# The role of ubiquitination and the p97-UBXD1 complex in regulating endosomal trafficking of caveolin-1

Inaugural-Dissertation

zur

Erlangung des Doktorgrades

Dr.rer.nat.

der Fakulät für

Biologie

an der

Universität Duisburg-Essen

vorgelegt von

Philipp Kirchner

aus Erlangen

Februar 2014

Die der vorliegenden Arbeit zugrunde liegenden Experimente wurden in der Abteilung für Molekularbiologie I am Zentrum für Medizinische Biotechnologie der Universität Duisburg-Essen durchgeführt.

1. Gutachter: Prof. Dr. Hemmo Meyer

2. Gutachter: Prof. Dr. Michael Ehrmann

Vorsitzender des Prüfungsausschusses: Prof. Dr. Peter Bayer

Tag der mündlichen Prüfung: 28. 05. 2014

# Table of contents

# Abbreviations

| | |
|---|---|
| AAA | ATPases Associated with diverse cellular Activities |
| ALIS | Aggresome-like Induced Structures |
| ALS | Amyotrophic Lateral Sclerosis |
| AMSH | Associated Molecule with the SH3 domain of STAM |
| ARF | ADP-ribosylation factor GTPase-activating protein 1 |
| ATP | Adenosine triphosphate |
| BCA | bicinchoninic acid protein assay |
| cCbl | Casitas B-lineage lymphoma proto-oncogene |
| CCD | Charge-coupled Device |
| cDNA | complementary DNA |
| CHMP | Charged Multivesicular body Protein |
| CIE | Clathrin-independent Endocytosis |
| CME | Clathrin-mediated Endocytosis |
| CUE | Coupling of Ubiquitin conjugation to Endoplasmic reticulum degradation |
| Cul3 | Cullin-3 |
| DAPI | 4',6-diamidino-2-phenylindole |
| DMEM | Dubecco's modified Eagles minimal essential medium |
| DNA | deoxyribonucleic acid |
| dNTP | deoxyribonucleotide |
| Doa4 | Degradation of α 4 |
| DOX | doxycycline |
| DTT | dithiothreitol |
| DUB | Deubiquitinating enzyme |
| DVC1 | DNA damage protein targeting VCP 1 |
| ECL | enhanced chemiluminescence |
| EEA1 | Early Endosome Antigen 1 |
| EGFR | Epidermal Growth Factor Receptor |
| EGTA | ethylene glycol tetraacetic acid |
| EMCCD | Electron-multiplying Charge-coupled Device |
| eNOS | endothelial Nitric Oxide Synthase |
| ER | Endoplasmic Reticulum |
| ERAD | ER-associated degradation |
| ESCRT | Endosomal Sorting Complex Required for Transport |
| FRT | Flp Recombination Target |
| GRB2 | Growth factor Receptor-bound protein 2 |
| GTP | Guanosine triphosphate |

| | |
|---|---|
| HECT | Homologous to the E6-AP Carboxyl Terminus |
| HEK293 | Human Embryonic Kidney 293 cells |
| HeLa | Henrietta Lacks human cervical carcinoma cell line |
| HEPES | 4-(2-hydroxyethyl)-1-piperazineethanesulfonic acid |
| HIF1α | Hypoxia-inducible Factor-1 α |
| HRP | horseradish peroxidase |
| HRS | Hepatocyte growth factor-regulated tyrosine kinase Substrate |
| HSC70 | Heat Shock Cognate 71 kDa protein |
| IF | immunofluorescence |
| IF | immunofluorescence |
| IGF-IR | Insulin-like Growth-factor I Receptor |
| ILV | Intralumenal Vesicle |
| LAMP1 | Lysosome-associated membrane glycoprotein 1 |
| LB | Luria-Bertani |
| LC3 | microtubule-associated proteins 1A/1B light chain 3 |
| MEM | minimal essential medium |
| MHC | Major Histocompatibility Complex |
| Mili-Q H2O | Mili-Q desalted water |
| MVE | Multivesicular Endosome |
| NA | Numerical Aperture |
| NEDD4 | Neural precursor cell Expressed Developmentally Down-regulated protein 4 |
| NEDD4L | NEDD4-like |
| NEM | N-Ethylmaleimide |
| NO | Nitric Oxide |
| NPL4 | Nuclear Protein Localization protein 4 homolog |
| NSF | NEM-sensitive fusion protein |
| PAGE | Polyacrylamide gel electrophoresis |
| PCR | polymerase chain reaction |
| PFU | PLAA Family Ubiquitin binding |
| PI3,5P2 | Phosphatidyinositol 3,5-bisphosphate |
| PI3P | Phosphatidyinositol 3-phosphate |
| PIP | Proliferating cell nuclear antigen-interacting Protein box |
| PIPES | piperazine-N,N'-bis(2-ethanesulfonic acid) |
| PLAA | Phospholipase A-2-activating protein |
| PTRF | Polymerase I and Transcript Release Factor |
| PUL | PLAA, Ufd3, lub1 |
| RING | Really Interesting New Gene |
| RISC | RNA induced silencing complex |

| | |
|---|---|
| RNA | ribonucleic acid |
| SDS | sodium dodecyl sulfate |
| SEP | Shp1, eyes-closed, p47 |
| SIMPLE | Small Integral Membrane Protein of Lysosome/late endosome |
| siRNA | small interfering RNA |
| SNARE | Soluble NSF Attachment Receptor |
| SRBC | Serum deprivation Response factor-related gene product that Binds to C-kinase |
| STAM | Signal Transducing Adapter Molecule |
| SUMO | Small Ubiquitin-related Modifier |
| TSG101 | Tumor susceptibility gene 101 protein |
| U | enzyme unit |
| U2OS | human osteosarcoma cell line U2 |
| UAS | Ubiquitin Associated |
| Ub | Ubiquitin |
| UBL | Ubiquitin-like |
| UBPY | Ubiquitin isopeptidase Y |
| UBX | Ubiquitin regulatory X |
| UBX-L | UBX-like |
| UBXD1 | UBX domain-containing protein 1 |
| UBZ | Ubiquitin-binding Zinc-finger |
| UFD1 | Ubiquitin fusion degradation protein 1 homolog |
| Ufd3 | Ubiquitin fusion degradation protein 3 |
| UIM | Ubiquitin Interacting Motif |
| VBM | VCP-binding Motif |
| VCP | Valosin-containing Protein |
| VCPIP1 | VCP/p47 complex-interacting protein 1 |
| VIM | VCP-interacting Motif |
| WB | Western blot |
| WWP1 | WW domain containing protein 1 |
| WWP2 | WW domain containing protein 2 |
| YOD1 | Ubiquitin thioesterase OTU1 |
| ZF | Zinc-finger |

# List of figures

# List of tables

## Summary

Caveolin-1 (CAV1) is the main structural component of cholesterol-rich microdomains in the plasma membrane, called caveolae. Caveolae occur in most mammalian cells and are involved in the regulation of cell signaling, lipid homeostasis, and response to mechanical stress. For turnover, CAV1 is ubiquitinated and sequestered in the lumen of multivesicular endosomes that eventually fuse with lysosomes. In addition to components of the ESCRT machinery, lysosomal sorting of ubiquitinated CAV1 requires the AAA-ATPase p97 together with the cofactor UBXD1. However, it is unknown at which site CAV1 is ubiquitinated and how ubiquitination is linked to endosomal sorting of CAV1. Moreover, it is unknown how the p97-UBXD1 complex interacts with ubiquitinated CAV1 and if p97 is a general regulator of endosomal sorting.

In this study, we show through systematic mutagenesis of lysine residues in CAV1 that ubiquitination of CAV1 occurs at any of the six lysines 5, 26, 30, 39, 47, and 57; and only the combined mutation of all six lysines together abolishes ubiquitination. The ubiquitination site is located in the flexible N-terminal region of CAV1 that is not involved in CAV1 oligomerization or membrane localization of CAV1. Importantly, mutation of the lysines 5 to 57 to arginine interfered with trafficking of CAV1 to early endosomes. As a consequence, the K5-57R variant accumulated at an early transport stage that was marked by the caveolar coat protein PTRF/cavin-1.

Previous studies established that overexpression of dominant negative p97 prevents sorting of CAV1 into the lumen of late endosomes. Consistently, we showed here that the ubiquitination site in the N-terminal region of CAV1 was necessary for the interaction between CAV1 and p97-UBXD1 as well as recruitment of p97-UBXD1 to endosomes. Moreover, cellular depletion or pharmacological inhibition of p97 accumulated ubiquitinated CAV1. These results indicate that p97-UBXD1 acts downstream of CAV1 ubiquitination and is required for the turnover of ubiquitinated CAV1 on late endosomes. In this context, we demonstrated that p97 also mediated lysosomal degradation of ligand-activated EGF receptor and, thus, acts as a general regulator of endosomal sorting.

## Zusammenfassung

Caveolin-1 (CAV1) ist ein wichtiger struktureller Bestandteil cholesterinreicher Mikrodomänen in der Plasmamembran, die Caveolae genannt werden. Caveolae finden sich in den meisten Säugerzellen und sind and der Regulation zellulärer Signalübertragung, des Fettstoffwechsels und der Reaktion auf mechanische Reize beteiligt. CAV1 wird für seinen eigenen Abbau ubiquitiniert und im Lumen multivesikulärer Endosomen, die letztendlich mit Lysosomen fusionieren, sequestriert. Der Transport von CAV1 zum Lysosom erfordert, neben Komponenten der ESCRT-Maschinerie, auch die AAA-ATPase p97 zusammmen mit dem Kofaktor UBXD1. Es ist allerdings unbekannt, an welcher Stelle CAV1 ubiquitiniert wird und wie Ubiquitinierung von CAV1 und endosomaler Transport miteinander verknüpft sind. Weiterhin ist unbekannt, wie genau der p97-UBXD1 Komplex mit CAV1 interagiert und ob p97 als allgemeiner Regulator für den endosomalen Transport fungiert.

Wir zeigen hier mittels systematischer Mutagenese, dass die Ubiquitinierung von CAV1 an einem beliebigen der sechs Lysine 5, 26, 30, 39, 47 und 57 in der N-terminalen Region stattfinden kann und dass die Mutation aller sechs Lysine zusammen notwendig ist, um die Ubiquitinierung zu verhindern. Die Ubiquitinierungsregion befindet sich in der flexiblen N-terminalen Region von CAV1, die nicht an der Oligomerisierung oder der Membranlokalisierung von CAV1 beteiligt ist. Bemerkenswerterweise behinderte die Mutation der Lysine 5 bis 57 den Transport von CAV1 zu frühen Endosomen. In der Folge akkumulierte CAV1 in einem frühen Transportschritt, der durch das caveoläre Hüllprotein PTRF/cavin-1 gekennzeichnet war.

Frühere Untersuchungen haben gezeigt, dass Expression einer dominant negativen Variante von p97 den Transport von CAV1 in das Lumen später Endosomen verhindert. In der Folge zeigten wir hier, dass die Ubiquitinierungsregion in CAV1 sowohl für die Interaktion zwischen CAV1 und dem p97-UBXD1 Komplex als auch die Rekrutierung von p97-UBXD1 zu Endosomen notwendig war. Weiterhin akkumulierte ubiquitiniertes CAV1 nach zellulärer Depletion oder pharmakologischer Inhibition von p97. Diese experimentellen Daten weisen darauf hin, dass p97-UBXD1 zeitlich nach der Ubiquitinierung von CAV1 agiert und notwendig für die Prozessierung von ubiquitiniertem CAV1 an späten Endosomen ist. In diesem

Zusammenhang zeigten wir weiterhin, dass p97 den lysosomalen Abbau von aktiviertem EGF Rezeptor vermittelte und deshalb als ein allgemeiner Regulator des endosomalen Transports agiert.

# 1 Introduction

## 1.1 Ubiquitination regulates protein turnover and activity

The term ubiquitination describes the posttranslational modification of lysine residues within a substrate protein with the small globular protein ubiquitin. This covalent modification is carried out by a three-step enzymatic cascade (Figure 1.1 A and B). Initially, ubiquitin is activated by an E1 ubiquitin-activating enzyme and subsequently transferred to an E2 ubiquitin-conjugating enzyme. Finally, an E3 ubiquitin ligase mediates the transfer of ubiquitin onto a specific substrate protein (Chen and Sun, 2009; Pickart, 2004). The E3 ubiquitin ligases constitute a large group of proteins with more than 600 members that can be divided into two families based on their catalytic domains. E3 ligases of the first family harbor a RING (Really Interesting New Gene) domain whereas members of the second family contain a HECT (Homology to E6AP C-terminus) domain (Deshaies and Joazeiro, 2009; Rotin and Kumar, 2009). Importantly, ubiquitin itself harbors seven lysines that can be ubiquitinated yielding poly-ubiquitin chains with specific linkages and specific cellular function. Ubiquitin binding proteins can discriminate between the different poly-ubiquitin chains and direct the ubiquitinated substrate protein into certain pathways (Ikeda and Dikic, 2008; Komander and Rape, 2012; Ye and Rape, 2009). The different topologies of ubiquitination are depicted in Figure 1.1 C.

Generally, poly-ubiquitin chains linked through lysine-48 induce proteasomal degradation of the substrate protein (Xu et al., 2009). In contrast, short poly-ubiquitin chains linked through lysine-63 mediate endocytosis of plasma membrane proteins (Duncan et al., 2006). However, other poly-ubiquitin chains, for example lysine-11 linked chains, can be a signal for proteasomal degradation as well as endocytosis (Boname et al., 2010; Xu et al., 2009). Chains that contain a mixture of different linkages further increase the complexity of the signals that are encoded by poly-ubiquitin chains (Ikeda and Dikic, 2008; Kim et al., 2007). Additionally, modification of proteins with a single ubiquitin is a signal for endocytosis and endosomal sorting of plasma membrane proteins. The substrate protein can be modified with a single ubiquitin (mono-ubiquitination), or several individual ubiquitin moieties (multiple mono-ubiquitination) (Haglund et al., 2003; Mosesson and Yarden, 2006; Sigismund et al., 2005; Stringer and Piper, 2011). Interestingly, poly-ubiquitin chains formed through lysine-63 linkages have an elongated conformation that makes them more

similar to mono-ubiquitin compared to the closed conformation of lysine-48 linked chains (Komander and Rape, 2012). In addition to mediating the turnover of cytosolic and membrane proteins, ubiquitination can regulate diverse cellular functions like DNA damage repair or cell signaling (Chen and Sun, 2009; Haglund and Dikic, 2005).

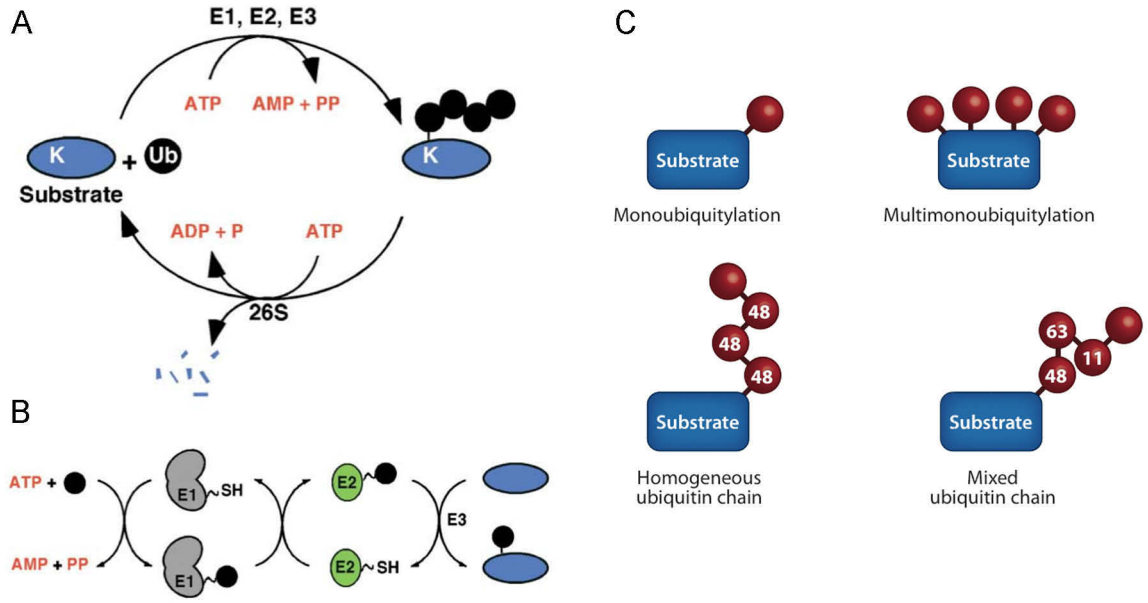


Figure 1.1 **Mechanism of ubiquitination and topologies of ubiquitination.**
A, schematic overview of the ubiquitination cycle. Substrates are ubiquitinated on surface lysines (K) by a cascade of E1 activating, E2 conjugating, and E3 ligase enzymes. Prior to substrate degradation for example in the 26S proteasome, ubiquitin is recovered and can be reused for ubiquitination. B, E1 ubiquitin-activating enzymes use the energy of ATP hydrolysis to form an ubiquitin thiol ester. Subsequently, ubiquitin is handed over to a cysteine residue in an E2 conjugating enzyme. Finally, an E3 ubiquitin ligase catalyzes the transfer of ubiquitin from the E2 conjugating enzyme to the substrate lysine. C, substrate proteins can be modified with a single lysine (mono-ubiquitination) or several individual ubiquitin moieties (multi/multiple-mono-ubiquitination). Poly-ubiquitin chains can contain homogenous ubiquitin linkages or a mixture of different ubiquitin linkages. (panel A and B are adopted from Pickart, 2004; panel C is adopted from Komander and Rape, 2012)

Ubiquitin-conjugated proteins can be deubiquitinated to recover ubiquitin prior to proteolysis of the substrate protein or to modify the ubiquitin signal (Komander and Rape, 2012). Deubiquitinating enzymes (DUBs) are vital to maintain sufficient cytosolic levels of free ubiquitin for proteasomal degradation as well as lysosomal degradation (Clague and Urbe, 2006; Finley, 2009). Additionally, deubiquitination is an important step prior to the extraction of ubiquitinated proteins from the endoplasmic reticulum (ER) (Claessen et al., 2012). Other cellular processes that are

regulated by deubiquitination are membrane fusion of Golgi fragments after mitosis or endosomal sorting of membrane proteins (Wang et al., 2004; Wright et al., 2011).

Finally, mammalian cells express several UBL (ubiquitin-like) proteins that can modify substrate proteins analogous to ubiquitin. The conjugation of UBL often modulates the activity and binding surfaces of proteins (Kerscher et al., 2006). For example, the lipid raft component caveolin-3 (CAV3) can be modified with the small ubiquitin like modifier SUMO and this modification affects the interaction with plasma membrane ion channels (Fuhs and Insel, 2011). Another example is autophagy that uses two highly specific ubiquitin conjugation systems to regulate the formation of autophagosomes (Ohsumi, 2001).

## 1.2 Endosomal sorting of plasma membrane proteins

Endosomal sorting of plasma membrane proteins is a process that has been extensively studied in yeast and mammalian cells. Many principles of endosomal sorting in mammalian cells have been elucidated using the epidermal growth factor receptor (EGFR) as a model substrate (Goh and Sorkin, 2013; Madshus and Stang, 2009). In general, small areas of the plasma membrane are internalized as vesicles in a process called endocytosis. Following endocytosis, these vesicles fuse with each other and early endosomes that act as an important sorting platform within the cell (Huotari and Helenius, 2011; Jovic et al., 2010). From early endosomes, proteins can recycle back to the plasma membrane (Maxfield and McGraw, 2004), engage in retrograde transport to the Golgi apparatus (Johannes and Popoff, 2008), or be targeted for lysosomal degradation (Huotari and Helenius, 2011). Furthermore, endosomes can regulate the timing and localization of intracellular signaling events (Scita and Di Fiore, 2010). Membrane proteins targeted for lysosomal degradation are sequestered on intralumenal vesicles (ILV) that bud inwards from the membrane of multivesicular endosomes (MVE) (Piper and Katzmann, 2007). Subsequently, these MVE mature into late endosomes and fuse with lysosomes to form endolysosomes. Endolysosomes are acidified organelles that contain a high concentration of proteases and digestive enzymes to degrade lumenal cargo (Huotari and Helenius, 2011; Luzio et al., 2007). Along this sorting pathway, endosomes can fuse to incorporate cargo proteins from different sources and also recycle membrane proteins back to the plasma membrane (Grant and Donaldson, 2009).

### 1.2.1 Clathrin dependent and independent endocytosis

The most prominent and fastest pathway for endocytosis of plasma membrane proteins and extracellular molecules is through clathrin-coated pits (McMahon and Boucrot, 2011; Ungewickell and Hinrichsen, 2007) (Figure 1.2 A, B, and C). The defining structural component of clathrin-mediated endocytosis is the clathrin hetero-hexamer, called triskelion (Greene et al., 2000; Liu et al., 1995). Plasma membrane proteins are clustered in clathrin-coated pits by adapter-proteins that mediate interaction between clathrin and endocytic cargo proteins. Most adapter-proteins, for example the abundant AP2 complex, additionally contain binding domains for phosphatidylinositol (PI)-4,5-bisphosphate ($PI3,5P_2$) lipids that mediate interaction with the plasma membrane (Mousavi et al., 2004). Cells express a wide variety of substrate adapters to mediate endocytosis of diverse cargo proteins (Ungewickell and Hinrichsen, 2007). For example, the Epsin, Eps15, and Eps15R adapters harbor ubiquitin-interacting motifs (UIM) and recognize ubiquitinated proteins (Tanno and Komada, 2013). These adapters can themselves be ubiquitinated in a process called coupled mono-ubiquitination to form a network of UIM-ubiquitin interactions that stabilizes the low affinity binding of the UIM to mono-ubiquitin (Barriere et al., 2006; Polo et al., 2002; Woelk et al., 2006). Interaction between adapter proteins, the plasma membrane, and cargo proteins induces nucleation of a clathrin coated-pit. Subsequently, clathrin is recruited to this seminal structure and induces further invagination of the plasma membrane. Finally, the GTPase dynamin mediates abscission of the clathrin-coated vesicle from the plasma membrane (McMahon and Boucrot, 2011; Ungewickell and Hinrichsen, 2007). Following endocytosis, the clathrin-coated vesicle fuses with the early endosome, where the clathrin coat is disassembled. However, clathrin can stay bound to early endosomes as part of special microdomains that contain ubiquitinated cargo proteins. These microdomains are important for recruitment of the downstream endosomal sorting machinery (Raiborg et al., 2002; Raiborg et al., 2006; Sachse et al., 2002).

In addition to the clathrin-dependent pathway, several pathways exist for clathrin-independent endocytosis (CIE) (Figure 1.2 A, and D). Generally, CIE requires lipid rafts and can be classified according to the requirement of dynamin for membrane abscission as well as the scaffold and regulatory proteins involved (Howes et al., 2010; Mayor and Pagano, 2007). The best-studied CIE pathway is the dynamin dependent endocytosis of plasma membrane caveolae that will be discussed in detail below. The second clathrin independent but dynamin dependent CIE mechanism

requires the small GTPase RHOA and no coat protein (Lamaze et al., 2001). In contrast, two small GTPases ARF1 and ARF6 were described to mediate plasma membrane endocytosis that is both independent of clathrin and dynamin (Howes et al., 2010; Mayor and Pagano, 2007). The ARF1 and ARF6 pathways possibly involve flotillin proteins that can induce membrane invaginations similar to caveolins (Glebov et al., 2006; Hansen and Nichols, 2009; Mayor and Pagano, 2007). Other mechanisms for endocytosis are phagocytosis and macropinocytosis. They are associated with actin-dependent membrane ruffles and generate large endocytic vesicles (Hansen and Nichols, 2009).

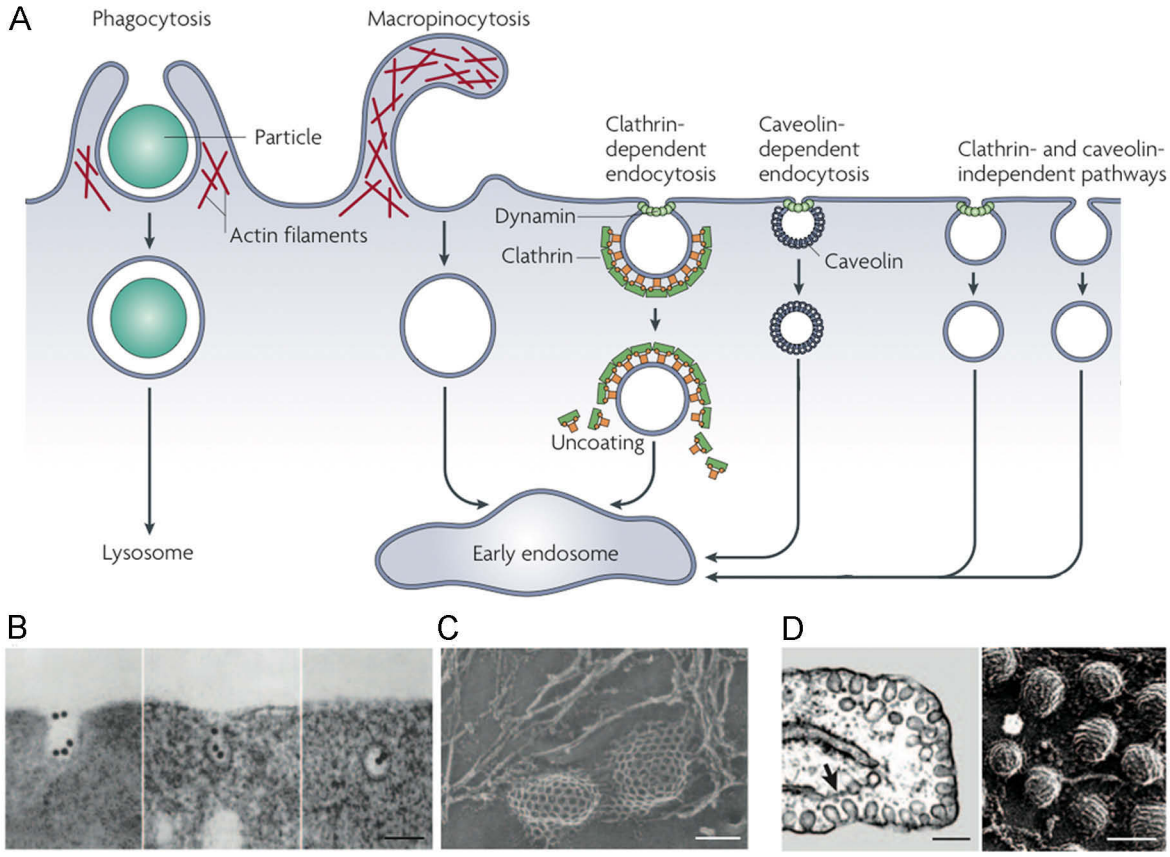


Figure 1.2 **Pathways of endocytosis**
A, Phagocytosis and macropinocytosis are actin-dependent pathways for the endocytosis of large particles or fluids respectively. Clathrin-mediated endocytosis is facilitated by the coat-protein clathrin and requires the GTPase dynamin for abscission of vesicles from the plasma membrane. Caveolae are specialized lipid raft domains that constitute a clathrin-independent but dynamin-dependent pathway for endocytosis. Other lipid raft-dependent endocytic pathways are independent of clathrin and caveolin but may require the activity of dynamin. Most internalized cargo molecules are delivered to the early endosome via clathrin- or caveolin-coated vesicles. B, thin section views of reticulocytes show clustering of gold-conjugated transferrin in clathrin-coated pits and endocytosis. C, Rapid-freeze, deep-etch view of clathrin lattices on the inner surface of a normal chick fibroblast. D, thin-section (left panel) and rapid-freeze, deep-etch (right panel) images of caveolae in endothelial cells. (modified from Mayor and Pagano, 2007)

### 1.2.2 The early endosome as a platform for protein sorting

Endocytic vesicles are short lived and either fuse homotypically to generate early endosomes *de novo* or fuse directly with the early endosomal compartment (Gruenberg and Maxfield, 1995; Ungewickell and Hinrichsen, 2007). Some endocytic vesicles might fuse with early endosomes only after several maturation steps as described for macropinocytosis of activated H-RAS (Porat-Shliom et al., 2008). Moreover, several studies found evidence for sorting of endocytic vesicles prior to the early endosome. These endocytic vesicles often carry unique membrane markers that distinguish them from early endosomes (Hayakawa et al., 2006; Lakadamyali et al., 2006; Zoncu et al., 2009). The early endosome is a pleomorphic organelle with a high rate of homotypic fusion and fission. It consists of vacuolar and tubular domains that accumulate cargo destined for degradation or recycling respectively (Gruenberg and Maxfield, 1995; Mellman, 1996) (Figure 1.3). Additionally, the early endosome can act as a coordination center for retrograde transport and quality control of plasma membrane proteins (Johannes and Popoff, 2008; Okiyoneda et al., 2010).

Due to the wide variety and vast number of endosomes, fusion between endocytic vesicles and endosomes has to be tightly regulated. This is achieved through small GTPases of the RAB family that are specific for the various endosomal compartments (Grosshans et al., 2006; Zerial and McBride, 2001). The RAB proteins recruit specific tethering factors that bridge between two vesicles to bring them in close proximity prior to fusion. Additionally, RAB proteins regulate the molecular machinery that facilitates membrane fusion together with a large number of effector proteins (Balderhaar and Ungermann, 2013; Zerial and McBride, 2001). In case of the early endosome, the small GTPase RAB5 governs the size and fusion rate of vesicles (Zeigerer et al., 2012). As an important effector protein, RAB5 recruits the PI3-kinase VPS34 that maintains the high levels of PI3P lipids that are specific for early endosomal membranes (Raiborg et al., 2013). The specific accumulation of PI3P lipids on early endosomes is necessary because tethering factors like EEA1 (Early Endosomal Antigen 1) require interaction with RAB5 and PI3P for their localization to early endosomes (Christoforidis et al., 1999). Consequently, removing PI3P from early endosomes inhibits endosomal trafficking through the early endosome (Raiborg et al., 2013).

Lysosomal degradation of membrane proteins involves the budding of intralumenal vesicles from the endosomal membrane into the lumen in a process called

multivesicular endosome (MVE) sorting (Figure 1.3). MVE sorting is mediated by the endosomal-sorting complex required for transport (ESCRT) that will be described in the next section. This process begins on early endosomes and continues during maturation into late endosomes. Late endosomes contain large numbers of intralumenal vesicles and are called multivesicular endosomes (Huotari and Helenius, 2011). The generation of intralumenal vesicles requires the induction of membrane curvature away from the cytoplasm (Raiborg and Stenmark, 2009). This topological change sequesters the cytoplasmic domains of transmembrane proteins from the cytoplasm and terminates signaling from activated transmembrane receptors (Goh and Sorkin, 2013; Huotari and Helenius, 2011).

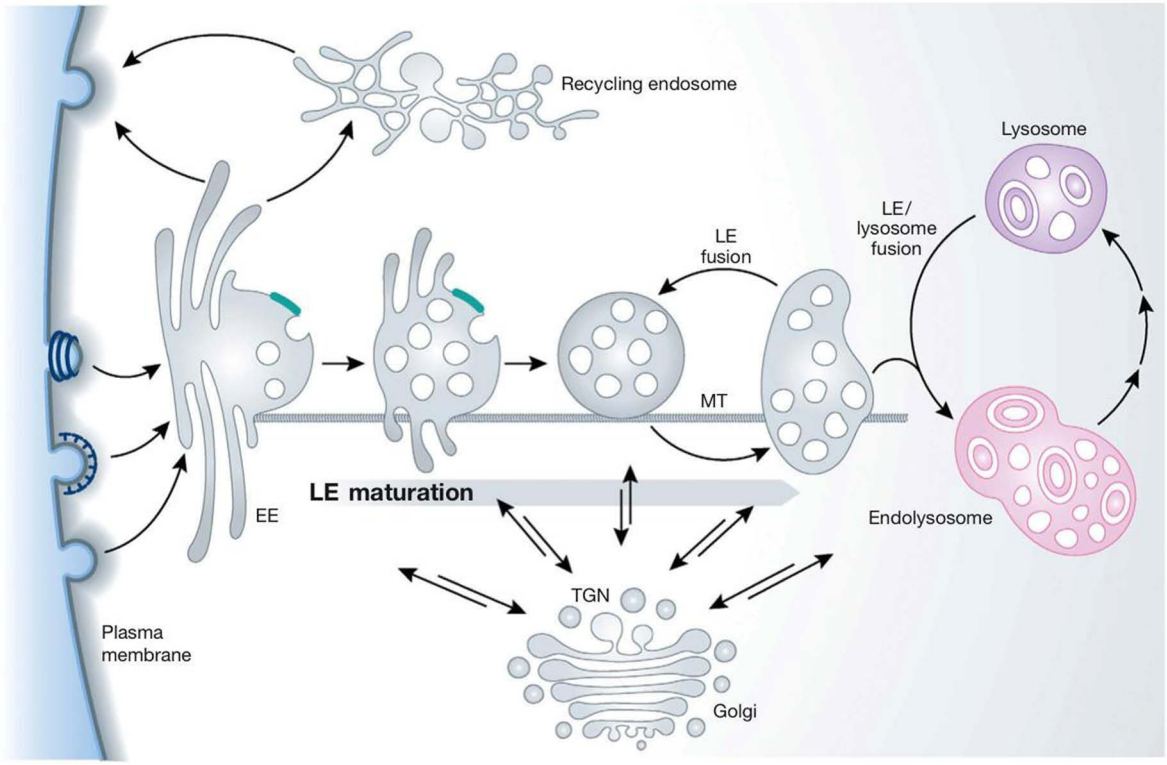


Figure 1.3 **The endosome/lysosome system.**
Endocytic vesicles from a variety of endocytic pathways deliver their contents and membranes to the early endosome. From the early endosome, cargo molecules can recycle back to the plasma membrane either directly or via the recycling endosome. Vacuolar domains of the early endosomes mature into late endosomes and eventually fuse with lysosomes. During maturation, endosomes grow in size through homotypic fusion and acquire intralumenal vesicles. The abscission of intralumenal vesicles that is mediated by the ESCRT machinery begins on early endosomes and continues throughout maturation. Additionally, endosomes can exchange membranes and content with the secretory pathway (retrograde transport). Late endosomes fuse with lysosomes and form endolysosomes where active degradation of the lumenal cargo takes place. (adopted from Huotari and Helenius, 2010)

Furthermore, during maturation into late endosomes the RAB5 GTPase is exchanged for the RAB7 GTPase, endosomes become increasingly acidified, and PI3P is converted into $PI3,5P_2$ (Huotari and Helenius, 2011; Rink et al., 2005).

### 1.2.3 The ESCRT machinery mediates MVE sorting of ubiquitinated substrates

The sorting of ubiquitinated membrane proteins into intralumenal vesicles by the ESCRT machinery has been extensively studied in the last years and is the subject of many comprehensive reviews (Henne et al., 2011; Piper and Katzmann, 2007; Raiborg and Stenmark, 2009; Roxrud et al., 2010). The signal for recognition of membrane proteins by the ESCRT machinery and subsequent MVE sorting are short lysine-63 linked poly-ubiquitin chains or mono-ubiquitin (Erpapazoglou et al., 2012; MacDonald et al., 2012; Sigismund et al., 2005; Stringer and Piper, 2011). The different architecture of this modification, in contrast to lysine-48 linked poly-ubiquitin chains, avoids targeting of membrane proteins to the proteasome (Komander and Rape, 2012). However, the affinity of the ESCRT ubiquitin-adapter proteins for single ubiquitin moieties is low and efficient sorting of mono-ubiquitinated proteins probably requires the clustering of mono-ubiquitin (Raiborg et al., 2002; Ren and Hurley, 2010). This is comparable to recognition of mono-ubiquitinated proteins in clathrin-mediated endocytosis (Barriere et al., 2006; Polo et al., 2002).

Many ubiquitinated membrane proteins engage ubiquitin adapters at the plasma membrane to initiate clathrin-mediated endocytosis. Following endocytosis, ubiquitinated substrates are recognized by the ESCRT-0 factors HRS (Hepatocyte growth factor-Regulated tyrosine kinase Substrate) and STAM (Signal Transducing Adapter Molecule) (Acconcia et al., 2009; Polo et al., 2002). Depletion of ESCRT-0 prevents the lysosomal degradation of ubiquitinated membrane proteins and induces recycling (Raiborg et al., 2008). The interaction between ubiquitinated membrane proteins and ESCRT-0 is localized on the early endosome and involves the clathrin coat protein (Raiborg et al., 2002; Raiborg et al., 2006; Sachse et al., 2002). HRS recruits another ubiquitin-receptor TSG101 (Tumor Susceptibility Gene 101) that constitutes the ESCRT-I complex together with additional protein factors (Henne et al., 2011; Roxrud et al., 2010). The ubiquitinated cargo is then handed over to VPS36 (vacuolar proteins sorting associated protein 36) that is a part of the ESCRT-II complex (Im and Hurley, 2008). Interestingly, several ESCRT components themselves are ubiquitinated and this directly regulates MVE-sorting (Amit et al., 2004; McCullough et al., 2004). In general, ubiquitinated proteins are captured by

ESCRT-0 and subsequently handed over to ESCRT-I and ESCRT-II. These protein complexes, in turn, mediate clustering on the endosomal membrane and possibly initiate membrane deformation (Henne et al., 2011; Roxrud et al., 2010). Finally, ESCRT-II recruits the multi-subunit ESCRT-III machinery that contains no ubiquitin binding motifs but is required for further deformation of the membrane and ILV abscission. After abscission of the ILV, the ESCRT proteins that have assembled on the endosomal membrane are recycled for subsequent rounds of ILV biogenesis. ESCRT-III proteins recruit the AAA-ATPase VPS4 that uses the energy of ATP hydrolysis to disassemble the ESCRT complexes (Henne et al., 2011; Roxrud et al., 2010) (Figure 1.4).

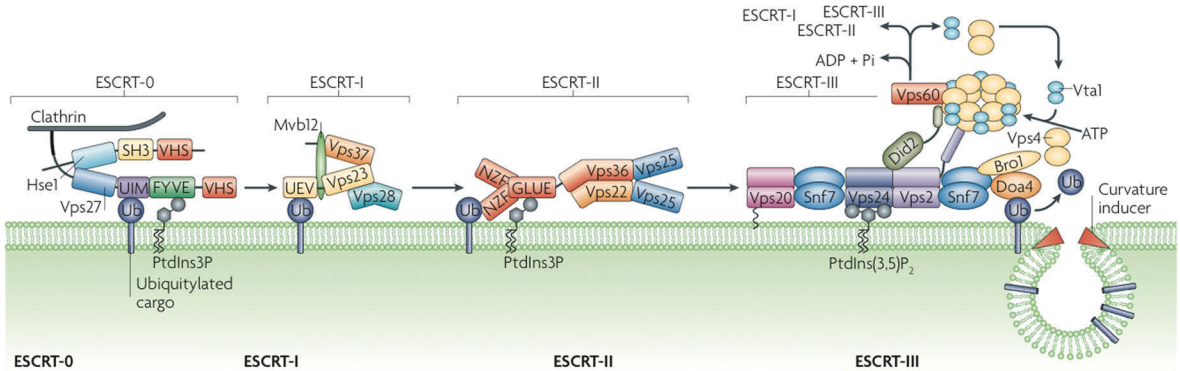


**ESCRT-0**

| *S. cerevisiae* | Mammalian |
|---|---|
| Vps27 | HRS (HGS) |
| Hse1 | STAM1, STAM2 |

**ESCRT-I**

| *S. cerevisiae* | Mammalian |
|---|---|
| Vps23 | VPS23 (TSG101) |
| Vps28 | VPS28 |
| Vps37 | VPS37A, B, C, D |
| Mvb12 | ? |

**ATPase complex**

| *S. cerevisiae* | Mammalian |
|---|---|
| Vps4 | VPS4A and VPS4B (SKD1) |
| Vta1 | LIP5 |

**ESCRT-II**

| *S. cerevisiae* | Mammalian |
|---|---|
| Vps22 | VPS22 (EAP30, SNF8) |
| Vps25 | VPS25 (EAP20) |
| Vps36 | VPS36 (EAP45) |

**Accessory**

| *S. cerevisiae* | Mammalian |
|---|---|
| Bro1 | ALIX (AIP1, PDCD6IP ) |
| Doa4 | UBPY? |
| ? | AMSH |

**ESCRT-III**

| *S. cerevisiae* | Mammalian |
|---|---|
| Vps2 | VPS2A, B (CHMP2A, B) |
| Vps24 | VPS24 (CHMP3) |
| Snf7 | SNF7-1, -2, -3 (CHMP4A, B, C) |
| Vps20 | VPS20 (CHMP6) |
| Did2 | CHMP1A, B |
| Vps60 | CHMP5 |
| - | CHMP7 |

Figure 1.4 **Schematic overview of the ESCRT machinery involved in intralumenal vesicle formation.**
Endosomal sorting of membrane protein into intralumenal vesicles requires the coordinated action of four multi-subunit complexes that constitute the ESCRT machinery. ESCRT-0 interacts with PI3P lipids, and clathrin complexes and captures ubiquitinated cargo proteins on the surface of endosomes. ESCRT-0 subsequently recruits ESCRT-I and ESCRT-II. These large protein complexes can interact with ubiquitinated cargo and, in the case of ESCRT-II with PI3P lipids. The action of ESCRT-I and ESCRT-II clusters ubiquitinated proteins on the surface of late endosomes. The ESCRT-III complex, in turn, is required to induce membrane deformation and vesicle abscission. This may require the help of membrane curvature inducing lipids, for example lysobisphosphatidic acid. Following vesicle abscission, the ESCRT complexes are recycled by the activity of the AAA-ATPase VPS4. The components of ESCRT complexes in yeast as well as mammalian cells are listed. (adopted from Williams and Urbe, 2007)

In light of the multiple protein interactions that are mediated through ubiquitin and ubiquitin binding domains it comes as no surprise that deubiquitination is an important step in MVE sorting (Clague and Urbe, 2006; Wright et al., 2011). In yeast,

Doa4 (Degradation of alpha 4) mediates deubiquitination of endosomal cargo. Even though deubiquitination is not required for MVE sorting, Doa4-deletion strains have reduced levels of free ubiquitin due to ubiquitin being degraded in the vacuole (Amerik et al., 2000; Luhtala and Odorizzi, 2004). In mammalian cells, the deubiquitinating enzymes UBPY (Ubiquitin-specific Protease Y) and AMSH (Associated Molecule with the SH3 domain of STAM) interact with the ESCRT-0 proteins HRS and STAM. Both DUBs can deubiquitinate cargo proteins, like the EGF receptor, as well as the ESCRT-0 ubiquitin-adapters. Depletion of AMSH promotes EGFR ubiquitination and subsequent degradation. (Bowers et al., 2006; McCullough et al., 2006). Likewise, knockdown of UBPY prevents deubiquitination of the EGF receptor; however, there is debate about the effect on MVE sorting (Berlin et al., 2010; Niendorf et al., 2007; Row et al., 2006). Deubiquitination of ESCRT-0 by AMSH and UBPY might prevent proteasomal degradation of these proteins and promote MVE sorting (Niendorf et al., 2007; Row et al., 2006). Importantly, both AMSH and UBPY cannot substitute for each other and likely perform other non-redundant functions. In general, deubiquitination of cargo after interaction with the ESCRT machinery favors degradation, while deubiquitination prior to ESCRT engagement favors recycling (Goh and Sorkin, 2013).

### 1.2.4 Endosomal sorting of ligand activated EGFR as an example for endocytosis and MVE sorting

Endocytosis and lysosomal degradation of the EGF receptor after ligand binding is a well-studied example for MVE sorting. Following binding of EGF, the EGF receptor dimerizes and auto-phosphorylates. This enables recruitment of phosphotyrosine-binding proteins like GRB2 (Growth factor Receptor-Bound protein 2) and activation of downstream signaling cascades (Goh and Sorkin, 2013; Madshus and Stang, 2009; Tomas et al., 2013). Simultaneously, the EGFR is ubiquitinated by ubiquitin ligases of the CBL (Casitas B-lineage Lymphoma) family and localizes together with GRB2 to clathrin-coated pits (Johannessen et al., 2006; Pennock and Wang, 2008). Following stimulation and ubiquitination, the receptor is endocytosed and transported to early endosomes (Figure 1.5). This might involve ubiquitination of not yet identified proteins, because also a non-ubiquitinatable EGFR variant is taken up efficiently (Huang et al., 2007; Huang et al., 2006). However, non-ubiquitinated EGFR is constitutively recycled back to the plasma membrane. Interestingly, even in the absence of stimulation, the EGFR undergoes constant rounds of endocytosis and recycling (Rush and Ceresa, 2013). The strength of EGF stimulation affects which

pathway is used for endocytosis and decides the subsequent fate of the receptor. Low levels of EGF favor clathrin-mediated endocytosis and recycling, while high levels of EGF induce clathrin-independent endocytosis and degradation (Sigismund et al., 2013; Sigismund et al., 2008). The EGF receptor has been shown to locate to caveolae in response to EGF stimulation. However, depletion of caveolin does not affect EGFR endocytosis (Kazazic et al., 2006; Sigismund et al., 2008).

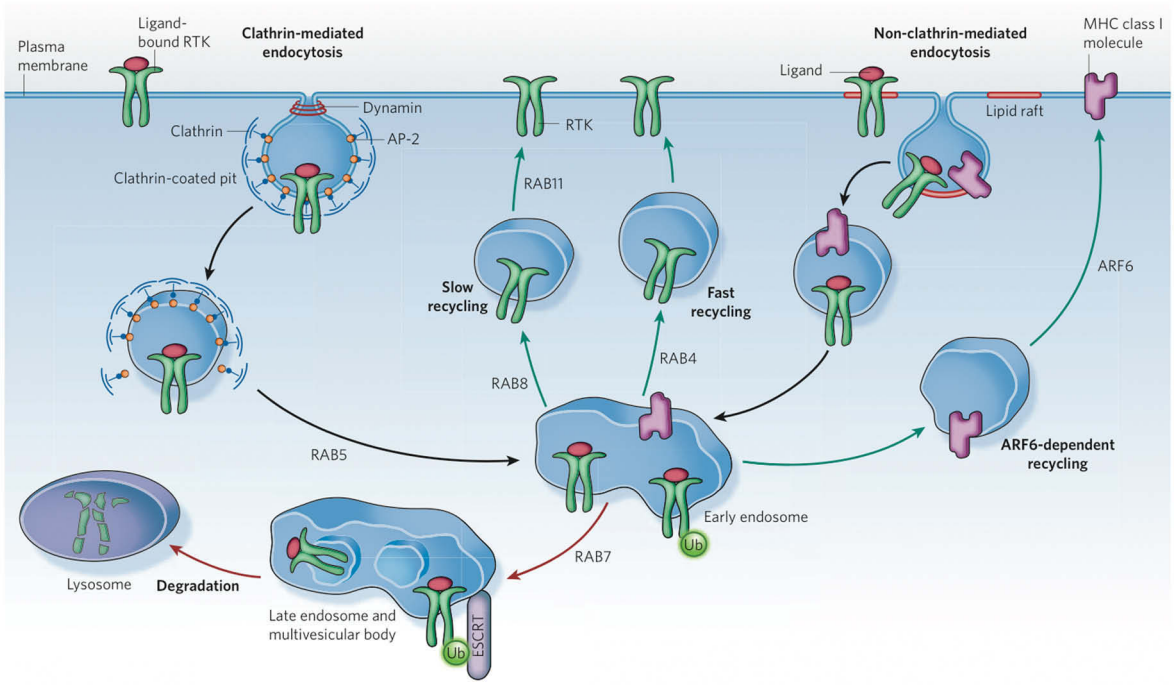


Figure 1.5 **Endocytic trafficking of transmembrane receptors.**
Receptor tyrosine kinases (RTKs) enter the cell through clathrin-mediated endocytosis but also can use lipid raft-dependent endocytosis under certain conditions. Clathrin-mediated endocytosis requires substrate-adapter proteins that recognize cargo proteins, like the AP-2 complex, and the GTPase dynamin for vesicle abscission. Other membrane proteins, for example MHC class I molecules, preferentially enter the cell via lipid raft-dependent endocytosis. Both pathways combine at the early endosome. From the early endosome, receptors can recycle back to the plasma membrane or engage in ESCRT-mediated sequestration in intralumenal vesicles and transport to the lysosome. Lysosomal degradation requires ubiquitination of the receptor and terminates signaling. Endosomal sorting is governed by small GTPases of the RAB family that specify separate endosomal compartments and pathways. (adopted from Scita and Di Fiore, 2010)

On early endosomes, the ubiquitinated EGFR engages the ESCRT-0 and this is necessary for sorting into ILVs and lysosomal degradation (Goh and Sorkin, 2013; Madshus and Stang, 2009) (Figure 1.5). Alternatively, the EGF receptor can be deubiquitinated on early endosomes to prevent lysosomal degradation. Along this line, a non-ubiquitinatable receptor constitutively recycles from late endosomes to the plasma membrane (Eden et al., 2012). Endocytosis of the EGFR can be a mechanism to control the duration of EGF-induced signaling. The decreased pH in the lumen of early endosomes in comparison to the extracellular space causes dissociation of EGF from the receptor and thus can terminate the signaling cascade (Roepstorff et al., 2009; Tomas et al., 2013). Furthermore, endocytosis of the activated EGFR offers a possibility to modify the interaction with signaling partners and modulate the EGF induced signaling (Scita and Di Fiore, 2010). However, once the EGFR is sequestered within MVE all signaling is terminated and the receptor is degraded.

This sequence of events is similar for most receptor tyrosine kinases (RTKs) but often involves specific adapters and effectors for each receptor (Goh and Sorkin, 2013; Madshus and Stang, 2009). For example, many RTK are ubiquitinated by members of the NEDD4 (Neural precursor cell expressed Developmentally Down-regulated protein 4) family of ubiquitin ligases (Rotin and Kumar, 2009). Other receptors like the transferrin receptor are not subject to lysosomal degradation after ligand binding but recycle to the plasma membrane after endocytosis (Grant and Donaldson, 2009).

### 1.2.5 Diseases associated with defects in MVE sorting

Defects in the ESCRT machinery in yeast and mammalian cells manifest in a distinctive abnormal subcellular structure that is called class E compartment. This compartment appears as stacked, flat cisternae that are not interconnected and represents aberrant MVE (Doyotte et al., 2005; Razi and Futter, 2006; Wollert et al., 2009). Depletion of ESCRT components in cell culture causes defects in MVE sorting and degradation of endosomal cargo proteins. For example, depletion of HRS (ESCRT-0) or TSG101 (ESCRT-I) causes a partial delay in EGFR degradation kinetics and induces recycling to the plasma membrane (Doyotte et al., 2005; Raiborg et al., 2008; Razi and Futter, 2006). Likewise, depletion of ESCRT-II or ESCRT-III components results in impaired EGF receptor degradation (Williams and Urbe, 2007). Importantly, this also affects signaling from the EGFR and can modulate

cell survival and apoptosis (Bache et al., 2004; Rush et al., 2012). Along this line, TSG101 and another mammalian ESCRT-I component, VPS37A, were originally identified as tumor-suppressor genes and map to chromosomal regions that are often deleted or mutated in cancers (Bache et al., 2004; Saksena and Emr, 2009). The control of cell signaling through endosomal sorting is an important regulator of growth-factor signaling and, therefore, associated with the origin of malignant growth (Goh and Sorkin, 2013; Tomas et al., 2013).

Furthermore, mutations in ESCRT proteins can affect cell cycle control, transcription regulation, and have been associated with neurodegenerative diseases (Saksena and Emr, 2009). Mutation in the ESCRT-III protein VPS2/CHMP2B causes a hereditary form of frontotemporal dementia (FTD) that is associated with ubiquitinated inclusions positive for the autophagy marker p62 (Urwin et al., 2010). Mutations in another ESCRT-III protein VPS24/CHMP3 inhibit the degradation of expanded poly-glutamine aggregates in Huntington's disease (Filimonenko et al., 2007). These mutations demonstrate that there is a connection between aggregate handling through autophagy and MVE sorting (Rusten and Simonsen, 2008). Interestingly, recent studies revealed that another hereditary neurological disorder, Charcot-Marie-Tooth disease type 1C, might be associated with MVE sorting. The SIMPLE (Small Integral Membrane Protein of Lysosome/late Endosome) protein interacts and colocalizes with ESCRT components and mutation of SIMPLE affects endosomal sorting of the RTK ErbB2 (Lee et al., 2012). In addition, the ability of the ESCRT machinery to induce membrane deformation can be hijacked by viruses to mediate budding of viral particles from the plasma membrane. For example, efficient release of the human immunodeficiency virus (HIV) requires interaction between TSG101 and viral surface proteins (Saksena and Emr, 2009).

## 1.3 Autophagy

Autophagy is used as a collective term for three related pathways that are highly conserved from yeast to mammals and facilitate degradation of cytosolic cargo in the lysosome (Weidberg et al., 2011). Macroautophagy is characterized by formation of a crescent shaped phagophore that expands to form a double-membrane autophagosome (Figure 1.6). Autophagosomes then fuse with endosomal compartments and eventually lysosomes to degrade the lumenal cargo. In microautophagy or chaperone mediated autophagy cytosolic proteins are directly delivered to the lumen of lysosomes by invagination of the lysosomal membrane or

translocation across the lysosomal membrane respectively (Kirkin et al., 2009b). Macroautophagy, here referred to simply as autophagy, can sequester and degrade large fractions of cytosolic material, for example as a reaction to starvation (Yang and Klionsky, 2010). In addition, cells can induce selective autophagy to degrade various cellular structures including protein aggregates, mitochondria, and microbes. Importantly, selective autophagy depends on the ubiquitination of substrates (Kirkin et al., 2009b).

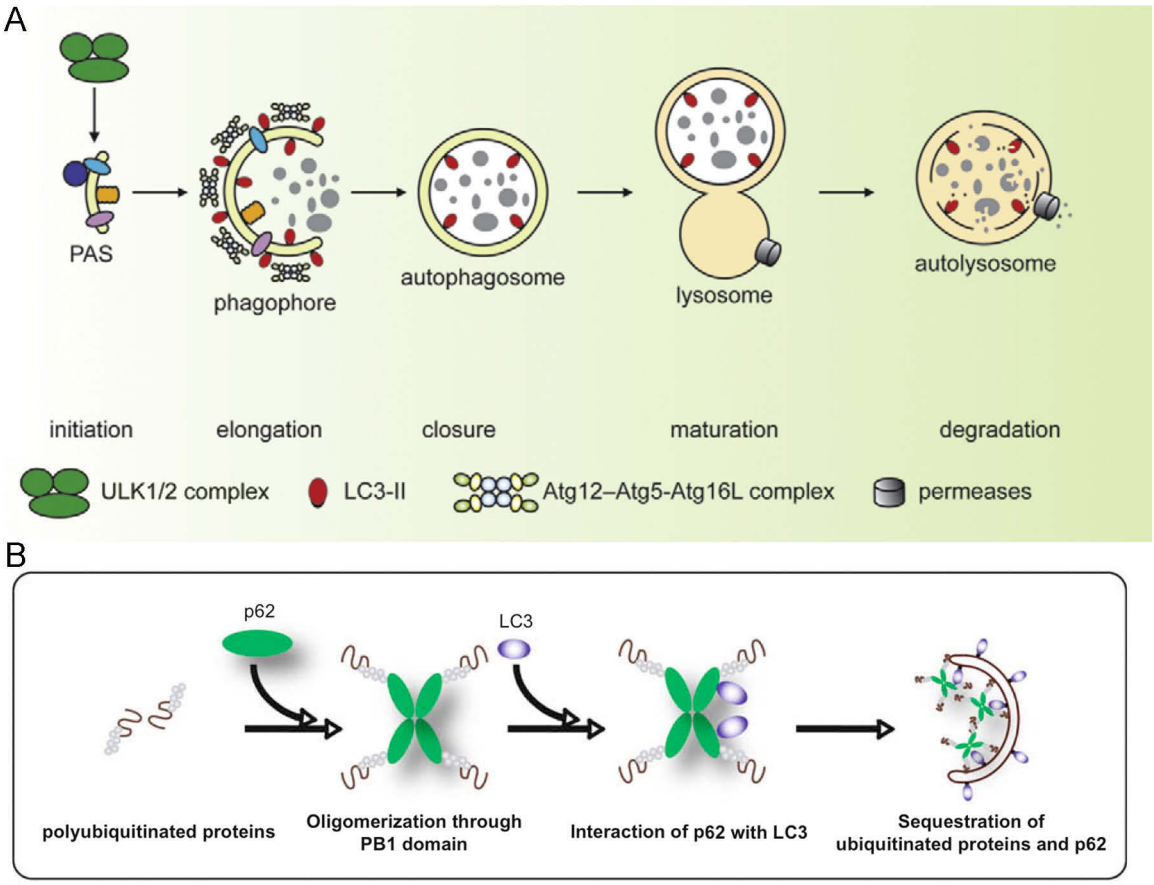


Figure 1.6 **Schematic overview of general end selective autophagy.**
A, Mammalian autophagy initiates at the phagophore assembly site (PAS) that incorporates signaling from upstream regulators. The ULK1/2 complex, for example, activates autophagy under starvation conditions. The phagophore is elongated by action of the two ubiquitin-like proteins ATG12 and ATG8 (LC3 in mammalian cells). This sequesters a fraction of the cytoplasm that is surrounded by a double membrane after phagophore closure. Autophagosomes dock at or fuse with lysosomes and form autolysosomes that degrade the sequestered cytoplasmic molecules. The resulting macromolecules are transported back into the cytoplasm through membrane permeases. B, the ubiquitin adapter p62 interacts with poly-ubiquitinated proteins and induces aggregation. Sequestration of these aggregates in autophagosomes is mediated by the direct interaction between p62 and the phagophore-membrane protein LC3. (panel A is modified from Yang and Klionsky, 2010; panel B is adopted from Komatsu and Ichimura, 2010)

Genetic studies in yeast revealed more than 30 autophagy-related (ATG) proteins that govern biogenesis, maturation, and degradation of the autophagosome (Suzuki and Ohsumi, 2007). Two pivotal elements of autophagosome formation are the ATG12 and ATG8 ubiquitin-like proteins. ATG12 is covalently attached to another autophagy protein ATG5, while ATG8 is conjugated to phosphatidylethanolamine (PE) lipids in the autophagosome membrane. In mammalian cells, several homologues of Atg8 are known of which LC3 (microtubule-associated proteins 1A/1B (MAP1) Light Chain 3) is the best characterized. ATG8-PE probably is the driving force that facilitates elongation of the phagophore and stays attached to the membrane through fusion of the autophagosome with the lysosome (Ohsumi, 2001). Therefore, Atg8 or LC3 are extensively used as markers for autophagosomes (Klionsky et al., 2008). However, the process of autophagosome formation is not completely understood and, for example, the source of autophagic membranes is still under debate (Hamasaki and Yoshimori, 2010).

### 1.3.1 Selective autophagy of ubiquitinated proteins

One important type of cargo for selective autophagy is aggregates of misfolded proteins that occur under stress condition or due to expression of aberrant peptides. Cells actively accumulate misfolded proteins in large aggregates called aggresomes. This requires microtubules together with motor proteins and the intermediate-filament protein vimentin (Kopito, 2000). In contrast, cells can form stress-induced aggregates, called aggresome-like induced structures (ALIS) that contain defective ribosomal products as well as long lived proteins and do not require active transport (Szeto et al., 2006). These intracellular aggregates are substrates for the proteasome and autophagy. Importantly, ALIS and other protein-aggregates are recognized by the ubiquitin-adapter p62 and directed towards autophagic degradation (Pankiv et al., 2007). The adapter protein p62 interacts with ubiquitin through an ubiquitin-associated domain (UBA) and dimerizes to aggregate ubiquitinated proteins. Additionally, p62 binds to the autophagosomal membrane protein LC3 trough an LC3-interacting region (LIR). Therefore, p62 can crosslink ubiquitinated substrates and target them to autophagy (Komatsu et al., 2007; Pankiv et al., 2007) (Figure 1.6). During autophagosome maturation, p62 stays bound to LC3 and is eventually degraded in lysosomes. As a consequence, abolishing autophagy causes accumulation of p62 and unspecific aggregation of ubiquitinated proteins in the cell that can lead to cell death (Komatsu et al., 2007; Korolchuk et al., 2009). In contrast, depletion of p62 does not result in visible accumulation of ubiquitinated aggregates

due to the presence of further ubiquitin-adapter proteins (Clausen et al., 2010; Kirkin et al., 2009a). In addition to protein aggregates, selective autophagy can facilitate the degradation of large protein complexes like ribosomes or whole organelles (Kirkin et al., 2009b). For example, damaged mitochondria are ubiquitinated by the E3 ubiquitin ligase Parkin and targeted for autophagic clearance. Interestingly, this too might involve p62 as an ubiquitin-adapter protein (Geisler et al., 2010). Taken together, the action of ubiquitin adapter proteins makes it possible to selectively target cytosolic components for autophagy (Kirkin et al., 2009b; Weidberg et al., 2011).

### 1.3.2 Autophagy and human disease.

Defects in selective autophagy are associated with a number of diseases that mainly arise from accumulation of protein aggregates in cells (Komatsu and Ichimura, 2010). Mutations in the ubiquitin-binding domain of p62 cause Paget disease of the bone (PDB). The disease mechanism of PDB has been originally attributed to defective NFκB signaling in osteoclasts. However, it is possible that mutations in p62 cause defects in autophagy that contribute to the disease phenotype (Goode and Layfield, 2010). Another congenital disorder with a similar bone phenotype is inclusion body myopathy, Paget disease of the bone and frontotemporal dementia (IBMPFD). Importantly, recent studies showed that IBMPFD is associated with inefficient clearance of autophagosomes (Ju et al., 2009; Tresse et al., 2010). Moreover, several neurological disorders are linked to defects in autophagy and inefficient degradation of protein aggregates. Mutations in ESCRT proteins that interfere with the fusion of autophagosomes and lysosomes and subsequent clearance of autophagosomes might be a cause for neurological disease (Rusten and Simonsen, 2008). In addition to cytosolic aggregates, autophagy was recently discovered to degrade misfolded proteins that accumulate in the ER in response to ER-stress (Yorimitsu and Klionsky, 2007). Moreover, autophagy can directly defend the cell against invading cytosolic pathogens. Recognition of *Salmonella* species by the ubiquitin-adapter optineurin induces enclosure of the bacterium in autophagosomes and autophagic degradation (Wild et al., 2011).

## 1.4 Caveolins and cavins.

The plasma membrane of all cells is composed of a phospholipids bilayer that separates the cytosol from the surrounding extracellular space. However, the plasma membrane is not homogenous but contains regions of higher and lower mobility. The liquid ordered regions of lower mobility, called lipid rafts, are enriched in sphingolipids and cholesterol and are stabilized by membrane proteins (Hancock, 2006). One special kind of cholesterol-rich lipid raft microdomains in the plasma membrane is defined by the 21 kD protein caveolin-1 (CAV1) and called caveolae for the distinctive flask-like shape (Figure 1.7 A). Caveolae have been implicated in a wide variety of cellular processes including endocytosis, cell signaling, membrane homeostasis, and mechanosensing (Parton and del Pozo, 2013).

### 1.4.1 Structure of caveolins and formation of caveolae.

The family of caveolin proteins is highly conserved between metazoan organisms and expression of most caveolins results in the spontaneous formation of caveolae in the plasma membrane (Kirkham et al., 2008). In humans, three caveolin isoforms are identified with CAV3 being expressed exclusively in muscle tissue and CAV1 and CAV2 in almost all other tissues. CAV1 and CAV2 show overlapping expression profiles and overexpressed CAV2 does not form caveolae on its own (Parton and del Pozo, 2013). Therefore, CAV2 possibly has a regulatory role in caveola formation and dynamics as observed in CAV2 deficient mice (Razani et al., 2002). All caveolins share a hairpin-like structure and insert into the cytoplasmic leaflet of the plasma membrane bilayer with a 33-residue intra membrane domain (Figure 1.7 B). As a consequence, both N- and C-terminus are facing the cytoplasm. During biogenesis, the C-terminal domain is palmitoylated; however, this modification is not required for targeting of CAV1 to caveolae (Parton et al., 2006). CAV1 and CAV3 can form high-molecular weight complexes through homo-oligomerization (Monier et al., 1995; Tang et al., 1996). In CAV1, the amino acids 61-101 are sufficient to form oligomers. In detail, the amino acids 79-96 form an alpha helix that mediates the oligomerization (Fernandez et al., 2002; Sargiacomo et al., 1995). The minimal CAV1 protein that can form caveolae spans the amino acids 49-147 and contains the oligomerization and intramembrane domains as well as two of three palmitoylation sites (Kirkham et al., 2008). Furthermore, CAV1 contains a scaffolding domain (CSD) that is made up by the amino acids 81-101 in CAV1 and has been described to take part in a wide variety of intermolecular interactions. For example, heterotrimeric G proteins, SRC

family tyrosine kinases, integrins, EGFR, and endothelial ion channels interact with CAV1 through a caveolin-binding motif (CBM). However, prediction of binding partners by bioinformatics based on the CBM proved to be difficult (Byrne et al., 2012; Collins et al., 2012). Additionally, studies using antibodies targeting the CSD suggest that this region is probably buried within CAV1 oligomers and not readily accessible for interaction (Parton and Simons, 2007; Pol et al., 2005).

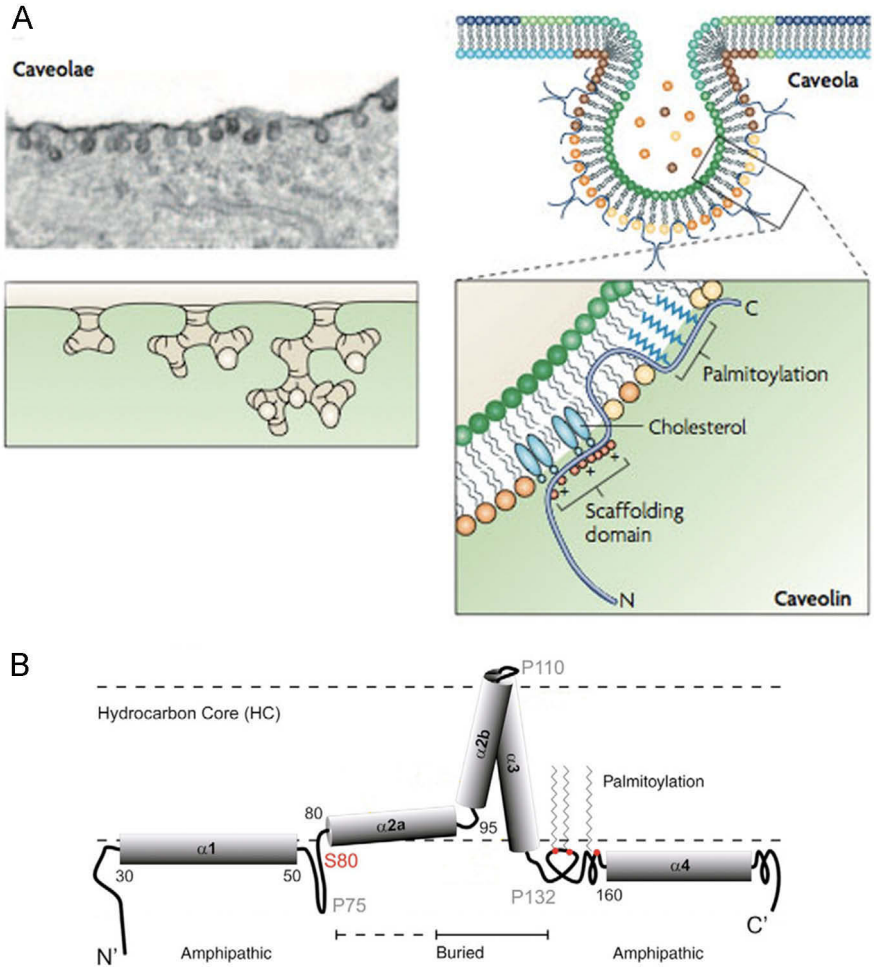


Figure 1.7 **Caveolae and membrane topology of CAV1.**
A, thin section image (upper left panel) of plasma membrane caveolae in adipocytes and schematic depiction of multiple caveolae forming continuous invaginations (lower left panel). The right panel illustrates a section through a single caveola and shows the flask-like shape. Cav1 is inserted into the cytoplasmic leaflet of the plasma membrane with N- and C-termini facing the cytoplasm (blowup). The scaffolding domain of CAV1 may directly interact with cholesterol. B, Topological model of CAV1 in the plasma membrane. The intra-membrane domain is buried in the plasma membrane with the N- and C-termini facing the cytoplasm. The scaffolding domain at least partially enters the hydrocarbon core of the membrane, while the C-terminal domain is anchored in the plasma membrane through palmitoylation. Parts of the N- and C-terminal regions form amphipathic helices at the plasma membrane interface. The very N-terminal region is more flexible and protrudes into the cytoplasm. (panel A is adopted from Parton and Simons, 2007; panel B is adopted from Parton et al., 2006)

CAV1 can be expressed from two distinct mRNAs as a full-length α-isoform or a β-isoform that is lacking the first 31 amino acids (Kogo and Fujimoto, 2000). However, the functional difference between the two isoforms is not clear (Parat, 2009). CAV1 is cotranslationally inserted into the endoplasmic reticulum (ER) in a signal recognition particle (SRP)-dependent manner (Monier et al., 1995). In the ER, CAV1 monomers assemble into 8S oligomers, named for their sedimentation coefficient, and are transported to the Golgi apparatus (Fernandez et al., 2002; Hayer et al., 2010a; Sargiacomo et al., 1995). If transport of CAV1 to the Golgi apparatus is inhibited, CAV1 re-localizes from the ER to lipid droplets (Ostermeyer et al., 2001). In the Golgi apparatus, 8S oligomers further assemble into larger 70S caveolar scaffolds and this causes the masking of certain epitopes that become buried within the oligomers (Pol et al., 2005). Importantly, this is accompanied by recruitment of cholesterol to the 70s complexes and resistance to extraction with the detergent Triton X-100. The 70S caveolar assemblies are subsequently transported to the plasma membrane in vesicular carriers that incorporate secretory cargo proteins (Hayer et al., 2010a). Each complex contains as many as 160 CAV1 proteins that arrive at the plasma membrane simultaneously (Hayer et al., 2010a; Pelkmans and Zerial, 2005). Crucially, several mutant variants of CAV1 that affect oligomerization cause accumulation of CAV1 in the Golgi apparatus (Ren et al., 2004). The best-studied mutation is the exchange of proline-132 to leucine that affects the intramembrane helix and favors dimerization over oligomerization (Rieth et al., 2012).

### 1.4.2 Cavins as regulators of caveolar stability

Recent studies identified several proteins that interact with caveolae and regulate their biogenesis and stability. These proteins were initially identified within diverse cellular processes and only later grouped together into the cavin family (Hansen and Nichols, 2010). PTRF (Polymerase I and Transcript Release Factor)/cavin-1 is a caveolar coat protein necessary for caveolae formation in cells usually lacking caveolae (Hill et al., 2008; Vinten et al., 2005). Depletion of PTRF/cavin-1 was shown to mobilize CAV1 from caveolae and induce bulk endocytosis of oligomeric CAV1 (Hayer et al., 2010b). In the absence of PTRF/cavin-1, CAV1 forms tubule-like structures on the plasma membrane while PTRF/cavin-1 overexpression stabilizes caveolae (Liu and Pilch, 2008; Verma et al., 2010). The stabilization of caveolae requires the interaction between PTRF/cavin-1 and the cytoskeleton (Liu and Pilch, 2008) (Figure 1.8). Interestingly, in the absence of CAV1 expression, PTRF/cavin-1 by itself can assemble into large oligomers that contain other cavin-family members

(Hayer et al., 2010b). Three more cavin-family proteins were identified and perform functions similar to PTRF/cavin-1 (Hansen and Nichols, 2010). For example, SRBC (Sdr-Related gene product that Binds to C-kinase)/cavin-3 associates with budding caveolae and might regulate vesicular trafficking through caveolae (McMahon et al., 2009). However, it is not known whether there is hierarchical binding of the cavins to caveolae or if cavins define special sub-populations of caveolae within the cell (Hansen and Nichols, 2010). Importantly, the different cavin-family proteins show tissue specific expression and function in the morphogenesis of caveolae (Hansen et al., 2013).

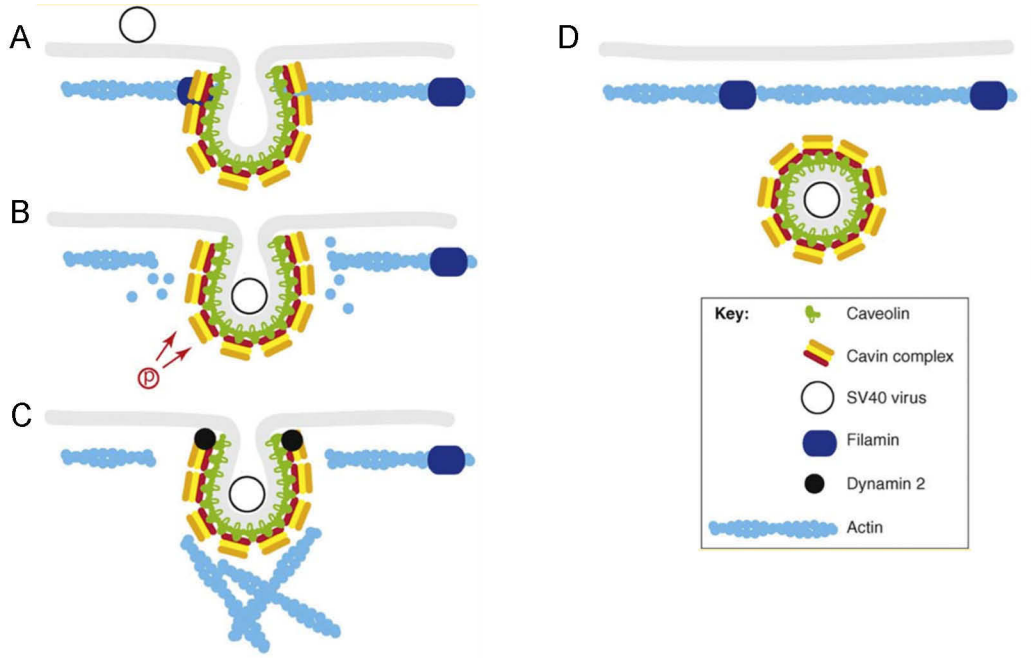


Figure 1.8 **Cavins mediate interaction between CAV1 and the cytoskeleton.** A, under normal conditions, caveolae are tightly associated with the cortical actin cytoskeleton and immobilized within the plasma membrane. This involves the F-actin binding protein Filamin that interacts with CAV1. Cavins probably form a second coat on the cytoplasmic site of caveolae and mediate the interaction with actin. B, after stimulation, for example by entry of SV40 virus, multiple signaling events are activated. This might involve phosphorylation of CAV1. C, the cortical actin disassembles and endocytic vesicles bud from the plasma membrane in a dynamin dependent fashion. D, importantly, the cavin-coat stays associated with the caveolar vesicle after budding. The CAV1 vesicle can then fuse with the early endosome to deliver its cargo. (adopted from Hansen and Nichols, 2010)

### 1.4.3 Endocytosis of caveolae

It has been shown in several studies that caveolae are stable domains in the plasma membrane that do not move laterally or exchange subunits (Hayer et al., 2010b; Mundy et al., 2002). However, caveolae can be mobilized and bud off from the plasma membrane in reaction to certain stimuli (Kirkham et al., 2005; Tagawa et al.,

2005) (Figure 1.8). Moreover, in addition to an immobile plasma membrane pool a cytoplasmic pool of caveolae can be observed to undergo repeated rounds of “kiss-and-run” interaction with the plasma membrane (Pelkmans and Zerial, 2005). Caveolae can engage in dynamin-dependent endocytosis and several extracellular cargo proteins can enter the cell via caveolae (Hansen and Nichols, 2009; Howes et al., 2010; Mayor and Pagano, 2007). However, the relevance of caveolae for endocytosis has been under debate because few cargo proteins require the presence of caveolae for endocytosis (Parton and del Pozo, 2013). Overexpression of CAV1 is sufficient to induce endocytosis of caveolae and ubiquitination dependent degradation in the lysosome (Hayer et al., 2010b). Importantly, we could show that a complex between the AAA-ATPase p97 and the UBX-domain containing cofactor UBXD1 regulates endosomal trafficking of ubiquitinated CAV1 (Ritz et al., 2011). In contrast, CAV1 enters the endosomal system as oligomers after destabilization of caveolae by cholesterol depletion or knockdown of PTRF/cavin-1 (Hayer et al., 2010b).

Following endocytosis, caveolae can fuse with the RAB5-positive early endosome and form stable domains (Pelkmans et al., 2004) (Figure 1.9). Interestingly, the coat of PTRF/cavin-1 proteins stays associated with caveolae during endocytosis and on early endosomes indicating that caveolae maintain the 70S scaffold on early endosomes (Boucrot et al., 2011; Hayer et al., 2010b; Parton and del Pozo, 2013). From the early endosome caveolae may recycle to the plasma membrane and the rate of recycling can regulate the number of plasma membrane caveolae (Parton and del Pozo, 2013; Pelkmans et al., 2004). For example, disruption of integrin-mediated adhesion induces endocytosis of caveolae and integrins. CAV1 recycles to the plasma membrane in a microtubule dependent manner after restoration of integrin adhesion (del Pozo et al., 2005; Parton and del Pozo, 2013). Along this line, caveolae redistribute from the plasma membrane to endosomal organelles during mitosis and this requires functional microtubules (Boucrot et al., 2011). Generally, microtubules mediate intracellular transport of endocytosed caveolae while the cortical actin cytoskeleton restricts the movement of caveolae in the plasma membrane (Mundy et al., 2002). Recent studies identified the ATPase EHD2 (Eps-15 Homology Domain-containing protein 2) as a linker between CAV1 and the actin cytoskeleton that regulates endocytosis of caveolae (Stoeber et al., 2012).

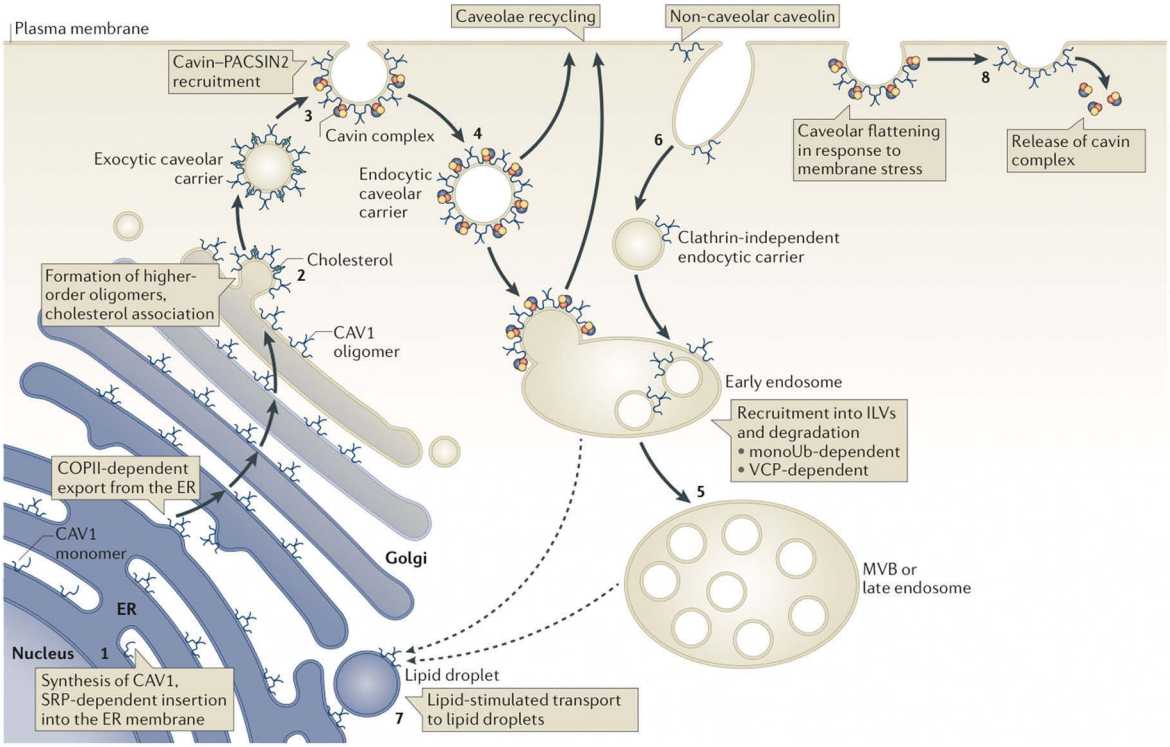


Figure 1.9 **Endocytic and exocytic trafficking of CAV1.**
Schematic representation of membrane trafficking of CAV1 in the biosynthetic and endosomal pathway. CAV1 is cotranslationally inserted into the ER and assembles into oligomers. Subsequently, CAV1 oligomers are transported to the Golgi apparatus, where they bind cholesterol and associate into large 70s scaffolds that are exported to the plasma membrane. On the plasma membrane CAV1 associates with cavin proteins that regulate the stability of caveolae. The cavin-coat stays bound to caveolar vesicles following stimulus dependent endocytosis. Non-caveolar CAV1 or CAV1 that is mobilized after cholesterol depletion can be taken up via other endocytic pathways. On early endosomes, the cavin-coat dissociates and CAV1 is disassembled into oligomers that are sorted into intralumenal vesicles (ILVs) and eventually degraded in the lysosome. This requires ubiquitination of CAV1 and the AAA-ATPase p97/VCP. Alternatively, after stimulation with lipids, CAV1 can be transported to lipid droplets in the vicinity of the nucleus. Flattening of caveolae in response to mechanical stress may release the cavin-coat proteins and induce downstream signaling events. (adopted from Parton and del Pozo, 2013)

### 1.4.4 Cellular functions of caveolins and caveolae.

Caveolae form distinct microdomains in the plasma membrane that contribute to the regulation of signaling, plasma membrane dynamics, and define a pathway for clathrin independent endocytosis (Parton and del Pozo, 2013). Plasma membrane receptors like the EGF receptor or the insulin-like growth factor-I receptor (IGF-IR) localize to caveolae upon stimulation. This has been shown to induce caveolae-mediated endocytosis of the IGF-IR but not the EGFR (Salani et al., 2010; Sigismund et al., 2005). Furthermore, the compartmentation of signaling molecules in lipid rafts and the interaction with CAV1 might be required to coordinate signaling events (Schwencke et al., 2006). A well-described membrane protein whose activity is

modulated through interaction with CAV1 is the endothelial nitric oxide synthase (eNOS) (Collins et al., 2012). Interaction between CAV1 and eNOS negatively regulates the eNOS activity and decreases nitric oxide (NO) production after induction. Interestingly, this interaction appears to be further regulated in a negative feedback loop through NO-induced phosphorylation of CAV1 in the N-terminal region (Chen et al., 2012). Additionally, caveolins regulate the surface expression of ion channels by mediating interaction between the ion channels and E3 ubiquitin ligases in the plasma membrane (Guo et al., 2012; Lee et al., 2009). Even though the interaction between CAV1 and signaling proteins in the plasma membrane is well documented, the molecular consequences are not yet understood (Byrne et al., 2012; Collins et al., 2012).

In addition to signaling, caveolae can mediate cellular adhesion, respond to mechanical stresses, and control lipid homeostasis (Parton and del Pozo, 2013) (Figure 1.9). Due to their flask-shaped nature, caveolae contain a large amount of membrane that can be released by flattening in response to mechanical stress. Additionally, cells might sense mechanical forces through signaling events created by the flattening of caveolae (Sinha et al., 2011; Yu et al., 2006). Caveolae sequester large amounts of cholesterol during biogenesis (Hayer et al., 2010b) and can regulate lipid homeostasis. For example, cholesterol treatment of adipocytes induces localization of CAV1 to lipid droplets, while knockdown of CAV1 depletes cholesterol from this organelle (Le Lay et al., 2006). Along this line, accumulation of cholesterol in late endosomes/lysosomes recruits CAV1 from the plasma membrane to the membranes of late endosomes/lysosomes (Mundy et al., 2012). Furthermore, non-caveolar as well as caveolar CAV1 can regulate integrin mediated cell adhesion. Phosphorylated CAV1 localizes to focal adhesions, and can induce their turnover to regulate cell migration (Nethe and Hordijk, 2011). As mentioned above, disruption of integrin adhesion triggers CAV1 dependent endocytosis of adhesion molecules (del Pozo et al., 2005). Importantly, the function of CAV1 and caveolae probably differs between cell types and depends on associated proteins, like cavins, or posttranslational modifications, for example phosphorylation (Parton and del Pozo, 2013).

### 1.4.5 Caveolins in human disease.

Even though caveolae are associated with many cellular processes the phenotypes of CAV1 knockout mice are rather mild. The mice are viable but show vascular disease, cardiomyopathy, and reduced life span. Interestingly, deletion of different exons of the CAV1 gene results in different phenotypes, in line with the multitude of functions associated with CAV1 (Parat, 2009). The vascular phenotypes are probably associated with altered eNOS function in the absence of caveolae (Chen et al., 2012; Wunderlich et al., 2008). In human patients, two homologous missense mutations in CAV1 and CAV3 have been described. The CAV3 P104L missense mutation is associated with limb girdle muscular dystrophy. This CAV3 variant fails to oligomerize in the Golgi apparatus and is subsequently degraded via the proteasome (Galbiati et al., 2000). The homologous mutation in CAV1, P132L, is associated with severe forms of breast cancer due to increased cell migration and invasiveness (Bonuccelli et al., 2009). Interestingly, CAV1 has been identified as a tumor suppressor gene as well as a proto-oncogene. The tumor-cell type and the surrounding tissue most likely determine if loss of plasma membrane CAV1 stimulates neoplastic growth or prevents tumor development (Schwencke et al., 2006). Moreover, CAV1 and caveolae have been implicated in insulin mediated signaling in diabetes, in cardiomyopathy, and in inflammatory signaling (Chidlow and Sessa, 2010; Schwencke et al., 2006). In the brain, CAV1 has a protective role after injury, regulates neurotransmitter signaling, and enhances dendritic growth (Head et al., 2011).

## 1.5 The AAA-ATPase p97

The hexameric protein p97 belongs to the group of AAA+ (ATPases associated with diverse cellular activities) ATPases. Hexameric AAA-ATPases are often involved in ATP-driven unfolding of proteins and reshaping of protein complexes (Bukau et al., 2006). The p97 AAA-ATPase (also known as valosin containing protein (VCP) in mammals, Cell division control protein 48 (Cdc48) in yeast, and transitional endoplasmic reticulum ATPase 94 (TER94) in fruit flies) is a highly conserved and abundant protein (Baek et al., 2013; Meyer et al., 2012; Yamanaka et al., 2012). It was identified as a factor for ubiquitin-mediated extraction of proteins from protein complexes or membranes as well as membrane fusion. Recent studies expand the functional spectrum of p97 to include regulation of the chromatin, endosomal sorting, and autophagy. Generally, p97 is recruited to ubiquitinated substrates and utilizes the

energy of ATP hydrolysis to segregate or unfold proteins (Meyer et al., 2012). This often facilitates degradation of the extracted proteins in the proteasome. A large number of protein cofactors associates with p97 that mediates interaction with ubiquitinated substrates or modulates posttranslational modifications and is important for the activity and functional diversity of p97 (Schuberth and Buchberger, 2008; Yeung et al., 2008). Mutations in p97 are associated with an autosomal dominant multisystemic disorder described as inclusion body myopathy associated with Paget disease of the bone and frontotemporal dementia (IBMPFD, OMIM 167320) (Ju and Weihl, 2010; Nalbandian et al., 2011) as well as amyotrophic lateral sclerosis (ALS) (Johnson et al., 2010).

### 1.5.1 Structure and segregase activity of p97

The AAA-ATPase protein superfamily constitutes a distinct sub-class of the P-loop NTPases. The large class of P-loop NTPases is characterized by the presence of a P-loop, also referred to as the Walker A motif, and a second, more variable region, called the Walker B motif (Snider and Houry, 2008). The Walker A motif is involved in ATP binding while the Walker B motif mediates ATP hydrolysis (Yakushiji et al., 2006). Each monomer of p97 consists of an N-terminal (N) domain, two AAA-ATPase domains D1 and D2, and a C-terminal region. Six p97 monomers together build an hourglass-like homo-hexamer with the D1 and D2 ATPase domains forming two concentric rings that are stacked on top of each other (DeLaBarre and Brunger, 2003; Rouiller et al., 2002) (Figure 1.10 A). The N domains are attached peripherally to the D1 ring and can move along the central axis of the p97 barrel. In all crystal structures of wild type p97, ADP is bound to the D1 domains and the N domains are located in one plane with the D1 ring (“down conformation”) (DeLaBarre and Brunger, 2003). However, cryo-electron microscopy shows that the N domains are flexible and move in response to the presence of different nucleotides (Rouiller et al., 2002).

The D1 domain has low ATPase activity and is mainly responsible for hexamerization of p97, while the main ATPase activity that provides the energy for the p97 function is located in the D2 domain (Song et al., 2003). Some studies reported that the two AAA-ATPase domains operate independently; however, other studies showed evidence of inter-dependence (Tang and Xia, 2012). Importantly, the p97 E578Q variant that cannot hydrolyze ATP in the D2 domain is dominant negative and traps ubiquitinated protein substrates after binding (Ramadan et al., 2007; Ye et al., 2003). The globular N domain can either mediate the recruitment of p97 cofactors or directly

engage with mono-ubiquitinated substrates (Rape et al., 2001; Schuberth and Buchberger, 2008Yeung, 2008 #304; Ye et al., 2003). Furthermore, the N domain can stabilize unfolded proteins, may regulate ATP hydrolysis in p97, and even couple substrate or adapter binding to hydrolysis (DeLaBarre and Brunger, 2005; Meyer et al., 2012). ATP hydrolysis in the D2 domain induces conformational changes that are propagated via the relatively immobile D1 domain onto the N domain (DeLaBarre and Brunger, 2005; Pye et al., 2006). These conformational changes enable p97 to unfold substrate proteins, take apart protein aggregates, or detach proteins from substrates like membranes or DNA (Meyer et al., 2012; Stolz et al., 2011; Yamanaka et al., 2012) (Figure 1.10 B). The interface between the N and D1 domains is of special importance because mutations in this region are associated with human disease (Nalbandian et al., 2011; Tang and Xia, 2012) that will be discussed in greater detail below. Several model exist how ATP hydrolysis could translate to the molecular segregase activity of p97. This could involve threading of the substrate protein through the central pore or unfolding of substrates on the surface of the p97 hexamer. However, the precise mechanism of ATP-driven action of p97 in cellular processes is not known (Baek et al., 2013).

The ability of p97 to segregate proteins was first postulated to be involved in the disassembly of SNARE (soluble N-ethylmaleimide-sensitive factor (NSF) attachment protein receptor) complexes following vesicles fusion (Rabouille et al., 1998). In the following, the yeast homologue of p97, Cdc48, was shown to act as a molecular segregase in the OLE pathway that is important for fatty acid synthesis and membrane fluidity (Hoppe et al., 2000). The transcription factor Spt23 localizes to the ER membrane as an inactive precursor called p120. Activation causes dimerization and mono-ubiquitination followed by proteasomal cleavage of one p120 molecule to yield the active p90 transcription factor. After processing, Cdc48 together with the UFD1-NPL4 cofactor recognizes the mono-ubiquitinated p90 and extracts it from the p90-p120 dimer. This allows p90 to translocate into the nucleus and activate transcription (Rape et al., 2001). The processing of p120 in yeast is similar to the activation of the NFκB transcription factor in higher eukaryotes. Interestingly, p97 was identified to regulate proteasomal degradation of ubiquitinated IκBα (inhibitor of NFκB signaling α) in response to cytokine signaling (Dai et al., 1998; Li et al., 2013).

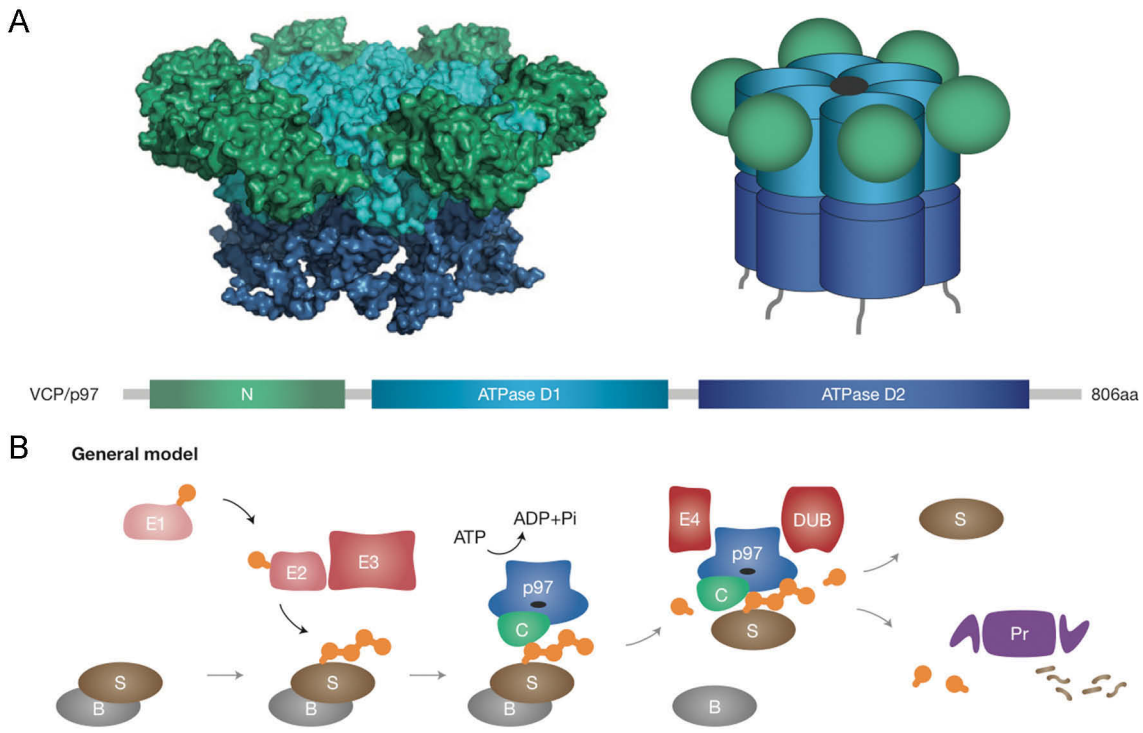


Figure 1.10 **Structure of p97 and general model for the p97 segregase activity.** A, crystal structure and schematic representation of the p97 hexamer. Each p97-monomer consists of an N domain and two ATPase domains D1 and D2. Six monomers associate to a p97-hexamer with the D1 (cyan) and D2 (blue) forming two concentric rings that are stacked on top of each other. The N domains (green) are attached in plane with the D1 ring. The C-terminal tails (grey) are less structured. B, schematic model of the general segregase activity of p97. A substrate protein (S) is ubiquitinated by a cascade of E1, E2, and E3 enzymes. This ubiquitinated substrate is recognized by p97 with the help of cofactor proteins (C). ATP hydrolysis in p97 segregates the substrate from binding partners (B) or cellular surfaces. Following extraction, ubiquitin chain-editing (E4) or deubiquitinating (DUB) enzymes may modulate the ubiquitination state of substrate proteins. This can process the substrate protein for degradation in the proteasome (Pr) or release it into the cytoplasm after deubiquitination. (panels A and B adopted from Meyer et al., 2012)

### 1.5.2 Cofactors regulate specificity and functional diversity of p97

A large number of cofactors associate with p97 to direct the p97 segregase activity toward specific cellular processes and regulate the activity of p97 temporally and spatially. While most p97 cofactors interact with the N domain, some cofactors can interact with the C-terminal region of p97 (Baek et al., 2013; Schuberth and Buchberger, 2008; Yeung et al., 2008). The largest family of cofactors binds to p97 via a UBX (ubiquitin-regulatory X) or UBX-like domain that assumes an ubiquitin-like fold and interacts with two partially overlapping binding sites on the p97 N domain (Kloppsteck et al., 2012; Meyer et al., 2012; Schuberth and Buchberger, 2008). Other general binding modules are the PUB (PNGase (peptide N-glycosidase)/ubiquitin-associated), or PUL (PLAA, Ufd3, Lub1) domains that interact with the C-terminal

region of p97. In addition, some cofactors bind to the p97 hexamer through shorter linear binding motifs like the VIM (VCP-interacting motif) or the SHP box. Importantly, cofactors can harbor more than one p97-binding site. For example, the cofactor UBXD1 (UBX domain containing cofactor 1) interacts with the N domain as well as the C-terminal region via a VIM motif and a PUB domain respectively (Madsen et al., 2008; Stapf et al., 2011).

The p97 cofactors can be divided into groups according to their p97-binding site, mutual exclusivity and enzymatic activity (Jentsch and Rumpf, 2007; Schuberth and Buchberger, 2008). Substrate-recruiting cofactors harbor an ubiquitin-binding domain in addition to a p97-binding site. Substrate-processing cofactors possess enzymatic activity and can modify p97-bound substrate proteins. However, this classification oversimplifies the connection between the molecular function of cofactors and their structural elements. For example, the UBXD1 protein is an important cofactor in p97-regulated endosomal sorting even though it harbors no ubiquitin-binding domain and does not interact with p97 via its UBX domain but through other interaction sites (Madsen et al., 2008; Ritz et al., 2011). Another possibility to categorize p97 cofactors is a hierarchical model (Meyer et al., 2012; Schuberth and Buchberger, 2008). Some cofactors bind mutually exclusive to p97 and can be called major cofactors. These major cofactors, including the UFD1 (ubiquitin fusion degradation protein 1)–NPL4 (nuclear protein localization protein 4) heterodimer, p47, or UBXD1 define core complexes of p97. Each core complex can act in several pathways by recruiting accessory protein factors that mediate localization to specific cellular compartments or catalyze additional enzymatic reactions. The main challenge of the p97 cofactor system is to investigate the interplay between p97 dependent pathways and to link cofactors to specific cellular processes (Meyer et al., 2012; Schuberth and Buchberger, 2008).

The two major cofactors UFD1-NPL4 and p47 harbor ubiquitin-binding domains and are examples of substrate-recruiting cofactors. Substrate-recruiting cofactors contain p97-binding sites together with one or more ubiquitin-binding domain and often mediate the interaction between p97 and ubiquitinated proteins (Jentsch and Rumpf, 2007; Meyer et al., 2002). However, p97 can also directly interact with ubiquitinated substrates via its N domain (Rape et al., 2001; Ye et al., 2003). The UFD1-NPL4 cofactor directs p97 to poly-ubiquitinated substrates on the ER membrane or chromatin and mediates their extraction (Ramadan et al., 2007; Rape et al., 2001;

Verma et al., 2011; Ye et al., 2003). In turn, the p47 cofactor predominantly binds to mono-ubiquitinated substrates and is important for p97-dependent fusion of ER or Golgi membranes (Totsukawa et al., 2011). Furthermore, p47 was identified as an important factor in the regulation of membranes in autophagy (Krick et al., 2010). In contrast, the third major cofactor UBXD1 does not harbor an ubiquitin-binding site and probably recruits additional unidentified protein factors that mediate binding to ubiquitinated substrates {Ritz, 2010 #164). The UBXD1 cofactor is involved in trafficking of membrane proteins in the exocytic and endocytic pathway (Haines et al., 2012; Ritz, 2010).

Another group of p97 cofactors modulates the posttranslational modification of substrate proteins and can be called substrate-processing cofactors (Jentsch and Rumpf, 2007). Many substrate-processing cofactors are ubiquitin ligases or deubiquitinating enzymes. This positions p97 as a coordination center of protein ubiquitination and add a further layer of control to the function of p97 in the ubiquitin system (Meyer et al., 2012). Several E3 ubiquitin ligases, like HRD1 or AMFR directly interact with p97 and regulate ubiquitination of proteins in ER-associated degradation (ERAD) (Claessen et al., 2012). Furthermore, several ubiquitin ligases of the cullin RING ligase family bind to p97 via the UBX domain containing cofactor UBXD7 and are implicated in HIF1α (hypoxia-inducible factor 1 α) turnover (Alexandru et al., 2008). Additionally, deubiquitinating enzymes like VCPIP1, Otu1, YOD1, or Ataxin-3 bind to p97 and are involved in various cellular pathways (Ernst et al., 2009; Rumpf and Jentsch, 2006; Wang et al., 2006; Wang et al., 2004). However, ubiquitination is not the only posttranslational modification that is regulated by p97 substrate-processing cofactors. For example, glycosylation of ER proteins is modulated by peptide N-glycanase (PNGase) that is recruited to p97 together as part of a larger regulatory complex (Li et al., 2006).

In addition to recruiting and modifying substrates, p97 cofactors can directly regulate the p97 hexamer. For example, UBXD9/TUG (tether, containing an UBX domain, for GLUT4) modulates the oligomeric state of p97 in the early secretory pathway (Orme and Bogan, 2012). Along this line, binding of the cofactor p47 regulates the ATPase activity of p97 (Meyer et al., 1998).

### 1.5.3 The function of p97 in the ubiquitin-proteasome system

As described above for the yeast OLE pathway, p97 acts as a driving force that segregates ubiquitinated protein complexes. This segregase function of p97 was shown to be involved in a wide variety of cellular processes that involve the extraction of ubiquitinated proteins from binding partners or cellular surfaces (Meyer et al., 2012). This is often connected to proteasomal degradation after extraction (Figure 1.11).

An important cellular process that requires p97 to extract proteins from membranes is ER-associated degradation (ERAD). Misfolded or incompletely assembled ER proteins are selectively exported from the ER in a process termed retro-translocation and degraded in the cytosol by the proteasome (Stolz et al., 2011; Ye, 2006). The energy required to extract the ERAD substrates from the ER membrane is provided by p97 together with the UFD1-NPL4 cofactor (Ye et al., 2003). The p97-UFD1-NPL4 complex is recruited to the ER membrane with the help of ER membrane localized cofactors, for example UBXD2, UBXD8, or VIMP (Claessen et al., 2012). Additionally, the UBX domain containing cofactors UBXD6 and SAKS1 were recently identified to localize at the ER membrane together with p97 (Glinka et al., 2013; Madsen et al., 2011). Furthermore, p97 associates with ubiquitin-processing factors that are necessary to mediate deubiquitination and re-ubiquitination of ERAD substrates for extraction and proteasomal degradation (Ballar et al., 2006; Ernst et al., 2009; Wang et al., 2006). Many of the large number of p97 cofactors that has been described to associate with p97 during ERAD might mediate extraction of special substrates or associate with p97 under certain conditions (Baek et al., 2013; Claessen et al., 2012). However, the complexity of p97 cofactors in ERAD is not understood. The ability of p97 to mobilize proteins from membranes is also utilized in other cellular processes. For example, p97 facilitates the extraction and degradation of ubiquitinated proteins from the outer mitochondrial membrane (Xu et al., 2011).

The activity of p97 is not limited to the extraction of proteins from membranes but furthermore can mobilize chromatin-bound proteins. During the final stages of mitosis, the chromatin-bound mitotic kinase Aurora B keeps the chromatin in a condensed state. At the exit from mitosis, Aurora B is ubiquitinated and subsequently extracted from the chromatin by the p97-UFD1-NPL4 complex and this enables de-condensation of chromosomes. (Dobrynin et al., 2011; Ramadan et al., 2007). Upon DNA damage, p97-UFD1-NPL4 facilitates proteasomal degradation of the CDC25A

phosphatase as an integral part of the $G_2$/M checkpoint (Riemer et al., 2014). Along this line, p97 is involved in the regulation of DNA replication and repair of double strand breaks in response to radiation damage. Moreover, p97 regulates the activity of cyclin-dependent kinases (CDKs) and controls bipolar spindle assembly during metaphase. In interphase cells, p97 regulates the stability and turnover of transcription factors (Meyer et al., 2012; Yamanaka et al., 2012).

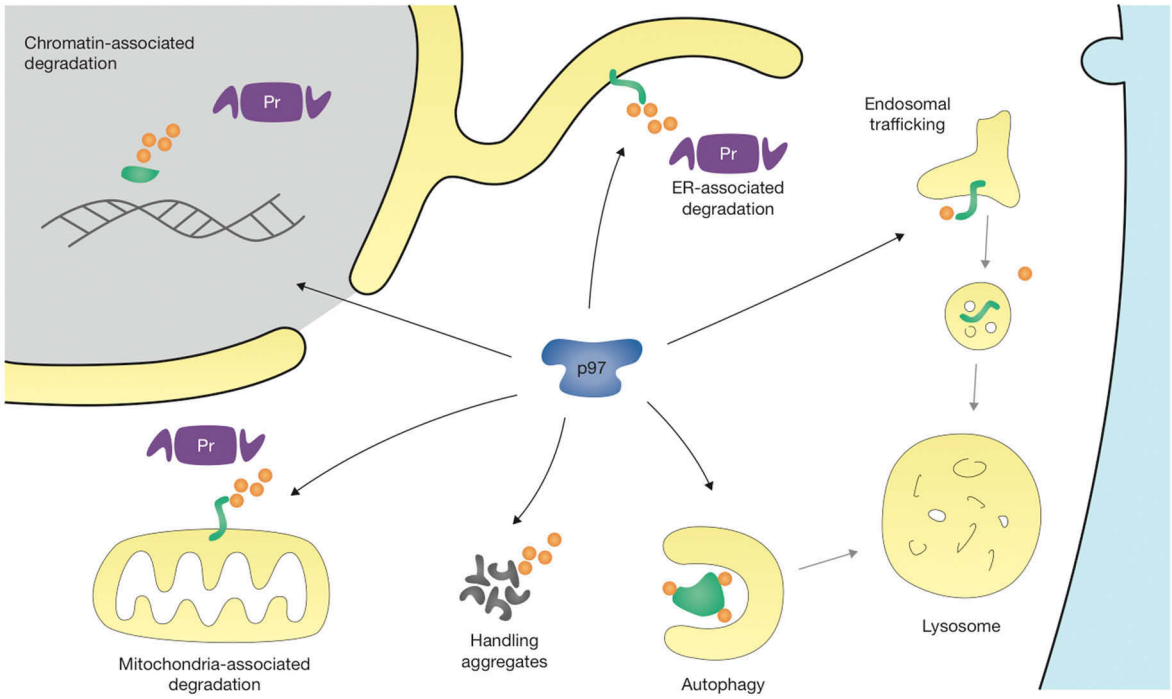


Figure 1.11 **Cellular functions of p97 in the ubiquitin-proteasome system and membrane trafficking.**
In interphase cells, p97 mediates a wide variety of cellular processes that involve degradation of substrate proteins in the proteasome (Pr). Other cellular roles of p97 are proteasome independent. Most prominently, p97 is required for the degradation of misfolded proteins in ER-associated degradation. Additionally, p97 facilitates the proteasome dependent degradation of chromatin-associated proteins or proteins of the outer mitochondrial membrane. The activity of p97 in the ubiquitin-proteasome system prevents the aggregation of misfolded proteins and protects the cell from protein stress. In addition, p97 controls cellular signaling and chromatin remodeling during DNA replication and repair. In parallel, p97 is involved in proteasome-independent membrane trafficking. For example, p97 regulates endosomal sorting of ubiquitinated membrane proteins to the lysosomes as well as clearance of ubiquitinated protein aggregates in autophagy. (adopted from Meyer et al., 2012)

### 1.5.4 p97 in membrane trafficking.

In addition to facilitating proteasomal degradation of ubiquitinated proteins, p97 was identified to regulate membrane fusion and trafficking. These functions are less extensively characterized compared to the proteasome-associated functions of p97 and probably involve the remodeling of large protein complexes (Figure 1.11).

During mitosis, the ER and Golgi apparatus are fragmented into vesicles that fuse again after exit from mitosis. The reformation of the Golgi apparatus requires the action of p97 together with one of the closely related cofactors p47 or p37 (Totsukawa et al., 2011). Furthermore, the deubiquitinating enzyme VCPIP1 is involved in both the p47 and p37 dependent vesicle fusion pathway. However, only p47-mediated fusion requires the deubiquitination activity of VCPIP1 (Totsukawa et al., 2011; Wang et al., 2004). It is not known which target protein is deubiquitinated by VCPIP1 and why deubiquitination is selectively required in the p47-mediated pathway. Importantly, the function of p97 in membrane fusion is independent of the proteasome and possibly involves cycles of deubiquitination and re-ubiquitination (Meyer, 2005). In this pathway, p97 is proposed to act together with a second AAA-ATPase, NSF, in the disassembly of SNARE complexes following vesicle fusion (Rabouille et al., 1998). Another membrane-associated cellular process that is regulated by p97 together with the p47 cofactor is autophagy (discussed below).

Several recent studies from our lab and others have linked p97 to trafficking of ubiquitinated membrane proteins to the lysosome (Baek et al., 2013; Bug and Meyer, 2012). We could show that p97 together with the recently identified cofactor UBXD1 mediates endosomal sorting of the ubiquitinated membrane protein CAV1 (Hayer et al., 2010b; Ritz et al., 2011). Overexpression of the dominant negative p97 variant E578Q prevents formation of intralumenal vesicles and this causes accumulation of CAV1 on late endosomes. The same phenotype is observed in cells overexpressing disease-associated variants of p97 as well as patient fibroblasts. Moreover, pharmacological inhibition of p97 prevents lysosomal degradation of ligand activated EGF receptor (Ritz et al., 2011). In yeast, protein sorting at multivesicular endosomes involves the substrate-recruiting cofactor Ufd3 and deletion of Ufd3 decreases the levels of free ubiquitin (Ren et al., 2008). In mammalian cells, p97 is recruited to the early endosome by the tethering factor EEA1. The segregase function of p97 might regulate the oligomeric state of the EEA1 and, as a consequence, sorting on the early endosome (Ramanathan and Ye, 2012). Another factor that recruits p97 to endosomes in dendritic cells is poly-ubiquitinated mannose receptor (Zehner et al., 2011). In the immune system, the segregase activity of p97 is required to extract antigens from endosomes for efficient cross-presentation. These data together indicate that p97 could regulate endosomal trafficking of diverse cargo proteins (Bug and Meyer, 2012).

Another proteasome independent degradation pathway that is regulated by p97 is autophagy. In yeast, a complex between Cdc48 and the cofactor p47 interacts with the ubiquitin-like Atg8 protein during autophagosome formation (Krick et al., 2010). The action of p97-p47 could be required to extract Atg8 from the growing phagophore. Similar to Golgi vesicle fusion, this function of p97 does not require the activity of the proteasome and probably involves segregation of protein complexes. In mammalian cells, defective autophagy was shown to be one of the hallmark features of the p97-associated congenital disease IBMPFD (Ju and Weihl, 2010). Importantly, accumulation of the autophagy marker proteins p62 and LC3 is reproduced in mammalian cells as well as transgenic mice that overexpress disease-associated variants of p97 (Custer et al., 2010; Ju et al., 2009; Tresse et al., 2010). Other examples for p97-mediated autophagy include the ubiquitin-mediated autophagic degradation of ribosomes in yeast. This requires the substrate-recruiting cofactor Ufd3 together with the deubiquitinating enzyme Ubp3 (Ossareh-Nazari et al., 2010). In eukaryotic cells, disease associated cytoplasmic aggregates of ribonucleoprotein complexes, called stress granules, are targeted for autophagic degradation in a p97-dependent fashion (Buchan et al., 2013). However, the mechanistic details of the function of p97 in autophagy remain unclear with many models being proposed (Bug and Meyer, 2012). Interestingly, endosomal sorting and autophagy are interconnected and it was shown that mutations in the membrane sorting machinery at multivesicular endosomes inhibit autophagy (Rusten and Simonsen, 2008). Therefore, the function of p97 in endosomal sorting and autophagy might be linked (Bug and Meyer, 2012).

### 1.5.5 Disease associated mutations in p97.

Several missense mutations in the N domain or the D1 domain of p97 are associated with the multi systemic disorder inclusion body myopathy associated with Paget disease of the bone and frontotemporal dementia (IBMPFD, Figure 1.12 A and B). The most frequent mutation is the exchange of lysine-155 for histidine (R155H). Importantly, all mutations cluster at the interface between the N- and D1-domain, which is not part of the nucleotide-binding pocket and not close to any known cofactor-binding site (Nalbandian et al., 2011; Tang and Xia, 2012). Importantly, the mutations do not abolish but rather increase the ATPase activity of the p97 D2 domain that provides the energy for p97 activity (Fernandez-Saiz and Buchberger, 2010; Niwa et al., 2012; Weihl et al., 2006). Moreover, overexpression of the pathogenic p97 variants in yeast rescues a lethal Cdc48 disruption in contrast to the

p97 wild type (Takata et al., 2012). However, recent studies suggest that the mutations could increase the mobility of the N domain in response to nucleotide binding in D1 and may affect the interaction between p97 and cofactors (Fernandez-Saiz and Buchberger, 2010; Ritz et al., 2011; Tang and Xia, 2012). The pathology of IBMPFD includes tissue degeneration with patient cells showing rimmed vacuoles, re-localization of the nuclear protein TDP-43 into the cytoplasm and accumulation in ubiquitin-positive protein aggregates (Nalbandian et al., 2011) (Figure 1.12 C). Because p97 is involved in a multitude of processes, it is not surprising that many cellular pathways are affected by mutations in p97 (Ju and Weihl, 2010; Nalbandian et al., 2011). This includes NFκB signaling, homeostasis of cellular ATP levels and, most prominently, autophagy. However, these imbalances are rather mild and take several decades to manifest in the IBMPFD phenotype.

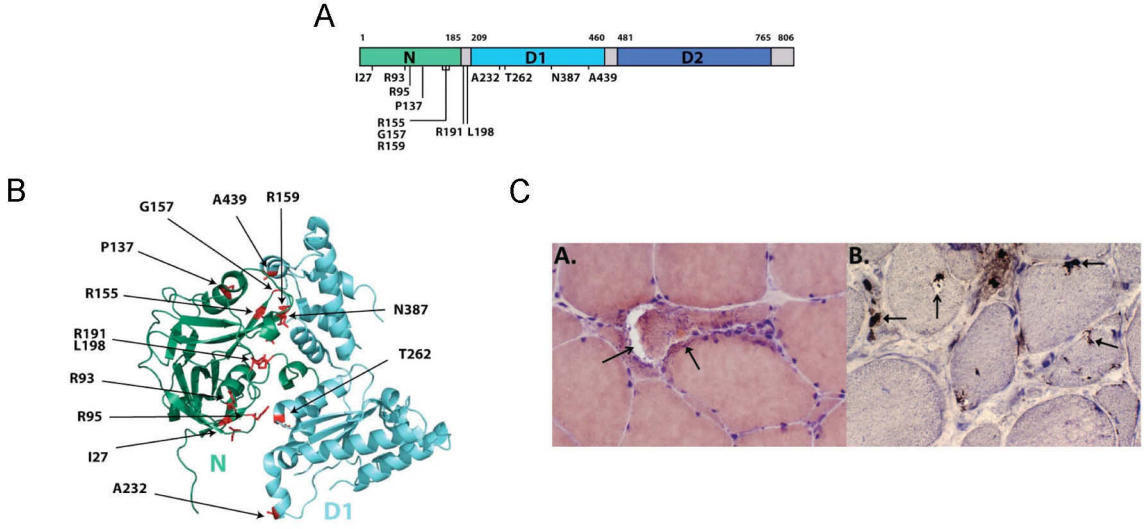


Figure 1.12 **Disease associated mutation in p97 and cellular phenotype.**
A, schematic representation of the p97 domain structure indicating the position of missense mutations associated with IBMPFD (inclusion body myopathy associated with Paget disease of the bone and frontotemporal dementia). B, cartoon model of the interface between N and D1 domain from crystal structures of p97 showing the three-dimensional position of the disease associated mutations. Importantly, all mutations are located within the interface of the N and D1 domain. C, IBMPFD patient muscle tissue processed for (A) congo red histochemistry or (B) TDP-43 (TAR DNA binding Protein-43) immunohistochemistry. The micrograph show large rimmed vacuoles (A) and re-localization of TDP-43 from the nucleus to cytoplasmic inclusions (B) in degenerating muscle fibers.

Importantly, IBMPFD mutations in p97 were shown to affect the interaction between p97 and cofactor proteins (Fernandez-Saiz and Buchberger, 2010; Ritz et al., 2011). The interaction of the two major cofactors UFD1-NPL4 and p47 with the IBMPFD variants is increased; however, the mutually exclusive binding of UFD1-NPL4 and

p47 is not affected by the mutations (Fernandez-Saiz and Buchberger, 2010). In addition, several substrate-processing cofactors show differential binding to disease-associated variants of p97. Importantly, we could show that the p97 R155H mutation prevents the interaction between p97 and the major cofactor UBXD1 and that this disrupts endosomal trafficking of ubiquitinated CAV1 (Ritz et al., 2011). In cells expressing p97 R155H, CAV1 accumulates on the limiting membrane of enlarged late endosomes. Crucially, in patient muscle tissue, p97 mutations cause a similar delocalization of the caveolin-family member CAV3. In this context, recent studies showed that defective autophagy is an important pathogenic feature of IBMPFD (Custer et al., 2010; Ju et al., 2009; Tresse et al., 2010). The defect in autophagy probably is responsible for the accumulation of ubiquitinated protein inclusions and vacuolization in patient tissue. As described above, endosomal sorting and autophagy are liked, probably because the sorting machinery on multivesicular endosomes is required for fusion of autophagosomes and lysosomes (Rusten and Simonsen, 2008). Therefore, the IBMPFD variants of p97 may affect the proteasome independent degradation of membrane proteins in endosomal sorting and clearance of cytoplasmic aggregates in autophagy through a common mechanism (Bug and Meyer, 2012; Custer et al., 2010; Ju et al., 2009; Ju and Weihl, 2010; Tresse et al., 2010).

## 1.6 The aims of the thesis

We recently showed that ubiquitinated CAV1 interacted with p97 in a complex with the cofactor UBXD1. Importantly, overexpression of dominant-negative or disease-associated variants of p97 prevented trafficking of CAV1 on late endosomes. However, the functional connection between CAV1 ubiquitination and endosomal sorting by the p97-UBXD1 complex remained unknown.

In this context, the goal of this study was to investigate the structural and functional consequences of CAV1 ubiquitination; as well as characterize the role of the p97-UBXD1 complex in trafficking at late endosomes. Therefore, we aimed at identifying the ubiquitination site in CAV1 and analyzing the effect of ubiquitination on the transport of CAV1 from the plasma membrane to lysosomes. Additionally, we wanted to characterize the interaction between CAV1 and the p97-UBXD1 complex; and investigate how the p97-UBXD1 complex affected the turnover of ubiquitinated CAV1 on late endosomes. Finally, we aimed at addressing the question if p97 mediated trafficking of further membrane proteins and could be established as a more general regulator of endosomal sorting.

# 2 Materials and methods

## 2.1 Cell culture

HEK293, U2OS and HeLa Kyoto cells were maintained in DMEM (Sigma) supplemented with 10% fetal bovine serum (FBS, PAA, Lot No: A10110-2432) and 1% penicillin/streptomycin (PAA). U2OS cell constitutively expressing CAV1-HA (U2OS-pIRES-CAV1-HA) were generated by random integration after transfection of the linearized pIRESpuro2b-CAV1-HA plasmid. Single clones were selected for integration with 0.4 µg/ml puromycin (PAA). U2OS-FRT cells carrying a single integrated FRT (Flp recombination target) site were generated by transfection of the pFRT/*Lac*ZEO plasmid (Invitrogen) according to the manufacturers instructions. Single integration was confirmed by Southern blotting (S. Bremer). The U2OS-FRT cells were transfected with the pcDNA6/TR plasmid (Invitrogen) to achieve stable integration of the tetracycline (Tet) repressor according to the manufacturers instructions. Single clones were selected for integration of the Tet repressor gene with 50 µg/ml Zeocin (Invitrogen). Presence of the Tet repressor was confirmed in Western blotting (M. Bug). The U2OS-FRT cells were used to generate U2OS cells expressing either p97-myc-strep (U2OS-p97) or CAV1-HA (U2OS-CAV1-HA) under control of a tetracycline-inducible promoter. U2OS-FRT cells were transfected with either pcDNA5-p97-myc-strep-FRT/TO or pcDNA5-CAV1-HA-FRT/TO plasmid together with the pOG44 Flp-recombinase plasmid (Invitrogen) to achieve integration into the FRT site. Single clones were selected. The inducible cell lines were maintained in DMEM supplemented with 10% tetracycline free FBS (PAN, Lot No: P2880209) and 1 % penicillin/streptomycin with additionally 4 µg/ml blasticidin S (PAA) and 130 µg/ml hygromycin B (PAA) for U2OS-p97 or 4 µg/ml blasticidin S and 120 µg/ml hygromycin B for U2OS-CAV1-HA. Expression was induced with 1 µg/ml doxycycline (Sigma-Aldrich). All cell lines were maintained at 37°C in 5% $CO_2$.

## 2.2 Transfections

HEK293 cells were transfected at 60 - 80% confluence using the JetPRIME reagent (Polyplus) or a $Ca_3(PO_4)_2$ based protocol. For JetPRIME transfection in a 3 cm diameter well (6 well plate) 2 µg DNA were diluted in 200 µl JetPRIME buffer (Polyplus) and briefly vortexed. To this dilution, 4 µl JetPRIME transfection reagent were added, vortexed briefly and dropped onto the cells after 10 to 15 minute incubation at room temperature. For transfection of HEK293 cells in a 10 cm dish 4

µg DNA were diluted in 1095 µl sterile Mili-Q $H_2O$. Then, 155 µl sterile 2M $CaCl_2$ were added and gently mixed. 1250 µl 2xHBS buffer were added dropwise while gently shaking and mixed by inverting the reaction tube 10 times. The transfection mix was added drop wise onto the cells without further incubation. U2OS cells and derived cell lines were transfected at 60 - 80% confluence using the JetPEI reagent (Polyplus). For a 3 cm diameter well (6 well plate) 2 µg DNA were diluted in 100 µl 150 mM NaCl and briefly vortexed. 4 µl of the JetPEI transfection reagent were diluted in 100 µl 150 mM NaCl, vortexed briefly and added to the DNA dilution. The mixture was vortexed briefly and dropped onto the cells after 20 minutes incubation at room temperature. The medium was exchanged for fresh growth medium 4 h after transfection. For transfection in 12 well plates half the amounts used for transfection in 6 well plates were used. All transiently transfected cells were analyzed 24 h post transfection.

## 2.3 Plasmid constructs

The plasmid constructs used in this study are detailed in Table 2.2. (page 54). Coding sequences were cloned from origin constructs into target plasmid backbones either directly through restriction and ligation or after polymerase chain reaction (PCR) amplification of the target sequence with DNA primers including novel restriction sites. DNA primers carrying restriction sites were designed with 10 to 15 nucleotides binding to the target sequence and one to three nucleotides overhang after the restriction site. The length of the overhang was chosen according to enzyme manufacturer recommendations (New England Biolabs). The DNA primers and the strategies used for cloning are given in Table 2.2 (page 56). DNA primers were purchased from Metabion. The target cDNA sequence was amplified using 2 U of Phusion DNA polymerase (Thermo scientific) with the 5x Phusion HF buffer (Thermo scientific) in 50 µl reactions. Forward and reverse primers were used at 400 nM together with 10 ng DNA template and 200 µM dNTPs. The PCR was carried out in a TPersonal thermocycler (Biometra). One PCR cycle consisted of 30 seconds denaturing at 98°C, annealing for 30 seconds at 50 – 54°C, and synthesis of the new DNA strand at 72°C. The annealing temperature was chosen depending on the primers used and the extension time was one minute per one kilobase of the target sequence. The PCR program consisted of 30 cycles with a final extension step at 72°C for 10 minutes. The PCR product was purified using a PCR clean-up kit (Machery-Nagel) or used directly for the restriction reaction if the restriction

endonucleases had sufficient activity in the Phusion HF buffer. Restriction endonucleases were used from New England Biolabs (NEB) in the appropriate buffers. 5 to 10 U of enzyme were used to digest one PCR reaction or 2 µg of plasmid DNA for 1 h at 37°C. Small DNA fragments were removed with a PCR clean-up kit (Machery-Nagel). To remove larger DNA fragments the digestion reaction was separated on a 0.8 to 1.5 % agarose gel, the band of the target DNA fragment was cut out, and purified with a gel extraction kit (Machery-Nagel). To ligate the target DNA fragment into a plasmid vector 100 ng of the digested vector were incubated with three times excess of the target fragment and 0.2 µl T4 DNA ligase (NEB) in 10 µl reactions for 2h at 16°C. Chemically competent DH5α cells were transformed with 2 µl of the ligation reaction with a 42°C heat shock for 45 seconds and grown on LB-agar plates containing 50 µg/ml ampicillin or 25 µg/ml kanamycin. Insertion of the target fragment into the plasmid vector was confirmed in control restrictions and directionality and identity of the insert was confirmed through sequencing (GATC Biotech).

## 2.4 Annealing of primer duplexes

Short complementary DNA fragments, purchased from Metabion, were designed with short overhangs to allow for direct ligation into digested plasmid vectors without need for endonuclease digestion. Equal amounts of forward and reverse primer (40 µM) were incubated in 25 µl reactions with 2.5 µl T4 ligase buffer (NEB) and 1 µl polynucleotide kinase (NEB) for 1h at 37°C to phosphorylate the primers for efficient ligation. The reactions were denatured at 95°C for 10 minutes and allowed to cool to 5°C below the calculated annealing temperature of the primer duplex and incubated at this temperature for another 1.5 h. The annealing reactions were allowed to cool to room temperature and ligated into appropriately digested plasmid vectors as detailed above.

Table 2.1 **DNA constructs used in this study.**

| name | vector | insert | tag | species | ref seq | source | database entry | comment |
|---|---|---|---|---|---|---|---|---|
| pcDNA 3.1 + | | | | | | Invitrogen | | |
| pcDNA 3.1 + myc-his C | | | myc-his | | | Invitrogen | | |
| pcDNA 5/FRT/TO | | | | | | Invitrogen | | |
| pEGFP | | | eGFP | | | Clontech | | |
| pcDNA 3.1 + 3xHA-strep | pcDNA 3.1 + | | 3xHA-strep | | | S. Bremer, Essen | 614 | |
| pcDNA 3.1 + HA | pcDNA 3.1 + | | HA | | | molecular cloning | 518 | |
| pIRESpuro2-mCherry | pIRESpuro2b | | mCherry | | | D. Ritz, Zurich | 401 | |
| pIRESpuro2b | pIRESpuro2 | | | | | D. Gerlich, Zurich | 199 | 1 |
| UBXD1-mCherry | pIRESpuro2-mCherry | UBXD1 | mCherry | human | NM_025241 | M. Vuk, Zurich | 411 | |
| GFP-RAB5 | pEGFP | RAB5 | GFP | human | NM_004162 | M. Zerial, Dresden | 488 | |
| PTRF-RFP | pcDNA 5/FRT/TO | PTRF | RFP | mouse | NM_008986 | A. Helenius, Zurich | 632 | |
| p97-myc-strep | pcDNA 5/FRT/TO | p97 | myc-strep | rat | NM_053863 | D. Ritz, Zurich | 242 | 2 |
| p97-myc-strep E578Q | pcDNA 5/FRT/TO | p97 E578Q | myc-strep | rat | n.a. | D. Ritz, Zurich | 243 | 2 |
| p97-GFP | pcDNA 5/FRT/TO | p97 | GFP | rat | NM_053863 | A. Eiteneuer | 514 | 2 |
| p97-GFP E578Q | pcDNA 5/FRT/TO | p97 E578Q | GFP | rat | n.a. | A. Eiteneuer | 515 | 2 |
| HA-ubiquitin | pcDNA 3.1 | HA-ubiquitin | HA | human | NM_018955 | P. deCamilli, Yale | 221 | |
| KDEL-GFP | pEGFP | KDEL sequence | GFP | n.a. | n.a. | | 106 | |
| LC3-GFP | pEGFP | LC3A | GFP | human | NM_032514 | T. Yoshimori | 489 | |
| CAV1-HA | pEGFP N1 | CAV1 | HA | dog | NM_001003296 | A. Helenius, Zurich | 254 | |
| CAV1-HA K5-176R | pEGFP N1 | CAV1 | HA | dog | n.a. | A. Helenius, Zurich | 541 | |
| CAV1-HA P132L | pEGFP N1 | CAV2 | HA | dog | n.a. | A. Helenius, Zurich | 648 | |
| CAV1-GFP | pEGFP N1 | CAV1 | HA | dog | NM_001003296 | A. Helenius, Zurich | 484 | |
| CAV1-myc | pcDNA 3.1 + myc-his C | CAV1 | myc | human | NM_001753 | J. Pessin, Stony Brook, NY | 503 | |
| CAV1-myc K155,176R | pcDNA 3.1 + myc-his C | CAV1 | myc | human | n.a. | site directed mutagenesis | 512 | |
| CAV1-myc K39-96R | pcDNA 3.1 + myc-his C | CAV1 | myc | human | n.a. | site directed mutagenesis | 513 | |
| CAV1-myc K5-96R | pcDNA 3.1 + myc-his C | CAV1 | myc | human | n.a. | site directed mutagenesis | 528 | |
| CAV1-myc K39-176R | pcDNA 3.1 + myc-his C | CAV1 | myc | human | n.a. | site directed mutagenesis | 529 | |
| CAV1-myc K5-57R | pcDNA 3.1 + myc-his C | CAV1 | myc | human | n.a. | site directed mutagenesis | 530 | |
| CAV1-myc K65-176R | pcDNA 3.1 + myc-his C | CAV1 | myc | human | n.a. | site directed mutagenesis | 532 | |
| comments: | | | | | | | | |
| 1, contains the multiple cloning site of pEGFP N1 | | | | | | | | |
| 2, contains a silent G to A transition at position 593 | | | | | | | | |

Table 2.1 (continued)

| name | vector | insert | tag | species | ref seq | source | database entry | comment |
|---|---|---|---|---|---|---|---|---|
| CAV1-HA | pcDNA 3.1 HA | CAV1 | HA | human | NM_001753 | molecular cloning | 533 | |
| CAV1-HA K155,176R | pcDNA 3.1 HA | CAV1 K155,176R | HA | human | n.a. | molecular cloning | 536 | |
| CAV1-HA K5-57R | pcDNA 3.1 HA | CAV1 K5-57R | HA | human | n.a. | molecular cloning | 537 | |
| CAV1-HA K65-176R | pcDNA 3.1 HA | CAV1 K65-176R | HA | human | n.a. | molecular cloning | 539 | |
| CAV1-HA K5-176R | pcDNA 3.1 HA | CAV1 K5-176R | HA | human | n.a. | molecular cloning | 540 | |
| CAV1-HA K5R | pcDNA 3.1 HA | CAV1 | HA | human | n.a. | site directed mutagenesis | 593 | |
| CAV1-HA K26R | pcDNA 3.1 HA | CAV1 | HA | human | n.a. | site directed mutagenesis | 594 | |
| CAV1-HA K30R | pcDNA 3.1 HA | CAV1 | HA | human | n.a. | site directed mutagenesis | 595 | |
| CAV1-HA K39R | pcDNA 3.1 HA | CAV1 | HA | human | n.a. | site directed mutagenesis | 596 | |
| CAV1-HA K47R | pcDNA 3.1 HA | CAV1 | HA | human | n.a. | site directed mutagenesis | 597 | |
| CAV1-HA K57R | pcDNA 3.1 HA | CAV1 | HA | human | n.a. | site directed mutagenesis | 598 | |
| CAV1-HA K30,39R | pcDNA 3.1 HA | CAV1 | HA | human | n.a. | site directed mutagenesis | 617 | |
| CAV1-HA K39,47R | pcDNA 3.1 HA | CAV1 | HA | human | n.a. | site directed mutagenesis | 616 | |
| CAV1-HA R5K | pcDNA 3.1 HA | CAV1 K5-176R | HA | human | n.a. | site directed mutagenesis | 619 | |
| CAV1-HA R26K | pcDNA 3.1 HA | CAV1 K5-176R | HA | human | n.a. | site directed mutagenesis | 620 | |
| CAV1-HA R30K | pcDNA 3.1 HA | CAV1 K5-176R | HA | human | n.a. | site directed mutagenesis | 621 | |
| CAV1-HA R39K | pcDNA 3.1 HA | CAV1 K5-176R | HA | human | n.a. | site directed mutagenesis | 622 | |
| CAV1-HA R47K | pcDNA 3.1 HA | CAV1 K5-176R | HA | human | n.a. | site directed mutagenesis | 623 | |
| CAV1-HA R57K | pcDNA 3.1 HA | CAV1 K5-176R | HA | human | n.a. | site directed mutagenesis | 624 | |
| CAV1 HA R30,39K | pcDNA 3.1 HA | CAV1 K5-176R | HA | human | n.a. | site directed mutagenesis | 625 | |
| CAV1 HA R39,47K | pcDNA 3.1 HA | CAV1 K5-176R | HA | human | n.a. | site directed mutagenesis | 633 | |
| CAV1-HA Y14F | pcDNA 3.1 HA | CAV1 | HA | human | n.a. | site directed mutagenesis | 631 | |
| CAV1-HA-strep | pcDNA 3.1 3xHA-strep | CAV1 | HA | human | NM_001753 | PCR cloning | 626 | |
| CAV1-HA-strep K155,176R | pcDNA 3.1 3xHA-strep | CAV1 K155,176R | HA | human | n.a. | PCR cloning | 627 | |
| CAV1-HA-strep K5-57R | pcDNA 3.1 3xHA-strep | CAV1 K5-57R | HA | human | n.a. | PCR cloning | 628 | |
| CAV1-HA-strep K65-176R | pcDNA 3.1 3xHA-strep | CAV1 K65-176R | HA | human | n.a. | PCR cloning | 629 | |
| CAV1-HA-strep K5-176R | pcDNA 3.1 3xHA-strep | CAV1 K5-176R | HA | human | n.a. | PCR cloning | 630 | |
| CAV1-HA-plRES | plRESpuro2b | CAV1 | HA | human | NM_001753 | PCR cloning | 557 | |
| CAV1-HA-plRES K5-176R | plRESpuro2b | CAV1 K5-176R | HA | human | n.a. | PCR cloning | 558 | |
| CAV1-HA-FRT/TO | pcDNA 5/FRT/TO | CAV1 | HA | human | NM_001753 | molecular cloning | 615 | |
| CAV1-HA-FRT/TO K5-176R | pcDNA 5/FRT/TO | CAV1 K5-176R | HA | human | n.a. | molecular cloning | 618 | |

Table 2.2 **DNA primers and cloning strategies.**

| mutation | orientation | sequence | database entry |
|---|---|---|---|
| Lys to Arg (missmatch codon in bold) | | | |
| R5R | for | CATGTCTGGGGGC**AGA**TACGTAGAC | 692 |
| | rev | GTCTACGTA**TCT**GCCCCCAGACATG | 693 |
| K26,30R | for | CATCTAC**AGG**CCCAACAAC**AGG**GCCATGG | 694 |
| | rev | CCATGGC**CCT**GTTGTTGGG**CCT**GTAGATG | 695 |
| K26R | for | GCAACATCTAC**AGG**CCCAACAACAAGG | 775 |
| | rev | CCTTGTTGTTGGG**CCT**GTAGATGTTGC | 776 |
| K30R | for | GCCCAACAAC**AGG**GCCATGGCAG | 777 |
| | rev | CTGCCATGGC**CCT**GTTGTTGGGC | 778 |
| K39R | for | GAGCTGAGCGAG**AGG**CAAGTGTACGAC | 676 |
| | rev | GTCGTACACTTG**CCT**CTCGCTCAGCTC | 677 |
| K47R | for | CGCGCACACC**AGG**GAGATCGACC | 678 |
| | rev | GGTCGATCTC**CCT**GGTGTGCGCG | 679 |
| K57R | for | CCGCGACCCT**AGA**CACCTCAACG | 680 |
| | rev | CGTTGAGGTG**TCT**AGGGTCGCGG | 681 |
| K65R | for | CGATGACGTGGTC**AGG**ATTGACTTTGAAG | 682 |
| | rev | CTTCAAAGTCAAT**CCT**GACCACGTCATCG | 683 |
| K86R | for | CGGCATTTGG**AGG**GCCAGCTTCAC | 684 |
| | rev | GTGAAGCTGGC**CCT**CCAAATGCCG | 685 |
| K96R | for | CACTGTGACG**AGA**TACTGGTTTTACCGC | 686 |
| | rev | GCGGTAAAACCAGTA**TCT**CGTCACAGTG | 687 |
| K135R | for | GTACCATGCATT**AGG**AGCTTCCTGATTG | 690 |
| | rev | CAATCAGGAAGCT**CCT**AATGCATGGTAC | 691 |
| K155R | for | GAAGCTGTTGGG**AGA**ATATTCAGCAATG | 672 |
| | rev | CATTGCTGAATAT**TCT**CCCAACAGCTTC | 673 |
| K176R | for | GCATCAACTTGCAG**AGA**GAAATAGCGGC | 674 |
| | rev | GCCGCTATTTC**TCT**CTGCAAGTTGATGC | 675 |
| Arg to Lys (missmatch codon in bold) | | | |
| R5K | for | CATGTCTGGGGGC**AAA**TACGTAGAC | 792 |
| | rev | GTCTACGTA**TTT**GCCCCCAGACATG | 793 |
| R26K | for | GCAACATCTAC**AAG**CCCAACAACAGGG | 794 |
| | rev | CCCTGTTGTTGGG**CTT**GTAGATGTTGC | 795 |
| R30K | for | GCCCAACAAC**AAG**GCCATGGCAG | 796 |
| | rev | CTGCCATGGC**CTT**GTTGTTGGGC | 797 |
| R39K | for | GAGCTGAGCGAG**AAG**CAAGTGTACGAC | 798 |
| | rev | GTCGTACACTTG**CTT**CTCGCTCAGCTC | 799 |
| R47K | for | CGCGCACACC**AAG**GAGATCGACC | 800 |
| | rev | GGTCGATCTC**CTT**GGTGTGCGCG | 801 |
| R57K | for | CCGCGACCCT**AAA**CACCTCAACG | 802 |
| | rev | CGTTGAGGTG**TTT**AGGGTCGCGG | 803 |
| other amino acid exchanges (missmatch codon in bold) | | | |
| Y14F | for | GGGACATCTC**TTC**ACCGTTCCCATC | 811 |
| | rev | GATGGGAACGGT**GAA**GAGATGTCCC | 812 |
| P132L | for | GGGCAGTTGTA**CTA**TGCATTAAGAGC | 877 |
| | rev | GCTCTTAATGCA**TAG**TACAACTGCCC | 878 |

Table 2.2 (continued)

| | | | |
|---|---|---|---|
| deletion mutagenesis on CAV1 wild type | | | |
| delta 61 - 178 | for | CCTAAACACCTCAACGAAATAGCGGCC | 865 |
| | rev | GGCCGCTATTTCGTTGAGGTGTTTAGG | 866 |
| delta 61 - 101 | for | CCTAAACACCTCAACTTGCTGTCTGCC | 869 |
| | rev | GGCAGACAGCAAGTTGAGGTGTTTAGG | 870 |
| delta 61 - 134 | for | CCTAAACACCTCAACAAGAGCTTCCTG | 873 |
| | rev | CAGGAAGCTCTTGTTGAGGTGTTTAGG | 874 |
| deletion mutagenesis on CAV1 K5-57R | | | |
| delta 61 - 178 | for | CCTAGACACCTCAACGAAATAGCGGCC | 867 |
| | rev | GGCCGCTATTTCGTTGAGGTGTCTAGG | 868 |
| delta 61 - 101 | for | CCTAGACACCTCAACTTGCTGTCTGCC | 871 |
| | rev | GGCAGACAGCAAGTTGAGGTGTCTAGG | 872 |
| delta 61 - 134 | for | CCTAGACACCTCAACAAGAGCTTCCTG | 875 |
| | rev | CAGGAAGCTCTTGTTGAGGTGTCTAGG | 876 |
| | | | |
| Primers and strategies used for molecular cloning | | | |
| | orientation | sequence | database entry |
| Annealed primer coding for an HA-tag with *Not*I/*Xho*I overhangs were cloned into pcDNA 3.1 (228) yielding pcDNA-HA (518). | | | |
| | for | GGCCGCATACCCATACGACGTCCCAGACTACGCTAGCTAGC | 1006 |
| | rev | TCGAGCTAGCTAGCGTAGTCTGGGACGTCGTATGGGTATGC | 1007 |
| the caveolin-1 sequence was cloned from CAV1/myc (503) into pcDNA-HA (518) as *Eco*RI/*Not*I fragment. | | | |
| The caveolin-1-HA sequence was cloned from CAV1-HA (533) into pIRESpuro2b (199) as *Eco*RI/*Bam*HI fragment | | | |
| | for | GATCGAATTCGGCACGAGGGGGCC | 750 |
| | rev | CGATGGATCCCTAGCTAGCGTAGTCTGG | 751 |
| The caveolin-1-HA sequence was cloned from CAV1-HA into pcDNA 5/FRT/TO as *Eco*RI/*Xho*I fragment | | | |
| The caveolin-1-HA sequence was cloned into pcDNA-3xHA-strep (614) as BamHI/AgeI fragment yielding CAV1-HA-strep | | | |
| | for | TACGAAGGATCCACTAGTCCAGTGTGG | 879 |
| | rev | CAACCGGTATGCATGCTAGCGTAGTCTGGGACG | 880 |

## 2.5 Site directed mutagenesis

To introduce single amino acid exchanges or longer deletions into the coding sequence of expression constructs, a site directed mutagenesis protocol was used. DNA primers were designed with a single base exchange flanked by at least 10 nucleotides. For larger mutations, at least 12 nucleotides were chosen flanking the DNA sequence that was to be looped out. Mutagenesis primers were purchased from Metabion and are listed in Table 2.2 (page 56). To introduce the mutation, the whole plasmid vector was amplified using 1.25 U PfuUltra II DNA polymerase (Agilent Technologies) in 50 µl reactions. The forward and reverse mutagenesis primers were used at 300 nM together with 50 – 100 ng template DNA and 400 µM dNTPs. The mutagenesis PCR was carried out in a TPersonal thermocycler (Biometra). One PCR cycle consisted of 30 seconds denaturing at 98°C, annealing for 60 seconds at 52°C

and synthesis of the new DNA strand at 72°C. The annealing temperature was fixed at 52°C for all primers and lowered to if the PCR yielded no product. The mutagenesis primers were designed to have an annealing temperature (Tm) of 70 to 72°C when calculated as: *Tm = 81.5 + 0.41(%GC) – 675/N - %mismatch*. Here %GC stands for the GC content of the primer, N denotes the primer length and %mismatch is the percentage of the whole primer not pairing with the target sequence. The extension time was one minute per one kilobase of plasmid DNA. The PCR program consisted of 16 cycles with a final extension step at 72°C for 15 minutes. To digest the template DNA, the reactions were incubated with 5 U *Dpn*I (NEB) for 1 h at 37°C. The template DNA is methylated and, therefore, specifically degraded by *Dpn*I. The digested PCR reactions were purified with a PCR clean-up kit (Machery-Nagel). DH5α cells were transformed with the mutated plasmid DNA using a heat shock at 42°C for 45 seconds. Transformed DH5α were grown on LB plates containing 50 µg/ml ampicillin or 25 µg/ml kanamycin. Presence of the introduced mutation and absence of additional mutations were confirmed by sequencing (GATC Biotech).

### 2.6 RNA interference (RNAi)

Small interfering RNA (siRNA) duplexes were purchased from Microsynth. RNA duplexes were designed with a 19 nucleotide core sequence specific for the targeted mRNA and 5’ and 3’ dTdT overhangs to improve incorporation into the RISC complex. RNA sequences are given in Table 2.3 (page 59). For RNA interference experiments cells were either seeded one day in advance (forward transfection) or at the same time as RNAi transfection (reverse transfection). The cells were transfected at 30 – 50% confluence using the Lipofectamine RNAiMAX transfection reagent (Invitrogen). For a forward transfection of 10 nM siRNA in a 6 well plate format, 1.25 µl of a 20 mM stock solution were diluted in 250 µl Opti-MEM I (Gibco) and vortexed briefly. 3.2 µl of the RNAiMAX transfection reagent (Invitrogen) were diluted in 250 µl Opti-MEM I, vortexed briefly and added to the diluted siRNA duplexes. The transfection reaction was vortexed briefly and drop wise added to the cells after 20 minutes incubation at room temperature. For transfection of higher concentrations of siRNA, like 20 or 40 nM, the volume of RNAiMAX was increased to 4.5 or 6 µl respectively. The higher siRNA amounts were used for depletion of the NEDD4, NEDD4L, WWP1, and WWP2 E3 ubiquitin ligases because they were published to deplete their targets at these concentrations. For transfection in 12 well plates half the volumes of 6 well plates were used. For reverse transfection of 10 nM siRNA

duplexes in 96 well plates 0.075 µl of a 20 mM stock solution were diluted in 25 µl Opti-MEM I and vortexed briefly. 0.2 µl of RNAiMAX transfection reagent were diluted in 25 µl Opti-MEM I, vortexed briefly and added to the diluted siRNA duplexes. The transfection reaction was vortexed briefly and added to a well on a 96 well plate. After 20 minutes incubation 100 µl of a suspension of U2OS-CAV1-HA cells with 8000 cell/ml were added to the well. RNAi transfected cells were analyzed 48 h or 72 h post transfection.

Table 2.3 **siRNA oligonucleotides used in this study.**

| name | core sequence | sense overhang | source | database entry |
|---|---|---|---|---|
| | | | | |
| AMFR s1 | GACGGAUUCAAGUACCUUU | dTdT | Burr et al., 2011 | 895 |
| Ataxin3 s1 | UGGCAGAAGGAGGAGUUAC | dTdT | Wang et al., 2012 | 893 |
| CBL s1 | CCUCUCUUCCAAGCACUGA | dTdT | Huang et al., 2006 | 815 |
| ctrl | UUCUCCGAACGUGUCACGU | dTdT | Ritz et al., 2011 | 714 |
| CUL3 s1 | CAACUUUCUUCAAACGCUA | dTdT | Huotari et al. 2012 | 710 |
| FAF1 s1 | CCACCUUCAUCAUCUAGUC | dTdT | Park et al., 2007 | 888 |
| HRS s1 | CGACAAGAACCCACACGUC | dTdT | Bache et al., 2003 | 764 |
| NEDD4L s1 | CCACAACACAAAGUCACAC | dTdT | Lin et al., 2010 | 817 |
| NEDD4L s2 | GUGGACAAUUUAGGCCGAA | dTdT | Yamada et al., 2012 | 949 |
| NEED4 s1 | CCAUGAAUCUAGAAGAACA | dTdT | Lin et al., 2010 | 816 |
| NPL4 s1 | CGUGGUGGAGGAUGAGAUU | dTdT | Dobrynin et al., 2011 | 737 |
| p47 s1 | AGCCAGCUCUUCCAUCUUA | dTdT | Dobrynin et al., 2011 | 589 |
| p97 s2 | AACAGCCAUUCUCAAACAGAA | dTdT | Quiagen, Hs_VCP_7 | 709 |
| p97 s3 | AAGUAGGGUAUGAUGACAUUG | dTdT | Wojcik et al., 2004 | 740 |
| PLAA s2 | CCAGUGAUGACCCUUGGUUAA | dTdT | Quiagen, Hs_PLAA_9 | 833 |
| PLAA s3 | GGACAGACUCGUCUAAUCA | dTdT | Quiagen, Hs_PLAA_6 | 834 |
| RAB7 s1 | GGAUGACCUCUAGGAAGAA | dTdT | Spinosa et al., 2008 | 883 |
| SAKS1 s1 | UAGGGAGGCAUGCCUAGGA | dTdT | Quiagen, Hs_LOC51035_2 | 889 |
| SAKS1 s2 | GCAGCGGGAGCGUGAAGAA | dTdT | Quiagen, Hs_LOC51035_5 | 948 |
| TSG101 | CGAUGGCAGUUCCAGGGAA | dTdT | Bishop et al., 2002 | 761 |
| UBXD1 s1 | CCAGGUGAGAAAGGAACUU | dTdT | Ritz et al., 2011 | 591 |
| UBXD1 s3 | UCAGAUACCACGUUGGUCC | dCdT | Quiagen, Hs_UBXD1_5 | 885 |
| UBXD6 s1 | GGAUGACGAGAAUUGGGUA | dTdT | Quiagen, Hs_UBXD6_2 | 791 |
| UBXD7 s1 | CAGCUUGAAAGGAGUGUUU | dTdT | Quiagen, Hs_KIAA0794_2 | 890 |
| UBXD8 s1 | GAAGUUAUUUCACUAAUAA | dTdT | Suzuki et al., 2012 | 891 |
| UBXD9 s1 | CCCUGUGAAUAUGAUCUGA | dTdT | Orme and Bogan, 2012 | 892 |
| UFD1 s2 | GUGGCCACCUACUCCAAAU | dTdT | Dobrynin et al., 2011 | 594 |
| VCPIP1 s1 | CCCGAUGAUUAUACUCCUG | dTdT | Quiagen, Hs_VCIPI135_3 | 826 |
| VCPIP1 s2 | CAGGGACAGACUUUAGUAA | dTdT | Quiagen, Hs_VCIPI135_2 | 827 |
| WAC s2 | CUCGAAGUCUUCAGCGCUC | dTdT | Quiagen, HS_WAC_5 | 829 |
| WWP1 s1 | GCAGAGAAAUACUGUUUAU | dTdT | Li et al., 2009 | 881 |
| WWP2 s1 | UGACAAAGUUGGCAAGGAA | dTdT | Maddika et al., 2011 | 882 |
| YOD1 s1 | GACCGUCAAAUUAGAGCUU | dTdT | Quiagen, Hs_Yod1_4 | 824 |
| YOD1 s2 | CAGCGUAACUUCCCUGAUC | dTdT | Quiagen, Hs_Yod1_5 | 825 |
| ZFAND2b s1 | GCAGCUCGAAGCCGUCCAA | dTdT | Quiagen, Hs_ZFAND2B_3 | 894 |

## 2.7 Pharmacological treatments

To inhibit p97 function cells were treated with 10 µM DBeQ (Interbioscreen or Sigma-Aldrich), or 10 µM I8, or 10 µM I5, or 10 µM I1 for 4 h. Because we received the unpublished inhibitors I8, I5, and I1 from for testing, unfortunately an information embargo prohibits us from giving up the full names and structures. To inhibit lysosomal degradation cells were treated with 200 ng/ml Bafilomycin A1 (Sigma-Aldrich), 20 mM ammonium chloride ($NH_4Cl$, Fluka), or a mixture of 10 µM leupeptin (Sigma-Aldrich) and pepstatin A (Sigma-Aldrich) for 18 h. Proteasomal degradation was blocked with 10 µM MG132 (Calbiochem) for 4 h.

## 2.8 Preparation of cell extracts

To stop biochemical processes and preserve proteins all steps during cell lysis were carried out on ice. For protein extraction from cells on a 6 well plate the cells were washed in 2 ml ice cold PBS. The cells were lysed in 60 µl extraction buffer (detailed below) added directly into the well. The extraction buffer was supplemented with 1:100 protease inhibitor (Roche, Complete EDTA-free) and, if required, 1:10 phosphatase inhibitor (Roche, PhosSTOP), or 10 mM NEM (Sigma-Aldrich) to inhibit deubiquitination by cysteine proteases. The cells were scraped from the well bottom using a cell scraper (BD Falcon) and transferred to reaction tubes. After incubation on ice for 20 minutes the extracts were centrifuged for 15 minutes at 14000 x g or 17000 x g to remove nuclei and heavy membrane fragments. Protein concentration was measured using a BCA assay (Interchim) in 96 well plate format. For storage the extracts were frozen in liquid nitrogen and kept at -80°C.

## 2.9 Immunoprecipitation

To affinity isolate proteins from cell extracts using specific antibodies, the protein concentration of the cell lysates was adjusted to 1 – 2 µg/ml in extraction buffer. Extracts were supplemented with 1:100 protease inhibitor (Roche, Complete EDTA-free) and 1 µg/ml BSA (Interchim). For one immunoprecipitation sample 250 µg to 500 µg protein were used. The samples were pre-cleared with 5 µl Dynabeads protein G (Invitrogen) (washed three times in extraction buffer) for 1 h at 4°C, rolling. All washing steps of Dynabeads protein G were carried out with a DynaMag Spin magnetic tube holder (Invitrogen). After pre-clearing the supernatant was collected

and 5 % were taken as an input sample. After addition of 0.6 µg antibody the samples were incubated 2 h at 4°C, rolling. To capture the antigen-antibody complexes 20 µl Dynabeads protein G were washed three times in extraction buffer and incubated with the samples for 1h at 4°C, rolling. From the supernatant, 5 % were taken as flow-through samples. The beads were washed three times in extraction buffer or once in extraction buffer and two times in PBS and resuspended in 18 µl extraction buffer. To the samples 6 µ l of 6x SDS loading buffer freshly supplemented with 1:10 1M DTT were added. The samples were boiled at 95°C for 5 minutes. After boiling, the Dynabeads protein G were removed and the supernatants analyzed in Western blotting.

### 2.10 SDS-PAGE and Western blotting

Protein samples from cell extracts or immunoprecipitations were separated by size in SDS polyacrylamide gels using a Tris/glycine buffer and the Mini Trans-Blot system (Bio-Rad). The polyacrylamide concentration, ranging from 7.5 to 13 %, was chosen to provide good resolution target proteins. The gels were run with constant current of 15 to 20 mA. The gels were either directly stained using Coomassie G-250 or used for Western blotting. For Western blotting, the proteins were transferred from the gels onto nitrocellulose Hybond-C Extra (Amersham) or PVDF Hybond-P (Amersham) using semi-dry or wet blotting protocols. The PVDF membrane was activated in methanol for one minute and than soaked in blotting buffer prior to usage. For semi-dry blots the membrane was placed on top of two filters soaked in blotting buffer. The gel was placed on top and the sandwich was finished with another layer of two filter papers soaked in blotting buffer. Air bubbles were forced out by rolling the sandwich with a plastic tube. Proteins were transferred in semi-dry Trans-blot SD transfer chambers (BioRad) at 120 mA constant current for 45 to 55 minutes. The membranes were stained in Ponceau-S dye to verify equal transfer and blocked in 10 % fat free milk in PBS-T or TBS-T for 1 h. For wet blotting, either the blotting buffer for semi dry transfer or a special wet blot transfer buffer with reduced SDS were used (detailed below). The blotting sandwich was assembled as described above. Proteins were transferred in Mini Trans-Blot (Bio-Rad) chambers at 4°C. Voltage was held constant at either 70 V for 3 h (blotting of the EGF-receptor) or at 30 V for 2 h. The membranes were then stained in Ponceau-S dye and blocked in 10% fat free milk in PBS-T or TBS-T. Membranes were washed 3 times for 5 minutes in PBS-T or TBS-T after blocking. Primary antibodies were diluted as detailed in Table 2.4 (page 63) and

incubated with the membranes over night at 4°C, or 2 h at room temperature in 50 ml tubes. Membranes were washed 3 times in PBS-T or TBS-T for 5 minutes. HRP-coupled Secondary antibodies were diluted 1:10000 or 1:20000 in either PBS-T or TBS-T and incubated with the membranes for 45 minutes at room temperature. For Western blots of immunoprecipitated proteins, HRP coupled secondary antibodies specific for the $F(ab')_2$ fragment were used to reduce recognition of the denatured light and heavy chain of the antibody that was used for capturing the target antigen in the immunoprecipitation. The membranes were washed 3 times in PBS-T or TBS-T for 15 minutes. To detect the bound secondary antibody, membranes were incubated with freshly prepared SuperSignal West Pico enhanced chemiluminescence (ECL) substrate (Pierce) for 3 minutes or ECL Plus substrate (Amersham) for 5 minutes. The light signals were detected on Super RX films (FUJIFILM). Films were developed in a Cawomat 200 IR (Cawo) developing machine. Films were digitalized with a ScanMaker i480 film scanner (Microtek). For quantification the signals were detected with a Fusion FX7 image acquisition system (Vilber Lourmat) using a cooled CCD camera. Digital images were quantified using Bio1D analysis software (Vilber Lourmat) or using ImageJ (1.45k, National Institutes of Health).

### 2.11 EGFR degradation assay

The ligand induced lysosomal degradation of the EGFR (epidermal growth factor receptor) is established as a model for endosomal sorting and lysosomal degradation of membrane proteins. This model was used to investigate the effect the p97 system on endosomal sorting. For RNAi experiments HeLa cells were transfected with siRNA for 72 h and then serum starved for 4h in DMEM without FCS. For inhibitor experiments HeLa or HEK293 cells were grown to confluence and serum starved for 4 h in DMEM containing p97 inhibitor or DMSO. Starvation accumulates the EGFR on the plasma membrane and poses it for stimulation by EGF. Internalization and degradation of the EGFR was induced by addition of 50 ng/ml (HEK293) or 100 ng/ml (HeLa) EGF. The cells were harvested in regular intervals after addition of EGF. Cell lysates were analyzed for the EGFR in Western blots as described above. The EGFR levels were calculated as percentage of the zero-minute time point.

Table 2.4 **Primary and secondary antibodies used in this study**

| primary antibodies | | | | |
|---|---|---|---|---|
| antigen | species | dilution in WB | dilution in IF | source |
| | | | | |
| alpha-tubulin | mouse | 1:8000 | n.d. | Sigma-Aldrich, T5168 |
| CAV1 (N20) | rabbbit | 1:1000 | 1:500 | Santa Cruz Biotechnology, sc-894 |
| DVC1 | rabbit | 1:500 | n.a. | Atlas, HPA025073 |
| EEA1 | mouse | n.d. | 1:200 | BD transduction labs, 610457 |
| EGFR | mouse | 1:500-1:1000 | n.d. | Santa Cruz Biotechnology, sc-81449 |
| EGFR | rabbit | 1:1000 | n.a. | Millipore, 06-847 |
| GM130 | rabbit | n.a. | 1:2000 | H. Meyer, ML07 |
| HA | rabbit | 1:1000 | 1:500 | Sigma-Aldrich, H6908 |
| HA | mouse | 1:1000 | 1:1000 | Covance, MMS-101P, HA.11 |
| HSC70 | mouse | 1:10000 | n.d. | Santa Cruz Biotechnology, sc-7298 |
| LAMP1 | mouse | n.d. | 1:500 | Santa Cruz Biotechnology, sc-5570 |
| myc | mouse | 1:1000 | 1:500 | hyboma cells, clone 9E10 |
| NEDD4L | rabbit | 1:1000 | n.d. | Cell Signaling, 4013 |
| NPL4 | rabbit | 1:500 | n.d. | H. Meyer, HME18 |
| p47 | rabbit | 1:2000 | n.a. | H. Meyer, HME22, serum |
| p62/SQSTM1 | rabbit | 1:4000 | 1:500 | Sigma-Aldrich, P0067 |
| p97/VCP | rabbit | 1:1000 | n.a. | H. Meyer, HME-8, serum |
| phospho-EGFR | rabbit | 1:500-1:1000 | n.d. | Cell Signaling, 2234 |
| PLAA | rabbit | 1:1000 | 1:500 | Epitomics, Y102 |
| PTRF/cavin-1 | rabbit | 1:1500 | 1:100 | Abcam, ab48824 |
| RAB5 | rabbit | 1:1000 | 1:200 | Cell Signaling, 3547 |
| RAB7 | rabbit | 1:1000 | 1:100 | Cell Signaling, 9367 |
| SAKS1 (LOC51035) | rabbit | 1:10000 | n.d. | Abcam , ab151723 |
| SEC31a | mouse | n.d. | 1:1000 | BD transduction labs, 612350 |
| TSG101 | rabbit | 1:1500 | n.d. | GeneTex, GTX118736 |
| ubiquitin | rabbit | 1:100 | n.a. | Sigma-Aldrich, U5379 |
| ubiquitin | mouse | 1:500 | n.d. | Cell Signaling, 3936, P4D1 |
| ubiquitin (chains) | mouse | 1:500-1:1000 | 1:500 | Millipore, 04-263, FK2 |
| UBXD1 | rabbit | 1:10000 | n.a. | H. Meyer, E43, serum |
| UBXD7 | sheep | 1:1500 | n.a. | G. Alexandrou, S409D |
| UBXD8 | rabbit | 1:1000 | n..d. | Novus Biologicals, NBP2-16381 |
| UFD1 | mouse | 1:500 | n.d. | C. Brasseur, 5E2, purified |
| VCPIP1 | rabbit | 1:2000 | n.a. | H. Meyer, HME 19, serum |
| YOD1 | rabbit | 1:1000 | n.a. | Sigma-Aldrich, SAB4502321 |

| secondary antibodies | | | | |
|---|---|---|---|---|
| antigen | species | dilution in WB | dilution in IF | source |
| HRP anti-mouse | goat | 1:10000-1:20000 | n.a. | BioRad, 170-6516 |
| HRP anti-rabbit | goat | 1:10000-1:20001 | n.a. | BioRad, 170-6515 |
| HRP anti-sheep | rabbit | 1:10000-1:20002 | n.a. | Pierce, 31480 |
| HRP anti-mouse F(ab')2 | goat | 1:20000 | n.a. | Jackson ImmunoResearch, 115-036-006 |
| HRP anti-rabbit F(ab')2 | goat | 1:20000 | n.a. | Jackson ImmunoResearch, 115-036-047 |
| Alexa 488 anti-mouse | goat | n.a. | 1:500 | Life Technologies, A-11029 |
| Alexa 568 anti-mouse | goat | n.a. | 1:500 | Life Technologies, A-11031 |
| Alexa 488 anti-rabbit | goat | n.a. | 1:500 | Life Technologies, A-11034 |
| Alexa 568 anti-rabbit | goat | n.a. | 1:500 | Life Technologies, A-11036 |

## 2.12 Fluorescence imaging

For visualization of cellular structures specific primary antibodies and fluorophore coupled secondary antibodies were used. U2OS Cells were seeded on glass cover slips (#1, 0.13 – 0.17 mm thickness, VWR) in cell culture dishes. The cells were seeded for sub-confluence at the time of fixation. After transfection or treatment the cells were fixed in 4% formaldehyde ($CH_2O$, PFA) in PBS or ice cold methanol. If it was desired to remove cytoplasmic proteins prior to fixation, the cells were incubated in pre-extraction buffer with 0.0025% saponin for 2 minutes. Cells were then washed in PBS and fixed in 4% PFA in PBS. For formaldehyde fixation, cells were washed twice in PBS and fixed in 4% PFA in PBS at room temperature for 20 minutes. The cells were washed twice in PBS and permeabilized in 0.1% Triton X-100 in PBS for 10 minutes. After washing three times five minutes in PBS the cells were blocked in 3% BSA in PBS for 30 minutes. For methanol fixation the cells were washed twice in PBS and fixed in ice-cold (-20°C) methanol for 10 minutes at room temperature. After washing three times five minutes in PBS the cells were blocked in 3% BSA in PBS for 30 minutes. After blocking, the cover slips were placed with the cell side down on drops of primary antibody solution on Parafilm (Pechiney) in a wet chamber and incubated for 90 minutes. The primary antibodies were diluted in 3% BSA in PBS as detailed in Table 2.4 (page 63). The cover slips were washed three times for five minutes in PBS and incubated in secondary antibody solution (1:500 in 3% BSA in PBS) for 30 minutes. The cover slips were washed three times for five minutes in PBS. After rinsing in Mili-Q $H_2O$ to remove residual salts, the cover slips were mounted with the cell side down onto drops of Mowiol (Calbiochem) solution, containing 0.5 µg/ml DAPI, on microscopy slides (Marienfeld). The microscopy slides were dried at room temperature and stored at 4°C. Imaging was performed on an inverted spinning-disc confocal microscope (Nikon Eclipse Ti equipped with a Yokogawa CSU X-1 spinning disk unit) using an x100, 1.49 NA or an x40, 0.94 NA objective. Images were acquired with an Andor iXon X3 EMCCD (electron multiplying charge coupled device) camera. Epifluorescence microscopy was carried out on an inverted fluorescence microscope (Axio Observer Z1, Zeiss) using an x 63, 1.4 NA objective. Images were acquired with an AxioCam MRm CCD camera.

## 2.13 Co-localization analysis

To quantify the colocalization of CAV1-HA or PTRF/cavin-1 positive vesicles with staining for ubiquitin or markers of the endosomal system an ImageJ (1.45k, National Institutes of Health) routine was developed. The routine identifies CAV1-HA or PTRF/cavin-1 positive vesicles in series of images acquired with equal laser intensity and exposure time. The vesicles are then classified as positive for colocalization if the signal of the ubiquitin or endosomal marker staining is above a certain threshold. In detail, the image of the CAV1-HA or PTRF/cavin-1 staining is thresholded to remove background signaling. The CAV1-HA or PTRF-cavin-1 threshold parameters for the different analyses are listed in Table 2.5 (page 66). The ImageJ Watershed algorithm is used to discriminate vesicles in close proximity. Vesicles are identified using the Analyze Particles function in ImageJ (vesicle size 10 – 400 pixel, roundness 0.5 – 1.0). For each vesicle the colocalizing signal of ubiquitin staining or staining for endosomal markers is measured. A vesicle is considered positive if the colocalizing signal is above a defined threshold and signal variation is not greater than four times the signal variation over the whole image. The thresholds used for the different markers are given in Table 2.5 (page 66). For each cell the total number of vesicles and of vesicles with colocalizing signal is given as a result. The complete algorithm is shown below.

Code for the ImageJ routine that was used for automated colocalization analysis:

```
/* The standard macro used to identify Cav1 vesicles (red) and measure colocalizing signal in the green channel. Results are buffered in an array and displayed in the results window after the run. For this only picture files may be present in the folder chosen for analysis. The thresholds for vesicles recognition and colocalization can be used to adapt the macro for different signal intensities and differences in background staining. The vesicles size can be further used to improve detection of vesicles. The table below contains information about the setting used for the different quantifications. Version from 12_08_10. This macro is based on the 1.45K version of ImageJ, NIH.  */
dir1 = getDirectory("Choose Directory ");  list = getFileList(dir1);
total = newArray(list.length);  positive = newArray(list.length);
setBatchMode(true);
for (i=0; i<list.length; i++) {  showProgress(i+1, list.length);
        open(dir1+list[i]);
        number_of_vesicles = 0;  positive_vesicles = 0;
        run("Stack to Images");
        selectWindow("Green");  run("Measure");
        mean_green = getResult('Mean',nResults-1);  std_green = getResult('StdDev',nResults-1);
        green_max = getResult('Max',nResults-1);
        selectWindow("Red");  run("Measure");
        mean_red = getResult('Mean',nResults-1);  std_red = getResult('StdDev',nResults-1);
        threshold_green = mean_green+3*std_green;  threshold_red = mean_red+3*std_red;
        threshold_red_std = 4*std_red;
        selectWindow("Green");  setThreshold(threshold_green,16384);
        run("Convert to Mask");  run("Watershed");
```

```
                run("Analyze Particles...", "size=10-400 pixel circularity=0.50-1.00 show=Nothing add");
                selectWindow("Red");
                count = roiManager("count");
                for (j = 0; j < count; j++) {                   roiManager("select", j);
                        run("Measure");
                        if (getResult('Mean',nResults-1) > threshold_red && getResult('StdDev',nResults-1) <
                        threshold_red_std) {            positive_vesicles++;            number_of_vesicles++;}
                        else                                    number_of_vesicles++;
                        }
                total[i] = number_of_vesicles;                  positive[i] = positive_vesicles;
                roiManager("delete");           run("Clear Results");
                while (nImages>0) {selectImage(nImages);        close();}
}
for (matrix=0; matrix<total.length; matrix++)
                {setResult("vesicles", matrix, total[matrix]);
                setResult("positive", matrix, positive[matrix]);}
updateResults();
```

Table 2.5 **Parameters used for the different colocalization analyses.**

| colocalization analyzed | threshold for vesicles | threshold for colocalization |
|---|---|---|
| CAV1-HA : ubiquitin | mean+3*stdev of CAV1-HA signal | mean+3*stdev of ubiquitin signal |
| CAV1-HA : LAMP1 | mean+3*stdev of CAV1-HA signal | mean+3*stdev of LAMP1 signal |
| CAV1-HA : EEA1 | mean+4*stdev of CAV1-HA signal | mean+2*stdev of EEA1 signal |
| CAV1-HA : RAB5 | mean+4*stdev of CAV1-HA signal | mean+2*stdev of RAB5 signal |
| CAV1-HA : PTRF/cavin-1 | mean+4*stdev of CAV1-HA signal | mean+3*stdev of PTRF/cavin-1 signal |
| CAV1-HA : p97-myc-strep | mean+3*stdev of CAV1-HA signal | mean+3*stdev of p97-myc-strep signal |
| CAV1-HA : UBXD1-mCherry | mean+2*stdev of CAV1-HA signal | mean+3*stdev of UBXD1-mCherry signal |
| PTRF/cavin-1 : EEA1 | mean+4*stdev of PTRF/cavin-1 signal | mean+3*stdev of EEA1 signal |
| PTRF/cavin-1 : ubiquitin | mean+4*stdev of PTRF/cavin-1 signal | mean+3*stdev of ubiquitin signal |

## 2.14 Statistical analyses

Statistical analyses were performed in SigmaPlot software (Systat) as Mann-Whitney *U* tests. Values of $p < 0.05$ (*), $p < 0.01$ (**) and $p < 0.001$ (***) were considered statistically significant. Box plots show median, lower and upper quartiles (line and box), $10^{th}$ and $90^{th}$ percentile (whiskers), and outliers (•).

## 2.15 Buffers and solutions

**2xHBS**

270 mM NaCl
10 mM KCl
1.5 mM $H_2PO_4$
10 mM glucose
40 mM HEPES
pH 7.05, sterile filter, store at 4°C

**extraction buffer**

150 mM KCl
5 mM $MgCl_2$
25 mM Tris-HCl
1% Triton X-100
5% Glycerol
2 mM ß-Mercaptoethanol
pH 7.4, store at -20°C

**protease inhibitor 100x**

Dissolve 1 protease inhibitor tablet (Roche, Complete EDTA-free) in 500 µl Mili-Q $H_2O$.
Store at -20°C.

**phosphatase inhibitor 10x**

Dissolve 1 phosphatase inhibitor tablet (Roche, PosSTOP) in 1 ml extraction buffer.
Store at -20°C

**6x SDS loading buffer**

0.35 M Tris, pH 6.8
30% glycerol (87%)
10% SDS
600 mM DTT
dissolve components completely
add 0.02% bromphenol blue

**10x SDS running buffer**

1.9 M glycine
250 mM Tris base
pH 8.8
1% SDS

**blotting buffer**

20% methanol
in 1x SDS running buffer

**10x wet blot transfer buffer**

1.92 mM glycine
205 mM Tris base
pH 8.3
0.04% SDS

add 20% methanol to 1x wet blot transfer buffer before use

**Western blot blocking solution**
3% BSA (Albumin fraction V, Applichem)
in PBS-T or TBS-T

**LB medium**
10g peptone (Fluka)
10 g NaCl
5 g yeast extract (Applichem)
ad 1 l Mili-Q $H_2O$
pH 7.0
autoclave

**LB agar**
20 g agar (Applichem)
ad 1 l LB medium
autoclave

**10x PBS pH 7.4**
100 mM $Na_2HPO_4$
21.7 $NaH_2PO_4$
1.54 M NaCl
pH 7.4

**PBS-T**
0.05 % Tween 20
in PBS pH 7.5

**10x TBS pH 7.6**
1.5 M NaCl
100 mM Tris
pH 7.6

**TBS-T**
0.1% Tween 20
in TBS pH 7.6

**stripping buffer**
200 mM gylcine
0.1% SDS
1% Tween 20
pH 2.2

**pre-extraction buffer**
80 mM PIPES
5 mM EGTA
1 mM $MgCl_2$
add 0.0025% saponin before use

**PFA solution**
4% paraformaldehyde
in PBS pH 7.4
store at -20°C
(store thawed aliquots at 4°C)

**IF blocking solution**
3% BSA (Albumin fraction V, Applichem)
in PBS pH 7.4

**Mowiol**
5 g Mowiol in 20 ml PBS
stir over night
add 10 ml glycerol (87%)
centrifuge 15 minutes at 17000 x g
add 0.5 µg/ml DAPI
store at -20°C

# 3 Results

## 3.1 CAV1 is ubiquitinated in the N-terminal region

Ubiquitination of the 178-amino acid membrane protein caveolin-1 (CAV1) was shown in previous studies. This modification is functional and governs the half-life of overexpressed caveolin-1 (Hayer et al., 2010b; Ritz et al., 2011). However, these analyses were performed using a lysine-less variant of CAV1 (K5-176R) in which all lysines were mutated to arginine. These extensive mutations in the CAV1 gene might affect the behavior of the protein in addition to preventing ubiquitination. The first goal of this study was, therefore, to define the ubiquitination site of CAV1 in more detail and possibly reduce the number of mutations necessary to abolish CAV1 ubiquitination.

### 3.1.1 Optimizing the assay to investigate ubiquitination of CAV1 variants

Previous studies of CAV1 ubiquitination in our lab made use of co-expression of human CAV1-myc and HA-ubiquitin to bolster the ubiquitination signal (Ritz et al., 2011). Therefore, we initially chose the same approach and mutated groups of lysines in CAV1-myc based on the CAV1 domain structure. Human caveolin-1 contains 12 lysine residues within four structural domains (Figure 3.1 A). First, we mutated the lysines 39 to 96 to arginine that are located N-terminally of the intra-membrane domain and are present in the both isoforms α-CAV1 and β-CAV1. In a second variant, we mutated the two lysines 155 and 176 in the C-terminal domain. These CAV1-myc variants were co-expressed with HA-ubiquitin in HEK293 cells and immunoprecipitated using myc-specific antibodies. We analyzed conjugation of HA-ubiquitin to CAV1-myc by Western blotting using HA-specific antibodies and could confirm the ubiquitination of CAV1 wild type shown in our lab (Ritz et al., 2011). In consistence with these data, we found that the lysine-less variant of CAV1 (K5-176R) displayed greatly reduced ubiquitination. Interestingly, we observed that mutation of the lysines 39 to 96 but not of lysine 155 and 176 reduced conjugation of HA-ubiquitin to CAV1-myc (data not shown). This prompted us to focus on the lysines in the N-terminal region. Therefore, we mutated the lysines 39 and 47, or 26 to 47, or all lysines in the N-terminal region (5 to 57) to arginine (Figure 3.1 A). We co-transfected these mutant CAV1 variants and HA-ubiquitin in HEK293 cells and immunoprecipitated CAV1-myc as described above. Again, we confirmed

modification of CAV1 wild type with HA-ubiquitin (Figure 3.1 B). Ubiquitinated CAV1 appeared as a slower migrating double band and additional slower migrating bands in Western blotting with HA-specific antibodies (Figure 3.1 B, double lines and arrow). This indicated that CAV1 was predominantly modified with mono-ubiquitin in addition to multi-ubiquitin (Ritz et al., 2011). Importantly, mutation of lysines in the N-terminal region greatly reduced modification of CAV1 with HA-ubiquitin comparable to mutation of all lysines in CAV1 to arginine (K5-176R). Furthermore, two important observations were made in this experiment. First, the mutation of lysines in CAV1 affected the running behavior of the CAV1 protein in SDS-gels. The lysine-less CAV1 K5-176R variant migrated faster in comparison to the wild type. In general, the CAV1 protein migrated faster the more lysines in CAV1 were mutated to arginine. Second, the lysine-less variant of CAV1-myc was still conjugated with HA-ubiquitin even though all lysines were mutated to arginine. This probably resulted from a lysine that is present in the myc epitope-tag and made CAV1-myc an unsuitable tool to investigate ubiquitination of CAV1. To circumvent the problem of unspecific ubiquitination of the myc-tag, we decided to use HA-tagged CAV1 instead because the HA-epitope contains no lysine. Furthermore, we chose to generate a CAV1-HA construct from human CAV1 cDNA instead of using the HA-tagged CAV1 from dog that was described by Hayer and colleagues (Hayer et al., 2010b). Since we exclusively used cell lines from human origin as our experimental systems, this excluded unspecific effects from differences in the CAV1 amino-acid sequence between the two species. To verify that ubiquitination and subcellular localization of human CAV1-HA in immunofluorescence microscopy was comparable to dog CAV1-HA or human CAV1-myc, we transfected these CAV1 variants into U2OS cells. The cells were stained with antibodies specific for either the HA- or myc-tag, and ubiquitin (FK2). Previous studies of overexpressed dog CAV1-HA showed that CAV1 localized to GFP-RAB marked early endosomes. Furthermore, CAV1 wild type but not the lysine-less CAV1 K5-176R colocalized with ubiquitin signal on endosomes (Hayer et al., 2010b; Ritz et al., 2011). Here, we confirmed the localization of dog CAV1-HA wild type and K5-176R to endosomes and the colocalization of dog CAV1-HA wild type positive endosomes with ubiquitin signal (Figure 3.1 C). Importantly, also the newly generated human CAV1-HA as well as the CAV1-myc constructs localized to endosomes. Consistently, only the wild type variants colocalized with ubiquitin signal comparable to dog CAV1-HA.

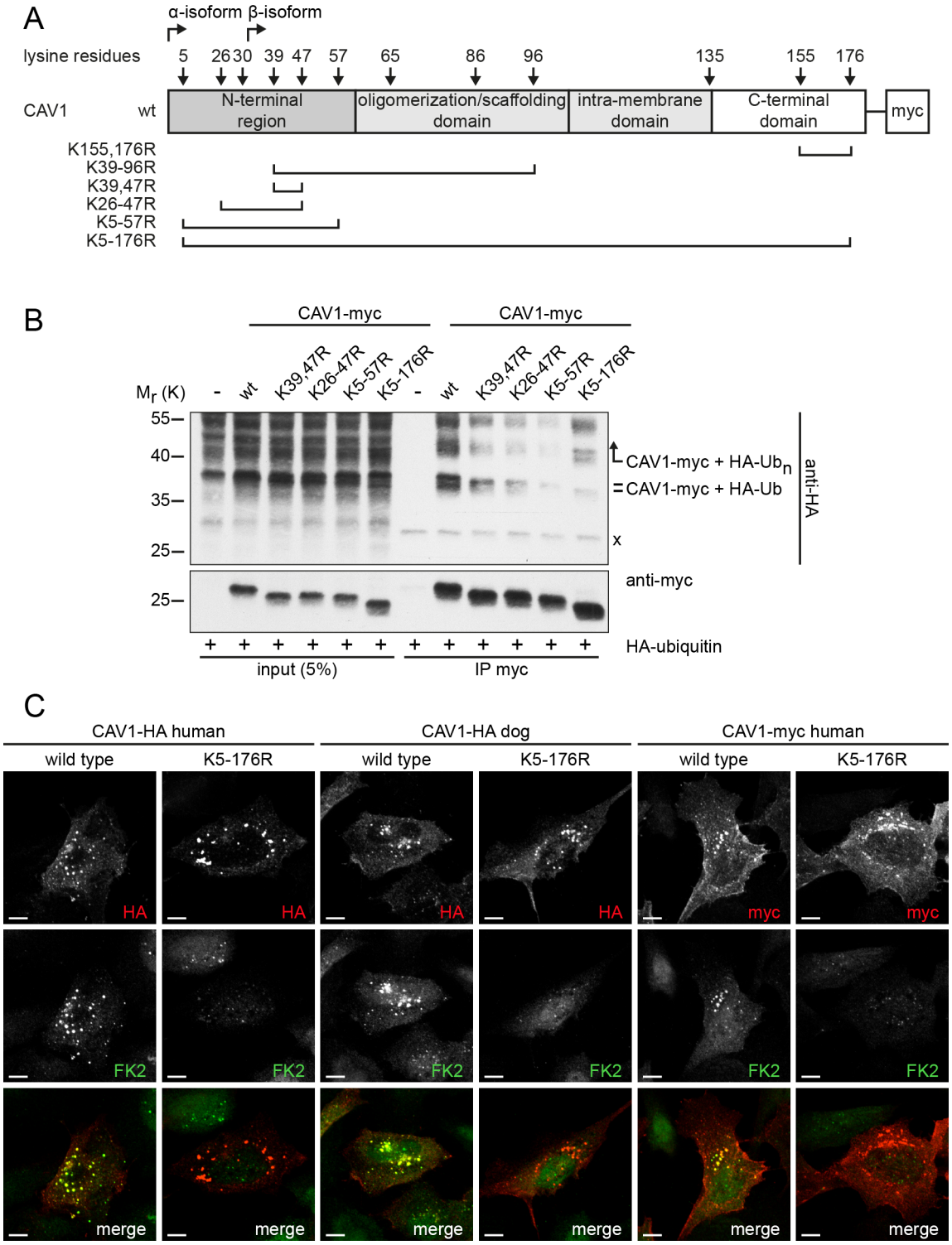


Figure 3.1 **CAV1-myc is modified with HA-ubiquitin and shows subcellular distribution and ubiquitination similar to human, or dog CAV1-HA.**
A, domain structure of the caveolin-1 (CAV1) protein showing the position of all lysine residues. Brackets indicate the groups of lysine residues in CAV1-myc that were mutated to arginine in this experiment. B, mutation of lysines in the N-terminal region interferes with ubiquitination of CAV1-myc. HEK293 cells were transfected with pcDNA3.1 empty vector (-), CAV1-myc wild type, or indicated variants in combination with HA-ubiquitin and lysed after 24 h. Cell lysates were immunoprecipitated using myc-specific antibodies. Immunoprecipitates (IP) were analyzed together with input samples in Western blotting using HA- and myc-specific antibodies. CAV1-myc modified with one (CAV1-myc + HA-Ub) or several (CAV1-myc + HA-Ub$_n$) HA-

ubiquitin moieties is indicated. The cross marks the position of the antibody light chain. C, CAV1 variants with different tags and from different species show the same localization and colocalization with ubiquitin. U2OS cells were transiently transfected with CAV1-HA wild type or K5-176R of either human or dog origin or CAV1-myc wild type or K5-57R of human origin and formaldehyde fixed after 24 h. The cells were stained with HA- and ubiquitin (FK2)-specific antibodies. Images were acquired by spinning disk microscopy using an x 100 objective. Representative images are shown. Scale bars = 10 µm.

Taken together, using CAV1-myc we could confirm modification of CAV1 with predominantly mono-ubiquitin and found indications that CAV1 might be ubiquitinated in the N-terminal region. Furthermore, we generated human HA-tagged CAV1 and could show that it localized to endosomes and colocalized with ubiquitin signal comparable to dog CAV1-HA. This human CAV1-HA enabled us to investigate the ubiquitination of a CAV1 variant that originated from the same species as our cell lines without introducing an additional lysine through the tag.

### 3.1.2 The lysines in the N-terminal region of CAV1 are sufficient and required for CAV1 ubiquitination

After establishing an appropriate experimental system to analyze the ubiquitination of CAV1, we investigated the effect of mutating groups of lysines in CAV1-HA to arginine. Based on the domain assignment of CAV1 (Figure 3.2 A) and the preliminary results gathered with CAV1-myc (Figure 3.1 B), we mutated the six lysines in the N-terminal region of CAV1-HA (K5-57R). A converse variant with the six lysines that are not part of the N-terminal region mutated to arginine (K65-176R) was generated additionally to a lysine-less CAV1-HA (K5-176R). The mutagenized CAV1-HA variants were transfected into U2OS cells and cell lysates were probed in Western blotting with caveolin-1-specific antibodies (Figure 3.2 B) CAV1-HA migrated slightly above endogenous CAV1 due to the additional residues of the HA-tag. In addition to the unmodified CAV1-HA wild type protein, we observed several slower migrating ubiquitinated species that correspond to the mono- and multi-ubiquitinated CAV1 described above and in previous studies (Ritz et al., 2011). This ubiquitination was unchanged by mutation of the six lysines that are not part of the N-terminal region of CAV1 (K65-176R). However, we did not observe ubiquitination of the CAV1 variant lacking the lysines of the N-terminal region (K5-57R) or the lysine-less CAV1 (K5-176R).

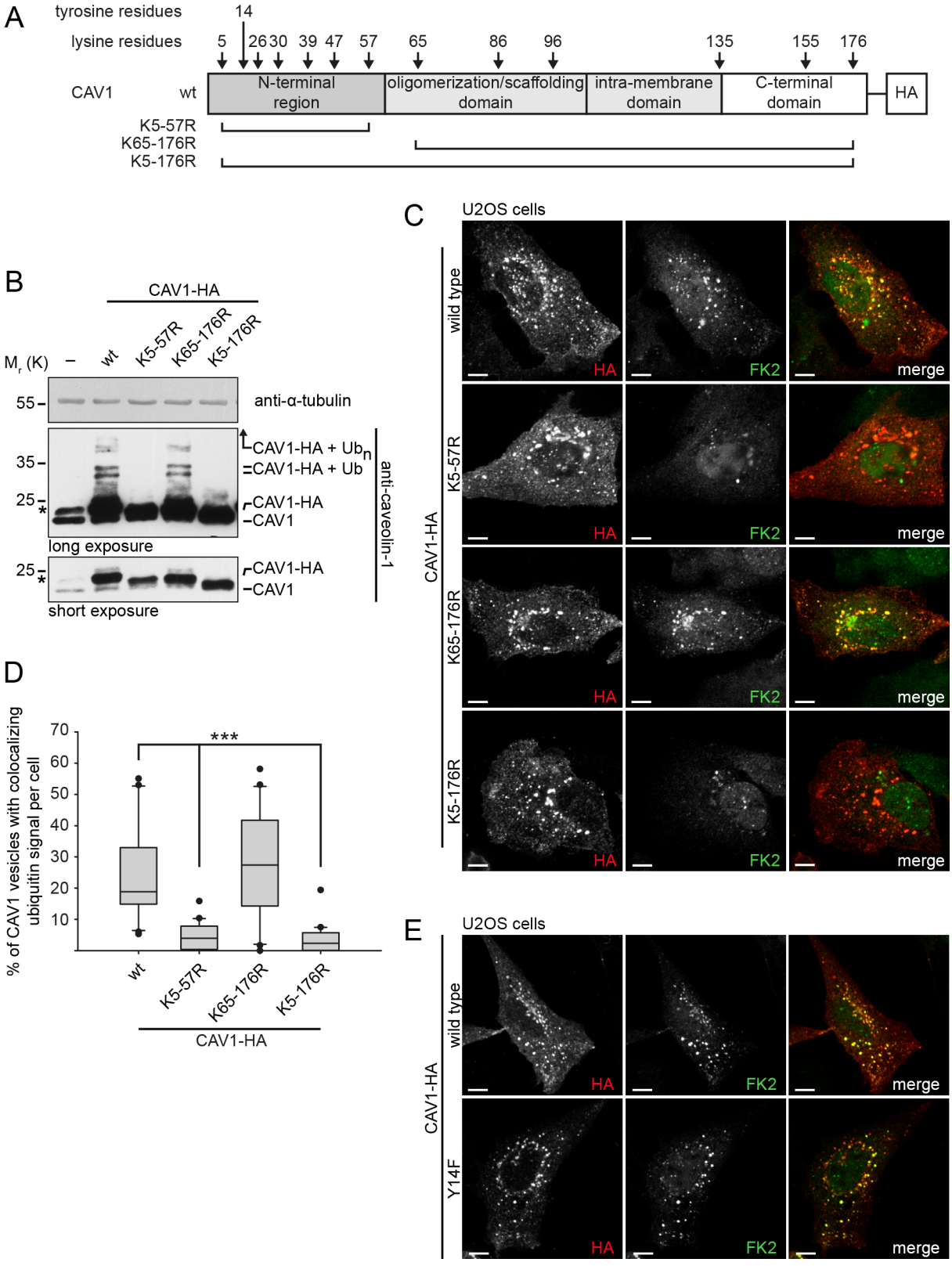


Figure 3.2 **Mutation of lysines in the N-terminal region prevents ubiquitination of CAV1.**
A, domain structure of the caveolin-1 (CAV1) protein showing the position of all lysine residues and the position of tyrosine-14 in the N-terminal region. Brackets indicate the groups of lysine residues in CAV1-HA that were mutated to arginine in this experiment. B, ubiquitination of CAV1-HA variants in U2OS cells. U2OS cells were transfected with pcDNA3.1 empty vector (-), CAV1-HA wild type, or indicated variants and lysed after 24 h. Cell lysates were analyzed in Western blotting using caveolin-1-

specific antibodies. Staining for α-tubulin served as a loading control. The asterisk indicates an unspecific band recognized by the anti-caveolin-1 antibody that was visible after long exposure. The position of mono-ubiquitinated (CAV1-HA + Ub) or multi-ubiquitinated (CAV1-HA + $Ub_n$) CAV1-HA is indicated. C, colocalization of CAV1-HA positive endosomes with ubiquitin signal in U2OS cells. U2OS cells were transfected with CAV1-HA wild type or indicated variants and formaldehyde fixed after 24 h. The cells were stained with HA- and ubiquitin (FK2)-specific antibodies and visualized by spinning disk microscopy using an x 100 objective. Representative images are shown. Scale bars = 10 µm. D, quantification of C. Automated identification of CAV1-HA vesicles and colocalization with ubiquitin (FK2) signal was carried out as detailed in "material and methods". Whiskers indicate the $10^{th}/90^{th}$ percentile and (•) indicates outliers. ***, $p < 0.001$, n = 20 cells/condition. E, ubiquitination of a phosphorylation-deficient CAV1 variant (Y14F). U2OS cells were transfected with CAV1-HA wild type or the Y14F variant and processed for immunofluorescence microscopy as in C. Scale bars = 10 µm.

To support the finding that the lysines 5 to 57 are required for ubiquitination of CAV1, we investigated localization of overexpressed CAV1 and colocalization with ubiquitin signal in immunofluorescence microscopy. Based on colocalization with the overexpressed early endosomal marker protein GFP-RAB5, we could confirm published data (Hayer et al., 2010b; Ritz et al., 2011) that CAV1 localized to endosomes independently of the mutations (data not shown). These CAV1 endosomes colocalized with ubiquitin signal in cells overexpressing CAV1 wild type but not the lysine-less CAV1 K5-176R (Figure 3.2 C). Importantly, also the CAV1 variant that was mutated in the N-terminal region (K5-57R) did not colocalize with ubiquitin. The CAV1 K65-176R variant, on the other hand, colocalized with ubiquitin signal comparable to CAV1 wild type. These differences were quantified using an ImageJ routine that measured colocalization with ubiquitin for each CAV1 vesicle within a cell. This analysis showed that a median of about 20% of CAV1 vesicles in CAV1 wild type expressing cells colocalized with the ubiquitin signal (Figure 3.2 D). The colocalization was significantly reduced for the N-terminal (K5-57R) and full (K5-176R) mutant of CAV1-HA. Mutation of the lysines that are not part of the N-terminal region of CAV1 (K65-176R) had no significant effect on colocalization. This suggests together with the data from Western blotting that the lysines in the N-terminal region but not the lysines in the other domains are critical for CAV1 ubiquitination. Interestingly, the N-terminal region harbors another regulatory residue. Phosphorylation on tyrosine-14 was described to regulate caveolae-mediated endocytosis and cell adhesion (del Pozo et al., 2005; Sverdlov et al., 2007). To investigate the effect of phosphorylation in the N-terminal region, we generated a phosphorylation-deficient variant of CAV1 with tyrosine-14 mutated to phenylalanine

(Y14F). The Y14F variant was expressed in U2OS cells and the cells were stained with HA- and ubiquitin (FK2)-specific antibodies (Figure 3.2 E). The CAV1 Y14F variant was less efficiently expressed compared to CAV1 wild type but showed no difference in localization to endosomal vesicles or colocalization with ubiquitin.

### 3.1.3 Ubiquitination of CAV1 in the N-terminal region is promiscuous

The ubiquitination site in the N-terminal region of CAV1 comprises half of all lysines in the CAV1 protein. In this context, we investigated the contribution of individual lysines in the N-terminal region towards CAV1 ubiquitination. First, we generated CAV1 variants with individual lysines of the N-terminal region mutated to arginine and expressed them in U2OS cells. The cell lysates were investigated by Western blotting using specific anti-caveolin-1 antibodies as described above. Interestingly, mutation of individual lysines did not affect the ubiquitination of CAV1 (Figure 3.3 A). The variation in intensity of the ubiquitination bands resulted from unequal expression of the CAV1 variants that was observed in shorter exposures of the caveolin-1 staining. This suggested that no individual lysine in the N-terminal region acted as the main acceptor for ubiquitin. To analyze if all lysines of the N-terminal region could be ubiquitinated equally well, we re-introduced individual lysines of the N-terminal region into the lysine-less variant of CAV1-HA and expressed these variants in U2OS cells (Figure 3.3 B). Importantly, re-introducing a single lysine at any of the six positions in the N-terminal region restored ubiquitination to the otherwise non-ubiquitinatable lysine-less CAV1 K5-176R. However, not all lysines were ubiquitinated with equal efficiency. While the lysines 39 and 47 were ubiquitinated the strongest, the lysines 30 and 57 served only as weak ubiquitin acceptors. Interestingly, re-introducing individual lysines into CAV1 K5-176R resulted in a single mono-ubiquitination band in contrast to the double band that was observed for CAV1 wild type mono-ubiquitination. In particular, ubiquitin conjugation at the lysines 5, 26, or 30 resulted in a slower migrating band, while conjugation at the lysines 39, 47, or 57 resulted in a slightly faster migrating band. Furthermore, if lysines from each sub-region were re-introduced into CAV1 K5-576R together (R30,39K) a double band was observed, but not if two lysines from the same sub-region (R39,47K) were re-introduced. This suggested that the site of ubiquitin conjugation influences the migratory behavior of CAV1 in SDS gels.

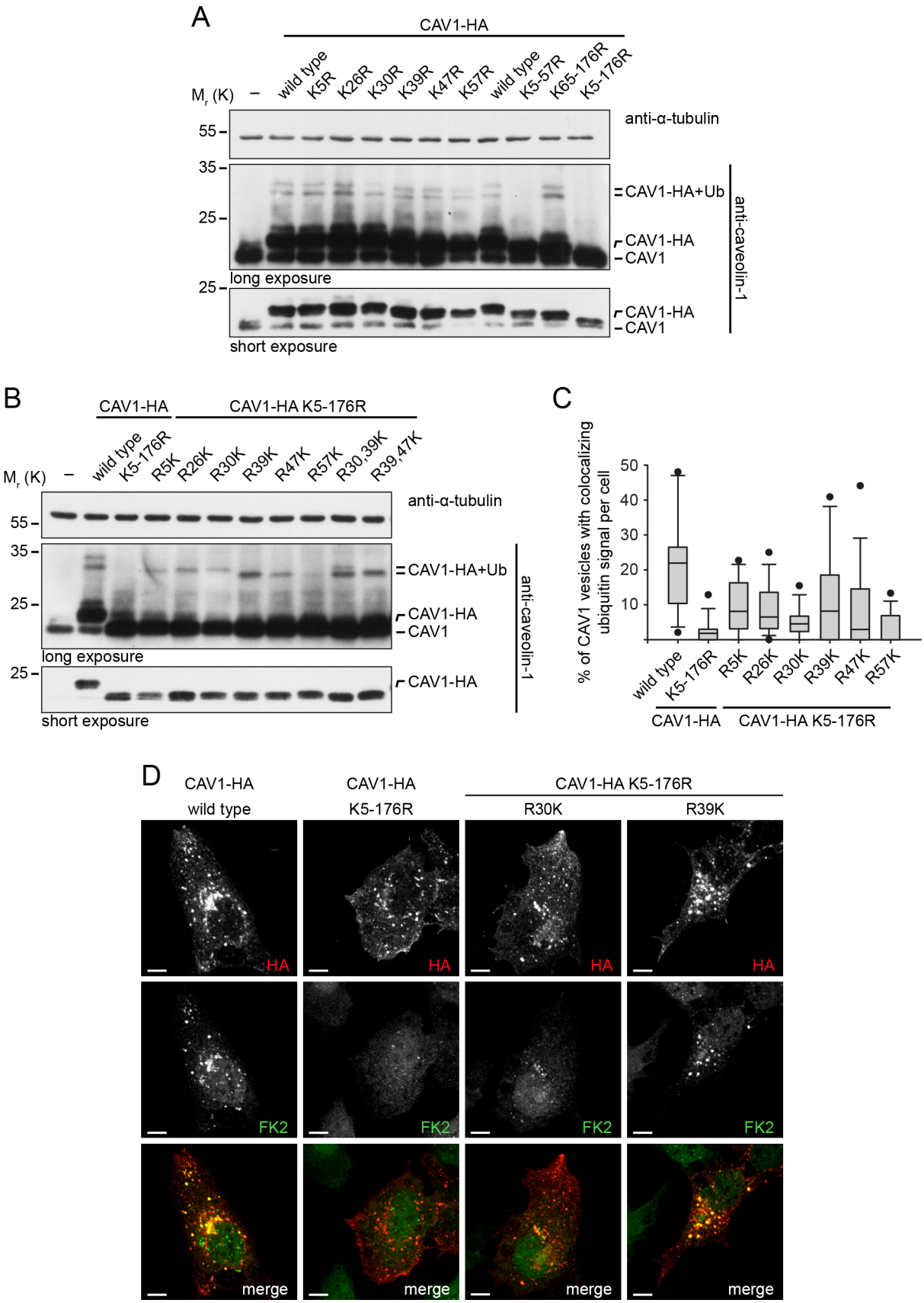


Figure 3.3 **Any lysine in the N-terminal region of CAV1 can serve as acceptor site for ubiquitination.**

A, mutation of single lysines in the N-terminal region does not affect CAV1 ubiquitination. U2OS cells were transfected with pcDNA3.1 empty vector (-), CAV1-HA wild type, or variants with a single lysine mutated to arginine, or the variants

described in Figure 3.2 B and lysed after 24 h. Cell lysates were analyzed in Western blotting using caveolin-1-specific antibodies. Staining for α -tubulin served as a loading control. The position of mono-ubiquitinated (CAV1-HA + Ub) CAV1-HA is indicated. B, ubiquitination of individual lysines in the N-terminal region of CAV1. U2OS cells were transfected with pcDNA3.1 empty vector (-), CAV1-HA wild type, K5-176R, or variants with individual lysines of the N-terminal region re-introduced into CAV1-HA K5-176R and processed for Western blotting as in A. Staining for α-tubulin served as a loading control. The position of mono-ubiquitinated (CAV1-HA + Ub) CAV1-HA is indicated. C, quantification of colocalization between CAV1 variants harboring individual lysines of the N-terminal region and ubiquitin signal. U2OS cells were transfected with CAV1-HA wild type, K5-176R, or the K5-176R variants harboring individual lysines and formaldehyde fixed after 24 h. The cells were stained with HA- and ubiquitin (FK2)-specific antibodies and visualized by spinning disk microscopy using an x 100 objective. Colocalization of CAV1 vesicles with ubiquitin signal was quantified by automated image analysis. Whiskers indicate the $10^{th}$/$90^{th}$ percentile and (•) indicates outliers. n = 15 cells/condition. D, exemplary micrographs of the images used for the quantification in C. Scale bars = 10 µm.

We confirmed these results by automated quantification of colocalization between CAV1 vesicles and ubiquitin signal in immunofluorescence microscopy (Figure 3.3 C and D). As expected from Western blotting, all CAV1 K5-176R variants harboring individual lysines of the N-terminal region showed colocalization with ubiquitin staining in contrast to lysine-less CAV1 K5-176R. However, the median percentage of CAV1 vesicles that colocalized with ubiquitin signal was reduced in comparison to CAV1 wild type. This difference was very pronounced for the R30K and R57K variants but less so for the R39K and R47K variants. This corresponds to the differences in ubiquitination that were observed in Western blotting. Representative micrographs of the images used in this analysis are shown for CAV1 wild type, K5-176R, R30K, and R39K (Figure 3.3 D).

Taken together, we established an experimental set up that allowed us to investigate the ubiquitination of CAV1 in Western blotting and immunofluorescence microscopy. Utilizing these assays, we could identify the lysines in the N-terminal region of CAV1 as necessary and sufficient for CAV1 ubiquitination. This enabled us in the following to investigate the functional consequences of CAV1 ubiquitination without mutating all lysines in the CAV1 protein.

## 3.2 Ubiquitination regulates endosomal trafficking of CAV1

The lysine-less CAV1 K5-176R variant has a markedly increased half-life compared to CAV1 wild type (Hayer et al., 2010b). Furthermore, treatment with lysosome inhibitors increases the half-life of overexpressed CAV1 wild type. In this context, we wanted to investigate the functional connection between CAV1 ubiquitination and endosomal sorting and lysosomal degradation of CAV1. Therefore, we transfected U2OS cells with CAV1 wild type or the non-ubiquitinatable CAV1 K5-57R variant and investigated the effect of mutating the ubiquitination site in the N-terminal region on endosomal sorting and lysosomal degradation of CAV1.

### 3.2.1 Transport of CAV1 to the lysosome depends on ubiquitination of CAV1

Lysosomal degradation of membrane proteins requires endosomal trafficking from early to late endosomes resulting in formation of multivesicular endosomes that fuse with lysosomes (Huotari and Helenius, 2011). Consequentially, we first investigated if the non-ubiquitinatable variants of CAV1 were efficiently transported to late endosomes and lysosomes. U2OS cells were transfected with CAV1-HA variants and stained with HA- and LAMP1 (lysosome-associated membrane glycoprotein)-specific antibodies. The LAMP1 protein localizes to membranes of the late endosomal and lysosomal compartment and stained many small vesicles throughout the cytoplasm in formaldehyde fixed cells (Figure 3.4 A). In cells overexpressing CAV1 wild type or the ubiquitinatable CAV1 K65-176R variant, a small number of CAV1 vesicles colocalized with LAMP1 vesicles. In contrast, if the non-ubiquitinatable CAV1 variants K5-57R or K5-176R were overexpressed the number of CAV1 vesicles colocalizing with LAMP1 signal was greatly reduced. This result was confirmed by automated quantification of colocalization with the same ImageJ routine we employed for analysis of colocalization between CAV1 vesicles and ubiquitin signal. The quantification showed that in cells expressing the CAV1 wild type a median of about 7% of CAV1 vesicles colocalized with LAMP1 signal (Figure 3.4 B). A comparable median percentage of CAV1 K65-176R vesicles colocalized with LAMP1, indicating an equally efficient transport to late endosomes/lysosomes. Crucially, the median percentage of CAV1 vesicles colocalizing with LAMP1 signal was significantly reduced in cells expressing the non-ubiquitinatable CAV1 K5-57R variant that is mutated in the N-terminal region. This reduction in colocalization was comparable to the lysine-less CAV1 K5-176R variant and was consistent with the phenotype observed in the micrographs. These data demonstrated that ubiquitination of CAV1 in

the N-terminal region was required for efficient transport of CAV1 to late endosome/lysosomes.

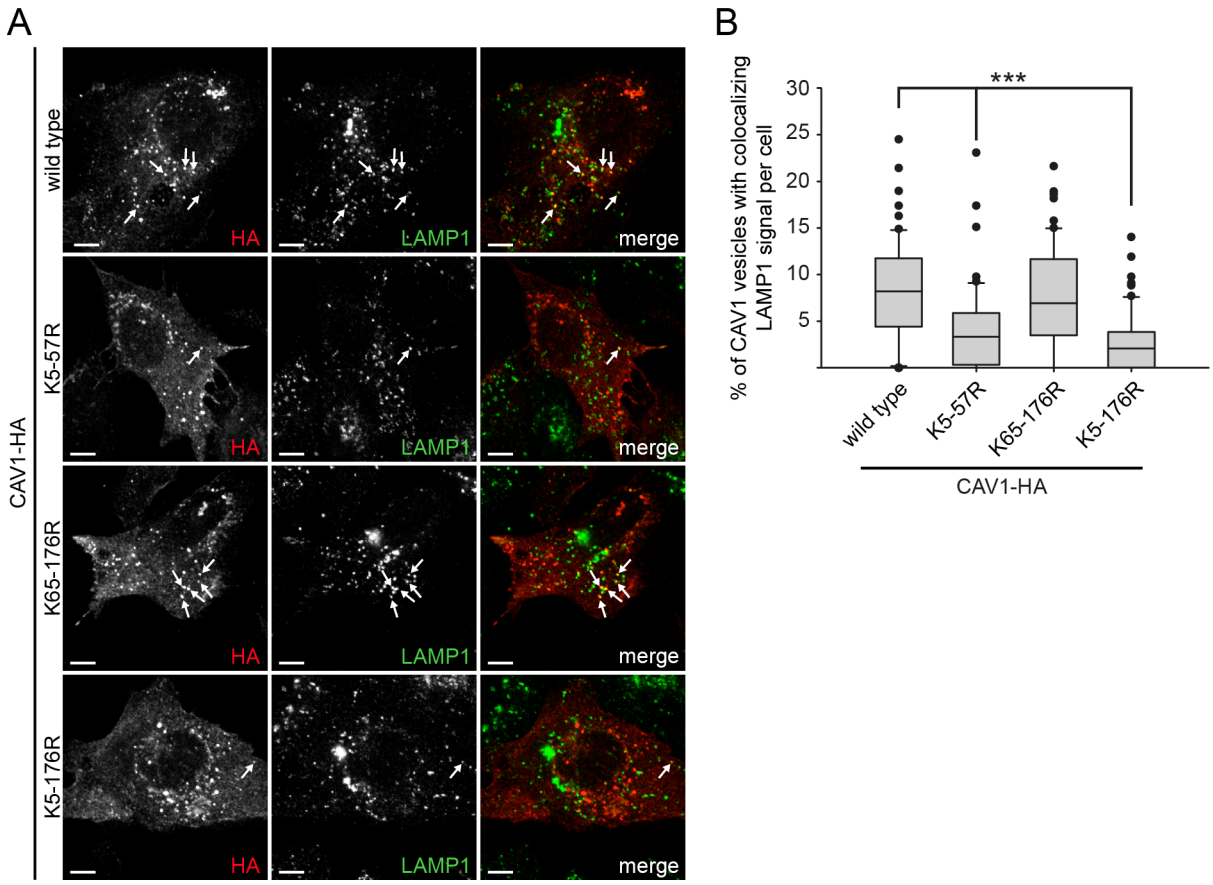


Figure 3.4 **Ubiquitinatable variants of CAV1 colocalize with the late endosome/lysosome marker protein LAMP1.**
A, trafficking of CAV1 to late endosomes/lysosomes requires the ubiquitination site in the N-terminal region. U2OS cells were transfected with CAV1-HA wild type or indicated variants and formaldehyde fixed after 24 h. The cells were stained with HA- and LAMP1-specific antibodies. Images were acquired by spinning disk microscopy using an x 100 objective. Representative images are shown, arrows indicate colocalizing vesicles. Scale bars = 10 µm. B, quantification of A. Automated identification of CAV1-HA vesicles and colocalization with LAMP1 signal was carried out as detailed in “material and methods”. Whiskers indicate the $10^{th}$/$90^{th}$ percentile and (•) indicates outliers. ***, $p < 0.001$, $n = 60$ cells/condition from three independent experiments.

### 3.2.2 Autophagy may partially play a role in degradation of overexpressed CAV1 wild type

We could show that CAV1 is trafficked to late endosomes/lysosomes in an ubiquitination dependent manner. In addition to endosomal sorting, ubiquitinated proteins can be delivered to the lysosome through ubiquitin-specific autophagy. In autophagy, a double-membrane structure encircles for example protein aggregates targeted for degradation and forms an autophagosome. Subsequently, autophagosomes fuse with multivesicular bodies or lysosomes to degrade their cargo

(Weidberg et al., 2011). Therefore, we investigated if autophagy could play a role in degradation of transiently overexpressed CAV1 in addition to endosomal sorting. We co-transfected U2OS cells with CAV1-HA variants and the autophagosome marker LC3 (microtubule-associated proteins 1A/1B light chain 3A)-GFP (Figure 3.5 A). In control-transfected cells LC3-GFP was distributed uniformly throughout cytoplasm and nucleus comparable to GFP alone. In few cells LC3-GFP accumulated in small perinuclear spots. Interestingly, overexpression of CAV1 wild type caused accumulation of LC3-GFP in few larger vesicles near the nucleus that colocalized with CAV1 vesicles. In contrast, overexpression of the non-ubiquitinatable CAV1 K5-57R variant did not result in accumulation of LC3-GFP in perinuclear vesicles and, as a consequence, no colocalization between CAV1 K5-57R and LC3-GFP could be observed. To confirm these data using a second marker for autophagosomes, we transfected U2OS cells with CAV1-HA variants and stained the cells with antibodies specific for the ubiquitin-adapter protein p62/SQSTM1. The ubiquitin-adapter p62 recognizes ubiquitinated protein aggregates and directs them to autophagy via direct binding to LC3 (Kirkin et al., 2009b). In control-transfected cells, p62 was observed in many small vesicles that concentrated around the nucleus (Figure 3.5 B). Furthermore, preventing the degradation of autophagosomes with the lysosome inhibitor bafilomycin A1 caused a striking accumulation of p62 vesicles (data not shown). After overexpression of CAV1-HA wild type, the number and also the staining intensity of p62 vesicles increased in comparison to control transfected cells and a large fraction of CAV1 vesicles colocalized with these p62 spots. It should be noted that the number of CAV1 vesicles colocalizing with p62 was markedly higher than the number of CAV1 vesicles colocalizing with LC3-GFP. However importantly, in cells overexpressing the non-ubiquitinatable CAV1-HA K5-57R no increase in number of p62 spots was observed. Consistently, colocalization between CAV1 K5-57R vesicles and p62 was rare. These experiments provided evidence that at least a fraction of overexpressed CAV1 might be funneled into the autophagy system in an ubiquitin-dependent manner.

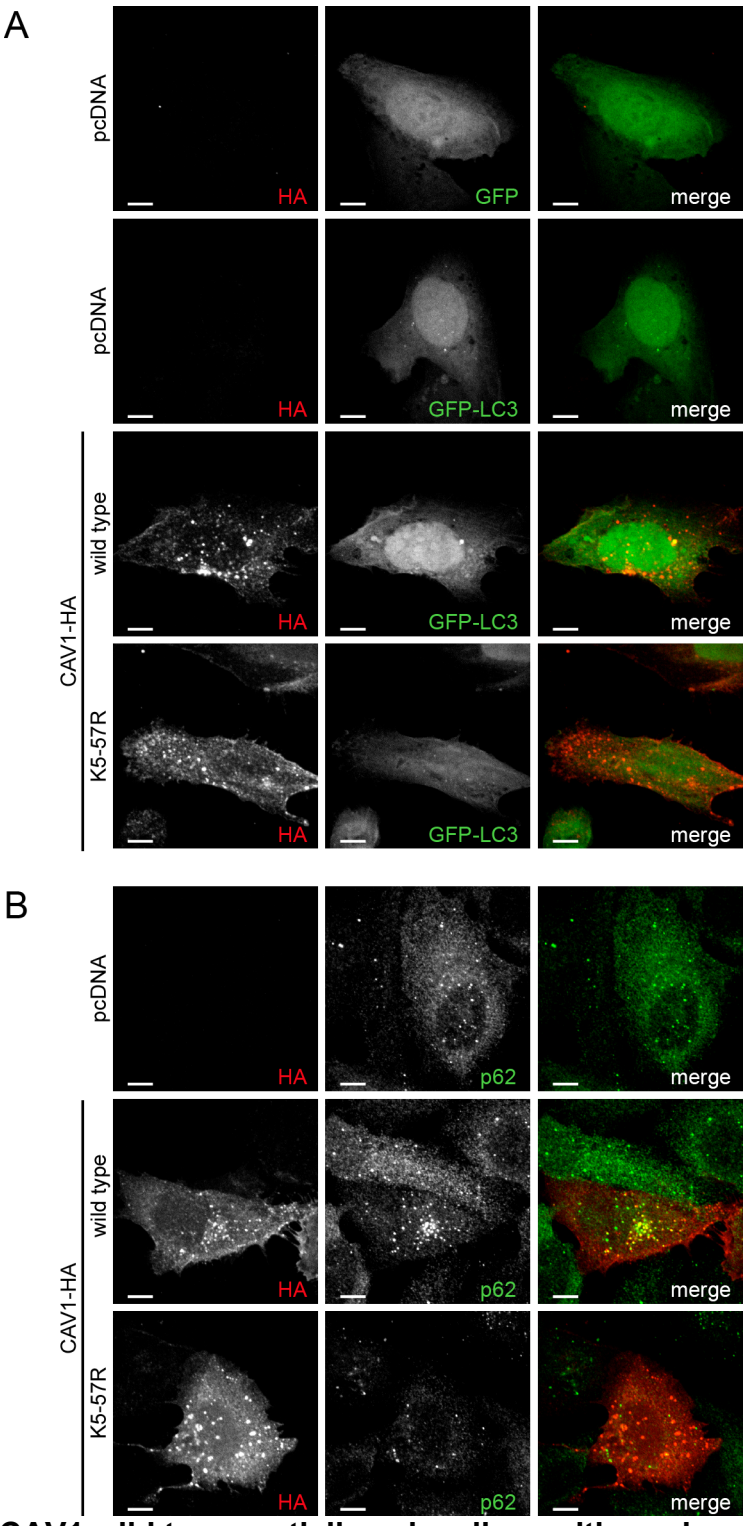


Figure 3.5 **CAV1 wild type partially colocalizes with markers for autophagy.** A, CAV1-HA wild type but not the non-ubiquitinatable CAV1-HA K5-57R partially colocalizes with LC3-GFP vesicles. U2OS cells were co-transfected with pcDNA3.1 empty vector, CAV1-HA wild type, or CAV1 K5-57R and GFP or LC3-GFP and formaldehyde fixed after 24 h. The cells were stained with HA-specific antibodies and visualized by spinning disk microscopy using an x 100 objective. Representative images are shown. Scale bars = 10 µm. B, CAV1-HA wild type colocalizes with the ubiquitin-adapter p62/SQSTM1. U2OS cells were transfected with pcDNA3.1 empty vector, CAV1-HA wild type, or CAV1 K5-57R and formaldehyde fixed after 24 h. The cells were stained with HA- and p62-specific antibodies. Images were acquired as in A. Representative images are shown. Scale bars = 10 µm.

### 3.2.3 Mutation of the N-terminal lysines has no effect on CAV1 biosynthesis and oligomerization

The CAV1 protein is cotranslationally inserted into the endoplasmic reticulum (ER) where it oligomerizes and subsequently transported to the Golgi apparatus. Oligomers assemble into higher order structures and are transported to the plasma membrane in vesicular carriers (Hayer et al., 2010a). Mutations in the CAV1 protein might not only affect ubiquitination and endosomal sorting but could also influence the biosynthesis of CAV1. To exclude that overexpressed CAV1 wild type or mutant variants accumulated in the biosynthetic pathway, we stained CAV1 in transiently transfected U2OS cells together with specific markers of the ER and Golgi apparatus. First, we investigated the colocalization of overexpressed CAV1 with the ER membrane protein UBXD8. UBXD8 is a cofactor of the AAA-ATPase p97 and associates with p97 for the extraction of misfolded protein during ER associated degradation (ERAD) (Mueller et al., 2008). U2OS cells were transfected with CAV1-HA variants and stained with HA- and UBXD8-specific antibodies (Figure 3.6 A). In control-transfected cells, UBXD8 was distributed in small spots throughout the cell with increasing density around the nucleus. This distribution was not visibly changed after expression of either CAV1 wild type or the non-ubiquitinatable K5-57R variant. Importantly, no CAV1-HA variant showed colocalization with the ER membrane protein UBXD8. To test if overexpressed CAV1 was able to exit the ER and was transported to the Golgi apparatus, we investigated colocalization of CAV1-HA with the ER-exit site marker SEC31A. ER-exit sites are special regions of the ER where vesicles bud off for ER to Golgi transport (Tang et al., 2000). In control-transfected cells the SEC31A staining appeared as small spots with increased density around the nucleus, comparable to the pattern of UBXD8 staining (Figure 3.6 B). This distribution was not affected by overexpression of either CAV1 wild type or the non-ubiquitinatable K5-57R variant. In fact, no colocalization between CAV1 vesicles and the ER exit site marker SEC31A could be observed. From the ER, CAV1 is further transported to the Golgi apparatus where it binds cholesterol and oligomerizes.

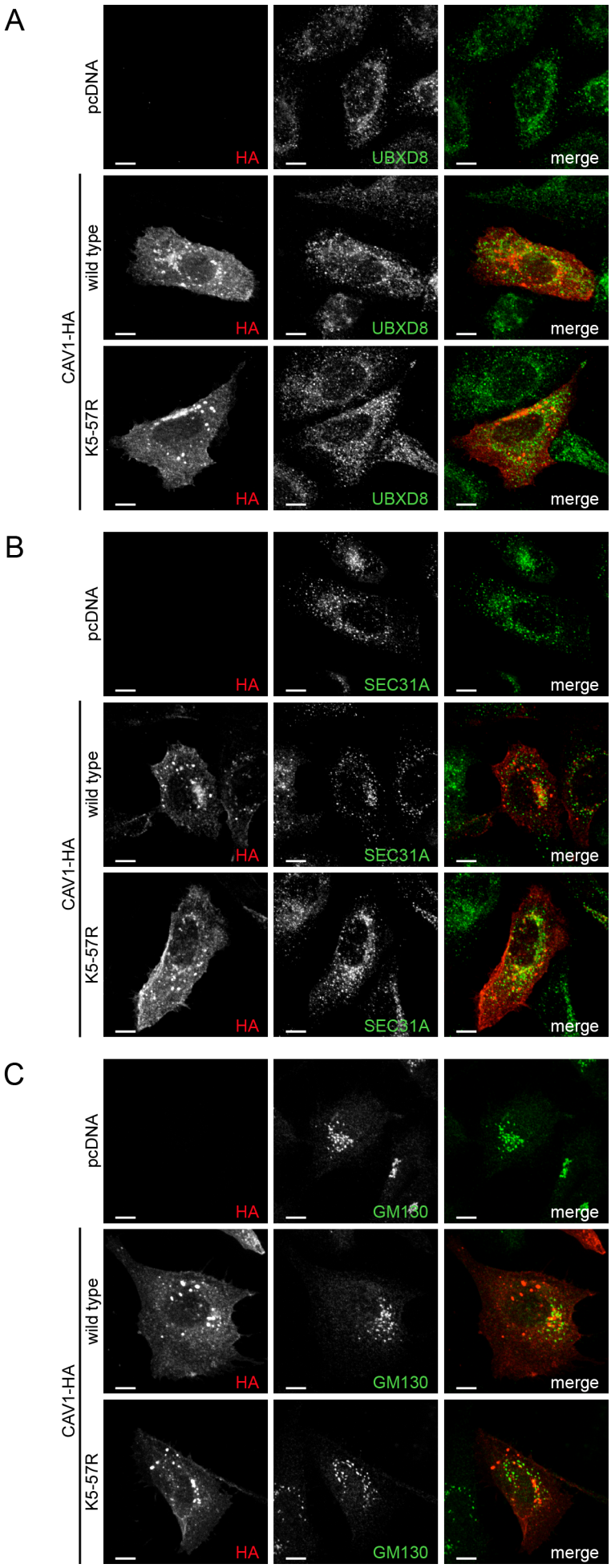
A
pcDNA
HA
UBXD8
merge
CAV1-HA
wild type
HA
UBXD8
merge
K5-57R
HA
UBXD8
merge
B
pcDNA
HA
SEC31A
merge
CAV1-HA
wild type
HA
SEC31A
merge
K5-57R
HA
SEC31A
merge
C
pcDNA
HA
GM130
merge
CAV1-HA
wild type
HA
GM130
merge
K5-57R
HA
GM130
merge

Figure 3.6 **Wild type and non-ubiquitinatable CAV1 do not colocalize with markers for ERAD or ER-exit sites and are exported from the Golgi apparatus.** A, CAV1-HA does not colocalize with the ERAD cofactor UBXD8. U2OS cells were transfected with pcDNA3.1 empty vector, CAV1-HA wild type, or CAV1 K5-57R and methanol fixed after 24 h. The cells were stained with HA- and UBXD8-specific antibodies and visualized by spinning disk microscopy using an x 100 objective. Representative images are shown. Scale bars = 10 µm. B, CAV1 does not accumulate at ER-exit sites marked by SEC31A. U2OS cells were transfected, processed for immunofluorescence microscopy as in A, and stained with HA- and SEC31A-specific antibodies. Images were acquired as in A. Scale bars = 10 µm. C, a small fraction of CAV1-HA vesicles colocalizes with GM130-positive Golgi vesicles. U2OS cells were transfected as in A, formaldehyde fixed after 24 h and stained with HA- and GM130-specific antibodies. Images were acquired as in A. Scale bars = 10 µm.

To exclude accumulation of CAV1 in the Golgi apparatus, we stained CAV1-HA transfected U2OS cells with specific antibodies for HA and the Golgi matrix protein GM130. In control-transfected cells, GM130 localized to a dense patch of large vesicles on one side of the nucleus and overexpression of CAV1 wild type or CAV1 K5-57R did not change the subcellular distribution of GM130 (Figure 3.6 C). Interestingly, we observed colocalization between a small fraction of CAV1 vesicles and GM130 staining that was comparable for CAV1 wild type and the non-ubiquitinatable K5-57R variant. In contrast, an oligomerization deficient mutant of CAV1 (P132L) that accumulates in the Golgi apparatus (Lee et al., 2002) strongly colocalized with GM130 signal in HeLa cells (data not shown). These experiments showed that the mutation of lysines in CAV1 had no effect on biosynthesis and oligomerization of CAV1.

### 3.2.4 Ubiquitination of CAV1 is required for sorting to early endosomes after endocytosis

We could confirm that the CAV1 vesicles we observed after overexpression of CAV1-HA variants did not result from accumulation of CAV1 in the biosynthetic pathway. Furthermore, we showed that trafficking of CAV1 to late endosomes/lysosomes required ubiquitination of CAV1 in the N-terminal region. Therefore, we analyzed if the non-ubiquitinatable variants accumulated in an endosomal compartment prior to the late endosome. We transfected U2OS cells with CAV1-HA and stained the cells with antibodies specific for marker proteins of the early endosomal compartment. In control-transfected cells, the early endosome antigen (EEA1) localized to many small vesicles that are dispersed throughout the cytoplasm with one denser cluster near the nucleus (Figure 3.7 A). Overexpression of CAV1 caused no visible changes in the subcellular localization of EEA1. However, in CAV1 wild type expressing cells,

the staining intensity of EEA1 vesicles was slightly increased and CAV1 vesicles frequently colocalized with EEA1 signal. Crucially, in cells transfected with the non-ubiquitinatable CAV1-HA K5-57R the colocalization between CAV1 and EEA1 was greatly reduced. We confirmed this observation using automated quantification of colocalization in ImageJ as described above. In CAV1 wild type expressing cells. a median of about 30% of CAV1 vesicles colocalized with EEA1. In consistence with the micrographs, this number was significantly reduced in cells expressing CAV1 K5-57R. To further support this result, we stained CAV1-HA transfected U2OS cells with antibodies specific for the small GTPase RAB5 as an additional marker for early endosomes. The intensity of the RAB5 staining was lower in comparison to EEA1 but showed the same subcellular localization (Figure 3.7 B). In a separate experiment, we could confirm that almost all RAB5 vesicles were also positive for EEA1 staining (data not shown). Overexpression of CAV1 wild type induced accumulation of RAB5 on larger vesicles near the nucleus that colocalized with CAV1. Consistently, no colocalization was observed in cells overexpressing the non-ubiquitinatable CAV1 K5-57R. Quantification of this colocalization in ImageJ confirmed that the number of CAV1 vesicles with colocalizing RAB5 staining was significantly reduced from a median of about 50% to less than 20% in cells expressing CAV1 K5-57R. The higher percentage of CAV1 vesicles that colocalized with RAB5 in contrast to EEA1 probably resulted from the low RAB5 staining intensity and, therefore, increased detection of background signal. In cells overexpressing CAV1-HA wild type, the caveolar-coat protein PTRF/cavin-1-mCherry colocalizes with CAV1 on RAB5-GFP positive early endosomes (Hayer et al., 2010b). PTRF/cavin-1 is stably associated with the cytoplasmic face of caveolae and stays bound during endocytosis (Hill et al., 2008). Therefore, we stained PTRF/cavin-1 as a marker for caveolar vesicles in U2OS cells overexpressing CAV1-HA variants (Figure 3.7 C). In control-transfected cells PTRF/cavin-1 uniformly stained the plasma membrane in small dots. Overexpression of CAV1 induced accumulation of PTRF/cavin-1 in large vesicles that almost completely colocalized with CAV1 vesicles. Crucially, this colocalization was independent of the N-terminal lysines in CAV1. Additionally, the PTRF/cavin-1 vesicles that were induced by overexpression of the non-ubiquitinatable CAV1 K5-57R variant were more brightly stained.

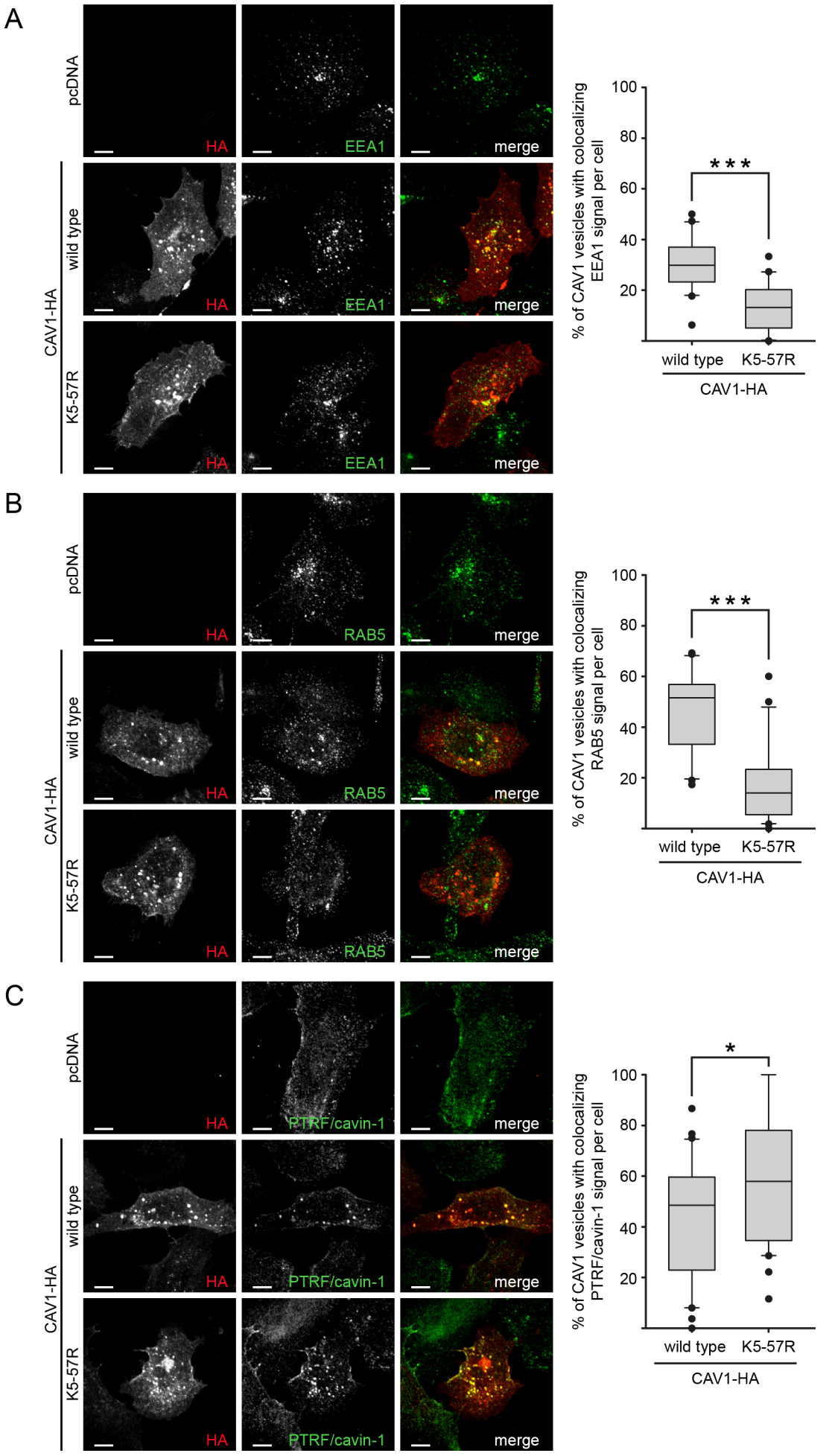
A
pcDNA
HA
EEA1
merge
CAV1-HA
wild type
HA
EEA1
merge
K5-57R
HA
EEA1
merge
% of CAV1 vesicles with colocalizing EEA1 signal per cell
100
80
60
40
20
* * *
wild type
K5-57R
CAV1-HA
B
pcDNA
HA
RAB5
merge
CAV1-HA
wild type
HA
RAB5
merge
K5-57R
HA
RAB5
merge
% of CAV1 vesicles with colocalizing RAB5 signal per cell
100
80
60
40
20
* * *
wild type
K5-57R
CAV1-HA
C
pcDNA
HA
PTRF/cavin-1
merge
CAV1-HA
wild type
HA
PTRF/cavin-1
merge
K5-57R
HA
PTRF/cavin-1
merge
% of CAV1 vesicles with colocalizing PTRF/cavin-1 signal per cell
100
80
60
40
20
*
wild type
K5-57R
CAV1-HA

Figure 3.7 **The non-ubiquitinatable CAV1 K5-57R does not colocalize with markers of the early endosome but accumulates together with PTRF/cavin-1.** A, localization of CAV1-HA to EEA1-positive early endosomes depends on ubiquitination of CAV1. U2OS cells were transfected with pcDNA3.1 empty vector, CAV1-HA wild type, or CAV1 K5-57R and formaldehyde fixed after 24 h. The cells were stained with HA- and EEA1-specific antibodies and visualized by spinning disk microscopy using an x 100 objective. Representative images are shown. Scale bars = 10 µm. Colocalization of CAV1-HA vesicles with EEA1 signal was quantified by automated image analysis. Whiskers indicate the $10^{th}/90^{th}$ percentile and (•) indicates outliers. ***, $p < 0.001$. n = 20 cells/condition from two independent experiments. B, ubiquitinated CAV1-HA colocalizes with the early endosome marker RAB5. U2OS cells were transfected and processed for immunofluorescence microscopy as in A. The cells were stained with HA- and RAB5-specific antibodies and images were acquired as in A. Scale bars = 10 µm. The percentage of CAV1-HA vesicles colocalizing with RAB5 signal was quantified as in A. Whiskers indicate the $10^{th}/90^{th}$ percentile and (•) indicates outliers. ***, $p < 0.001$. n = 20 cells/condition from two independent experiments. C, the non-ubiquitinatable CAV1-HA K5-57R accumulates together with PTRF/cavin-1. U2OS cells were transfected and processed for immunofluorescence microscopy as in A. The cells were stained with HA- and PTRF/cavin-1-specific antibodies and images were acquired as in A. Scale bars = 10 µm. The percentage of CAV1-HA vesicles colocalizing with PTRF/cavin-1 signal was quantified as in A. Whiskers indicate the $10^{th}/90^{th}$ percentile and (•) indicates outliers. *, $p < 0.05$. n = 30 cells/condition from three independent experiments.

To confirm this observation, we quantified the colocalization between CAV1 and PTRF/cavin-1 in ImageJ. In CAV1 wild type expressing cells, a median of about 50% of CAV1 vesicles colocalized with PTRF/cavin-1 signal. This colocalization was significantly increased to a median of above 60% of CAV1 vesicles in cells overexpressing the non-ubiquitinatable CAV1 K5-57R. These data indicated that ubiquitination of CAV1 might be necessary for trafficking of PTRF/cavin-1 positive caveolar vesicles to early endosomes.

Because the non-ubiquitinatable CAV1 K5-57R did not localize to the early endosome, we expected that the PTRF/cavin-1 vesicles that accumulate after CAV1 K5-57R expression would be negative for markers of the early endosome. Therefore, we overexpressed CAV1-HA variants in U2OS cells and stained the cells with PTRF/cavin-1- and EEA1-specific antibodies. The overexpressed CAV1-HA was not visualized due to technical limitations. However, as shown in Figure 3.7 C, large PTRF/cavin-1 vesicles were only observed after CAV1 overexpression and were almost identical with CAV1 vesicles. In control-transfected cells, PTRF/cavin-1 and EEA1 stained the plasma membrane or small vesicles respectively (Figure 3.8 A).

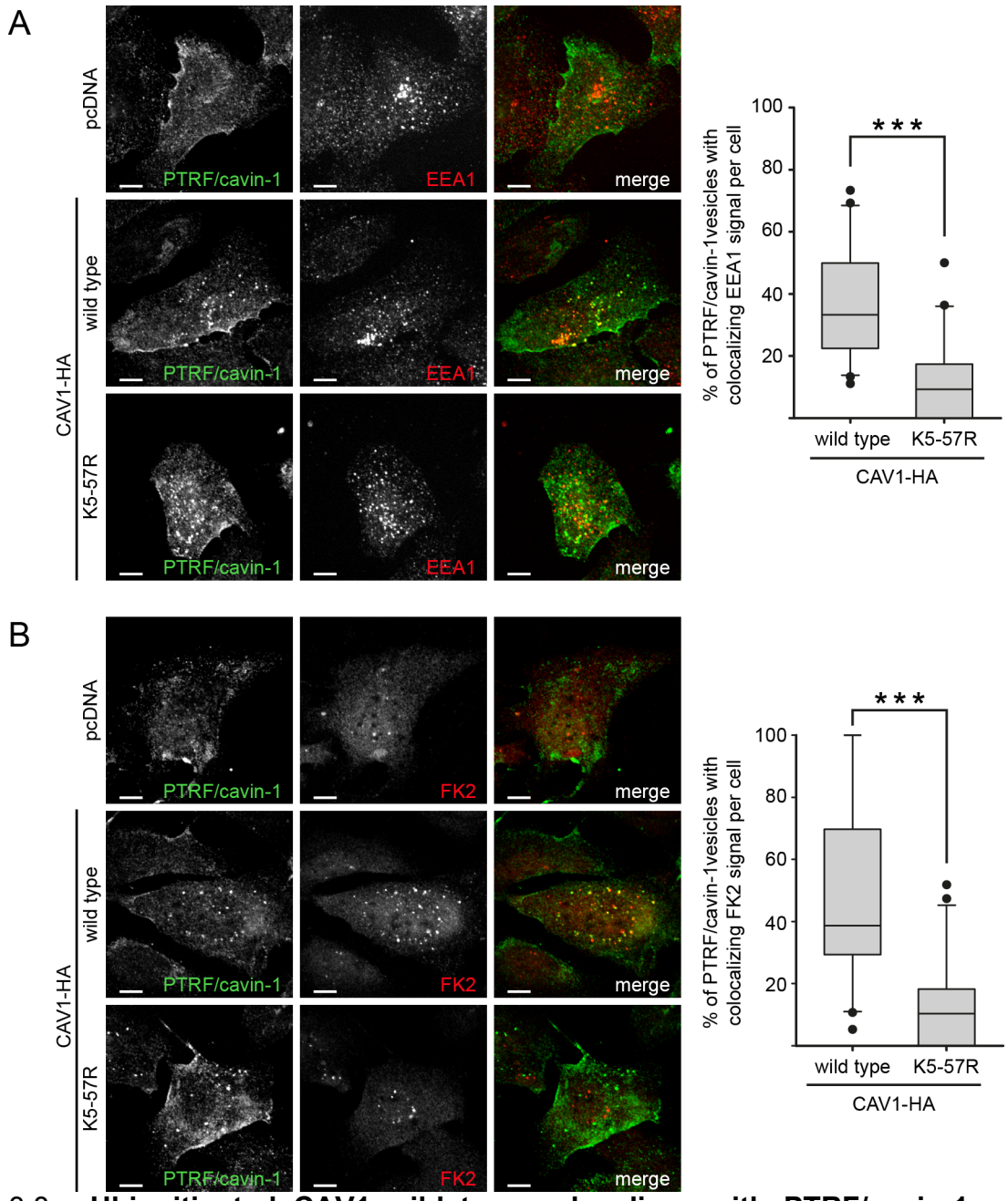


Figure 3.8 **Ubiquitinated CAV1 wild type colocalizes with PTRF/cavin-1 on early endosomes.**

A, PTRF/cavin-1 vesicles in CAV1-HA wild type expressing cells colocalize with the early endosome marker EEA1. U2OS cells were transfected with pcDNA3.1 empty vector, CAV1-HA wild type, or CAV1 K5-57R and formaldehyde fixed after 24 h. The cells were stained with PTRF/cavin-1- and EEA1-specific antibodies and visualized by spinning disk microscopy using an x 100 objective. Representative images are shown. Scale bars = 10 µm. Colocalization of PTRF/cavin-1 vesicles with EEA1 signal was quantified by automated image analysis. Whiskers indicate the $10^{th}$/$90^{th}$ percentile and (•) indicates outliers. ***, $p < 0.001$. n = 20 cells/condition from two independent experiments. B, CAV1-HA wild type is ubiquitinated on PTRF/cavin-1 vesicles. U2OS cells were transfected and processed for immunofluorescence microscopy as in A. The cells were stained with PTRF/cavin-1- and ubiquitin (FK2)-specific antibodies and images were acquired as in A. Scale bars = 10 µm. The percentage of PTRF/cavin-1 vesicles colocalizing with ubiquitin signal was quantified as in A. Whiskers indicate the $10^{th}$/$90^{th}$ percentile and (•) indicates outliers. ***, $p < 0.001$. n = 20 cells/condition from two independent experiments.

Crucially, overexpression of wild type CAV1 caused accumulation of PTRF/cavin-1 on vesicles that at least partially colocalized with EEA1-positive vesicles. Moreover, the colocalization between PTRF/cavin-1 vesicles and EEA1 was reduced in cells that overexpressed the non-ubiquitinatable CAV1 K5-57R. We confirmed this result by automated quantification of colocalization in ImageJ. In CAV1 wild type expressing cells, a median of more than 30% of PTRF/cavin-1 vesicles colocalized with EEA1 signal. This colocalization was significantly reduced in cells expressing CAV1 K5-57R. Finally, we analyzed if the wild type CAV1 on PTRF/cavin-1 positive vesicles is ubiquitinated. Therefore, we transfected U2OS cells with CAV1-HA and stained the cells with PTRF/cavin1- and ubiquitin (FK2)-specific antibodies (Figure 3.8 B). Again, CAV1-HA was not stained due to technical limitations. In control-transfected cells, ubiquitin was distributed evenly through the cell with few spots of higher intensity in the nucleus. Overexpression of CAV1 wild type induced accumulation of ubiquitin on vesicles that frequently colocalized with PTRF/cavin-1 vesicles. In contrast, in cells transfected with the non-ubiquitinatable K5-57R variant no ubiquitin-positive vesicles were observed and colocalization with PTRF/cavin-1 vesicles was rare. Quantification of these images in ImageJ revealed that in CAV1 wild type expressing cells a median of about 40% of PTRF/cavin-1 vesicles colocalized with ubiquitin signal. This percentage was significantly reduced in cells expressing CAV1 K5-57R.

We could confirm that ubiquitination of CAV1 was important for trafficking of CAV1 to late endosomes/lysosomes. Importantly, this CAV1 transport defect correlates with decreased degradation of the non-ubiquitinatable CAV1 K5-176R (Hayer et al., 2010b). Additionally, we found evidence that autophagy might at least partially be involved in degradation of ubiquitinated CAV1. In contrast, mutation of lysines in CAV1 did not affect biosynthesis of CAV1 and trafficking to the plasma membrane. Importantly, we showed that ubiquitination of CAV1 was required for trafficking of CAV1 to early endosomes after endocytosis on PTRF/cavin-1 positive vesicles.

## 3.3 Establishing a microscopy-based RNAi screen to identify E3 ligases that ubiquitinate CAV1

In the previous experiments, we established a functional link between ubiquitination of CAV1 in the N-terminal region and endosomal trafficking of CAV1. However, to expand the possibilities for functional studies of CAV1 ubiquitination, we wanted to identify the E3 ubiquitin ligase that ubiquitinates CAV1. Therefore, we wanted to establish an immunofluorescence microscopy based assay of CAV1 ubiquitination. This assay could then be used to screen a large library of siRNAs targeting E3 ligases for changes in CAV1 ubiquitination.

### 3.3.1 Characterizing an inducible U2OS-CAV1-HA cell line with the help of a small set of candidate E3 ubiquitin ligases

The initial requirement for a microscopy-based screening protocol was to generate a cell system with robust overexpression of CAV1. Therefore, we generated two U2OS cell lines to circumvent the need for transient transfection of CAV1. The first cell line constitutively expressed CAV1-HA after random integration of the CAV-HA cDNA sequence into the genome (U2OS-pIRES-CAV1-HA). Several clones of this cell line were tested and the clone #6 was chosen for its high expression of the transgene (data not shown). The second cell line expressed CAV1-HA under control of a doxycycline inducible promoter (U2OS-CAV1-HA). Several clones were tested and the clone #8 was chosen on basis of its high expression of CAV1-HA after induction with doxycycline (data not shown). The constitutively and inducibly expressing U2OS cell lines were compared in Western blotting with transient transfection of CAV1-HA in U2OS cells (Figure 3.9 A). Transient transfection resulted in high overexpression of CAV1-HA and strong ubiquitination. In comparison, the U2OS-pIRES-CAV1-HA cell line showed less strong expression and ubiquitination. The inducible U2OS-CAV1-HA displayed further reduced, but still well detectable, overexpression and ubiquitination of CAV1 after induction with doxycycline. The induction efficiency was later improved by seeding the cells more dense (data not shown).

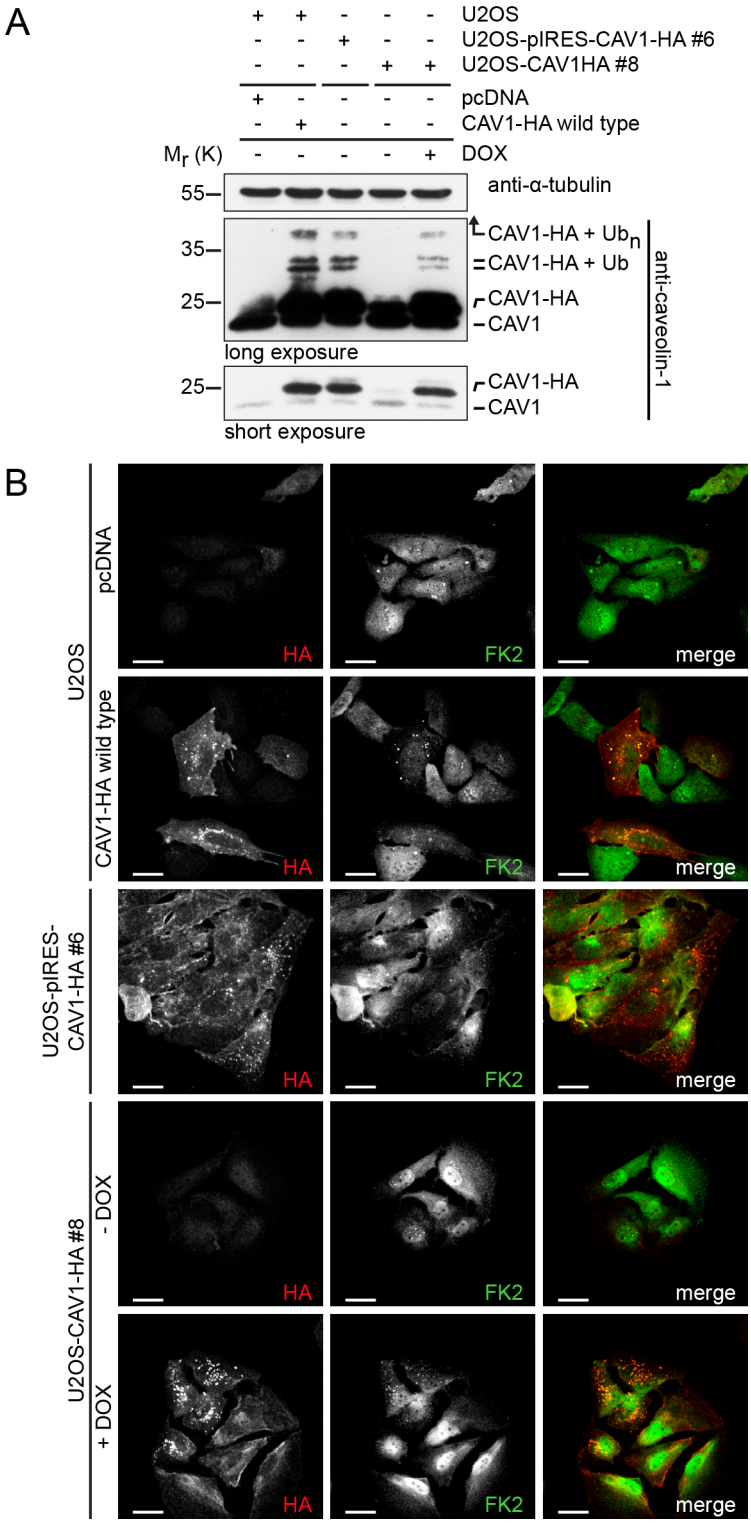


Figure 3.9 **Comparison of constitutive or inducible overexpression of CAV1 with transient overexpression in U2OS cells.**
A, ubiquitinated CAV1-HA accumulates after constitutive or inducible overexpression in U2OS cell lines. U2OS cells were transfected with pcDNA3.1 empty vector or CAV1-HA for 24 h. U2OS-CAV1-HA cells were left untreated or induced with doxycycline (DOX) for 24 h. The cells were harvested together with U2OS-pIRES-CAV1-HA cells in lysis-buffer and analyzed in Western blotting using caveolin-1-specific antibodies. Staining for α-tubulin served as a loading control. The position of mono-ubiquitinated (CAV1-HA + Ub) or multi-ubiquitinated (CAV1-HA + $Ub_n$) CAV1-HA is indicated. B, U2OS-CAV1-HA cells show localization of CAV1-HA to

endosomes and colocalization with ubiquitin signal. U2OS, U2OS-CAV1-HA, and U2OS-pIRES-CAV1-HA cells were treated as in A. After formaldehyde fixation, the cells were stained with HA- and ubiquitin (FK2)-specific antibodies and visualized by spinning disk microscopy using an x 40 objective. Representative images are shown. Scale bars = 20 µm.

To confirm endosomal localization of CAV1-HA and colocalization with ubiquitin, we stained the cell lines with HA- and ubiquitin (FK2)-specific antibodies and compared them to transiently transfected U2OS cells (Figure 3.9 B). Transiently transfected U2OS cells were very heterogeneous for CAV1-HA expression. Many cells expressed low levels of CAV1-HA or accumulated overexpressed CAV1-HA in aggregates. Few cells showed localization of CAV1-HA to endosomes and colocalization with ubiquitin signal. The U2OS-pIRES-CAV1-HA cell line showed high expression of CAV1-HA and localization to endosomal vesicles in most cells. However, these vesicles often did not colocalize with ubiquitin signal. Overall, the distribution of ubiquitin was very variable and many cells displayed morphological alterations and were polynucleated. Finally, the inducible U2OS-CAV1-HA cell line showed overexpression of CAV1-HA in almost every cell after induction, though overexpression not always resulted in localization of CAV1 to endosomal vesicles. Crucially, the CAV1 vesicles frequently colocalized with ubiquitin signal. However, It has to be noted that the intensity of the ubiquitin signal was weaker in comparison to transient overexpression of CAV1 in U2OS cells. Based on the immunofluorescence microcopy, we chose the U2OS-CAV1-HA cell line clone #8 for further studies. The cells appeared healthy and frequently showed ubiquitin positive CAV1 vesicles.

Next, we tested two assays to measure the levels of ubiquitinated CAV1 in response to depletion of E3 ubiquitin ligases in the inducible cell line. We either analyzed accumulation of ubiquitinated CAV1 in Western blotting or investigated colocalization between CAV1 endosomes and ubiquitin signal in immunofluorescence microcopy. To test these assays, we chose a set of candidate E3 ubiquitin ligases that are known to ubiquitinate membrane proteins. The candidate ligases contain four members (NEDD4, NEDD4L, WWP1, WWP2) of the NEDD4 family of HECT-type E3 ligases that is associated with endocytosis of membrane proteins (Ingham et al., 2004). Furthermore, we chose the RING finger E3 ligase cCbl that ubiquitinates the EGF receptor and mediates its lysosomal degradation (Haglund et al., 2003). Additionally, we selected the cullin-RING ligase cullin-3 (Cul3) because it was shown to be involved in the maturation of lysosomes (Huotari et al., 2012). We transfected

U2OS-CAV1-HA cells with siRNA oligonucleotides targeting the E3 ubiquitin ligases and induced CAV1-HA expression with doxycycline.

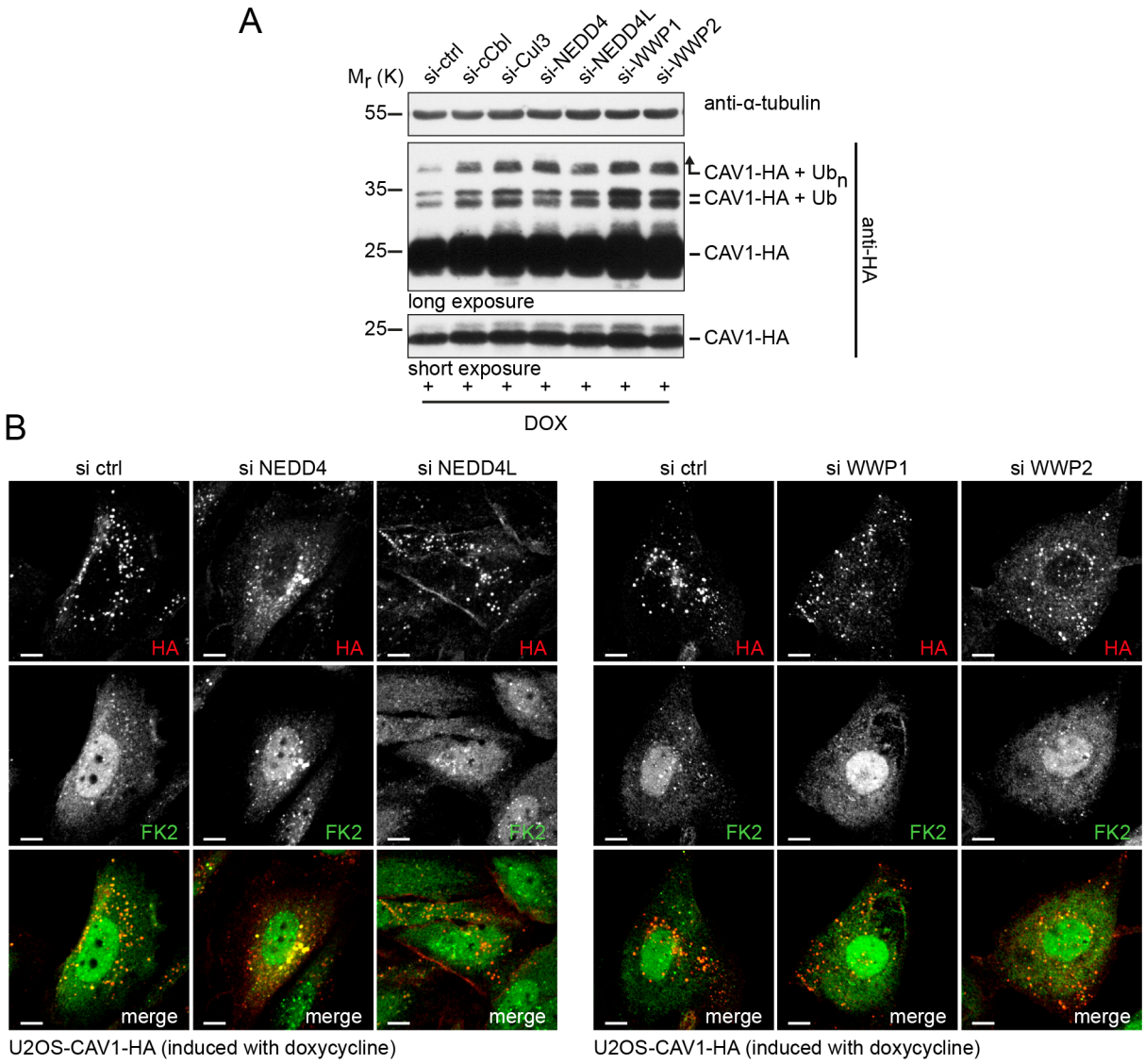


Figure 3.10 **Depletion of E3 ligases causes cellular accumulation of ubiquitinated CAV1 but has diverse effects on CAV1-HA localization.**
A, depletion of a set of E3 ubiquitin ligases leads to accumulation of ubiquitinated CAV1-HA. U2OS-CAV1-HA cells were transfected with control siRNA (si-ctrl) oligonucleotides or the indicated siRNAs for a total of 48 h. The siRNA treated U2OS-CAV1-HA cells were later induced with doxycycline (DOX) to express CAV1-HA 24 h prior to lysis. Cell lysates were analyzed in Western blotting using HA-specific antibodies. Staining for α-tubulin served as a loading control. The position of mono-ubiquitinated (CAV1-HA + Ub) and multi-ubiquitinated (CAV1-HA + $Ub_n$) CAV1-HA is indicated. B, depletion of NEDD4L induces localization of CAV1-HA to the plasma membrane and possibly reduces colocalization with ubiquitin. U2OS-CAV1-HA cells were transfected and induced as described in A. The cells were formaldehyde fixed and stained with HA- and ubiquitin (FK2)-specific antibodies and visualized by spinning disk microscopy using an x 100 objective. Representative images are shown. Scale bars = 10 µm.

First, we analyzed cell lysates in Western blotting using HA-specific antibodies (Figure 3.10 A). Interestingly, we observed that depletion of any of the tested E3 ligases increased the levels of ubiquitinated CAV1. In detail, knockdown of the two HECT-type ligases NEDD4 or NEDD4L caused weak accumulation of ubiquitinated CAV1. Knockdown of cCbl or Cul3 resulted in intermediate accumulation, while depletion of the two HECT-type ligases WWP1 or WWP2 resulted in strong accumulation of ubiquitinated CAV1. Second, we stained siRNA transfected and induced U2OS-CAV1-HA cells with antibodies specific for HA and ubiquitin (FK2) (Figure 3.10 B). In the control-depleted condition CAV1 localized to endosomal vesicles that colocalized with ubiquitin signal. In contrast, depletion of NEDD4 caused accumulation of CAV1 in enlarged perinuclear and clearly ubiquitin positive vesicles. Interestingly, after knockdown of the E3 ligase NEDD4L CAV1 frequently showed increased localization to the plasma membrane in comparison to the control depletion. Moreover, the colocalization between CAV1 vesicles and ubiquitin staining appeared to be reduced. Because NEDD4L directly interacts with the caveolin-family member CAV3 (Guo et al., 2012), we chose to further investigate this phenotype. In contrast, depletion of either WWP1 or WWP2 increased the overall number of cells with CAV1 endosomes as well as the number of ubiquitin positive CAV1 endosomes per cell.

### 3.3.2 Automated image quantification can detects changes in CAV1 ubiquitination over a wide range

We decided to improve the detection of CAV1 ubiquitination in immunofluorescence microscopy by using automated image analysis together with chemical inhibition of CAV1 degradation. Therefore, we treated siRNA transfected and induced U2OS-CAV1-HA cells with $NH_4Cl$ to block lysosomal degradation of CAV1 (Hayer et al., 2010b) and accumulate ubiquitinated CAV1 in the cells. As a negative control we used the proteasome inhibitor MG132 that was shown by Hayer and colleagues to have no effect on CAV1 half-life. Cell lysates of siRNA transfected and inhibitor treated U2OS-CAV1-HA cells were analyzed in Western blotting using HA- and NEDD4L-specific antibodies (Figure 3.11 A). Importantly, we could confirm efficient depletion of NEDD4L by the NEDD4L siRNA oligonucleotide. In control depleted cells, ubiquitinated CAV1 accumulated after lysosome inhibition with $NH_4Cl$ but decreased after proteasome inhibition.

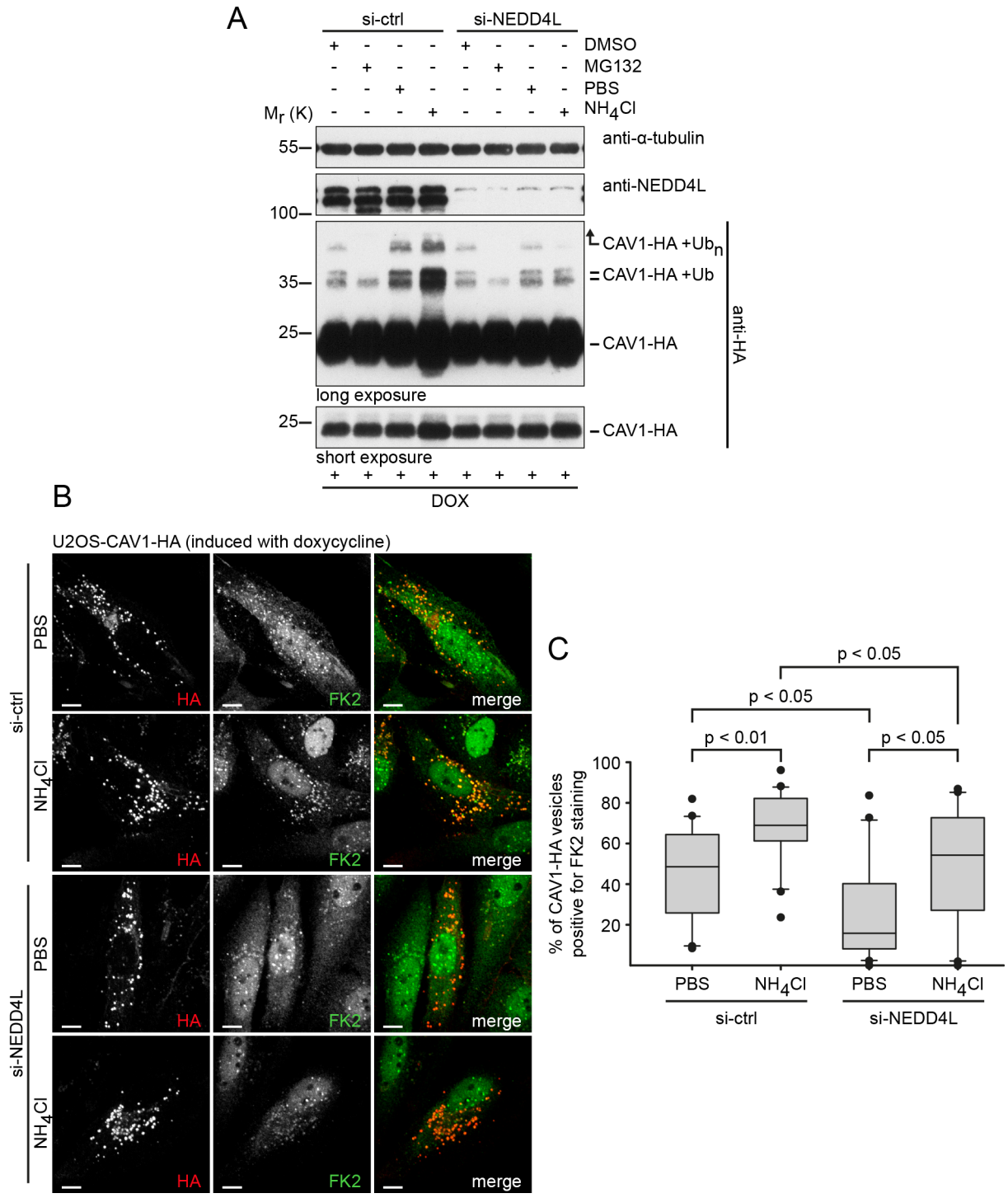


Figure 3.11 **In NEDD4L depleted cells ubiquitinated CAV1 does not accumulate after lysosome inhibition.**
A, in NEDD4L depleted cells lysosome inhibition causes no accumulation of ubiquitinated CAV1-HA. U2OS-CAV1-HA cells were transfected with control siRNA (si-ctrl) oligonucleotides or siRNA targeting NEDD4L for a total or 48 h and induced with doxycycline (DOX) to express CAV1-HA for 24 h. The cells were treated with $NH_4Cl$ or solvent alone (PBS) for 18 h prior to lysis. Cell lysates were analyzed in Western blotting using HA-and NEDD4L-specific antibodies. Staining for α -tubulin served as a loading control. The position of mono-ubiquitinated (CAV1-HA + Ub) and multi-ubiquitinated (CAV1-HA + $Ub_n$) CAV1-HA is indicated. B, NEDD4L depletion reduces the colocalization of CAV1 vesicles with ubiquitin signal in mock or $NH_4Cl$ treated cells. U2OS-CAV1-HA cells were transfected and induced as described in A.

The cells were formaldehyde fixed and stained with HA- and ubiquitin (FK2)-specific antibodies and visualized by spinning disk microscopy using an x 100 objective. Representative images are shown. Scale bars = 10 µm. C, quantification of B. Colocalization of CAV1-HA vesicles with ubiquitin signal was quantified by automated image analysis as detailed in “material and methods”. Whiskers indicate the $10^{th}$/$90^{th}$ percentile and (•) indicates outliers. Calculated p-values are indicated. n = 20 cells/condition from two independent experiments.

Interestingly, in NEDD4L depleted cells, lysosome inhibition caused no accumulation of ubiquitinated CAV1, while the decrease in ubiquitinated CAV1 after proteasome inhibition was not affected. This suggested that NEDD4L had an influence on the levels of ubiquitinated CAV1 destined for lysosomal degradation. In the next step, we wanted to reproduce this effect in immunofluorescence microscopy and stained siRNA transfected and inhibitor treated U2OS-CAV1-HA cells with HA- and ubiquitin (FK2)-specific antibodies (Figure 3.11 B). In the control-depleted cells, $NH_4Cl$ caused a marked accumulation of CAV1 positive endosomes accompanied by an increase in colocalization with ubiquitin signal. In NEDD4L depleted cells, CAV1 endosomes accumulated after $NH_4Cl$ treatment but there was less increase in colocalization with ubiquitin signal, supporting the phenotype that we observed in Western blotting. This experiment was quantified using automated colocalization analysis in ImageJ (Figure 3.11 C). $NH_4Cl$ treatment of the control-depleted cells significant increased the median number of CAV1 vesicles colocalizing with ubiquitin from 50% to 70%. Consistently, treatment of NEDD4L depleted cells with $NH_4Cl$ significantly increased the median percentage of CAV1 vesicles colocalizing with ubiquitin from 20% to more than 50%. However, the median percentage of CAV1 vesicles colocalizing with ubiquitin signal was always significantly lower in NEDD4L depleted cells in comparison to control-depleted cells. Overall, we could detect significant differences in the median percentage of CAV1 endosomes that colocalize with ubiquitin signal ranging from 20% up to 70%.

We established an inducible U2OS-CAV1-HA cell line for robust overexpression of CAV1. With this cell line, we tested several E3 ubiquitin ligases in Western blotting and immunofluorescence microscopy for effects on the levels of ubiquitinated CAV1. Depletion of these ligases resulted in accumulation of ubiquitinated CAV1. Furthermore, we observed that NEDD4L depletion decreased the levels of ubiquitinated CAV1 after lysosome inhibition but not in control-treated cells. Importantly, we could show that automated analysis was able to detect differences in colocalization between CAV1 vesicles and ubiquitin signal over a wide range.

## 3.4 The p97-UBXD1 complex interacts with CAV1 and regulates lysosomal turnover of CAV1

In our lab we previously showed that wild type CAV1 but not the lysine-less CAV1 K5-176R interacts with the AAA-ATPase p97 and the cofactor UBXD1. Furthermore, expression of the dominant negative p97 E578Q variant caused accumulation of CAV1 on enlarged endosomes (Ritz et al., 2011). In this study we observed that ubiquitination of CAV1 in the N-terminal region was important for endosomal sorting of CAV1. Therefore, we asked if the lysines in the N-terminal region of CAV1 also were required for the interaction between CAV1 and p97 and how p97 regulated endosomal sorting of ubiquitinated CAV1.

### 3.4.1 The ubiquitination site in the N-terminal region of CAV1 is required for interaction with p97-UBXD1 on endosomes

Initially, we analyzed if mutation of the six lysines in the N-terminal region of CAV1 was sufficient to abolish interaction with p97 and the p97 cofactor UBXD1. Therefore, we immunoprecipitated CAV1-myc from cell lysates of transiently transfected HEK293 cells using myc-specific antibodies and investigated co-precipitation of p97 and UBXD1 in Western blotting (Figure 3.12 A). Co-precipitation of p97 and UBXD1 was observed with the CAV1 wild type as well as with the CAV1 K65-176R variant. Both variants harbor a wild type N-terminal region and were shown to be ubiquitinated. Crucially, mutating the N-terminal lysines (K5-57R) or all lysines in CAV1 (K5-176R) abolished the co-precipitation of p97 and UBXD1. Since we observed that ubiquitinated CAV1 localized to endosomes, we analyzed if the interaction between CAV1 and the p97-UBXD1 complex takes place on endosomes. Because specific localization studies of endogenous or transiently overexpressed p97 were previously unsuccessful, we generated an U2OS cell line that expresses low levels of p97-myc-strep (U2OS-p97-myc-strep) under control of a doxycycline inducible promoter (Figure 3.12 B). The U2OS-p97-myc-strep cells were transfected with CAV1-HA variants, induced to express p97-myc-strep, and stained with HA- and myc-tag-specific antibodies. Importantly, in cells overexpressing CAV1 wild type or the ubiquitinatable K65-176R variant, p97-myc-strep accumulated on CAV1-positive vesicles (Figure 3.12 C). In contrast, if the non-ubiquitinatable CAV1 variants K5-57R and K5-176R were overexpressed the localization of p97-myc-strep to CAV1 endosomes was greatly reduced although not completely abolished.

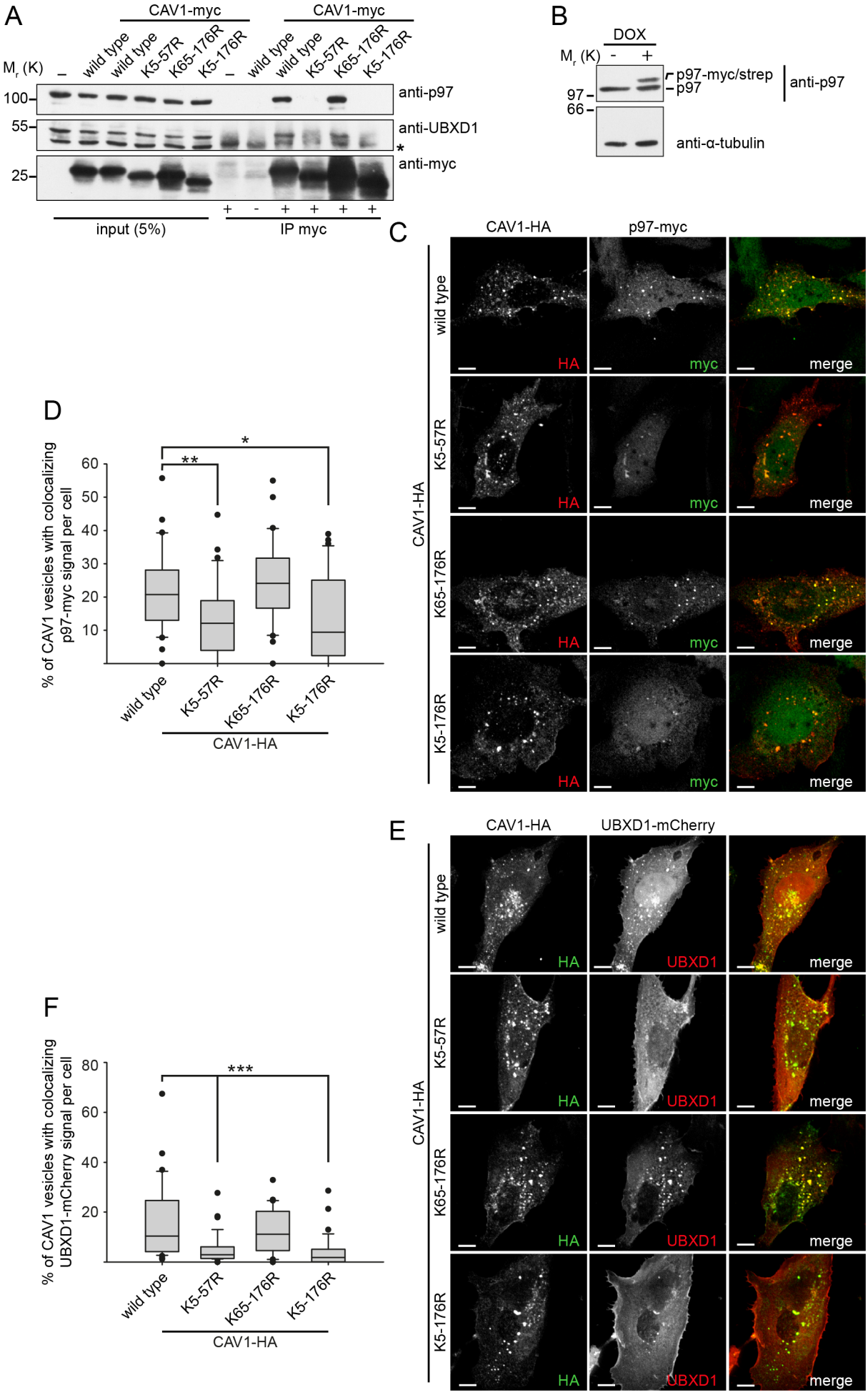
A
CAV1-myc
CAV1-myc
wild type
wild type
K5-57R
K65-176R
K5-176R
wild type
wild type
K5-57R
K65-176R
K5-176R
M r (K)
100
55
25
anti-p97
anti-UBXD1
*
anti-myc
input (5%)
IP myc
B
DOX
M r (K)
97
66
p97-myc/strep
p97
anti-p97
anti-α-tubulin
C
CAV1-HA
p97-myc
wild type
K5-57R
K65-176R
K5-176R
CAV1-HA
HA
myc
merge
D
% of CAV1 vesicles with colocalizing p97-myc signal per cell
*
**
wild type
K5-57R
K65-176R
K5-176R
CAV1-HA
E
CAV1-HA
UBXD1-mCherry
wild type
K5-57R
K65-176R
K5-176R
CAV1-HA
HA
UBXD1
merge
F
% of CAV1 vesicles with colocalizing UBXD1-mCherry signal per cell
***
wild type
K5-57R
K65-176R
K5-176R
CAV1-HA

Figure 3.12 **The lysines in the N-terminal region of CAV1 are required for interaction with P97-UBXD1 and recruitment to endosomes.**
A, ubiquitinatable CAV1 interacts with p97-UBXD1. HEK293 cells were transfected with pcDNA3.1 empty vector (-), CAV1-myc wild type or the indicated variants and lysed after 24 h. Cell lysates were immunoprecipitated using myc-specific antibodies. Immunoprecipitation with HA-specific antibodies was used as a negative control (-). Immunoprecipitates (IP) were analyzed together with input samples in Western blotting using myc-, UBXD1-, and p97-specific antibodies. The asterisk indicates the position of the antibody heavy chain. B, expression of p97-myc-strep in U2OS cells under a doxycycline inducible promoter. U2OS-p97 cells were left untreated or induced with doxycycline (DOX) to express p97-myc-strep and lysed after 24 h. Cell lysates were analyzed in Western blotting using p97-specific antibodies. Staining for α-tubulin served as a loading control. The position of endogenous p97 and p97-myc-strep is indicated. C, ubiquitinatable CAV1 variants recruit p97 to endosomes. U2OS-p97-myc-strep cells were induced with doxycycline (DOX) to express p97-myc-strep and transiently transfected with CAV1-HA wild type and the indicated variants. The cells were formaldehyde fixed and stained with HA- and myc-specific antibodies. Images were acquired on a spinning disk microscope using an x 100 objective. Representative images are shown. Scale bars = 10 µm. D, quantification of C. Colocalization between CAV1-HA and p97-myc positive vesicles was quantified by automated image analysis. Whiskers indicate the $10^{th}$/$90^{th}$ percentile and (•) indicates outliers. *, $p < 0.05$, **, $p < 0.01$. n = 30 cells/condition from three independent experiments. E, ubiquitinatable CAV1 variants localize UBXD1-mCherry to endosomes. U2OS cells were transiently transfected with UBXD1-mCherry and CAV1-HA wild type or the indicated variants and processed for immunofluorescence microscopy using HA-specific antibodies as in C. Scale bars = 10 µm. F, quantification of E as in D. Whiskers indicate the $10^{th}$/$90^{th}$ percentile and (•) indicates outliers. ***, $p < 0.001$. n = 30 cells/condition from three independent experiments.

We quantified these images using automated colocalization analysis in ImageJ as described above. In cells expressing the ubiquitinatable CAV1 wild type or K65-176R a median of above 20% of CAV1 vesicles colocalized with p97-myc-strep (Figure 3.12 D). Importantly, this colocalization was significantly reduced in cells expressing the non-ubiquitinatable CAV1 variants. However, a median of above 10% of CAV1 endosomes still showed colocalization with p97-myc-strep comparable to the phenotype observed by eye. Along this line, we investigated if the p97 cofactor UBXD1 showed a comparable localization to endosomes after overexpression of ubiquitinatable CAV1. Importantly, previous experiments showed colocalization of UBXD1-mCherry with wild type CAV1-GFP in life cell microscopy (Ritz et al., 2011). We expressed the CAV1-HA variants and UBXD1-mCherry in U2OS cells and confirmed colocalization of UBXD1-mCherry with wild type CAV1 and CAV1 K65-176R in fixed cells (Figure 3.12 E). In contrast, in cells expressing the non-ubiquitinatable variants of CAV1-HA, UBXD1-mCherry did not localize to CAV1 endosomes. Quantification of this colocalization in ImageJ confirmed that a median of about 10% of CAV1 wild type and CAV1 K65-176R vesicles colocalized with

UBXD1-mCherry (Figure 3.12 F). In contrast, the percentage of CAV1 vesicles colocalizing with UBXD1-mCherry was significantly reduced in cells expressing the non-ubiquitinatable CAV1 variants. This colocalization study indicated together with the CAV1 immunoprecipitations that the six N-terminal lysines in CAV1 are important for interaction with p97-UBXD1. Moreover, this interaction probably takes place on endosomes.

### 3.4.2 CAV1 is degraded in the lysosome and this requires p97 activity

We have established that ubiquitination of CAV1 is required for endosomal transport of CAV1 to late endosomes/lysosomes and could show that p97 interacts with ubiquitinated CAV1. Therefore, we investigated a functional connection between p97 and endosomal sorting of ubiquitinated CAV1. We utilized the inducible U2OS-CAV1-HA cell line that we generated for the siRNA screen of E3 ubiquitin ligases (Figure 3.9) to confirm that ubiquitinated CAV1 is degraded in the lysosome. U2OS-CAV1-HA cells were induced and treated with inhibitors of lysosomal or proteasomal degradation. The cell lysates were investigated in Western blotting using caveolin-1- and ubiquitin (FK2)-specific antibodies (Figure 3.13 A). Inhibition of lysosomal degradation with either bafilomycin A1 or ammonium chloride ($NH_4Cl$) accumulated ubiquitinated and unmodified CAV1. This was not the case if the cells were treated with the proteasome inhibitor MG132 even though proteasome inhibition caused a general accumulation of ubiquitinated substrates as seen in the ubiquitin staining. Interestingly, the levels of ubiquitinated CAV1, especially of multi-ubiquitinated CAV1 (CAV1-HA + $Ub_n$), were reduced after proteasome inhibition. This is consistent with a depletion of free ubiquitin and reduced ubiquitin conjugation in MG132 treated cells (Melikova et al., 2006). After confirming that ubiquitinated CAV1 was degraded in the lysosome, we investigated the effect of pharmacological inhibition of p97 on the levels of ubiquitinated CAV1. Due to the high toxicity of the p97 inhibitor DBeQ (Chou et al., 2011) we could not extend the treatment beyond 4 h in comparison to the 18 h treatment we used for lysosome inhibitors. Nonetheless, we observed some accumulation of ubiquitinated CAV1 in comparison to the DMSO control (Figure 3.13 B).

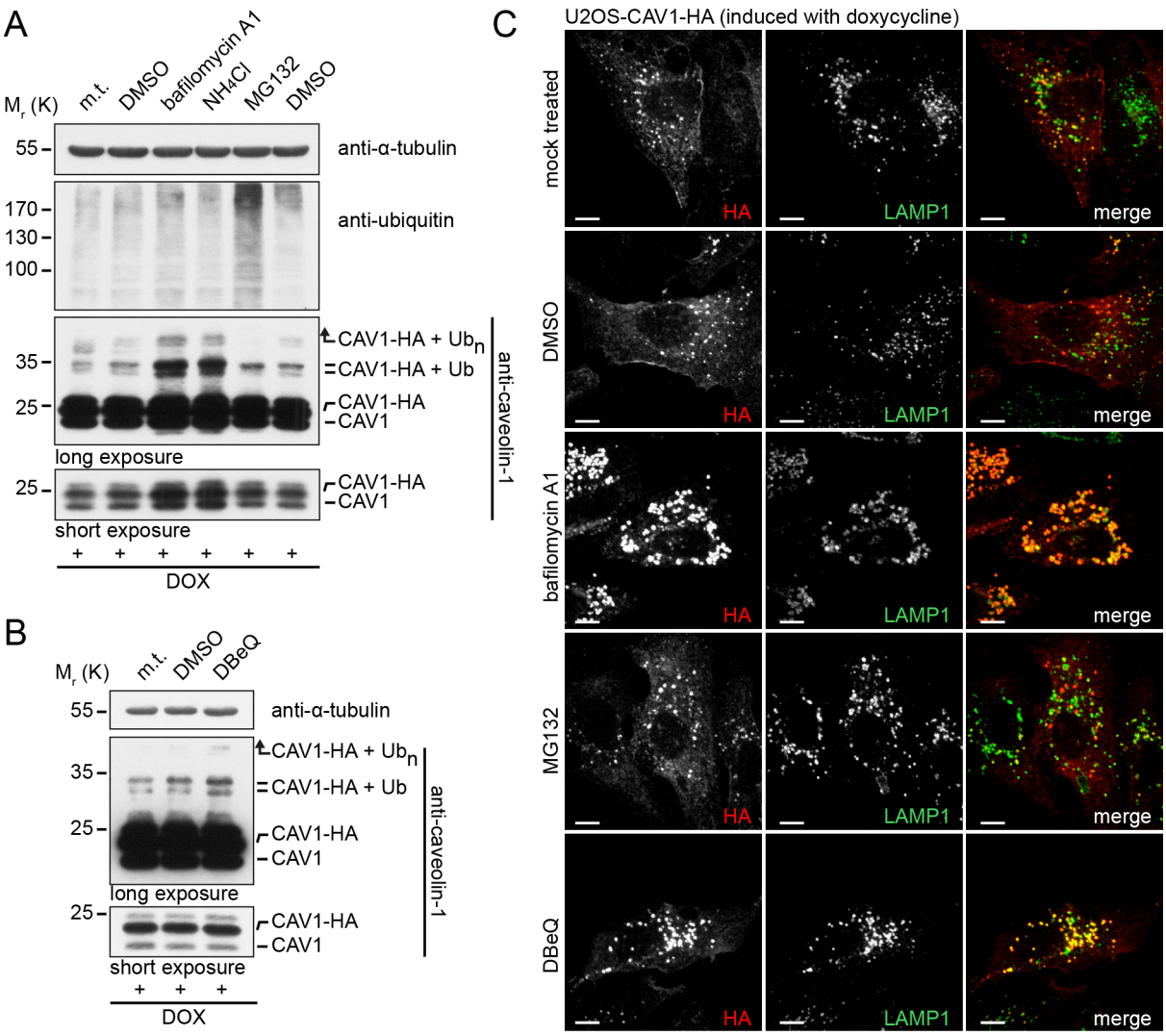


Figure 3.13 **Ubiquitinated CAV1 accumulates after pharmacological inhibition of the lysosome or p97.**
A, inhibitors of the lysosome but not of the proteasome cause accumulation of ubiquitinated CAV1. U2OS-CAV1-HA cells were induced with doxycycline (DOX) for 24 h to express CAV1-HA. The cells were mock treated (m.t.), treated with DMSO or the lysosome inhibitors bafilomycin A1 or $NH_4Cl$ for 18 h or treated with the proteasome inhibitor MG132 for 4 h prior to lysis. Cell lysates were analyzed in Western blotting using HA- and ubiquitin (FK2)-specific antibodies. Staining for α-tubulin served as a loading control. The position of mono-ubiquitinated (CAV1-HA + Ub) and multi-ubiquitinated (CAV1-HA + $Ub_n$) CAV1-HA is indicated. B, short pharmacological inhibition of p97 causes weak accumulation of ubiquitinated CAV1. U2OS-CAV1-HA cells were induced as in A. The cells were mock treated (m.t.), or treated with DMSO, or DBeQ for 4 h prior to lysis. Cell lysates were analyzed in Western blotting as in A using caveolin-1-specific antibodies. C, CAV1 accumulates on late endosomes after inhibition of the lysosome or p97. U2OS cells were induced and treated with lysosome, proteasome, or p97 inhibitors as in A and B. The cells were formaldehyde fixed and stained with HA- and LAMP1-specific antibodies. Images were acquired on a spinning disk microscope using an x 100 objective. Representative images are shown. Scale bars = 10 µm.

To investigate the subcellular localization of CAV1 after treatment with lysosome, proteasome, or p97 inhibitors, we stained U2OS-CAV1-HA cells with antibodies specific for HA and the late endosome/lysosome marker protein LAMP1. In the untreated or DMSO control-treated cells, CAV1 localized to many small endosomal vesicles that were frequently positive for LAMP1 (Figure 3.13 C). Interestingly, the colocalization between CAV1 and LAMP was increased in the inducible cell line compared to transiently transfected U2OS (Figure 3.4 A). After lysosome inhibition with bafilomycin A1, CAV1 accumulated on many large endosomes that strongly colocalized with LAMP1 staining. Additionally, the LAMP1 vesicles appeared clumped and enlarged compared to the control. Treatment with the proteasome inhibitor MG132 caused no accumulation of CAV1 and did not affect the colocalization between CAV1 vesicles and LAMP1. However, treatment with the p97 inhibitor DBeQ induced accumulation of CAV1 on LAMP1-positive enlarged endosomes. In comparison to bafilomycin A1 treated cells the vesicles were smaller and the colocalization with LAMP1 was less stringent. Along this line, we could show that after lysosome or p97 inhibition CAV1 accumulated together with ubiquitin (data not shown).

We chose an RNAi approach to analyze the function of p97 in lysosomal degradation of CAV1 from an additional angle. Therefore, we depleted p97 and the cofactor UBXD1 that interacted with ubiquitinated CAV1. The inducible U2OS-CAV1-HA cells were transfected with specific siRNA oligonucleotides targeting p97 and UBXD1 and CAV1-HA expression was induced with doxycycline. Cell lysates were probed in Western blotting with specific antibodies and efficient depletion of p97 and UBXD1 was shown (Figure 3.14 A). Importantly, transfection of siRNA oligonucleotides targeting p97 or UBXD1 but not of non-targeting control siRNA or mock transfection caused a strong accumulation of ubiquitinated CAV1. Recently, we identified several p97 cofactors including the deubiquitinating enzymes (DUBs) YOD1 and VCPIP1 and the substrate-recruiting cofactor PLAA to be involved in endosomal trafficking and lysosomal degradation of the EGF receptor (M. Bug, unpublished data). Therefore, we investigated if these p97 cofactors were also involved in lysosomal turnover of ubiquitinated CAV1. We transfected U2OS-CAV1-HA cells with siRNA oligonucleotides targeting p97, UBXD1, p47, YOD1, VCPIP1, and PLAA and induced expression of CAV1-HA as above. Effective knockdown efficiency was confirmed for the siRNA targeting PLAA (Figure 3.14 B), as well as the other siRNAs (data not shown). As described above, strong accumulation of ubiquitinated CAV1-HA was

observed after depletion of p97 and UBXD1. Interestingly, depletion of the substrate-recruiting cofactor PLAA and the DUB VCPIP1 but not YOD1 showed a comparable effect. However, knockdown of another substrate-recruiting cofactor, p47, did not affect the levels of ubiquitinated CAV1. This shows that functional p97 is required for lysosomal degradation of ubiquitinated CAV1 and may require additional cofactors.

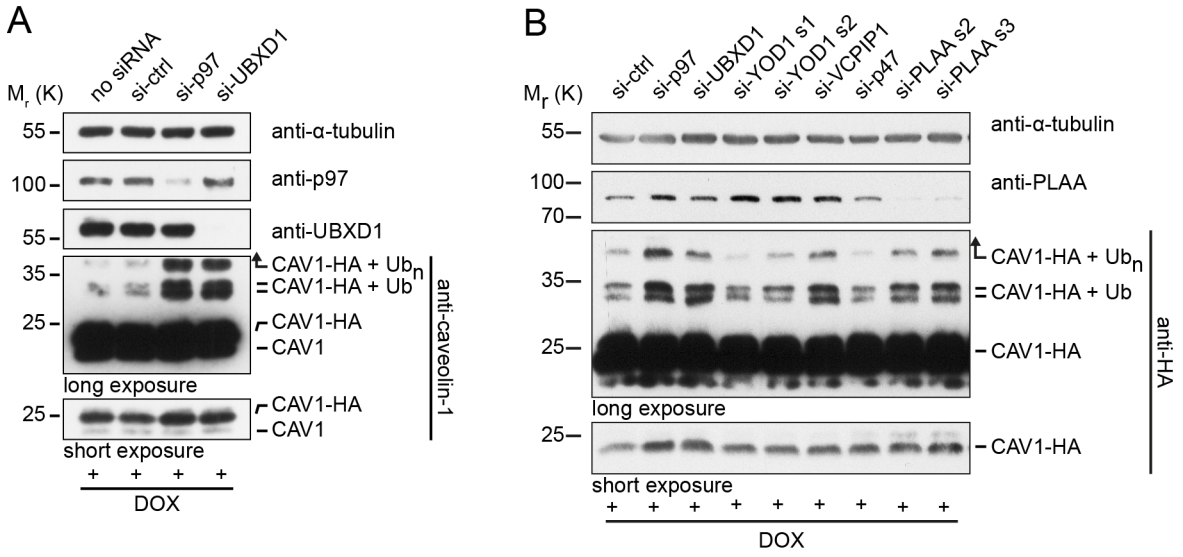


Figure 3.14 **Depletion of p97, UBXD1, VCPIP1, or PLAA causes accumulation of ubiquitinated CAV1.**
A, depletion of p97 or UBXD1 leads to accumulation of ubiquitinated CAV1. U2OS-CAV1-HA cells were left untreated (no siRNA) or transfected with control siRNA oligonucleotides (si-ctrl), siRNAs targeting p97, or UBXD1 for a total of 48 h. The cells were induced with doxycycline (DOX) to express CAV1-HA 24 h prior to lysis. Cell lysates were analyzed in Western blotting using caveolin-1-specific antibodies. Staining for α-tubulin served as a loading control. The position of mono-ubiquitinated (CAV1-HA + Ub) or multi-ubiquitinated (CAV1-HA + Ub$_n$) CAV1-HA is indicated. B, depletion of the substrate-recruiting cofactor PLAA or the deubiquitinating enzyme VCPIP1 causes accumulation of ubiquitinated CAV1. U2OS-CAV1-HA cells were transfected with control siRNA oligonucleotides (si-ctrl) or the indicated siRNAs for a total of 48 h and induced as in A. Two different siRNA oligonucleotides were tested for YOD1 (s1 and s2) and PLAA (s2 and s3). Cell lysates were analyzed in Western blotting using HA-specific antibodies. Staining for α -tubulin served as a loading control. The position of mono-ubiquitinated (CAV1-HA + Ub) or multi-ubiquitinated (CAV1-HA + Ub$_n$) CAV1-HA is indicated.

### 3.4.3 A systematic screen identifies no ubiquitin-binding cofactor that is required for the interaction between CAV1 and p97

The finding that the substrate-recruiting cofactor PLAA is involved in CAV1 turnover prompted us to investigate the molecular details of the interaction between CAV1 and the p97-UBXD1 complex. While p97 by itself has weak affinity for ubiquitin it usually interacts with ubiquitinated substrates through substrate-recruiting cofactors (Jentsch and Rumpf, 2007; Meyer et al., 2002). Importantly, no p97 cofactor was known to mediate the interaction between ubiquitinated CAV1 and p97. PLAA can bind to p97

via a PUL domain and to ubiquitin through a WD40 and a PFU domain (Mullally et al., 2006). We immunoprecipitated CAV1-myc from HEK293 cells in the background of siRNA mediated PLAA depletion (Figure 3.15 A). As a control we depleted the p97 cofactor UBXD1 that contains no ubiquitin-binding motif and was shown in our lab to be not required for the interaction between CAV1 and p97 (Ritz et al., 2011). The non-ubiquitinatable K5-57R variant of CAV1 was transfected as an additional control that does not bind p97. Efficient depletion of UBXD1 and PLAA was confirmed in the input samples. As expected, p97 and UBXD1 were found to interact with CAV1 wild type but not with CAV1 K5-57R in control-depleted cells. Furthermore, depletion of UBXD1 did not interfere with binding of p97 to CAV1 wild type. Importantly, also depletion of PLAA had no effect on the co-precipitation of p97 and UBXD1 with CAV1 wild type. This is supported by the observation that PLAA itself did not co-precipitate with CAV1 wild type or K5-57R. However, the levels of PLAA detected in the input samples were close to the detection threshold of the Western blot. Therefore, weak or transient interaction of PLAA and CAV1 might not have been detected in this experiment. Moreover, in mass spectrometry analyses, D. Ritz could identify PLAA only in precipitates of the substrate trapping p97 E578Q variant (Ritz et al., 2011). Therefore, we co-expressed p97-GFP wild type or E578Q and CAV1-myc variants in HEK293 cells and immunoprecipitated CAV1-myc from the cell lysates using specific antibodies. Overexpression of p97-GFP wild type and E578Q was confirmed in the input samples, although at lower levels compared to endogenous p97 (Figure 3.15 B). We observed no difference in expression of the CAV1 variants between p97-GFP wild type and E578Q expressing cells. However, the levels of ubiquitinated CAV1 that were precipitated from the lysates of p97-GFP E578Q expressing cells were slightly reduced in comparison to p97-GFP wild type expressing cells. As expected, the p97-UBXD1 complex co-isolated with CAV1 wild type in p97-GFP wild type expressing cells. Additionally, weak co-precipitation of p97 and UBXD1 was observed with the non-ubiquitinatable CAV1 K5-176R variant. However, HEK293 cells express endogenous wild type CAV1 that can be ubiquitinated and possibly forms hetero-oligomers together with the exogenous non-ubiquitinatable CAV1. This may be sufficient to precipitate the p97-UBXD1 complex if p97-GFP wild type is overexpressed. In p97-GFP E578Q expressing cells p97 and UBXD1 co-precipitated with CAV1 wild type although at lower levels in comparison to cells expressing p97-GFP wild type. Importantly, PLAA was not found to co-precipitate with CAV1 under any tested condition.

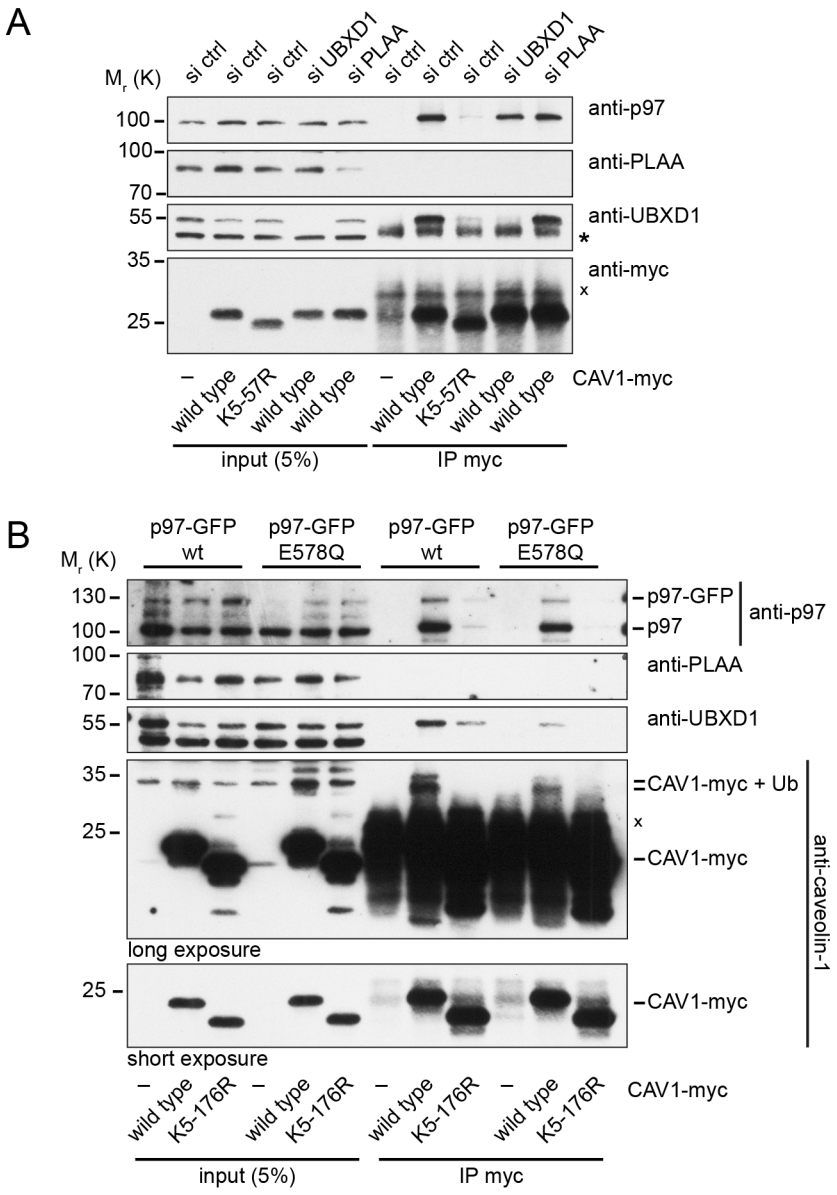


Figure 3.15 **Depletion of PLAA does not affect interaction between CAV1 and the p97-UBXD1 complex.**

A, UBXD1 and PLAA are not required for the interaction between CAV1 and p97. HEK293 cells were transfected with control siRNA oligonucleotides (si-ctrl) or siRNAs targeting UBXD1 or PLAA for a total of 48 h. The siRNA treated cells were transiently transfected with pcDNA3.1 empty vector (-), CAV1-myc wild type or CAV1-myc K5-57R 24 h prior to lysis. Cell lysates were immunoprecipitated using myc-specific antibodies. Immunoprecipitates (IP) were analyzed together with input samples in Western blotting using myc-, PLAA-, UBXD1-, and p97-specific antibodies. The asterisk and the cross indicate the position of the antibody heavy and light chain respectively. B, Overexpression of the substrate trapping p97 E578Q variant does not stabilize co-precipitation of PLAA with CAV1. HEK293 cell were co-transfected with CAV1-myc wild type or K5-176R and p97-GFP wild type or E578Q for 24 h. Cell lysates were immunoprecipitated as in A and analyzed in Western blotting using caveolin-1-, PLAA-, UBXD1-, and p97-specific antibodies. The cross marks the position of the antibody light chain. The position of mono-ubiquitinated (CAV1-HA + Ub) CAV1-HA is indicated.

Because we found no evidence that PLAA mediated the interaction between ubiquitinated CAV1 and p97, we performed a small-scale RNAi screen of all known substrate-recruiting cofactors. Graphical representations of the substrate-recruiting cofactors with the respective p97- and ubiquitin-binding domains are shown in Figure 3.16 A. The siRNA oligonucleotides targeting p97, UBXD1, UFD1, NPL4, p47, PLAA, and DVC1 were already established in the lab and shown in Western blotting to deplete their target proteins (Figure 3.16 B, Figure 3.17) (Dobrynin et al., 2011). The NPL4 siRNA oligonucleotide co-depleted UFD1 as described by G. Dobrynin. We confirmed efficient depletion of UBXD7 and UBXD8 with the specific siRNA oligonucleotides in this and the following experiment. Importantly, the SAKS1 siRNA used in this screen was later shown to have no knockdown efficiency (Figure 3.17). HEK293 cells were transfected with siRNA oligonucleotides and additionally transfected with CAV1-myc prior to lysis. The cell lysates were immunoprecipitated with anti-myc antibodies and co-precipitation of p97 and UBXD1 was investigated in Western blotting using specific antibodies. As described above, depletion of UBXD1 and PLAA did not affect the interaction between CAV1 and p97. Importantly, depletion of none of the other substrate-recruiting cofactors affected co-precipitation of p97 and UBXD1 with CAV1 (Figure 3.16 B). However, we could not control the knockdown efficiency of all siRNAs used in this screen. Interestingly, we observed that the p97 cofactor UBXD8 co-precipitated with CAV1. This was the only p97 cofactor so far, apart from UBXD1 that we observed to interact with CAV1. Therefore, we tested the possibility that UBXD1 and UBXD8 mediated the interaction between CAV1 and p97 together. However, co-depletion of UBXD1 and UBXD8 did not abolish with the interaction between CAV1 and p97 (data not shown).

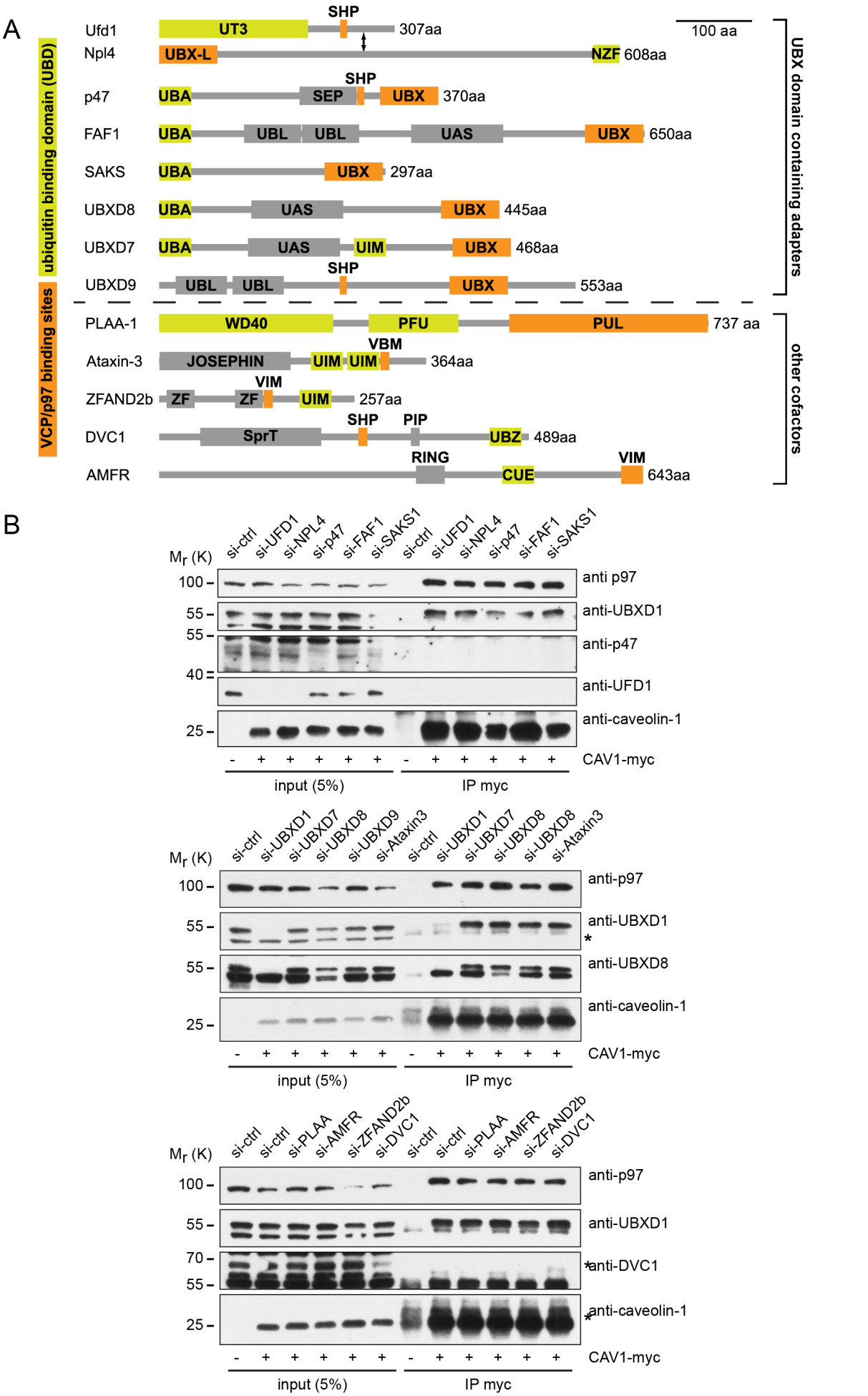
A
ubiquitin binding domain (UBD)
VCP/p97 binding sites
UBX domain containing adapters
other cofactors
100 aa
Ufd1
UT3
SHP
307aa
Npl4
UBX-L
NZF
608aa
p47
UBA
SEP
SHP
UBX
370aa
FAF1
UBA
UBL
UBL
UAS
UBX
650aa
SAKS
UBA
UBX
297aa
UBXD8
UBA
UAS
UBX
445aa
UBXD7
UBA
UAS
UIM
UBX
468aa
UBXD9
UBL
UBL
SHP
UBX
553aa
PLAA-1
WD40
PFU
PUL
737 aa
Ataxin-3
JOSEPHIN
UIM
UIM
VBM
364aa
ZFAND2b
ZF
ZF
VIM
UIM
257aa
DVC1
SprT
SHP
PIP
UBZ
489aa
AMFR
RING
CUE
VIM
643aa
B
Mr (K)
si-ctrl
si-UFD1
si-NPL4
si-p47
si-FAF1
si-SAKS1
anti p97
anti-UBXD1
anti-p47
anti-UFD1
anti-caveolin-1
CAV1-myc
input (5%)
IP myc
si-UBXD1
si-UBXD7
si-UBXD8
si-UBXD9
si-Ataxin3
anti-UBXD8
si-PLAA
si-AMFR
si-ZFAND2b
si-DVC1
anti-DVC1

Figure 3.16 **RNAi screen for a substrate-recruiting cofactor that mediates the interaction between ubiquitinated CAV1 and p97-UBXD1.**
A, siRNA mediated depletion of substrate-recruiting cofactors did not affect the interaction between CAV1 and p97-UBXD1. HEK293 cells were transfected with control siRNA (si-ctrl) or the indicated siRNA oligonucleotides for a total of 48 h. The siRNA treated cells were transiently transfected with pcDNA3.1 empty vector (-) or CAV1-myc wild type for 24 h prior to lysis. The cell lysates were immunoprecipitated using myc-specific antibodies. Immunoprecipitates (IP) were analyzed together with input samples in Western blotting using the indicated specific antibodies. The cross marks the position of the antibody light chain.

### 3.4.4 Cellular depletion of substrate-recruiting cofactors affects turnover of ubiquitinated CAV1

Owing to the fact that depletion of PLAA caused accumulation of ubiquitinated CAV1 even though it did not mediate interaction between CAV1 and p97-UBXD1, we tested the cofactor library that was used in the siRNA screen for effects on the levels of ubiquitinated CAV1. U2OS-CAV1-HA cells were transfected with siRNA oligonucleotides for and induced to express CAV1-HA prior to lysis. Cell lysates were analyzed in Western blotting using specific antibodies. In addition to the previously confirmed siRNA oligonucleotides we confirmed depletion of UBXD7 with the specific siRNA oligonucleotide. However, the original siRNA oligonucleotide targeting SAKS1 (s1) was shown to have no knockdown efficiency and was replaced by a second siRNA (s2) that efficiently depleted SAKS1 (Figure 3.17). We confirmed that depletion of p97, UBXD1, and PLAA accumulated ubiquitinated CAV1 as shown above. Depletion of UFD1 or NPL4 had no effect on ubiquitinated CAV1, while depletion of p47 and FAF1 decreased the levels of ubiquitinated CAV1. Interestingly, knockdown of SAKS1 with the second oligo (s2) caused a marked accumulation of ubiquitinated CAV1, as did depletion of DVC1. This was accompanied by accumulation of the unmodified CAV1. Intermediate levels of ubiquitinated CAV1 accumulated after Ataxin3 depletion comparable to depletion of PLAA. The knockdown of ZFAND2b, AMFR, UBXD7, UBXD8, or UBXD9 caused minor to strong accumulation of ubiquitinated CAV1. However, these effects showed high variation between experiments. Especially the effect of UBXD7 depletion was sometimes on par with or greater than the effect of UBXD9 depletion.

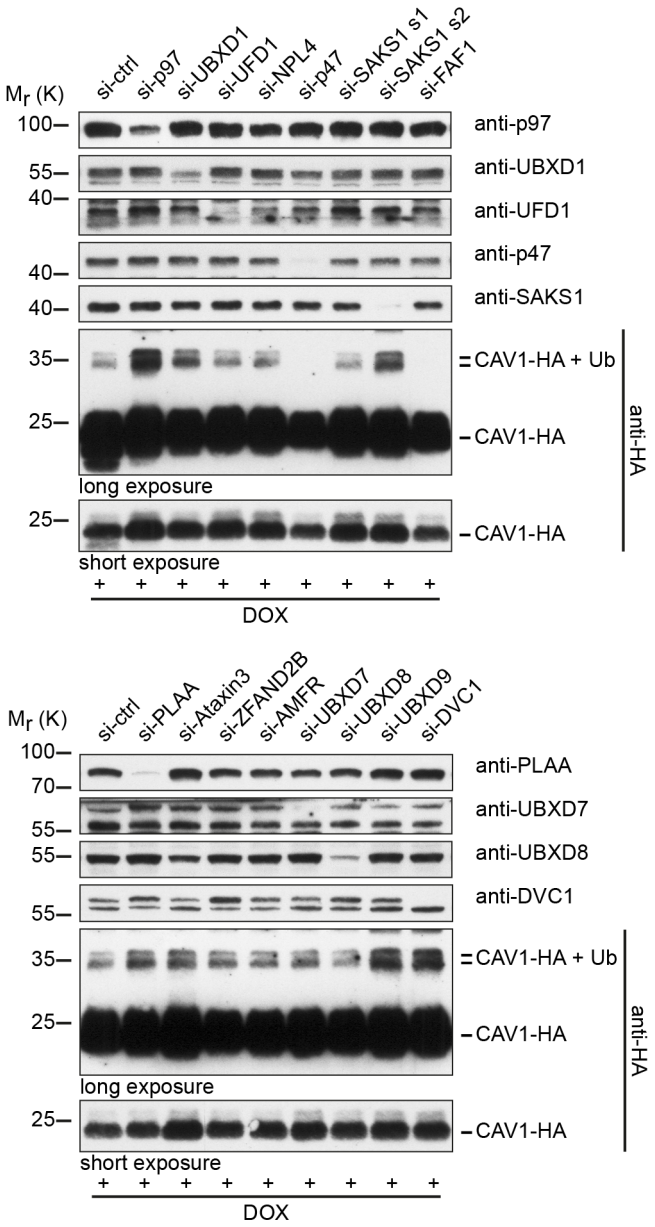


Figure 3.17 **Depletion of some substrate-recruiting cofactors accumulates or decreases ubiquitinated CAV1**.
A, depletion of SAKS1 or DVC1 accumulates, while depletion of p47 or FAF1 decreases ubiquitinated CAV1. U2OS-CAV1-HA cells were transfected with control siRNA (si-ctrl) oligonucleotides or the indicated siRNAs for a total of 48 h. The siRNA treated U2OS-CAV1-HA cells were then induced with doxycycline (DOX) to express CAV1-HA for 24 prior to lysis. Cell lysates were analyzed in Western blotting using the indicated specific antibodies. The position of mono-ubiquitinated (CAV1-HA + Ub) CAV1-HA is indicated.

Summarizing, we could show that the lysines in the N-terminal region of CAV1 were required for interaction of CAV1 with the p97-UBXD1 complex on endosomes. Furthermore, inhibition of the lysosome but not of the proteasome resulted in accumulation of ubiquitinated CAV1 on late endosomes. Additionally, we confirmed that p97 ATPase activity was required for endosomal sorting of CAV1 and that pharmacological inhibition of p97 accumulated CAV1 on late endosomes. Moreover,

depletion of p97, UBXD1, the deubiquitinating enzyme YOD1, or the substrate-recruiting cofactor PLAA caused accumulation of ubiquitinated CAV1. In contrast, we found no evidence that PLAA mediated the interaction between ubiquitinated CAV1 and p97-UBXD1. Moreover, an RNAi-based screen of all known substrate-recruiting cofactors yielded no cofactor that was required for this interaction. Cellular depletion of these p97 cofactors, however, had diverse effects on the levels of ubiquitinated CAV1.

## 3.5 Establishing p97 as a general regulator of endocytosis

We showed that p97 was involved in sorting of ubiquitinated CAV1 to the lysosome and asked if p97 may function as a general regulator of endosomal sorting. The ligand-induced endocytosis and lysosomal degradation of the EGF receptor (EGFR) is a widely used model system for endosomal sorting (Madshus and Stang, 2009). Following endocytosis the EGFR is sorted into the lumen of late endosomes and eventually degraded in the lysosome (Bache et al., 2004). We investigated the effect of chemical inhibition and siRNA mediated depletion of p97 on the ligand-induced degradation of the EGFR.

### 3.5.1 Pharmacological inhibition of p97 delays degradation of the EGFR

We used small molecule inhibitors of p97 as a fast way of modulating p97 ATPase activity. Confluent HEK293 cells were starved for 4 h to accumulate the EGF receptor on the plasma membrane in the presence of either the p97 inhibitor DBeQ (Chou et al., 2011) or vehicle alone. The cells were stimulated with EGF and harvested after 0, 30, 60, and 90 minutes. EGFR levels were analyzed in Western blotting using EGFR specific antibodies (Figure 3.18 A). The intensities of the EGFR bands were quantified and calculated relative to the first time point. In the DMSO-treated controls, 80% of the EGFR was degraded after 90 minutes of stimulation. In contrast, in the cells treated with the p97 inhibitor DBeQ, EGFR degradation was significantly inhibited as early as 30 minutes and only little degradation was observed after 90 minutes. This result showed that p97 ATPase activity is important for lysosomal degradation of the EGFR.

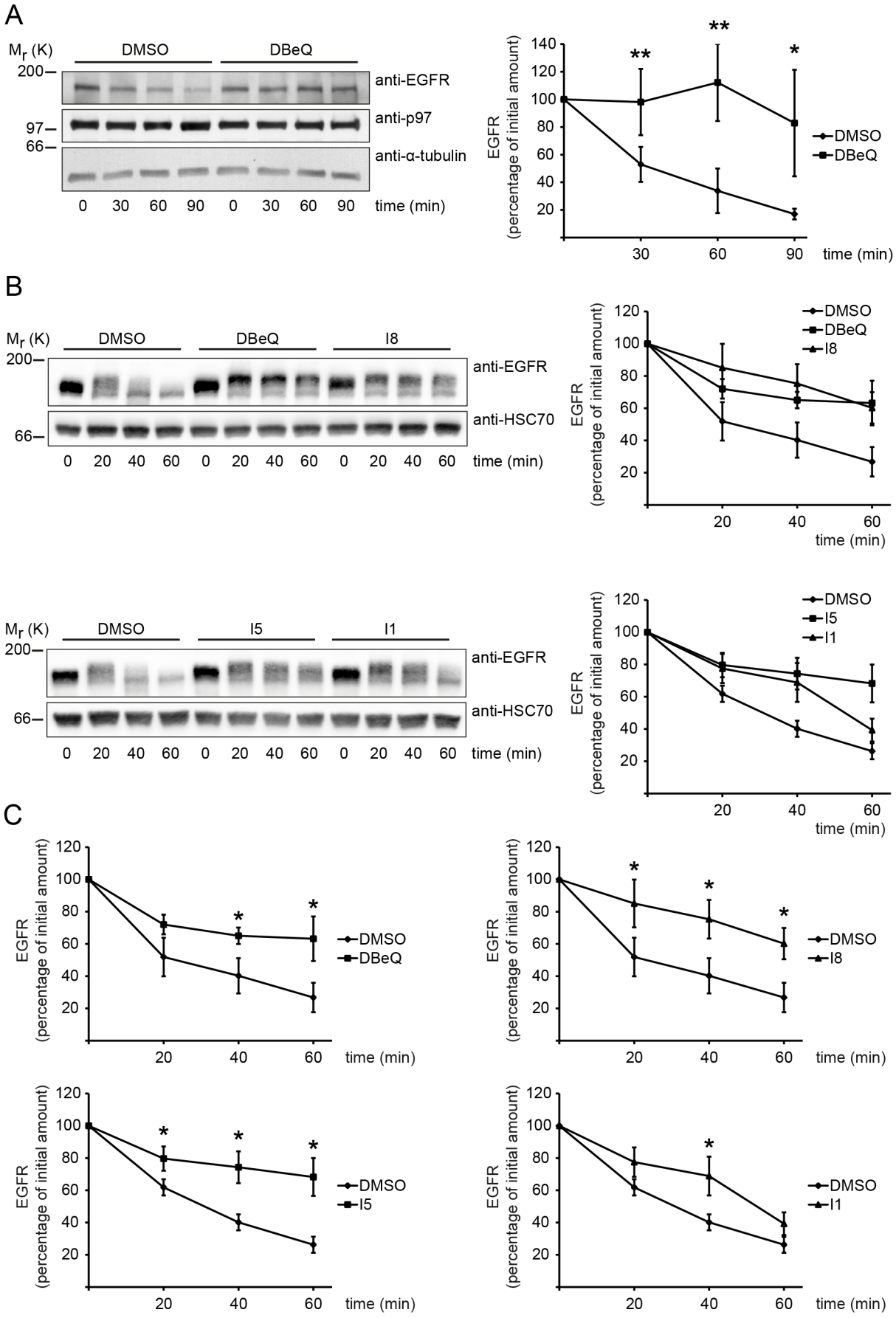
A
Mr (K)
DMSO
DBeQ
200
97
66
anti-EGFR
anti-p97
anti-α-tubulin
0 30 60 90 0 30 60 90 time (min)
EGFR (percentage of initial amount)
DMSO
DBeQ
time (min)
B
Mr (K)
DMSO
DBeQ
I8
anti-EGFR
anti-HSC70
0 20 40 60 0 20 40 60 0 20 40 60 time (min)
DMSO
DBeQ
I8
Mr (K)
DMSO
I5
I1
anti-EGFR
anti-HSC70
DMSO
I5
I1
C
DMSO
DBeQ
DMSO
I8
DMSO
I5
DMSO
I1

Figure 3.18 **Pharmacological inhibition of p97 delays degradation of the EGFR.** A, the p97 inhibitor DBeQ prevents EGFR degradation in HEK293 cells. HEK293 cells were grown to confluence, serum-starved in serum-free DMEM for 4h, and at the same time treated with DMSO or DBeQ. EGFR degradation was induced by addition of 50 ng/ml EGF and cells were harvested in lysis buffer 0, 30, 60, and 90 minutes after stimulation. Cell lysates were analyzed in Western blotting using EGFR- and p97-specific antibodies. Staining for α-tubulin served as a loading control. Electrochemiluminescence signals were quantified from scanned X-ray films using the Bio1D software (Vilber Lourmat) and normalized to the first time point. Error bars represent standard deviation, n = 5. *, $p < 0.05$. **, $p < 0.01$. B, chemical inhibition of p97 delays degradation of the EGFR in HeLa cells. HeLa cells were grown to confluence, serum-starved in serum-free DMEM for 4h, and at the same time treated with DMSO, DBeQ, I8, I5, or I1. EGFR degradation was induced by addition of 100 ng/ml EGF and cells were harvested in lysis buffer 0, 20, 40, and 60 minutes after stimulation. Cell lysates were analyzed in Western blotting using EGFR-specific antibodies. Staining for HSC70 served as a loading control. Electrochemiluminescence signals were digitally acquired using a CCD camera, quantified in ImageJ (1.45k, NIH), and normalized to the first time point. Error bars represent standard deviation, n = 3. C, EGFR degradation curves from B plotted for each inhibitor individually together with the respective DMSO control. Error bars represent standard deviation, n = 3. *, $p < 0.05$.

We confirmed this finding in HeLa cells that express more EGFR and are more widely used to study EGFR regulation. Moreover, we expanded the portfolio of p97 inhibitors to include three additional inhibitors that were made available to the lab for characterization. These unpublished inhibitors (I8, I5 and I1) were identified in high throughput screens to inhibit p97 ATPase activity. Unfortunately, due to an information embargo, we cannot provide structural and biochemical details on these compounds. We starved confluent HeLa cells for 4 h to accumulate the EGFR on the plasma membrane in the presence of p97 inhibitor or vehicle alone. The cells were then stimulated with EGF and harvested after 0, 20, 40, and 60 minutes. EGFR levels were analyzed in Western blotting as described above. The quantification showed that in HeLa cells about 70% of the EGFR was degraded after 60 minutes (Figure 3.18 B). The p97 inhibitor DBeQ delayed EGFR degradation and only 30% of the protein were degraded after 60 minutes. In cells treated with the p97 inhibitor I8, about 30% of EGFR was degraded after 60 minutes comparable to DBeQ treatment. Interestingly, the amount of EGFR at the first time point was slightly lower in I8 treated cells in comparison to DMSO or DBeQ treated cells. The p97 inhibitor I5 showed an inhibitory effect on EGFR degradation that was comparable to DBeQ and I8. In contrast, the p97 inhibitor I1 delayed EGFR degradation only up to 40 minutes. Beyond that time point, the EGFR levels quickly dropped and about 60% of the EGFR was degraded after 60 minutes. In Figure 3.18 C the effect of each inhibitor is

plotted individually together with the respective DMSO control. For DBeQ, I8, and I5 significant differences in EGFR levels were observed at the 40- and 60-minute time points. Furthermore the inhibitors I8 and I5 already caused significant delay of EGFR degradation after 20 minutes of stimulation. The inhibitor I1 caused a significant difference in EGFR levels only at the 40-minute time point but not after 60 minutes of EGFR treatment.

### 3.5.2 Depletion of p97 and PLAA inhibits EGFR degradation

To identify the p97 cofactors that work together with p97 in endosomal sorting and lysosomal degradation of the EGFR, we performed a siRNA-mediated screen in the lab (M. Bug, unpublished data). In this screen, p97 and several cofactors were identified as putative regulators of EGFR sorting. Depletion of the substrate-recruiting cofactor PLAA or the deubiquitinating enzymes YOD1 and VCPIP1 in HeLa cells caused accumulation of the EGFR on enlarged endosomes. To confirm this result in Western blotting, we depleted the cofactors in HeLa cells and investigated the EGFR degradation after EGF stimulation. As a control, we depleted the ESCRT factor TSG101 that is required for endosomal sorting of membrane proteins and to delays EGFR degradation (Raiborg et al., 2008). Knockdown efficiency was tested and confirmed for the TSG101, p97, PLAA, and VCPIP1 siRNAs (data not shown). The YOD1 protein could not be stained in these experiments due to technical problems. However, depletion of YOD1 was shown In HEK293 cells (data not shown). In the control-depleted cells, the EGFR was quickly degraded (Figure 3.19). In contrast, in cells depleted for TSG101, the cellular levels of EGFR were already decreased at the first time point but still a substantial fraction of the initial amount remained after 60 minutes of EGF treatment. Importantly, depletion of p97 did not affect the cellular levels of EGFR but markedly stabilized the EGFR after stimulation. Depletion of PLAA prevented degradation of the EGFR comparable to p97 knockdown. Interestingly, we observed no shift of the EGFR to higher molecular weights after EGF stimulation in this condition. In YOD1 depleted cells the initial levels of EGFR appeared slightly increased and the degradation rate was lower in comparison to the control. In VCPIP1 depleted cells, the cellular EGFR levels were already decreased prior to EGF stimulation comparable to the TSG101 depleted condition. However, in contrast to TSG101 knockdown, the EGFR was not stabilized and at the 60-minute time point almost all EGFR was degraded.

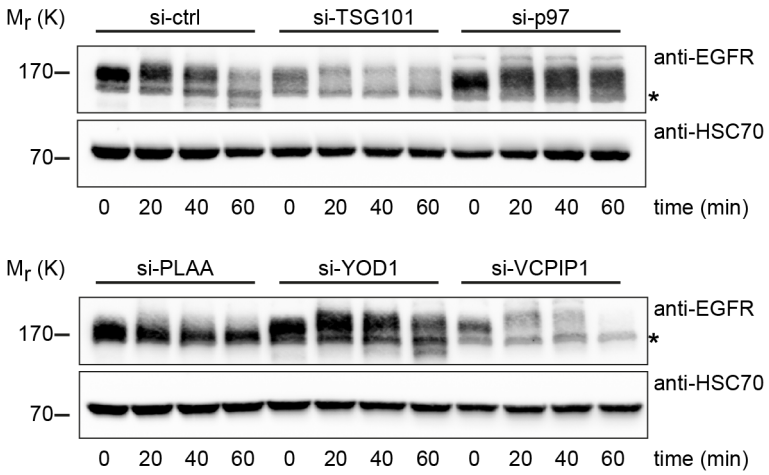


Figure 3.19 **Depletion of p97 or p97 cofactors affects the cellular EGFR levels and the EGFR degradation rate.**
A, cellular depletion of p97 and PLAA causes a marked delay in EGFR degradation. HeLa cells were transfected with control siRNA (si-ctrl) oligonucleotides or siRNAs targeting TSG101, p97, PLAA, YOD1 or VCPIP1 for a total of 72 h. The cells were serum-starved in serum-free DMEM for 4 h and then EGFR degradation was induced by addition of 100 ng/ml EGF. The cells were harvested in lysis buffer 0, 20, 40, and 60 minutes after stimulation. Cell lysates were analyzed in Western blotting using EGFR-specific antibodies. Staining for HSC70 served as a loading control. The asterisk indicates an unspecific band that is recognized by the EGFR antibody.

We could show in two cell lines and using three inhibitors that the ATPase activity of p97 was required for EGF induced degradation of the EGFR. These data were confirmed by siRNA-mediated depletion of p97. Furthermore, depletion of the substrate-recruiting cofactor PLAA delayed EGFR degradation comparable to p97 knockdown. Knockdown of the deubiquitinating enzyme YOD1 caused a small delay of EGFR degradation, while depletion of TSG101 and VCPIP1 decreased the cellular EGFR levels already prior to stimulation.

# 4 Discussion

In this study, we identified the six lysines 5 to 57 in the N-terminal region of CAV1 as critical for ubiquitination of CAV1. We used this information to investigate the functional role of CAV1 ubiquitination in endosomal sorting and lysosomal degradation of CAV1. Furthermore, we showed that the ubiquitination site in the N-terminal region is required for interaction between CAV1 and the AAA-ATPase p97 and performed detailed analyses of this interaction. We found that p97 is involved in endosomal sorting and lysosomal degradation of CAV1 and, importantly, also in endosomal sorting of the EGF receptor. These findings will be discussed with regard to the structural details of CAV1 ubiquitination, the functional relevance of CAV1 ubiquitination for endosomal sorting, the interaction between CAV1 and p97, and the functional role of p97 in endosomal sorting.

## 4.1 Ubiquitination of CAV1 in the N-terminal region

Caveolae are stable cholesterol-rich microdomains in the plasma membrane that do not move laterally or exchange subunits (Mundy et al., 2002; Pelkmans and Zerial, 2005; Tagawa et al., 2005; Thomsen et al., 2002). Still, overexpression of CAV1 is sufficient to mobilize CAV1 and induce endocytosis and degradation in the lysosome. For this process, CAV1 is modified mostly with mono-ubiquitin in addition to short ubiquitin chains (Hayer et al., 2010b). As a consequence, mutating all lysines in CAV1 to arginine (K5-176R) inhibits ubiquitination and lysosomal degradation of CAV1. However, the lysine-less CAV1 K5-176R variant does not provide information about which functional domain in CAV1 is ubiquitinated and how ubiquitination affects the CAV1 protein. Therefore, our initial goal was to define the ubiquitination site in CAV1 more closely.

### 4.1.1 CAV1 is exclusively ubiquitinated in the N-terminal region

We confirmed our data that overexpressed CAV1-myc is modified with HA-ubiquitin (Ritz et al., 2011) and found indication that mutation of the lysines of the N-terminal region interfered with ubiquitination. To improve detection of changes in CAV1 ubiquitination, we generated a human CAV1-HA expression-construct. We chose to use human CAV1 cDNA in contrast to earlier studies (Hayer et al., 2010a; Hayer et al., 2010b) to avoid unspecific effects from expressing dog cDNA in human cell culture. Using this tool, we showed in Western blotting that mutation of the six lysines

in the N-terminal region (K5-57R) was sufficient to abolish CAV1 ubiquitination. In contrast, mutation of the six lysines in the other structural domains of CAV1 (K65-176R) did not affect CAV1 ubiquitination. Consistently, we observed in immunofluorescence microscopy that mutation of the lysines in the N-terminal region significantly reduced the colocalization between CAV1 endosomes and ubiquitin signal. Crucially, the mutation of lysines in CAV1 did not affect the trafficking of CAV1 in the biosynthetic pathway. CAV1 did not accumulate in the ER, at ER-exit sites, or in the Golgi apparatus as shown with specific marker proteins for these cellular compartments. This is important in light of a recent study by Hanson and colleagues that showed that adding a GFP-tag was sufficient to induce defects in CAV1 trafficking (Hanson et al., 2013). Our findings are supported by published data that confirm comparable localization of CAV1 wild type and the lysine-less CAV1 K5-176R to the plasma membrane (Hayer et al., 2010b).

During the course of this study, two large-scale analyses of the ubiquitinated proteome were published (Kim et al., 2011; Wagner et al., 2011). In these screens, ubiquitinated proteins were isolated on the basis of a characteristic diglycine remnant on ubiquitin-conjugated lysines (Peng et al., 2003) and identified in mass spectrometry. Crucially, both studies together identify characteristic diglycine modification of all six lysines in the N-terminal region in CAV1 in line with our mutagenesis data. In addition, Kim and colleagues find evidence for ubiquitination of lysine-176 in the C-terminal domain of CAV1. In our hands, mutation of all lysines that are not part of the N-terminal region (K65-176R) had no effect on CAV1 ubiquitination, while mutation of the lysines in the N-terminal region was sufficient to abolish CAV1 ubiquitination. This argues against involvement of lysine-176 in the mono-ubiquitination of overexpressed CAV1. Importantly, the mass spectrometry approach does not distinguish if a lysine-residue is modified with mono-ubiquitin or poly-ubiquitin chains. It is possible that lysine-176 is modified with poly-ubiquitin chains in cellular processes other than endosomal sorting. For example, an oligomerization deficient variant (P104L) of the caveolin-family member CAV3 is ubiquitinated with K48-linked ubiquitin chains and degraded by the proteasome because it accumulates in the Golgi apparatus (Galbiati et al., 2000).

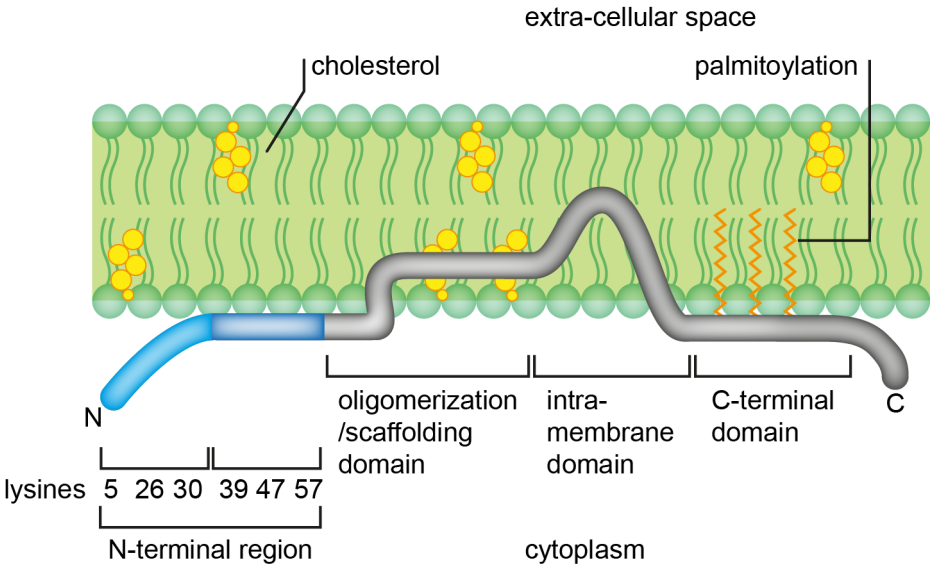


Figure 4.1 **The site of CAV1 ubiquitination is located in the N-terminal region.** Topology model of CAV1 in the plasma membrane. CAV1 is inserted into the plasma membrane through a hairpin-like intra-membrane domain with both N- and C-termini facing the cytoplasm. The oligomerization/scaffolding domain is partially inserted into the hydrophobic core of the membrane where it may associate with cholesterol. The C-terminal domain is palmitoylated on three cysteines and anchored in the plasma membrane. In contrast, the N-terminal region is more flexible and protrudes into the cytoplasm. We show that the six lysines in the N-terminal region are sufficient and required for CAV1 ubiquitination. Interestingly, ubiquitination of the first three lysines (5, 26, 30), or the following three lysines (39, 47, 57) produces a small difference in the running behavior of mono-ubiquitinated CAV1 in SDS gels. The second sub-region partially overlaps with a putative membrane interface helix (Parton et al., 2006). (modified from Parton and del Pozo, 2013)

Interestingly, ubiquitination of CAV1 appears to be promiscuous in a manner similar to sumoylation of CAV3 (Fuhs and Insel, 2011). Mutation of individual lysines in the N-terminal region had no effect on CAV1 ubiquitination. Consistently, re-introducing any lysine of the N-terminal region into the lysine-less CAV1 K5-176R variant resulted in a partial restoration of ubiquitination. However, not all lysines could serve as ubiquitin acceptor sites equally well. Ubiquitination of lysines 39 and 47 was the most prominent, while the lysines 30 and 57 were only marginally ubiquitinated. Interestingly, the faintly ubiquitinated lysine-57 is located within the minimal CAV1 required for caveolae formation (Kirkham et al., 2008; Parton et al., 2006) and might not be readily accessible for ubiquitination. Likewise, the minor ubiquitin-acceptor lysine-30 is positioned at the start of a predicted amphipathic helix between residues 30 and 50 (Parton et al., 2006) (Figure 4.1). The two most efficiently ubiquitinated lysines (K39 and K47) are present in both CAV1 isoforms α and β (Kogo and Fujimoto, 2000). This might allow efficient ubiquitination of the β-isoform by the same ubiquitin ligase as the α-isoform. Furthermore, the conjugation of ubiquitin to the first

three lysines (K5, K26, K30) or the following three lysines (K39, K47, K57) resulted in a small difference in the migration speed of mono-ubiquitinated CAV1 in SDS gels. This indicates that the observed double band of mono-ubiquitinated CAV1 wild type probably is the result of ubiquitin conjugation in both sub-regions with equal frequency.

### 4.1.2 The N-terminal region of CAV1 is accessible for posttranslational modifications

The finding that CAV1 is ubiquitinated in the N-terminal region provides insight into the molecular consequences of CAV1 ubiquitination. The CAV1 protein contains several membrane-binding domains in addition to the intra-membrane domain (Figure 4.1). The C-terminal domain is palmitoylated on three conserved cysteines, while the scaffolding domain is partially buried in the inner leaflet of the plasma membrane (Epand et al., 2005; Parton et al., 2006). Additionally, the oligomerization and scaffolding domains are involved in intermolecular interactions and oligomerization of CAV1 (Fernandez et al., 2002; Sargiacomo et al., 1995). In contrast, the N-terminal region is less structured and protrudes into the cytoplasm apart from predicted helix between residues 30 and 50 that may interact with the plasma membrane interface (Parton et al., 2006). We speculate that this allows ubiquitination of oligomerized CAV1 without disruption of caveolae. Consistently, we observed that ubiquitinated CAV1 colocalized with PTRF/cavin-1, a coat protein that only associates with caveolar CAV1 but not biosynthetic pools of CAV1 (Hill et al., 2008; Kirkham et al., 2008; Liu and Pilch, 2008). The lysines of the N-terminal region are conserved in CAV1 from zebrafish, chicken, and mouse (data not shown); also the closely related CAV3 harbors lysines corresponding to position 47 and 57 in CAV1 plus one additional lysine close to the N-terminus. This is consistent with the notion that ubiquitination in the N-terminal region is a conserved mechanism of regulating caveolin proteins and can take place prior to disassembly of the caveolar scaffold. However, fusion of the N-terminal region alone to GFP was not sufficient to serve as an ubiquitination signal (data not shown). One explanation is that ubiquitination of the N-terminal region of CAV1 may require localization to lipid raft domains in the plasma membrane and does not occur if the N-terminal domain is fused to freely diffusible GFP.

Another posttranslational modification in the N-terminal region is the phosphorylation of tyrosine-14 that has been described as a regulator of caveolar endocytosis (Aoki et al., 2007; del Pozo et al., 2005; Gaus et al., 2006; Sverdlov et al., 2007). In

agreement with the work from del Pozo and colleagues, we observed that a phosphorylation-deficient CAV1 variant (Y14F) localized to the plasma membrane similar to wild type CAV1. Yet crucially, we found no evidence for reduced endocytosis or ubiquitination of CAV1 Y14F.

### 4.1.3 Establishing a microscopy-based assay of CAV1 ubiquitination in E3 ubiquitin ligase depleted cells

The non-ubiquitinatable CAV1 K5-57R variant makes it possible to analyze the functional consequences of CAV1 ubiquitination. However, for a comprehensive analysis it would be interesting to directly influence the ubiquitination state of wild type CAV1 by depleting or overexpressing the E3 ubiquitin ligase that modifies CAV1. Because to date no E3 ligase was known to ubiquitinate CAV1, we decided to establish a microscopy-based assay of CAV1 ubiquitination in parallel to performing functional analyses of the non-ubiquitinatable CAV1 K5-57R variant. This assay could then be used to screen a large library of siRNA oligonucleotides targeting E3 ubiquitin ligases for effects on CAV1 ubiquitination. For this purpose, we generated an U2OS cell line that expresses CAV1-HA under control of a doxycycline inducible promoter to investigate ubiquitination of CAV1 in Western blotting and immunofluorescence microscopy. In this cell line, we tested a small number of E3 ubiquitin ligases that are known to ubiquitinate membrane proteins. In particular, the HECT-type ligase NEDD4L interacts with transiently overexpressed CAV3 in HEK293 cells (Guo et al., 2012). Depletion of NEDD4L caused accumulation of ubiquitinated CAV1 in untreated cells but prevented accumulation of ubiquitinated CAV1 in cells treated with a lysosome inhibitor. However, this probably represents an unspecific effect of NEDD4L depletion since NEDD4L is also involved in the ubiquitination of several important regulators of endosomal sorting (Yang and Kumar, 2010). Nevertheless, we were able to establish that the automated analysis of colocalization between CAV1 vesicles and ubiquitin is a suitable assay to quantify CAV1 ubiquitination in E3 ubiquitin ligase depleted cells. Due to time limitations, this analysis was only performed with a small number of pre-selected E3 ligases.

## 4.2 What are the functional consequences of CAV1 ubiquitination?

Previous studies showed that mutation of all lysines in CAV1 increases the half-life of CAV1 by preventing lysosomal degradation (Hayer et al., 2010b; Ritz et al., 2011). Along this line, lysosomal inhibitors but not proteasome inhibitors prevent degradation of overexpressed CAV1 (Hayer et al., 2010b) and inhibit stimulated degradation of CAV1 (Martinez-Outschoorn et al., 2010; Peterson et al., 2003; Vassilieva et al., 2009). Importantly, sorting of CAV1 into multivesicular endosomes requires the AAA-ATPase p97, and overexpression of the dominant negative p97 E578Q variant prevents the formation of intralumenal vesicles (Ritz et al., 2011). Moreover, CAV1 wild type but not the lysine-less CAV1 K5-176R interacts with the p97 and the cofactor UBXD1 supporting a role of p97 in the endosomal sorting of ubiquitinated CAV1. However, the functional connection between CAV1 ubiquitination and endosomal trafficking of CAV1 was not known.

### 4.2.1 Sorting of ubiquitinated CAV1 on late endosomes requires p97

We could confirm that inhibition of the lysosome, but not of the proteasome accumulated ubiquitinated CAV1 on late endosomes. Moreover, also cellular depletion or pharmacological inhibition of the p97-UBXD1 complex caused accumulation of ubiquitinated CAV1. Along this line, we observed that the non-ubiquitinatable CAV1 variants showed significantly reduced colocalization with the late endosome marker LAMP1 in comparison to wild type CAV1. These data indicate that p97-UBXD1 acts downstream of CAV1 ubiquitination and regulates sorting of ubiquitinated CAV1 on late endosomes prior to degradation in the lysosome. Crucially, we could show that the ubiquitination site in the N-terminal region of CAV1 was required for interaction between CAV1 and the p97-UBXD1 complex and mediated recruitment of p97-UBXD1 to endosomes. The functional connection between CAV1 ubiquitination and endosomal sorting by the p97-UBXD1 complex will be discussed in more detail below.

### 4.2.2 CAV1 ubiquitination regulates trafficking of CAV1 to the early endosome after endocytosis

Importantly we could show that, in addition to mediating interaction with p97-UBXD1 and sorting at the late endosome, ubiquitination of CAV1 was already required for trafficking of CAV1 to the early endosome. Following stimulus dependent endocytosis, CAV1 localizes to stable membrane domains on early endosomes (Hayer et al., 2010b; Pelkmans et al., 2004; Pelkmans and Zerial, 2005).

Consequently, we observed that wild type CAV1 colocalized with the early endosome markers EEA1 and RAB5. However, this was not the case for the non-ubiquitinatable K5-57R variant. Moreover, non-ubiquitinatable CAV1 accumulated on ubiquitin- and EEA1-negative endocytic vesicles that were marked by the caveolar coat protein PTRF/cavin-1. PTRF/cavin-1 associates with large 70S caveolar scaffolds and regulates the stability of caveolae and interaction with the cytoskeleton (Hansen et al., 2013; Liu and Pilch, 2008; Vinten et al., 2005). Importantly, PTRF/cavin-1 stays associated with CAV1 oligomers after endocytosis and during trafficking to early endosomes (Hayer et al., 2010b; Hill et al., 2008). The PTRF/cavin-1 positive vesicles that accumulate after CAV1 overexpression probably are related to RAB5-negative endocytic vesicles prior to fusion with the early endosome (Sharma et al., 2003). However, these vesicles are usually small and short-lived but might be enlarged and stabilized by the high levels of CAV1 after transient overexpression.

Data by Hayer and colleagues and our own experiments showed that, in contrast to endogenous RAB5, CAV1 colocalized with overexpressed GFP-RAB5 independently of ubiquitination (Hayer et al., 2010b). The discrepancy between these observations may be explained by the fact that overexpression of GFP-RAB5 increases the size of the early endosomal compartment (Bucci et al., 1992; Roberts et al., 1999). This might reduce the need for CAV1 ubiquitination by increasing the rate of fusion between endocytic vesicles and the early endosome (Zeigerer et al., 2012). It is not known how CAV1 ubiquitination regulates trafficking to the early endosome but a recent study showed that CAV1 could directly interact with RAB5 and increase the GTPase activity of RAB5 (Hagiwara et al., 2009). Interestingly, RAB5 has to be present on both the incoming vesicle and the early endosome for fusion to occur (Barbieri et al., 1998). Thus, ubiquitination of CAV1 may be required to effectively recruit or activate RAB5 on endocytic vesicles. Figure 4.2 shows a graphical representation of our model for trafficking of CAV1 after endocytosis. Life cell microscopy could help to clarify this endosomal sorting event by following the fate of individual CAV1-positive vesicles from endocytosis to fusion with the early endosome. In a similar experiment, Zoncu and colleagues tracked single endosomes after endocytosis and investigated the sequential recruitment of membrane proteins upstream of the early endosome (Zoncu et al., 2009).

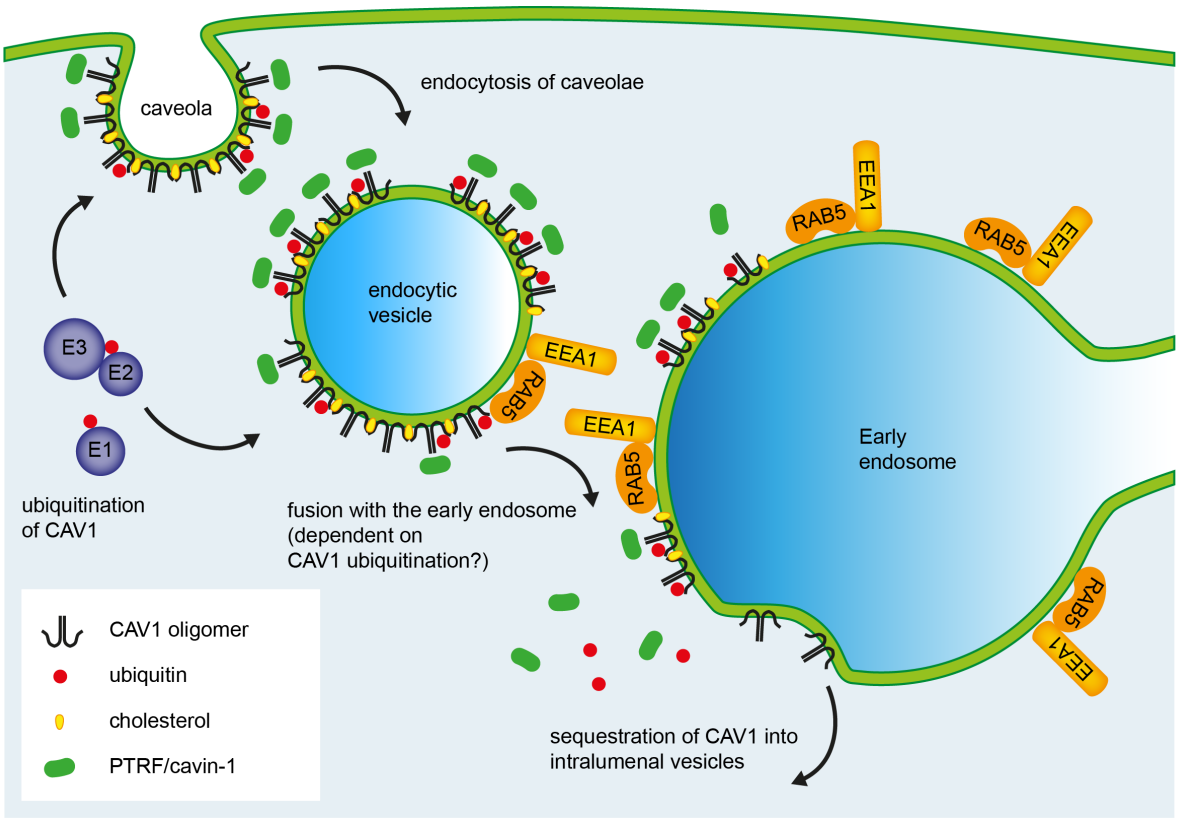


Figure 4.2 **Model for the sorting of ubiquitinated CAV1 after endocytosis.** Ubiquitination of CAV1 may mediate trafficking of caveolar vesicles to the early endosome. CAV1 may be ubiquitinated in caveolae at the plasma membrane or on endocytic vesicles. The endocytic vesicles are marked by the coat protein PTRF-cavin-1 that associates with caveolar scaffolds. From early endosomes, CAV1 is further sequestered into intralumenal vesicles and transported to the lysosome for degradation. In contrast, non-ubiquitinatable CAV1 is endocytosed on PTRF/cavin-1 positive vesicles comparable to CAV1 wild type but does not colocalize with the early endosome markers EEA1 and RAB5. Therefore, we propose that ubiquitination of CAV1 may be required for fusion of endocytic vesicles with the early endosome. The molecular connection between CAV1 ubiquitination and trafficking to early endosomes is not known but might involve direct interaction of ubiquitinated CAV1 and the endosomal GTPase RAB5.

### 4.2.3 Autophagy might be involved in the degradation of ubiquitinated CAV1

In addition to endosomal markers, CAV1 wild type colocalized with the autophagosome marker LC3-GFP. This interaction was limited to few vesicles per cell but strikingly absent in cells expressing the non-ubiquitinatable CAV1 K5-57R variant. Moreover, a substantial fraction of CAV1 wild type vesicles colocalized with a second autophagy marker, the ubiquitin adapter protein p62. Again, this was specific for CAV1 wild type and not observed with non-ubiquitinatable CAV1. It is unclear why more CAV1 vesicles colocalize with p62 in comparison to LC3-GFP. It could be possible that quenching of the GFP fluorescence in acidified endosomes reduces the number of LC3-GFP vesicles we can visualize (Pankiv et al., 2007). However, this

appears unlikely in light of the small percentage (7%) of CAV1 vesicles that colocalize with acidified LAMP1-positive late endosomes.

In selective autophagy, p62 aggregates ubiquitinated cytoplasmic proteins and directs them to the autophagosome via direct interaction with the autophagic membrane protein LC3 (Kirkin et al., 2009b). However, In addition to degradation of cytoplasmic proteins, autophagy can be involved in degradation of proteins that accumulate in the ER (Yorimitsu and Klionsky, 2007). Importantly, we could exclude that the colocalization of CAV1 with LC3-GFP or p62 was due to accumulation of misfolded or aggregated CAV1 in the biosynthetic pathway. We showed that overexpressed CAV1 did not colocalize with UBXD8, a p97 cofactor that resides in the ER membrane and is involved in retro-translocation of misfolded proteins. Moreover, we did not observe accumulation of CAV1 on ER-exit sites or in the Golgi apparatus. Therefore, we suggest that the source of colocalization between CAV1 and LC3-GFP or p62 is not ubiquitinated CAV1 in the biosynthetic pathway but rather on endosomes.

We do not know if the colocalization between CAV1 and p62 or LC3-GFP is the result of a direct interaction and how autophagy is involved in endosomal sorting of CAV1. One possibility is that interaction between ubiquitinated CAV1 and p62 on endosomes induces sequestration of CAV1 vesicles in autophagosomes. Interestingly, it has been shown that overexpression of a mono-ubiquitin fused protein that localizes to peroxisomes was sufficient to recruit p62 and induce degradation of these vesicles in autophagy (Kim et al., 2008). In this context, p97 has been shown to regulate autophagy of ubiquitinated proteins (Chou et al., 2011; Ju et al., 2009; Tresse et al., 2010) and could be equally required for CAV1 degradation via endosomal sorting and autophagy. Interestingly, in addition to its function as an ubiquitin adapter in autophagy, p62 is reported to interact with a wide variety of membrane proteins and mediate ubiquitination or deubiquitination in endosomal sorting (Duran et al., 2011; Geetha et al., 2005; Geetha et al., 2008; Layfield and Shaw, 2007). Therefore, p62 may facilitate endosomal sorting of CAV1 by mediating CAV1 deubiquitination. A model for the functional connection between p62 and trafficking of ubiquitinated CAV1 is presented in Figure 4.3.

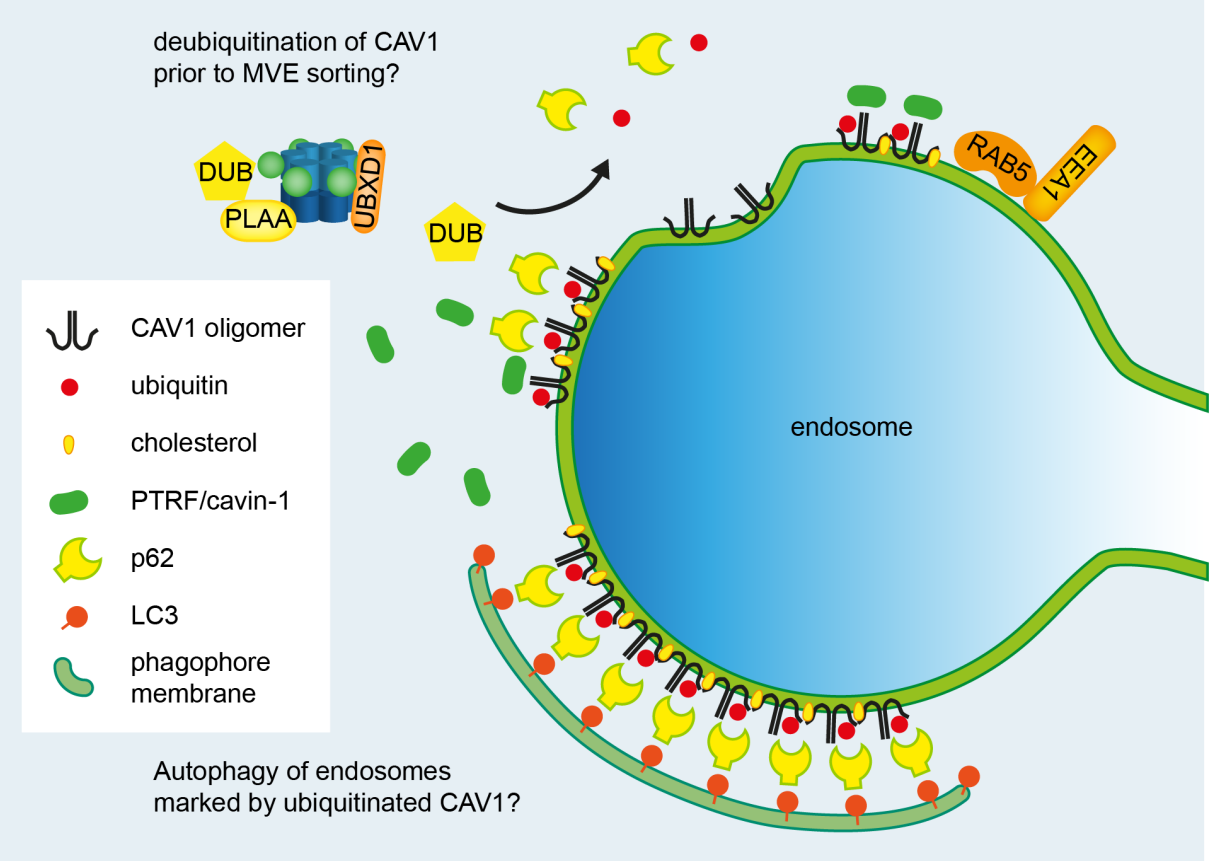


Figure 4.3 **Possible functions for p62 on CAV1 endosomes.**
After overexpression of ubiquitinatable CAV1, the ubiquitin adapter protein p62 colocalizes with CAV1 on endosomes. Furthermore, a smaller percentage of CAV1 vesicles colocalizes with the autophagic membrane protein LC3-GFP. Interaction between ubiquitinated CAV1 and p62 might be a signal for degradation of CAV1-positive endosomes in autophagy. As an alternative, p62 could recognize ubiquitinated CAV1 on endosomes and coordinate deubiquitination. This may involve the activity of unknown deubiquitinating enzymes in association with the p97-UBXD1 complex (discussed below).

## 4.3 How does p97 interact with ubiquitinated CAV1?

We have established that ubiquitination of CAV1 in the N-terminal region regulates sorting of CAV1 on early and late endosomes. Previous studies by our group showed that overexpression of the dominant negative p97 variant E578Q accumulates CAV1 on the limiting membrane of enlarged late endosomes (Ritz et al., 2011). Furthermore, CAV1 wild type but not the non-ubiquitinatable CAV1 K5-176R variant interacts with the AAA-ATPase p97 in a complex with the cofactor UBXD1. In the following, we will discuss the functional connection between the p97-UBXD1 complex and sorting of ubiquitinated CAV1 on late endosomes.

### 4.3.1 The p97-UBXD1 mediates turnover of ubiquitinated CAV1

Importantly, we could show that the ubiquitination site in the N-terminal region of CAV1 was required for interaction with p97 and UBXD1. Along this line, we observed that CAV1 wild type but not the non-ubiquitinatable CAV1 variants recruited p97 and UBXD1 to endosomes. However, a fraction of p97 localized to endosomes also in the absence of CAV1 ubiquitination. This indicates that additional factors might be able to target p97 to endosomes. Interestingly, a recent study described direct interaction between p97 and the early endosomal marker protein EEA1 that could recruit p97 to early endosomes (Ramanathan and Ye, 2012). Taken together, our data suggest that the p97-UBXD1 complex interacts with ubiquitinated CAV1 on endosomes and directly regulates endosomal trafficking of CAV1. Crucially, we could show that siRNA mediated depletion of p97 or UBXD1 caused accumulation of ubiquitinated CAV1 comparable to lysosome inhibition. Furthermore, short pharmacological inhibition of p97 with the inhibitor DBeQ (Chou et al., 2011) caused a weak but consistent accumulation of ubiquitinated CAV1 on late endosomes. This indicates that p97 and UBXD1 act downstream of CAV1 ubiquitination and regulate turnover of ubiquitinated CAV1. During the course of this study, Chen and colleagues published their finding that CAV1 interacts with p97 in a complex with UFD1 and Derlin-1 and facilitates the extraction of ubiquitinated COX2 proteins from the ER (Chen et al., 2013). In contrast, we never observed localization of overexpressed CAV1 to the ER. Additionally, in previous studies we showed that CAV1 exclusively precipitated UBXD1 but not the p97 cofactor UFD1 (Ritz et al., 2011).

### 4.3.2 The interaction between p97 and ubiquitinated CAV1 might not require an ubiquitin-binding cofactor

The interaction between p97 and ubiquitinated substrates is generally mediated through substrate-recruiting cofactors (Jentsch and Rumpf, 2007; Meyer et al., 2002). Therefore, we investigated if an ubiquitin-binding cofactor is required for the interaction between p97 and ubiquitinated CAV1. Initially, we tested the substrate-recruiting cofactor PLAA because we observed that depletion of PLAA caused accumulation of ubiquitinated CAV1 comparable to depletion of p97. Furthermore, the yeast homologue Ufd3 is known to be involved in sorting of ubiquitinated cargo proteins on multivesicular endosomes (Ren et al., 2008). PLAA interacts with the C-terminus of p97 through a PUL domain and can bind ubiquitin through and a PFU domain together with a WD40 β -propeller (Mullally et al., 2006). Nevertheless, cellular depletion of PLAA did not affect the interaction between p97 and

ubiquitinated CAV1. Along this line, PLAA did not co-isolate with p97 in CAV1 immunoprecipitates. However, it is possible that we cannot co-precipitate PLAA because the interaction between the PLAA cofactor and p97 is only transient. Importantly, we found in previous mass spectrometry analyses (Ritz et al., 2011) that PLAA only interacted with the dominant negative E578Q variant of p97 that cannot release protein substrates after binding (Ramadan et al., 2007; Ye et al., 2003). However, expressing the substrate-trapping p97 E578Q variant together with CAV1 did not stabilize co-isolation of the PLAA cofactor in CAV1 immunoprecipitates. Interestingly, the interaction between CAV1 and p97 E578Q was rather decreased in comparison to p97 wild type. One possible explanation could be that the p97 E578Q variant is trapped in many substrate-protein complexes and thus sequestered away from ubiquitinated CAV1.

To systematically address the question if a substrate-recruiting cofactor mediates the interaction between p97 and ubiquitinated CAV1, we screened a siRNA library of all known p97 cofactors that harbor ubiquitin-binding motifs. Interestingly, depletion of none of these cofactors affected the interaction between ubiquitinated CAV1 and p97-UBXD1. However, not all siRNAs used in the screen were confirmed to deplete their target protein efficiently. Especially, the siRNA targeting SAKS1 used in this screen was later found ineffective to deplete SAKS1. Additionally, several cofactors might facilitate the interaction between CAV1 and p97 in a redundant fashion. In the scope of this study, however, it was not possible to verify the depletion efficiency of all siRNAs and to exclude cofactor redundancy in the CAV1-p97-UBXD1 complex. At least, the results from this screen suggest that p97 might be able to interact with ubiquitinated CAV1 without the help of an ubiquitin-adapter protein. Along this line, a recent study in yeast described a group of proteasome substrates that accumulate after deletion of Cdc48 but not after deletion of substrate-recruiting cofactors (Kolawa et al., 2013). Furthermore, p97 has a weak affinity for mono-ubiquitinated substrates (Rape et al., 2001; Ye et al., 2003) and even can recognize non-ubiquitinated protein substrates (Ye et al., 2003). The ubiquitin-binding site resides on the N domain of p97 that is structurally similar to the UFD1 cofactor (Park et al., 2005; Pye et al., 2007). Additionally, the N-domain interacts with ubiquitin-like domains, for example the UBX domain that is present in several p97 cofactors (Schuberth and Buchberger, 2008). The weak binding affinity of p97 to mono-ubiquitin might be amplified by simultaneous interaction with several ubiquitinated CAV1 molecules. In this context,

we found in a previous study that p97 preferentially binds SDS-resistant CAV1 oligomers (Ritz et al., 2011).

## 4.4 How does p97 regulate endosomal sorting of CAV1 and the EGFR?

We established p97, together with the cofactor UBXD1, as a regulator of endosomal sorting of ubiquitinated CAV1. In this context, we asked if p97 is a more general regulator of endosomal sorting and investigated the lysosomal degradation of the EGF receptor. Additionally, we investigated the involvement of further p97 cofactors in p97-mediated endosomal sorting.

### 4.4.1 Lysosomal turnover of ubiquitinated CAV1 might involve the p97 cofactors PLAA and VCPIP1

Mass spectrometry and immunoprecipitation studies in our lab (D. Ritz and M. Bug, unpublished data) identified an interaction between the p97-UBXD1 complex and the substrate-recruiting cofactor PLAA. Moreover, the deubiquitinating enzymes YOD1 and VCPIP1 were also indentified in this complex. The yeast homologue of PLAA, Ufd3, was shown to genetically interact with deubiquitinating enzymes and regulate the mono-ubiquitination of histone H2B is response to DNA damage (Lis and Romesberg, 2006). Furthermore, Ufd3 is involved in sorting of ubiquitinated proteins on multivesicular endosomes (Ren et al., 2008). Importantly, we could show that depletion of PLAA or the deubiquitinating enzyme VCPIP1 resulted in accumulation of ubiquitinated CAV1 comparable to depletion of p97 or UBXD1. The DUB activity of VCPIP1 in p97-p47-mediated reassembly of the Golgi apparatus is regulated through the activator protein WAC (Totsukawa et al., 2011). Consequentially, depletion of WAC caused accumulation of ubiquitinated CAV1 comparable to VCPIP1 depletion (data not shown). The function of PLAA might be to bring VCPIP1 into close contact with ubiquitinated CAV1. However, as discussed above, we could not identify an interaction between ubiquitinated CAV1 and PLAA. In this context, we tested the effect of cellular depletion of all known substrate-recruiting cofactors on the levels of ubiquitinated CAV1 to identify other components of the p97-UBXD1 complex. Knockdown of several cofactors such as SAKS1 and DVC1 caused accumulation of ubiquitinated CAV1, while depletion of p47 or FAF1 decreased the levels of ubiquitinated CAV1. However, the results gathered from this experiment are only preliminary.

### 4.4.2 p97 regulates lysosomal degradation of activated EGF receptor

To investigate if p97 is a general regulator in endosomal trafficking of membrane proteins, we analyzed degradation of the EGF receptor. Ligand-induced endocytosis and degradation of the EGF receptor is a widely studied model for ubiquitin-dependent degradation of plasma membrane proteins in the lysosome (Goh and Sorkin, 2013; Madshus and Stang, 2009). Importantly, we could show that treatment of HEK293 cells with the p97 inhibitor DBeQ (Chou et al., 2011) inhibited the ligand-induced degradation of the EGF receptor. This was confirmed in HeLa cells using DBeQ and two new p97 inhibitors that were supplied to our lab for characterization. A third inhibitor with lower inhibitory activity in vitro (R. Pöhler, unpublished data), consistently, had a weak effect on EGFR degradation. We further confirmed that p97 was required for EGFR degradation by cellular depletion of p97 with specific siRNA oligonucleotides. This establishes p97 as a general regulator of endosomal trafficking. To elucidate the cofactors that work together with p97 in endosomal sorting of ligand stimulated EGFR, we screened a siRNA library of p97 cofactors using immunofluorescence microscopy (M. Bug unpublished data). In this screen we found that depletion of PLAA or the deubiquitinating enzymes YOD1 and VCPIP1 caused accumulation of the EGF receptor on enlarged endosomes. Consistently, we observed in Western blotting that depletion of PLAA, and to a lesser extend YOD1, delayed EGFR degradation. In contrast, depletion of VCPIP1 had no effect on the rate of EGFR degradation. However, knockdown of VCPIP1 decreased the cellular levels of EGFR similar to depletion of the ESCRT-I protein TSG101. This could indicate that the knockdown of VCPIP1 affects endosomal recycling of the EGFR, as was proposed for depletion of TSG101 (Morris et al., 2012; Rush and Ceresa, 2013).

### 4.4.3 What is the functional connection between p97 and endosomal sorting?

Cellular depletion of PLAA had a comparable effect on the endosomal trafficking of both ubiquitinated CAV1 and EGFR. In contrast, depletion of the DUB VCPIP1 specifically caused accumulation of ubiquitinated CAV1, while depletion of YOD1 inhibited EGFR degradation. Therefore, we speculate that p97, together with PLAA, could form a scaffold that associates with substrate-specific deubiquitinases to regulate membrane trafficking (Figure 4.4). As mentioned above, this model is similar to the regulation of histone H2b ubiquitination in yeast by the PLAA homologue Ufd3 in association with deubiquitinases (Lis and Romesberg, 2006). It is well established that deubiquitination is a crucial step in the MVE sorting of membrane proteins on late endosomes (Goh and Sorkin, 2013). In this context, we discussed above that the

ubiquitin-adapter protein p62 might be recruited to ubiquitinated CAV1 on endosomes to mediate deubiquitination and MVE sorting. It could be possible that such a deubiquitination step involves p97 together with deubiquitinating enzymes.

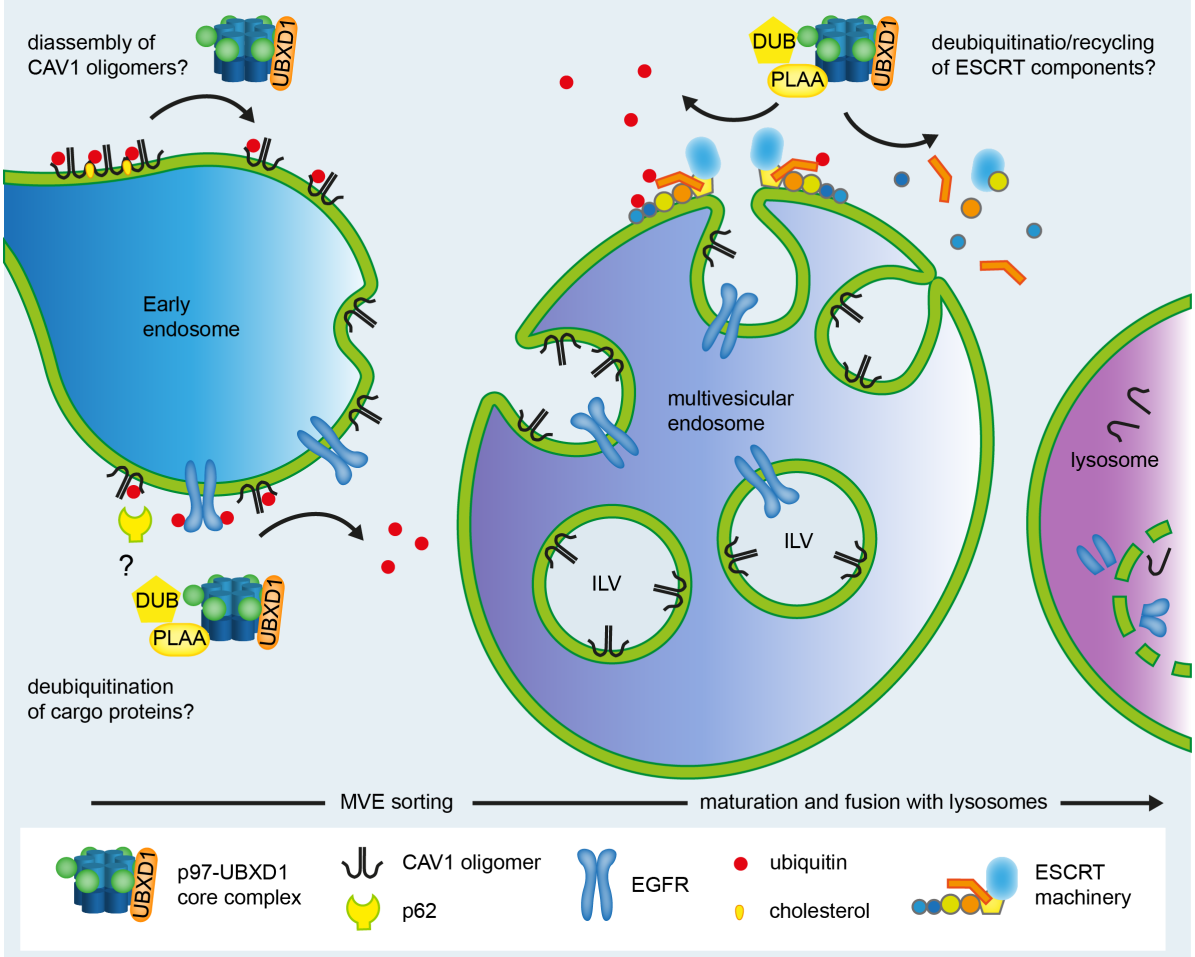


Figure 4.4 **Hypothetical model for the functions of p97 in endosomal sorting of ubiquitinated CAV1 and the EGFR**

We could show that p97 is an important regulator in endosomal sorting and lysosomal degradation of ubiquitinated CAV1 and the EGFR. There are several possible models that could explain the molecular function of p97 in endosomal sorting. Deubiquitination of cargo proteins is essential for their sorting into intralumenal vesicles (ILVs) and degradation in the lysosome. This deubiquitination may could be mediated by p97-associated deubiquitinases and involve targeting factors like PLAA. Furthermore, this could be connected to the localization of the ubiquitin-adapter p62 to CAV1-positive endosomes. As an alternative, the segregase activity of p97 might be required to disassemble the large caveolar scaffolds prior to intralumenal vesicle formation. Finally, p97 might regulate the endosomal sorting machinery on multivesicular endosomes (MVEs) that facilitates ILV formation. In this model, p97 could mediate deubiquitination of ESCRT component and prevent their proteasomal degradation, or enable recycling of the ESCRT machinery after vesicle abscission.

In an alternative model, the p97-PLAA-DUB complex could be required to deubiquitinate and thus stabilize factors that are involved in multivesicular endosome biogenesis, for example VPS34 PI3P-kinase subunits (Abrahamsen et al., 2012; Raiborg et al., 2013) or ESCRT components (Clague and Urbe, 2006; Wright et al., 2011). Finally, p97 utilizes the energy of ATP hydrolysis to segregate ubiquitinated protein complexes, for example in ERAD (Meyer et al., 2012; Stolz et al., 2011; Ye, 2006) or in mitosis (Ramadan et al., 2007). Given that caveolae induce membrane curvature towards the cytosol (Parton et al., 2006), disassembly of the caveolar scaffold is probably required for MVE sorting of CAV1 because intralumenal vesicles curve away from the cytosol (Raiborg and Stenmark, 2009). Interestingly, we showed in a previous study that p97 predominantly interacted with SDS-resistant CAV1 oligomers (Ritz et al., 2011). In an alternative model, the segregase activity of p97 may be required to recycle subunits of the ESCRT endosomal-sorting machinery after vesicle abscission, similar to the activity of the AAA-ATPase VPS4 (Wollert et al., 2009). Interestingly, p97 was proposed to regulate vesicle fusion by regenerating free Syntaxin-5 from SNARE complexes following vesicle fusion (Rabouille et al., 1998). The models for the molecular function of p97 in endosomal sorting of ubiquitinated CAV1 and the EGFR are presented in Figure 4.4. However, further work is required to define the molecular function of p97 in endosomal sorting of ubiquitinated cargo proteins in more detail.

## References

Abrahamsen, H., Stenmark, H., and Platta, H.W. (2012). Ubiquitination and phosphorylation of Beclin 1 and its binding partners: Tuning class III phosphatidylinositol 3-kinase activity and tumor suppression. FEBS Lett *586*, 1584-1591.

Acconcia, F., Sigismund, S., and Polo, S. (2009). Ubiquitin in trafficking: the network at work. Exp Cell Res *315*, 1610-1618.

Alexandru, G., Graumann, J., Smith, G.T., Kolawa, N.J., Fang, R., and Deshaies, R.J. (2008). UBXD7 binds multiple ubiquitin ligases and implicates p97 in HIF1alpha turnover. Cell *134*, 804-816.

Amerik, A.Y., Nowak, J., Swaminathan, S., and Hochstrasser, M. (2000). The Doa4 deubiquitinating enzyme is functionally linked to the vacuolar protein-sorting and endocytic pathways. Mol Biol Cell *11*, 3365-3380.

Amit, I., Yakir, L., Katz, M., Zwang, Y., Marmor, M.D., Citri, A., Shtiegman, K., Alroy, I., Tuvia, S., Reiss, Y.*, et al.* (2004). Tal, a Tsg101-specific E3 ubiquitin ligase, regulates receptor endocytosis and retrovirus budding. Genes Dev *18*, 1737-1752.

Aoki, T., Hagiwara, H., Matsuzaki, T., Suzuki, T., and Takata, K. (2007). Internalization of caveolae and their relationship with endosomes in cultured human and mouse endothelial cells. Anat Sci Int *82*, 82-97.

Bache, K.G., Slagsvold, T., and Stenmark, H. (2004). Defective downregulation of receptor tyrosine kinases in cancer. EMBO J *23*, 2707-2712.

Baek, G.H., Cheng, H., Choe, V., Bao, X., Shao, J., Luo, S., and Rao, H. (2013). Cdc48: A Swiss Army Knife of Cell Biology. J Amino Acids *2013*, 183421.

Balderhaar, H.J., and Ungermann, C. (2013). CORVET and HOPS tethering complexes - coordinators of endosome and lysosome fusion. J Cell Sci *126*, 1307-1316.

Ballar, P., Shen, Y., Yang, H., and Fang, S. (2006). The role of a novel p97/valosin-containing protein-interacting motif of gp78 in endoplasmic reticulum-associated degradation. J Biol Chem *281*, 35359-35368.

Barbieri, M.A., Hoffenberg, S., Roberts, R., Mukhopadhyay, A., Pomrehn, A., Dickey, B.F., and Stahl, P.D. (1998). Evidence for a symmetrical requirement for Rab5-GTP in in vitro endosome-endosome fusion. J Biol Chem *273*, 25850-25855.

Barriere, H., Nemes, C., Lechardeur, D., Khan-Mohammad, M., Fruh, K., and Lukacs, G.L. (2006). Molecular basis of oligoubiquitin-dependent internalization of membrane proteins in Mammalian cells. Traffic *7*, 282-297.

Berlin, I., Schwartz, H., and Nash, P.D. (2010). Regulation of epidermal growth factor receptor ubiquitination and trafficking by the USP8.STAM complex. J Biol Chem *285*, 34909-34921.

Boname, J.M., Thomas, M., Stagg, H.R., Xu, P., Peng, J., and Lehner, P.J. (2010). Efficient internalization of MHC I requires lysine-11 and lysine-63 mixed linkage polyubiquitin chains. Traffic *11*, 210-220.

Bonuccelli, G., Casimiro, M.C., Sotgia, F., Wang, C., Liu, M., Katiyar, S., Zhou, J., Dew, E., Capozza, F., Daumer, K.M.*, et al.* (2009). Caveolin-1 (P132L), a common breast cancer mutation, confers mammary cell invasiveness and defines a novel stem cell/metastasis-associated gene signature. Am J Pathol *174*, 1650-1662.

Boucrot, E., Howes, M.T., Kirchhausen, T., and Parton, R.G. (2011). Redistribution of caveolae during mitosis. J Cell Sci *124*, 1965-1972.

Bowers, K., Piper, S.C., Edeling, M.A., Gray, S.R., Owen, D.J., Lehner, P.J., and Luzio, J.P. (2006). Degradation of endocytosed epidermal growth factor and virally ubiquitinated major histocompatibility complex class I is independent of mammalian ESCRTII. J Biol Chem *281*, 5094-5105.

Bucci, C., Parton, R.G., Mather, I.H., Stunnenberg, H., Simons, K., Hoflack, B., and Zerial, M. (1992). The small GTPase rab5 functions as a regulatory factor in the early endocytic pathway. Cell *70*, 715-728.

Buchan, J.R., Kolaitis, R.M., Taylor, J.P., and Parker, R. (2013). Eukaryotic stress granules are cleared by autophagy and Cdc48/VCP function. Cell *153*, 1461-1474.

Bug, M., and Meyer, H. (2012). Expanding into new markets--VCP/p97 in endocytosis and autophagy. J Struct Biol *179*, 78-82.

Bukau, B., Weissman, J., and Horwich, A. (2006). Molecular chaperones and protein quality control. Cell *125*, 443-451.

Byrne, D.P., Dart, C., and Rigden, D.J. (2012). Evaluating caveolin interactions: do proteins interact with the caveolin scaffolding domain through a widespread aromatic residue-rich motif? PLoS One *7*, e44879.

Chen, S.F., Wu, C.H., Lee, Y.M., Tam, K., Tsai, Y.C., Liou, J.Y., and Shyue, S.K. (2013). Caveolin-1 Interacts with Derlin-1 and Promotes Ubiquitination and Degradation of Cyclooxygenase-2 via Collaboration with p97 Complex. J Biol Chem *288*, 33462-33469.

Chen, Z., Bakhshi, F.R., Shajahan, A.N., Sharma, T., Mao, M., Trane, A., Bernatchez, P., van Nieuw Amerongen, G.P., Bonini, M.G., Skidgel, R.A.*, et al.* (2012). Nitric oxide-dependent Src activation and resultant caveolin-1 phosphorylation promote eNOS/caveolin-1 binding and eNOS inhibition. Mol Biol Cell *23*, 1388-1398.

Chen, Z.J., and Sun, L.J. (2009). Nonproteolytic functions of ubiquitin in cell signaling. Mol Cell *33*, 275-286.

Chidlow, J.H., Jr., and Sessa, W.C. (2010). Caveolae, caveolins, and cavins: complex control of cellular signalling and inflammation. Cardiovasc Res *86*, 219-225.

Chou, T.F., Brown, S.J., Minond, D., Nordin, B.E., Li, K., Jones, A.C., Chase, P., Porubsky, P.R., Stoltz, B.M., Schoenen, F.J.*, et al.* (2011). Reversible inhibitor of

p97, DBeQ, impairs both ubiquitin-dependent and autophagic protein clearance pathways. Proc Natl Acad Sci U S A *108*, 4834-4839.

Christoforidis, S., McBride, H.M., Burgoyne, R.D., and Zerial, M. (1999). The Rab5 effector EEA1 is a core component of endosome docking. Nature *397*, 621-625.

Claessen, J.H., Kundrat, L., and Ploegh, H.L. (2012). Protein quality control in the ER: balancing the ubiquitin checkbook. Trends Cell Biol *22*, 22-32.

Clague, M.J., and Urbe, S. (2006). Endocytosis: the DUB version. Trends Cell Biol *16*, 551-559.

Clausen, T.H., Lamark, T., Isakson, P., Finley, K., Larsen, K.B., Brech, A., Overvatn, A., Stenmark, H., Bjorkoy, G., Simonsen, A.*, et al.* (2010). p62/SQSTM1 and ALFY interact to facilitate the formation of p62 bodies/ALIS and their degradation by autophagy. Autophagy *6*, 330-344.

Collins, B.M., Davis, M.J., Hancock, J.F., and Parton, R.G. (2012). Structure-based reassessment of the caveolin signaling model: do caveolae regulate signaling through caveolin-protein interactions? Dev Cell *23*, 11-20.

Custer, S.K., Neumann, M., Lu, H., Wright, A.C., and Taylor, J.P. (2010). Transgenic mice expressing mutant forms VCP/p97 recapitulate the full spectrum of IBMPFD including degeneration in muscle, brain and bone. Hum Mol Genet *19*, 1741-1755.

Dai, R.M., Chen, E., Longo, D.L., Gorbea, C.M., and Li, C.C. (1998). Involvement of valosin-containing protein, an ATPase Co-purified with IkappaBalpha and 26 S proteasome, in ubiquitin-proteasome-mediated degradation of IkappaBalpha. J Biol Chem *273*, 3562-3573.

del Pozo, M.A., Balasubramanian, N., Alderson, N.B., Kiosses, W.B., Grande-Garcia, A., Anderson, R.G., and Schwartz, M.A. (2005). Phospho-caveolin-1 mediates integrin-regulated membrane domain internalization. Nat Cell Biol *7*, 901-908.

DeLaBarre, B., and Brunger, A.T. (2003). Complete structure of p97/valosin-containing protein reveals communication between nucleotide domains. Nat Struct Biol *10*, 856-863.

DeLaBarre, B., and Brunger, A.T. (2005). Nucleotide dependent motion and mechanism of action of p97/VCP. J Mol Biol *347*, 437-452.

Deshaies, R.J., and Joazeiro, C.A. (2009). RING domain E3 ubiquitin ligases. Annu Rev Biochem *78*, 399-434.

Dobrynin, G., Popp, O., Romer, T., Bremer, S., Schmitz, M.H., Gerlich, D.W., and Meyer, H. (2011). Cdc48/p97-Ufd1-Npl4 antagonizes Aurora B during chromosome segregation in HeLa cells. J Cell Sci *124*, 1571-1580.

Doyotte, A., Russell, M.R., Hopkins, C.R., and Woodman, P.G. (2005). Depletion of TSG101 forms a mammalian "Class E" compartment: a multicisternal early endosome with multiple sorting defects. J Cell Sci *118*, 3003-3017.

Duncan, L.M., Piper, S., Dodd, R.B., Saville, M.K., Sanderson, C.M., Luzio, J.P., and Lehner, P.J. (2006). Lysine-63-linked ubiquitination is required for endolysosomal degradation of class I molecules. EMBO J *25*, 1635-1645.

Duran, A., Amanchy, R., Linares, J.F., Joshi, J., Abu-Baker, S., Porollo, A., Hansen, M., Moscat, J., and Diaz-Meco, M.T. (2011). p62 is a key regulator of nutrient sensing in the mTORC1 pathway. Mol Cell *44*, 134-146.

Eden, E.R., Huang, F., Sorkin, A., and Futter, C.E. (2012). The role of EGF receptor ubiquitination in regulating its intracellular traffic. Traffic *13*, 329-337.

Epand, R.M., Sayer, B.G., and Epand, R.F. (2005). Caveolin scaffolding region and cholesterol-rich domains in membranes. J Mol Biol *345*, 339-350.

Ernst, R., Mueller, B., Ploegh, H.L., and Schlieker, C. (2009). The otubain YOD1 is a deubiquitinating enzyme that associates with p97 to facilitate protein dislocation from the ER. Mol Cell *36*, 28-38.

Erpapazoglou, Z., Dhaoui, M., Pantazopoulou, M., Giordano, F., Mari, M., Leon, S., Raposo, G., Reggiori, F., and Haguenauer-Tsapis, R. (2012). A dual role for K63-linked ubiquitin chains in multivesicular body biogenesis and cargo sorting. Mol Biol Cell *23*, 2170-2183.

Fernandez, I., Ying, Y., Albanesi, J., and Anderson, R.G. (2002). Mechanism of caveolin filament assembly. Proc Natl Acad Sci U S A *99*, 11193-11198.

Fernandez-Saiz, V., and Buchberger, A. (2010). Imbalances in p97 co-factor interactions in human proteinopathy. EMBO Rep *11*, 479-485.

Filimonenko, M., Stuffers, S., Raiborg, C., Yamamoto, A., Malerod, L., Fisher, E.M., Isaacs, A., Brech, A., Stenmark, H., and Simonsen, A. (2007). Functional multivesicular bodies are required for autophagic clearance of protein aggregates associated with neurodegenerative disease. J Cell Biol *179*, 485-500.

Finley, D. (2009). Recognition and processing of ubiquitin-protein conjugates by the proteasome. Annu Rev Biochem *78*, 477-513.

Fuhs, S.R., and Insel, P.A. (2011). Caveolin-3 undergoes SUMOylation by the SUMO E3 ligase PIASy: sumoylation affects G-protein-coupled receptor desensitization. J Biol Chem *286*, 14830-14841.

Galbiati, F., Volonte, D., Minetti, C., Bregman, D.B., and Lisanti, M.P. (2000). Limb-girdle muscular dystrophy (LGMD-1C) mutants of caveolin-3 undergo ubiquitination and proteasomal degradation. Treatment with proteasomal inhibitors blocks the dominant negative effect of LGMD-1C mutanta and rescues wild-type caveolin-3. J Biol Chem *275*, 37702-37711.

Gaus, K., Le Lay, S., Balasubramanian, N., and Schwartz, M.A. (2006). Integrin-mediated adhesion regulates membrane order. J Cell Biol *174*, 725-734.

Geetha, T., Jiang, J., and Wooten, M.W. (2005). Lysine 63 polyubiquitination of the nerve growth factor receptor TrkA directs internalization and signaling. Mol Cell *20*, 301-312.

Geetha, T., Seibenhener, M.L., Chen, L., Madura, K., and Wooten, M.W. (2008). p62 serves as a shuttling factor for TrkA interaction with the proteasome. Biochem Biophys Res Commun *374*, 33-37.

Geisler, S., Holmstrom, K.M., Skujat, D., Fiesel, F.C., Rothfuss, O.C., Kahle, P.J., and Springer, W. (2010). PINK1/Parkin-mediated mitophagy is dependent on VDAC1 and p62/SQSTM1. Nat Cell Biol *12*, 119-131.

Glebov, O.O., Bright, N.A., and Nichols, B.J. (2006). Flotillin-1 defines a clathrin-independent endocytic pathway in mammalian cells. Nat Cell Biol *8*, 46-54.

Glinka, T., Alter, J., Braunstein, I., Tzach, L., Wei Sheng, C., Geifman, S., Edelmann, M., Kessler, B., and Stanhill, A. (2013). Signal-peptide mediated translocation is regulated by a P97-AIRAPL complex. Biochem J.

Goh, L.K., and Sorkin, A. (2013). Endocytosis of receptor tyrosine kinases. Cold Spring Harb Perspect Biol *5*, a017459.

Goode, A., and Layfield, R. (2010). Recent advances in understanding the molecular basis of Paget disease of bone. J Clin Pathol *63*, 199-203.

Grant, B.D., and Donaldson, J.G. (2009). Pathways and mechanisms of endocytic recycling. Nat Rev Mol Cell Biol *10*, 597-608.

Greene, B., Liu, S.H., Wilde, A., and Brodsky, F.M. (2000). Complete reconstitution of clathrin basket formation with recombinant protein fragments: adaptor control of clathrin self-assembly. Traffic *1*, 69-75.

Grosshans, B.L., Ortiz, D., and Novick, P. (2006). Rabs and their effectors: achieving specificity in membrane traffic. Proc Natl Acad Sci U S A *103*, 11821-11827.

Gruenberg, J., and Maxfield, F.R. (1995). Membrane transport in the endocytic pathway. Curr Opin Cell Biol *7*, 552-563.

Guo, J., Wang, T., Li, X., Shallow, H., Yang, T., Li, W., Xu, J., Fridman, M.D., Yang, X., and Zhang, S. (2012). Cell surface expression of human ether-a-go-go-related gene (hERG) channels is regulated by caveolin-3 protein via the ubiquitin ligase Nedd4-2. J Biol Chem *287*, 33132-33141.

Hagiwara, M., Shirai, Y., Nomura, R., Sasaki, M., Kobayashi, K., Tadokoro, T., and Yamamoto, Y. (2009). Caveolin-1 activates Rab5 and enhances endocytosis through direct interaction. Biochem Biophys Res Commun *378*, 73-78.

Haglund, K., and Dikic, I. (2005). Ubiquitylation and cell signaling. EMBO J *24*, 3353-3359.

Haglund, K., Sigismund, S., Polo, S., Szymkiewicz, I., Di Fiore, P.P., and Dikic, I. (2003). Multiple monoubiquitination of RTKs is sufficient for their endocytosis and degradation. Nat Cell Biol *5*, 461-466.

Haines, D.S., Lee, J.E., Beauparlant, S.L., Kyle, D.B., den Besten, W., Sweredoski, M.J., Graham, R.L., Hess, S., and Deshaies, R.J. (2012). Protein interaction profiling of the p97 adaptor UBXD1 points to a role for the complex in modulating ERGIC-53 trafficking. Mol Cell Proteomics *11*, M111 016444.

Hamasaki, M., and Yoshimori, T. (2010). Where do they come from? Insights into autophagosome formation. FEBS Lett *584*, 1296-1301.

Hancock, J.F. (2006). Lipid rafts: contentious only from simplistic standpoints. Nat Rev Mol Cell Biol *7*, 456-462.

Hansen, C.G., and Nichols, B.J. (2009). Molecular mechanisms of clathrin-independent endocytosis. J Cell Sci *122*, 1713-1721.

Hansen, C.G., and Nichols, B.J. (2010). Exploring the caves: cavins, caveolins and caveolae. Trends Cell Biol *20*, 177-186.

Hansen, C.G., Shvets, E., Howard, G., Riento, K., and Nichols, B.J. (2013). Deletion of cavin genes reveals tissue-specific mechanisms for morphogenesis of endothelial caveolae. Nat Commun *4*, 1831.

Hanson, C.A., Drake, K.R., Baird, M.A., Han, B., Kraft, L.J., Davidson, M.W., and Kenworthy, A.K. (2013). Overexpression of caveolin-1 is sufficient to phenocopy the behavior of a disease-associated mutant. Traffic *14*, 663-677.

Hayakawa, A., Leonard, D., Murphy, S., Hayes, S., Soto, M., Fogarty, K., Standley, C., Bellve, K., Lambright, D., Mello, C.*, et al.* (2006). The WD40 and FYVE domain containing protein 2 defines a class of early endosomes necessary for endocytosis. Proc Natl Acad Sci U S A *103*, 11928-11933.

Hayer, A., Stoeber, M., Bissig, C., and Helenius, A. (2010a). Biogenesis of caveolae: stepwise assembly of large caveolin and cavin complexes. Traffic *11*, 361-382.

Hayer, A., Stoeber, M., Ritz, D., Engel, S., Meyer, H.H., and Helenius, A. (2010b). Caveolin-1 is ubiquitinated and targeted to intralumenal vesicles in endolysosomes for degradation. J Cell Biol *191*, 615-629.

Head, B.P., Hu, Y., Finley, J.C., Saldana, M.D., Bonds, J.A., Miyanohara, A., Niesman, I.R., Ali, S.S., Murray, F., Insel, P.A.*, et al.* (2011). Neuron-targeted caveolin-1 protein enhances signaling and promotes arborization of primary neurons. J Biol Chem *286*, 33310-33321.

Henne, W.M., Buchkovich, N.J., and Emr, S.D. (2011). The ESCRT pathway. Dev Cell *21*, 77-91.

Hill, M.M., Bastiani, M., Luetterforst, R., Kirkham, M., Kirkham, A., Nixon, S.J., Walser, P., Abankwa, D., Oorschot, V.M., Martin, S.*, et al.* (2008). PTRF-Cavin, a conserved cytoplasmic protein required for caveola formation and function. Cell *132*, 113-124.

Hoppe, T., Matuschewski, K., Rape, M., Schlenker, S., Ulrich, H.D., and Jentsch, S. (2000). Activation of a membrane-bound transcription factor by regulated ubiquitin/proteasome-dependent processing. Cell *102*, 577-586.

Howes, M.T., Mayor, S., and Parton, R.G. (2010). Molecules, mechanisms, and cellular roles of clathrin-independent endocytosis. Curr Opin Cell Biol *22*, 519-527.

Huang, F., Goh, L.K., and Sorkin, A. (2007). EGF receptor ubiquitination is not necessary for its internalization. Proc Natl Acad Sci U S A *104*, 16904-16909.

Huang, F., Kirkpatrick, D., Jiang, X., Gygi, S., and Sorkin, A. (2006). Differential regulation of EGF receptor internalization and degradation by multiubiquitination within the kinase domain. Mol Cell *21*, 737-748.

Huotari, J., and Helenius, A. (2011). Endosome maturation. EMBO J *30*, 3481-3500.

Huotari, J., Meyer-Schaller, N., Hubner, M., Stauffer, S., Katheder, N., Horvath, P., Mancini, R., Helenius, A., and Peter, M. (2012). Cullin-3 regulates late endosome maturation. Proc Natl Acad Sci U S A *109*, 823-828.

Ikeda, F., and Dikic, I. (2008). Atypical ubiquitin chains: new molecular signals. 'Protein Modifications: Beyond the Usual Suspects' review series. EMBO Rep *9*, 536-542.

Im, Y.J., and Hurley, J.H. (2008). Integrated structural model and membrane targeting mechanism of the human ESCRT-II complex. Dev Cell *14*, 902-913.

Ingham, R.J., Gish, G., and Pawson, T. (2004). The Nedd4 family of E3 ubiquitin ligases: functional diversity within a common modular architecture. Oncogene *23*, 1972-1984.

Jentsch, S., and Rumpf, S. (2007). Cdc48 (p97): a "molecular gearbox" in the ubiquitin pathway? Trends Biochem Sci *32*, 6-11.

Johannes, L., and Popoff, V. (2008). Tracing the retrograde route in protein trafficking. Cell *135*, 1175-1187.

Johannessen, L.E., Pedersen, N.M., Pedersen, K.W., Madshus, I.H., and Stang, E. (2006). Activation of the epidermal growth factor (EGF) receptor induces formation of EGF receptor- and Grb2-containing clathrin-coated pits. Mol Cell Biol *26*, 389-401.

Johnson, J.O., Mandrioli, J., Benatar, M., Abramzon, Y., Van Deerlin, V.M., Trojanowski, J.Q., Gibbs, J.R., Brunetti, M., Gronka, S., Wuu, J.*, et al.* (2010). Exome sequencing reveals VCP mutations as a cause of familial ALS. Neuron *68*, 857-864.

Jovic, M., Sharma, M., Rahajeng, J., and Caplan, S. (2010). The early endosome: a busy sorting station for proteins at the crossroads. Histol Histopathol *25*, 99-112.

Ju, J.S., Fuentealba, R.A., Miller, S.E., Jackson, E., Piwnica-Worms, D., Baloh, R.H., and Weihl, C.C. (2009). Valosin-containing protein (VCP) is required for autophagy and is disrupted in VCP disease. J Cell Biol *187*, 875-888.

Ju, J.S., and Weihl, C.C. (2010). Inclusion body myopathy, Paget's disease of the bone and fronto-temporal dementia: a disorder of autophagy. Hum Mol Genet *19*, R38-45.

Kazazic, M., Roepstorff, K., Johannessen, L.E., Pedersen, N.M., van Deurs, B., Stang, E., and Madshus, I.H. (2006). EGF-induced activation of the EGF receptor does not trigger mobilization of caveolae. Traffic *7*, 1518-1527.

Kerscher, O., Felberbaum, R., and Hochstrasser, M. (2006). Modification of proteins by ubiquitin and ubiquitin-like proteins. Annu Rev Cell Dev Biol *22*, 159-180.

Kim, H.T., Kim, K.P., Lledias, F., Kisselev, A.F., Scaglione, K.M., Skowyra, D., Gygi, S.P., and Goldberg, A.L. (2007). Certain pairs of ubiquitin-conjugating enzymes (E2s) and ubiquitin-protein ligases (E3s) synthesize nondegradable forked ubiquitin chains containing all possible isopeptide linkages. J Biol Chem *282*, 17375-17386.

Kim, P.K., Hailey, D.W., Mullen, R.T., and Lippincott-Schwartz, J. (2008). Ubiquitin signals autophagic degradation of cytosolic proteins and peroxisomes. Proc Natl Acad Sci U S A *105*, 20567-20574.

Kim, W., Bennett, E.J., Huttlin, E.L., Guo, A., Li, J., Possemato, A., Sowa, M.E., Rad, R., Rush, J., Comb, M.J.*, et al.* (2011). Systematic and quantitative assessment of the ubiquitin-modified proteome. Mol Cell *44*, 325-340.

Kirkham, M., Fujita, A., Chadda, R., Nixon, S.J., Kurzchalia, T.V., Sharma, D.K., Pagano, R.E., Hancock, J.F., Mayor, S., and Parton, R.G. (2005). Ultrastructural identification of uncoated caveolin-independent early endocytic vehicles. J Cell Biol *168*, 465-476.

Kirkham, M., Nixon, S.J., Howes, M.T., Abi-Rached, L., Wakeham, D.E., Hanzal-Bayer, M., Ferguson, C., Hill, M.M., Fernandez-Rojo, M., Brown, D.A.*, et al.* (2008). Evolutionary analysis and molecular dissection of caveola biogenesis. J Cell Sci *121*, 2075-2086.

Kirkin, V., Lamark, T., Sou, Y.S., Bjorkoy, G., Nunn, J.L., Bruun, J.A., Shvets, E., McEwan, D.G., Clausen, T.H., Wild, P.*, et al.* (2009a). A role for NBR1 in autophagosomal degradation of ubiquitinated substrates. Mol Cell *33*, 505-516.

Kirkin, V., McEwan, D.G., Novak, I., and Dikic, I. (2009b). A role for ubiquitin in selective autophagy. Mol Cell *34*, 259-269.

Klionsky, D.J., Abeliovich, H., Agostinis, P., Agrawal, D.K., Aliev, G., Askew, D.S., Baba, M., Baehrecke, E.H., Bahr, B.A., Ballabio, A.*, et al.* (2008). Guidelines for the use and interpretation of assays for monitoring autophagy in higher eukaryotes. Autophagy *4*, 151-175.

Kloppsteck, P., Ewens, C.A., Forster, A., Zhang, X., and Freemont, P.S. (2012). Regulation of p97 in the ubiquitin-proteasome system by the UBX protein-family. Biochim Biophys Acta *1823*, 125-129.

Kogo, H., and Fujimoto, T. (2000). Caveolin-1 isoforms are encoded by distinct mRNAs. Identification Of mouse caveolin-1 mRNA variants caused by alternative transcription initiation and splicing. FEBS Lett *465*, 119-123.

Kolawa, N., Sweredoski, M.J., Graham, R.L., Oania, R., Hess, S., and Deshaies, R.J. (2013). Perturbations to the ubiquitin conjugate proteome in yeast deltaubx mutants identify ubx2 as a regulator of membrane lipid composition. Mol Cell Proteomics *12*, 2791-2803.

Komander, D., and Rape, M. (2012). The ubiquitin code. Annu Rev Biochem *81*, 203-229.

Komatsu, M., and Ichimura, Y. (2010). Physiological significance of selective degradation of p62 by autophagy. FEBS Lett *584*, 1374-1378.

Komatsu, M., Waguri, S., Koike, M., Sou, Y.S., Ueno, T., Hara, T., Mizushima, N., Iwata, J., Ezaki, J., Murata, S.*, et al.* (2007). Homeostatic levels of p62 control cytoplasmic inclusion body formation in autophagy-deficient mice. Cell *131*, 1149-1163.

Kopito, R.R. (2000). Aggresomes, inclusion bodies and protein aggregation. Trends Cell Biol *10*, 524-530.

Korolchuk, V.I., Mansilla, A., Menzies, F.M., and Rubinsztein, D.C. (2009). Autophagy inhibition compromises degradation of ubiquitin-proteasome pathway substrates. Mol Cell *33*, 517-527.

Krick, R., Bremer, S., Welter, E., Schlotterhose, P., Muehe, Y., Eskelinen, E.L., and Thumm, M. (2010). Cdc48/p97 and Shp1/p47 regulate autophagosome biogenesis in concert with ubiquitin-like Atg8. J Cell Biol *190*, 965-973.

Lakadamyali, M., Rust, M.J., and Zhuang, X. (2006). Ligands for clathrin-mediated endocytosis are differentially sorted into distinct populations of early endosomes. Cell *124*, 997-1009.

Lamaze, C., Dujeancourt, A., Baba, T., Lo, C.G., Benmerah, A., and Dautry-Varsat, A. (2001). Interleukin 2 receptors and detergent-resistant membrane domains define a clathrin-independent endocytic pathway. Mol Cell *7*, 661-671.

Layfield, R., and Shaw, B. (2007). Ubiquitin-mediated signalling and Paget's disease of bone. BMC Biochem *8 Suppl 1*, S5.

Le Lay, S., Hajduch, E., Lindsay, M.R., Le Liepvre, X., Thiele, C., Ferre, P., Parton, R.G., Kurzchalia, T., Simons, K., and Dugail, I. (2006). Cholesterol-induced caveolin targeting to lipid droplets in adipocytes: a role for caveolar endocytosis. Traffic *7*, 549-561.

Lee, H., Park, D.S., Razani, B., Russell, R.G., Pestell, R.G., and Lisanti, M.P. (2002). Caveolin-1 mutations (P132L and null) and the pathogenesis of breast cancer: caveolin-1 (P132L) behaves in a dominant-negative manner and caveolin-1 (-/-) null mice show mammary epithelial cell hyperplasia. Am J Pathol *161*, 1357-1369.

Lee, I.H., Campbell, C.R., Song, S.H., Day, M.L., Kumar, S., Cook, D.I., and Dinudom, A. (2009). The activity of the epithelial sodium channels is regulated by caveolin-1 via a Nedd4-2-dependent mechanism. J Biol Chem *284*, 12663-12669.

Lee, S.M., Chin, L.S., and Li, L. (2012). Charcot-Marie-Tooth disease-linked protein SIMPLE functions with the ESCRT machinery in endosomal trafficking. J Cell Biol *199*, 799-816.

Li, G., Zhao, G., Zhou, X., Schindelin, H., and Lennarz, W.J. (2006). The AAA ATPase p97 links peptide N-glycanase to the endoplasmic reticulum-associated E3 ligase autocrine motility factor receptor. Proc Natl Acad Sci U S A *103*, 8348-8353.

Li, J.M., Wu, H., Zhang, W., Blackburn, M.R., and Jin, J. (2013). The p97-UFD1L-NPL4 Protein Complex Mediates Cytokine-induced IkappaBalpha Proteolysis. Mol Cell Biol.

Lis, E.T., and Romesberg, F.E. (2006). Role of Doa1 in the Saccharomyces cerevisiae DNA damage response. Mol Cell Biol *26*, 4122-4133.

Liu, L., and Pilch, P.F. (2008). A critical role of cavin (polymerase I and transcript release factor) in caveolae formation and organization. J Biol Chem *283*, 4314-4322.

Liu, S.H., Wong, M.L., Craik, C.S., and Brodsky, F.M. (1995). Regulation of clathrin assembly and trimerization defined using recombinant triskelion hubs. Cell *83*, 257-267.

Luhtala, N., and Odorizzi, G. (2004). Bro1 coordinates deubiquitination in the multivesicular body pathway by recruiting Doa4 to endosomes. J Cell Biol *166*, 717-729.

Luzio, J.P., Pryor, P.R., and Bright, N.A. (2007). Lysosomes: fusion and function. Nat Rev Mol Cell Biol *8*, 622-632.

MacDonald, C., Buchkovich, N.J., Stringer, D.K., Emr, S.D., and Piper, R.C. (2012). Cargo ubiquitination is essential for multivesicular body intralumenal vesicle formation. EMBO Rep *13*, 331-338.

Madsen, L., Andersen, K.M., Prag, S., Moos, T., Semple, C.A., Seeger, M., and Hartmann-Petersen, R. (2008). Ubxd1 is a novel co-factor of the human p97 ATPase. Int J Biochem Cell Biol *40*, 2927-2942.

Madsen, L., Kriegenburg, F., Vala, A., Best, D., Prag, S., Hofmann, K., Seeger, M., Adams, I.R., and Hartmann-Petersen, R. (2011). The tissue-specific Rep8/UBXD6 tethers p97 to the endoplasmic reticulum membrane for degradation of misfolded proteins. PLoS One *6*, e25061.

Madshus, I.H., and Stang, E. (2009). Internalization and intracellular sorting of the EGF receptor: a model for understanding the mechanisms of receptor trafficking. J Cell Sci *122*, 3433-3439.

Martinez-Outschoorn, U.E., Pavlides, S., Whitaker-Menezes, D., Daumer, K.M., Milliman, J.N., Chiavarina, B., Migneco, G., Witkiewicz, A.K., Martinez-Cantarin, M.P., Flomenberg, N.*, et al.* (2010). Tumor cells induce the cancer associated fibroblast phenotype via caveolin-1 degradation: implications for breast cancer and DCIS therapy with autophagy inhibitors. Cell Cycle *9*, 2423-2433.

Maxfield, F.R., and McGraw, T.E. (2004). Endocytic recycling. Nat Rev Mol Cell Biol *5*, 121-132.

Mayor, S., and Pagano, R.E. (2007). Pathways of clathrin-independent endocytosis. Nat Rev Mol Cell Biol *8*, 603-612.

McCullough, J., Clague, M.J., and Urbe, S. (2004). AMSH is an endosome-associated ubiquitin isopeptidase. J Cell Biol *166*, 487-492.

McCullough, J., Row, P.E., Lorenzo, O., Doherty, M., Beynon, R., Clague, M.J., and Urbe, S. (2006). Activation of the endosome-associated ubiquitin isopeptidase AMSH by STAM, a component of the multivesicular body-sorting machinery. Curr Biol *16*, 160-165.

McMahon, H.T., and Boucrot, E. (2011). Molecular mechanism and physiological functions of clathrin-mediated endocytosis. Nat Rev Mol Cell Biol *12*, 517-533.

McMahon, K.A., Zajicek, H., Li, W.P., Peyton, M.J., Minna, J.D., Hernandez, V.J., Luby-Phelps, K., and Anderson, R.G. (2009). SRBC/cavin-3 is a caveolin adapter protein that regulates caveolae function. EMBO J *28*, 1001-1015.

Melikova, M.S., Kondratov, K.A., and Kornilova, E.S. (2006). Two different stages of epidermal growth factor (EGF) receptor endocytosis are sensitive to free ubiquitin depletion produced by proteasome inhibitor MG132. Cell Biol Int *30*, 31-43.

Mellman, I. (1996). Endocytosis and molecular sorting. Annu Rev Cell Dev Biol *12*, 575-625.

Meyer, H., Bug, M., and Bremer, S. (2012). Emerging functions of the VCP/p97 AAA-ATPase in the ubiquitin system. Nat Cell Biol *14*, 117-123.

Meyer, H.H. (2005). Golgi reassembly after mitosis: the AAA family meets the ubiquitin family. Biochim Biophys Acta *1744*, 481-492.

Meyer, H.H., Kondo, H., and Warren, G. (1998). The p47 co-factor regulates the ATPase activity of the membrane fusion protein, p97. FEBS Lett *437*, 255-257.

Meyer, H.H., Wang, Y., and Warren, G. (2002). Direct binding of ubiquitin conjugates by the mammalian p97 adaptor complexes, p47 and Ufd1-Npl4. EMBO J *21*, 5645-5652.

Monier, S., Parton, R.G., Vogel, F., Behlke, J., Henske, A., and Kurzchalia, T.V. (1995). VIP21-caveolin, a membrane protein constituent of the caveolar coat, oligomerizes in vivo and in vitro. Mol Biol Cell *6*, 911-927.

Morris, C.R., Stanton, M.J., Manthey, K.C., Oh, K.B., and Wagner, K.U. (2012). A knockout of the Tsg101 gene leads to decreased expression of ErbB receptor tyrosine kinases and induction of autophagy prior to cell death. PLoS One *7*, e34308.

Mosesson, Y., and Yarden, Y. (2006). Monoubiquitylation: a recurrent theme in membrane protein transport. Isr Med Assoc J *8*, 233-237.

Mousavi, S.A., Malerod, L., Berg, T., and Kjeken, R. (2004). Clathrin-dependent endocytosis. Biochem J *377*, 1-16.

Mueller, B., Klemm, E.J., Spooner, E., Claessen, J.H., and Ploegh, H.L. (2008). SEL1L nucleates a protein complex required for dislocation of misfolded glycoproteins. Proc Natl Acad Sci U S A *105*, 12325-12330.

Mullally, J.E., Chernova, T., and Wilkinson, K.D. (2006). Doa1 is a Cdc48 adapter that possesses a novel ubiquitin binding domain. Mol Cell Biol *26*, 822-830.

Mundy, D.I., Li, W.P., Luby-Phelps, K., and Anderson, R.G. (2012). Caveolin targeting to late endosome/lysosomal membranes is induced by perturbations of lysosomal pH and cholesterol content. Mol Biol Cell *23*, 864-880.

Mundy, D.I., Machleidt, T., Ying, Y.S., Anderson, R.G., and Bloom, G.S. (2002). Dual control of caveolar membrane traffic by microtubules and the actin cytoskeleton. J Cell Sci *115*, 4327-4339.

Nalbandian, A., Donkervoort, S., Dec, E., Badadani, M., Katheria, V., Rana, P., Nguyen, C., Mukherjee, J., Caiozzo, V., Martin, B.*, et al.* (2011). The multiple faces of valosin-containing protein-associated diseases: inclusion body myopathy with Paget's disease of bone, frontotemporal dementia, and amyotrophic lateral sclerosis. J Mol Neurosci *45*, 522-531.

Nethe, M., and Hordijk, P.L. (2011). A model for phospho-caveolin-1-driven turnover of focal adhesions. Cell Adh Migr *5*, 59-64.

Niendorf, S., Oksche, A., Kisser, A., Lohler, J., Prinz, M., Schorle, H., Feller, S., Lewitzky, M., Horak, I., and Knobeloch, K.P. (2007). Essential role of ubiquitin-specific protease 8 for receptor tyrosine kinase stability and endocytic trafficking in vivo. Mol Cell Biol *27*, 5029-5039.

Niwa, H., Ewens, C.A., Tsang, C., Yeung, H.O., Zhang, X., and Freemont, P.S. (2012). The role of the N-domain in the ATPase activity of the mammalian AAA ATPase p97/VCP. J Biol Chem *287*, 8561-8570.

Ohsumi, Y. (2001). Molecular dissection of autophagy: two ubiquitin-like systems. Nat Rev Mol Cell Biol *2*, 211-216.

Okiyoneda, T., Barriere, H., Bagdany, M., Rabeh, W.M., Du, K., Hohfeld, J., Young, J.C., and Lukacs, G.L. (2010). Peripheral protein quality control removes unfolded CFTR from the plasma membrane. Science *329*, 805-810.

Orme, C.M., and Bogan, J.S. (2012). The ubiquitin regulatory X (UBX) domain-containing protein TUG regulates the p97 ATPase and resides at the endoplasmic reticulum-golgi intermediate compartment. J Biol Chem *287*, 6679-6692.

Ossareh-Nazari, B., Bonizec, M., Cohen, M., Dokudovskaya, S., Delalande, F., Schaeffer, C., Van Dorsselaer, A., and Dargemont, C. (2010). Cdc48 and Ufd3, new partners of the ubiquitin protease Ubp3, are required for ribophagy. EMBO Rep *11*, 548-554.

Ostermeyer, A.G., Paci, J.M., Zeng, Y., Lublin, D.M., Munro, S., and Brown, D.A. (2001). Accumulation of caveolin in the endoplasmic reticulum redirects the protein to lipid storage droplets. J Cell Biol *152*, 1071-1078.

Pankiv, S., Clausen, T.H., Lamark, T., Brech, A., Bruun, J.A., Outzen, H., Overvatn, A., Bjorkoy, G., and Johansen, T. (2007). p62/SQSTM1 binds directly to Atg8/LC3 to facilitate degradation of ubiquitinated protein aggregates by autophagy. J Biol Chem *282*, 24131-24145.

Parat, M.O. (2009). The biology of caveolae: achievements and perspectives. Int Rev Cell Mol Biol *273*, 117-162.

Park, S., Isaacson, R., Kim, H.T., Silver, P.A., and Wagner, G. (2005). Ufd1 exhibits the AAA-ATPase fold with two distinct ubiquitin interaction sites. Structure *13*, 995-1005.

Parton, R.G., and del Pozo, M.A. (2013). Caveolae as plasma membrane sensors, protectors and organizers. Nat Rev Mol Cell Biol *14*, 98-112.

Parton, R.G., Hanzal-Bayer, M., and Hancock, J.F. (2006). Biogenesis of caveolae: a structural model for caveolin-induced domain formation. J Cell Sci *119*, 787-796.

Parton, R.G., and Simons, K. (2007). The multiple faces of caveolae. Nat Rev Mol Cell Biol *8*, 185-194.

Pelkmans, L., Burli, T., Zerial, M., and Helenius, A. (2004). Caveolin-stabilized membrane domains as multifunctional transport and sorting devices in endocytic membrane traffic. Cell *118*, 767-780.

Pelkmans, L., and Zerial, M. (2005). Kinase-regulated quantal assemblies and kiss-and-run recycling of caveolae. Nature *436*, 128-133.

Peng, J., Schwartz, D., Elias, J.E., Thoreen, C.C., Cheng, D., Marsischky, G., Roelofs, J., Finley, D., and Gygi, S.P. (2003). A proteomics approach to understanding protein ubiquitination. Nat Biotechnol *21*, 921-926.

Pennock, S., and Wang, Z. (2008). A tale of two Cbls: interplay of c-Cbl and Cbl-b in epidermal growth factor receptor downregulation. Mol Cell Biol *28*, 3020-3037.

Peterson, T.E., Guicciardi, M.E., Gulati, R., Kleppe, L.S., Mueske, C.S., Mookadam, M., Sowa, G., Gores, G.J., Sessa, W.C., and Simari, R.D. (2003). Caveolin-1 can regulate vascular smooth muscle cell fate by switching platelet-derived growth factor signaling from a proliferative to an apoptotic pathway. Arterioscler Thromb Vasc Biol *23*, 1521-1527.

Pickart, C.M. (2004). Back to the future with ubiquitin. Cell *116*, 181-190.

Piper, R.C., and Katzmann, D.J. (2007). Biogenesis and function of multivesicular bodies. Annu Rev Cell Dev Biol *23*, 519-547.

Pol, A., Martin, S., Fernandez, M.A., Ingelmo-Torres, M., Ferguson, C., Enrich, C., and Parton, R.G. (2005). Cholesterol and fatty acids regulate dynamic caveolin trafficking through the Golgi complex and between the cell surface and lipid bodies. Mol Biol Cell *16*, 2091-2105.

Polo, S., Sigismund, S., Faretta, M., Guidi, M., Capua, M.R., Bossi, G., Chen, H., De Camilli, P., and Di Fiore, P.P. (2002). A single motif responsible for ubiquitin recognition and monoubiquitination in endocytic proteins. Nature *416*, 451-455.

Porat-Shliom, N., Kloog, Y., and Donaldson, J.G. (2008). A unique platform for H-Ras signaling involving clathrin-independent endocytosis. Mol Biol Cell *19*, 765-775.

Pye, V.E., Beuron, F., Keetch, C.A., McKeown, C., Robinson, C.V., Meyer, H.H., Zhang, X., and Freemont, P.S. (2007). Structural insights into the p97-Ufd1-Npl4 complex. Proc Natl Acad Sci U S A *104*, 467-472.

Pye, V.E., Dreveny, I., Briggs, L.C., Sands, C., Beuron, F., Zhang, X., and Freemont, P.S. (2006). Going through the motions: the ATPase cycle of p97. J Struct Biol *156*, 12-28.

Rabouille, C., Kondo, H., Newman, R., Hui, N., Freemont, P., and Warren, G. (1998). Syntaxin 5 is a common component of the NSF- and p97-mediated reassembly pathways of Golgi cisternae from mitotic Golgi fragments in vitro. Cell *92*, 603-610.

Raiborg, C., Bache, K.G., Gillooly, D.J., Madshus, I.H., Stang, E., and Stenmark, H. (2002). Hrs sorts ubiquitinated proteins into clathrin-coated microdomains of early endosomes. Nat Cell Biol *4*, 394-398.

Raiborg, C., Malerod, L., Pedersen, N.M., and Stenmark, H. (2008). Differential functions of Hrs and ESCRT proteins in endocytic membrane trafficking. Exp Cell Res *314*, 801-813.

Raiborg, C., Schink, K.O., and Stenmark, H. (2013). Class III phosphatidylinositol 3-kinase and its catalytic product PtdIns3P in regulation of endocytic membrane traffic. FEBS J *280*, 2730-2742.

Raiborg, C., and Stenmark, H. (2009). The ESCRT machinery in endosomal sorting of ubiquitylated membrane proteins. Nature *458*, 445-452.

Raiborg, C., Wesche, J., Malerod, L., and Stenmark, H. (2006). Flat clathrin coats on endosomes mediate degradative protein sorting by scaffolding Hrs in dynamic microdomains. J Cell Sci *119*, 2414-2424.

Ramadan, K., Bruderer, R., Spiga, F.M., Popp, O., Baur, T., Gotta, M., and Meyer, H.H. (2007). Cdc48/p97 promotes reformation of the nucleus by extracting the kinase Aurora B from chromatin. Nature *450*, 1258-1262.

Ramanathan, H.N., and Ye, Y. (2012). The p97 ATPase associates with EEA1 to regulate the size of early endosomes. Cell Res *22*, 346-359.

Rape, M., Hoppe, T., Gorr, I., Kalocay, M., Richly, H., and Jentsch, S. (2001). Mobilization of processed, membrane-tethered SPT23 transcription factor by CDC48(UFD1/NPL4), a ubiquitin-selective chaperone. Cell *107*, 667-677.

Razani, B., Wang, X.B., Engelman, J.A., Battista, M., Lagaud, G., Zhang, X.L., Kneitz, B., Hou, H., Jr., Christ, G.J., Edelmann, W.*, et al.* (2002). Caveolin-2-deficient mice show evidence of severe pulmonary dysfunction without disruption of caveolae. Mol Cell Biol *22*, 2329-2344.

Razi, M., and Futter, C.E. (2006). Distinct roles for Tsg101 and Hrs in multivesicular body formation and inward vesiculation. Mol Biol Cell *17*, 3469-3483.

Ren, J., Pashkova, N., Winistorfer, S., and Piper, R.C. (2008). DOA1/UFD3 plays a role in sorting ubiquitinated membrane proteins into multivesicular bodies. J Biol Chem *283*, 21599-21611.

Ren, X., and Hurley, J.H. (2010). VHS domains of ESCRT-0 cooperate in high-avidity binding to polyubiquitinated cargo. EMBO J *29*, 1045-1054.

Ren, X., Ostermeyer, A.G., Ramcharan, L.T., Zeng, Y., Lublin, D.M., and Brown, D.A. (2004). Conformational defects slow Golgi exit, block oligomerization, and reduce raft affinity of caveolin-1 mutant proteins. Mol Biol Cell *15*, 4556-4567.

Riemer, A., Dobrynin, G., Dressler, A., Bremer, S., Soni, A., Iliakis, G., and Meyer, H. (2014). The p97-Ufd1-Npl4 ATPase complex ensures robustness of the G /M checkpoint by facilitating CDC25A degradation. Cell Cycle *13*.

Rieth, M.D., Lee, J., and Glover, K.J. (2012). Probing the caveolin-1 P132L mutant: critical insights into its oligomeric behavior and structure. Biochemistry *51*, 3911-3918.

Rink, J., Ghigo, E., Kalaidzidis, Y., and Zerial, M. (2005). Rab conversion as a mechanism of progression from early to late endosomes. Cell *122*, 735-749.

Ritz, D. (2010). Mass spectrometry-based and functional analysis of novel VCP/p97 cofactor complexes in health and disease (ETH Zurich).

Ritz, D., Vuk, M., Kirchner, P., Bug, M., Schutz, S., Hayer, A., Bremer, S., Lusk, C., Baloh, R.H., Lee, H.*, et al.* (2011). Endolysosomal sorting of ubiquitylated caveolin-1 is regulated by VCP and UBXD1 and impaired by VCP disease mutations. Nat Cell Biol *13*, 1116-1123.

Roberts, R.L., Barbieri, M.A., Pryse, K.M., Chua, M., Morisaki, J.H., and Stahl, P.D. (1999). Endosome fusion in living cells overexpressing GFP-rab5. J Cell Sci *112 ( Pt 21)*, 3667-3675.

Roepstorff, K., Grandal, M.V., Henriksen, L., Knudsen, S.L., Lerdrup, M., Grovdal, L., Willumsen, B.M., and van Deurs, B. (2009). Differential effects of EGFR ligands on endocytic sorting of the receptor. Traffic *10*, 1115-1127.

Rotin, D., and Kumar, S. (2009). Physiological functions of the HECT family of ubiquitin ligases. Nat Rev Mol Cell Biol *10*, 398-409.

Rouiller, I., DeLaBarre, B., May, A.P., Weis, W.I., Brunger, A.T., Milligan, R.A., and Wilson-Kubalek, E.M. (2002). Conformational changes of the multifunction p97 AAA ATPase during its ATPase cycle. Nat Struct Biol *9*, 950-957.

Row, P.E., Prior, I.A., McCullough, J., Clague, M.J., and Urbe, S. (2006). The ubiquitin isopeptidase UBPY regulates endosomal ubiquitin dynamics and is essential for receptor down-regulation. J Biol Chem *281*, 12618-12624.

Roxrud, I., Stenmark, H., and Malerod, L. (2010). ESCRT & Co. Biol Cell *102*, 293-318.

Rumpf, S., and Jentsch, S. (2006). Functional division of substrate processing cofactors of the ubiquitin-selective Cdc48 chaperone. Mol Cell *21*, 261-269.

Rush, J.S., and Ceresa, B.P. (2013). RAB7 and TSG101 are required for the constitutive recycling of unliganded EGFRs via distinct mechanisms. Mol Cell Endocrinol *381*, 188-197.

Rush, J.S., Quinalty, L.M., Engelman, L., Sherry, D.M., and Ceresa, B.P. (2012). Endosomal accumulation of the activated epidermal growth factor receptor (EGFR) induces apoptosis. J Biol Chem *287*, 712-722.

Rusten, T.E., and Simonsen, A. (2008). ESCRT functions in autophagy and associated disease. Cell Cycle *7*, 1166-1172.

Sachse, M., Urbe, S., Oorschot, V., Strous, G.J., and Klumperman, J. (2002). Bilayered clathrin coats on endosomal vacuoles are involved in protein sorting toward lysosomes. Mol Biol Cell *13*, 1313-1328.

Saksena, S., and Emr, S.D. (2009). ESCRTs and human disease. Biochem Soc Trans *37*, 167-172.

Salani, B., Passalacqua, M., Maffioli, S., Briatore, L., Hamoudane, M., Contini, P., Cordera, R., and Maggi, D. (2010). IGF-IR internalizes with Caveolin-1 and PTRF/Cavin in HaCat cells. PLoS One *5*, e14157.

Sargiacomo, M., Scherer, P.E., Tang, Z., Kubler, E., Song, K.S., Sanders, M.C., and Lisanti, M.P. (1995). Oligomeric structure of caveolin: implications for caveolae membrane organization. Proc Natl Acad Sci U S A *92*, 9407-9411.

Schuberth, C., and Buchberger, A. (2008). UBX domain proteins: major regulators of the AAA ATPase Cdc48/p97. Cell Mol Life Sci *65*, 2360-2371.

Schwencke, C., Braun-Dullaeus, R.C., Wunderlich, C., and Strasser, R.H. (2006). Caveolae and caveolin in transmembrane signaling: Implications for human disease. Cardiovasc Res *70*, 42-49.

Scita, G., and Di Fiore, P.P. (2010). The endocytic matrix. Nature *463*, 464-473.

Sharma, D.K., Choudhury, A., Singh, R.D., Wheatley, C.L., Marks, D.L., and Pagano, R.E. (2003). Glycosphingolipids internalized via caveolar-related endocytosis rapidly merge with the clathrin pathway in early endosomes and form microdomains for recycling. J Biol Chem *278*, 7564-7572.

Sigismund, S., Algisi, V., Nappo, G., Conte, A., Pascolutti, R., Cuomo, A., Bonaldi, T., Argenzio, E., Verhoef, L.G., Maspero, E.*, et al.* (2013). Threshold-controlled ubiquitination of the EGFR directs receptor fate. EMBO J *32*, 2140-2157.

Sigismund, S., Argenzio, E., Tosoni, D., Cavallaro, E., Polo, S., and Di Fiore, P.P. (2008). Clathrin-mediated internalization is essential for sustained EGFR signaling but dispensable for degradation. Dev Cell *15*, 209-219.

Sigismund, S., Woelk, T., Puri, C., Maspero, E., Tacchetti, C., Transidico, P., Di Fiore, P.P., and Polo, S. (2005). Clathrin-independent endocytosis of ubiquitinated cargos. Proc Natl Acad Sci U S A *102*, 2760-2765.

Sinha, B., Koster, D., Ruez, R., Gonnord, P., Bastiani, M., Abankwa, D., Stan, R.V., Butler-Browne, G., Vedie, B., Johannes, L.*, et al.* (2011). Cells respond to mechanical stress by rapid disassembly of caveolae. Cell *144*, 402-413.

Snider, J., and Houry, W.A. (2008). AAA+ proteins: diversity in function, similarity in structure. Biochem Soc Trans *36*, 72-77.

Song, C., Wang, Q., and Li, C.C. (2003). ATPase activity of p97-valosin-containing protein (VCP). D2 mediates the major enzyme activity, and D1 contributes to the heat-induced activity. J Biol Chem *278*, 3648-3655.

Stapf, C., Cartwright, E., Bycroft, M., Hofmann, K., and Buchberger, A. (2011). The general definition of the p97/valosin-containing protein (VCP)-interacting motif (VIM) delineates a new family of p97 cofactors. J Biol Chem *286*, 38670-38678.

Stoeber, M., Stoeck, I.K., Hanni, C., Bleck, C.K., Balistreri, G., and Helenius, A. (2012). Oligomers of the ATPase EHD2 confine caveolae to the plasma membrane through association with actin. EMBO J *31*, 2350-2364.

Stolz, A., Hilt, W., Buchberger, A., and Wolf, D.H. (2011). Cdc48: a power machine in protein degradation. Trends Biochem Sci *36*, 515-523.

Stringer, D.K., and Piper, R.C. (2011). A single ubiquitin is sufficient for cargo protein entry into MVBs in the absence of ESCRT ubiquitination. J Cell Biol *192*, 229-242.

Suzuki, K., and Ohsumi, Y. (2007). Molecular machinery of autophagosome formation in yeast, Saccharomyces cerevisiae. FEBS Lett *581*, 2156-2161.

Sverdlov, M., Shajahan, A.N., and Minshall, R.D. (2007). Tyrosine phosphorylation-dependence of caveolae-mediated endocytosis. J Cell Mol Med *11*, 1239-1250.

Szeto, J., Kaniuk, N.A., Canadien, V., Nisman, R., Mizushima, N., Yoshimori, T., Bazett-Jones, D.P., and Brumell, J.H. (2006). ALIS are stress-induced protein storage compartments for substrates of the proteasome and autophagy. Autophagy *2*, 189-199.

Tagawa, A., Mezzacasa, A., Hayer, A., Longatti, A., Pelkmans, L., and Helenius, A. (2005). Assembly and trafficking of caveolar domains in the cell: caveolae as stable, cargo-triggered, vesicular transporters. J Cell Biol *170*, 769-779.

Takata, T., Kimura, Y., Ohnuma, Y., Kawawaki, J., Kakiyama, Y., Tanaka, K., and Kakizuka, A. (2012). Rescue of growth defects of yeast cdc48 mutants by pathogenic IBMPFD-VCPs. J Struct Biol *179*, 93-103.

Tang, B.L., Zhang, T., Low, D.Y., Wong, E.T., Horstmann, H., and Hong, W. (2000). Mammalian homologues of yeast sec31p. An ubiquitously expressed form is localized to endoplasmic reticulum (ER) exit sites and is essential for ER-Golgi transport. J Biol Chem *275*, 13597-13604.

Tang, W.K., and Xia, D. (2012). Structural and functional deviations in disease-associated p97 mutants. J Struct Biol *179*, 83-92.

Tang, Z., Scherer, P.E., Okamoto, T., Song, K., Chu, C., Kohtz, D.S., Nishimoto, I., Lodish, H.F., and Lisanti, M.P. (1996). Molecular cloning of caveolin-3, a novel member of the caveolin gene family expressed predominantly in muscle. J Biol Chem *271*, 2255-2261.

Tanno, H., and Komada, M. (2013). The ubiquitin code and its decoding machinery in the endocytic pathway. J Biochem *153*, 497-504.

Thomsen, P., Roepstorff, K., Stahlhut, M., and van Deurs, B. (2002). Caveolae are highly immobile plasma membrane microdomains, which are not involved in constitutive endocytic trafficking. Mol Biol Cell *13*, 238-250.

Tomas, A., Futter, C.E., and Eden, E.R. (2013). EGF receptor trafficking: consequences for signaling and cancer. Trends Cell Biol.

Totsukawa, G., Kaneko, Y., Uchiyama, K., Toh, H., Tamura, K., and Kondo, H. (2011). VCIP135 deubiquitinase and its binding protein, WAC, in p97ATPase-mediated membrane fusion. EMBO J *30*, 3581-3593.

Tresse, E., Salomons, F.A., Vesa, J., Bott, L.C., Kimonis, V., Yao, T.P., Dantuma, N.P., and Taylor, J.P. (2010). VCP/p97 is essential for maturation of ubiquitin-containing autophagosomes and this function is impaired by mutations that cause IBMPFD. Autophagy *6*, 217-227.

Ungewickell, E.J., and Hinrichsen, L. (2007). Endocytosis: clathrin-mediated membrane budding. Curr Opin Cell Biol *19*, 417-425.

Urwin, H., Authier, A., Nielsen, J.E., Metcalf, D., Powell, C., Froud, K., Malcolm, D.S., Holm, I., Johannsen, P., Brown, J.*, et al.* (2010). Disruption of endocytic trafficking in frontotemporal dementia with CHMP2B mutations. Hum Mol Genet *19*, 2228-2238.

Vassilieva, E.V., Ivanov, A.I., and Nusrat, A. (2009). Flotillin-1 stabilizes caveolin-1 in intestinal epithelial cells. Biochem Biophys Res Commun *379*, 460-465.

Verma, P., Ostermeyer-Fay, A.G., and Brown, D.A. (2010). Caveolin-1 induces formation of membrane tubules that sense actomyosin tension and are inhibited by polymerase I and transcript release factor/cavin-1. Mol Biol Cell *21*, 2226-2240.

Verma, R., Oania, R., Fang, R., Smith, G.T., and Deshaies, R.J. (2011). Cdc48/p97 mediates UV-dependent turnover of RNA Pol II. Mol Cell *41*, 82-92.

Vinten, J., Johnsen, A.H., Roepstorff, P., Harpoth, J., and Tranum-Jensen, J. (2005). Identification of a major protein on the cytosolic face of caveolae. Biochim Biophys Acta *1717*, 34-40.

Wagner, S.A., Beli, P., Weinert, B.T., Nielsen, M.L., Cox, J., Mann, M., and Choudhary, C. (2011). A proteome-wide, quantitative survey of in vivo ubiquitylation sites reveals widespread regulatory roles. Mol Cell Proteomics *10*, M111 013284.

Wang, Q., Li, L., and Ye, Y. (2006). Regulation of retrotranslocation by p97-associated deubiquitinating enzyme ataxin-3. J Cell Biol *174*, 963-971.

Wang, Y., Satoh, A., Warren, G., and Meyer, H.H. (2004). VCIP135 acts as a deubiquitinating enzyme during p97-p47-mediated reassembly of mitotic Golgi fragments. J Cell Biol *164*, 973-978.

Weidberg, H., Shvets, E., and Elazar, Z. (2011). Biogenesis and cargo selectivity of autophagosomes. Annu Rev Biochem *80*, 125-156.

Weihl, C.C., Dalal, S., Pestronk, A., and Hanson, P.I. (2006). Inclusion body myopathy-associated mutations in p97/VCP impair endoplasmic reticulum-associated degradation. Hum Mol Genet *15*, 189-199.

Wild, P., Farhan, H., McEwan, D.G., Wagner, S., Rogov, V.V., Brady, N.R., Richter, B., Korac, J., Waidmann, O., Choudhary, C.*, et al.* (2011). Phosphorylation of the autophagy receptor optineurin restricts Salmonella growth. Science *333*, 228-233.

Williams, R.L., and Urbe, S. (2007). The emerging shape of the ESCRT machinery. Nat Rev Mol Cell Biol *8*, 355-368.

Woelk, T., Oldrini, B., Maspero, E., Confalonieri, S., Cavallaro, E., Di Fiore, P.P., and Polo, S. (2006). Molecular mechanisms of coupled monoubiquitination. Nat Cell Biol *8*, 1246-1254.

Wollert, T., Wunder, C., Lippincott-Schwartz, J., and Hurley, J.H. (2009). Membrane scission by the ESCRT-III complex. Nature *458*, 172-177.

Wright, M.H., Berlin, I., and Nash, P.D. (2011). Regulation of endocytic sorting by ESCRT-DUB-mediated deubiquitination. Cell Biochem Biophys *60*, 39-46.

Wunderlich, C., Schober, K., Kasper, M., Heerwagen, C., Marquetant, R., Ebner, B., Forkmann, M., Schoen, S., Braun-Dullaeus, R.C., Schmeisser, A*., et al.* (2008). Nitric oxide synthases are crucially involved in the development of the severe cardiomyopathy of caveolin-1 knockout mice. Biochem Biophys Res Commun *377*, 769-774.

Xu, P., Duong, D.M., Seyfried, N.T., Cheng, D., Xie, Y., Robert, J., Rush, J., Hochstrasser, M., Finley, D., and Peng, J. (2009). Quantitative proteomics reveals the function of unconventional ubiquitin chains in proteasomal degradation. Cell *137*, 133-145.

Xu, S., Peng, G., Wang, Y., Fang, S., and Karbowski, M. (2011). The AAA-ATPase p97 is essential for outer mitochondrial membrane protein turnover. Mol Biol Cell *22*, 291-300.

Yakushiji, Y., Nishikori, S., Yamanaka, K., and Ogura, T. (2006). Mutational analysis of the functional motifs in the ATPase domain of Caenorhabditis elegans fidgetin homologue FIGL-1: firm evidence for an intersubunit catalysis mechanism of ATP hydrolysis by AAA ATPases. J Struct Biol *156*, 93-100.

Yamanaka, K., Sasagawa, Y., and Ogura, T. (2012). Recent advances in p97/VCP/Cdc48 cellular functions. Biochim Biophys Acta *1823*, 130-137.

Yang, B., and Kumar, S. (2010). Nedd4 and Nedd4-2: closely related ubiquitin-protein ligases with distinct physiological functions. Cell Death Differ *17*, 68-77.

Yang, Z., and Klionsky, D.J. (2010). Mammalian autophagy: core molecular machinery and signaling regulation. Curr Opin Cell Biol *22*, 124-131.

Ye, Y. (2006). Diverse functions with a common regulator: ubiquitin takes command of an AAA ATPase. J Struct Biol *156*, 29-40.

Ye, Y., Meyer, H.H., and Rapoport, T.A. (2003). Function of the p97-Ufd1-Npl4 complex in retrotranslocation from the ER to the cytosol: dual recognition of nonubiquitinated polypeptide segments and polyubiquitin chains. J Cell Biol *162*, 71-84.

Ye, Y., and Rape, M. (2009). Building ubiquitin chains: E2 enzymes at work. Nat Rev Mol Cell Biol *10*, 755-764.

Yeung, H.O., Kloppsteck, P., Niwa, H., Isaacson, R.L., Matthews, S., Zhang, X., and Freemont, P.S. (2008). Insights into adaptor binding to the AAA protein p97. Biochem Soc Trans *36*, 62-67.

Yorimitsu, T., and Klionsky, D.J. (2007). Eating the endoplasmic reticulum: quality control by autophagy. Trends Cell Biol *17*, 279-285.

Yu, J., Bergaya, S., Murata, T., Alp, I.F., Bauer, M.P., Lin, M.I., Drab, M., Kurzchalia, T.V., Stan, R.V., and Sessa, W.C. (2006). Direct evidence for the role of caveolin-1 and caveolae in mechanotransduction and remodeling of blood vessels. J Clin Invest *116*, 1284-1291.

Zehner, M., Chasan, A.I., Schuette, V., Embgenbroich, M., Quast, T., Kolanus, W., and Burgdorf, S. (2011). Mannose receptor polyubiquitination regulates endosomal recruitment of p97 and cytosolic antigen translocation for cross-presentation. Proc Natl Acad Sci U S A *108*, 9933-9938.

Zeigerer, A., Gilleron, J., Bogorad, R.L., Marsico, G., Nonaka, H., Seifert, S., Epstein-Barash, H., Kuchimanchi, S., Peng, C.G., Ruda, V.M.*, et al.* (2012). Rab5 is necessary for the biogenesis of the endolysosomal system in vivo. Nature *485*, 465-470.

Zerial, M., and McBride, H. (2001). Rab proteins as membrane organizers. Nat Rev Mol Cell Biol *2*, 107-117.

Zoncu, R., Perera, R.M., Balkin, D.M., Pirruccello, M., Toomre, D., and De Camilli, P. (2009). A phosphoinositide switch controls the maturation and signaling properties of APPL endosomes. Cell *136*, 1110-1121.

## Acknowledgments

I would like to thank Hemmo Meyer for providing me with the opportunity to work on the exciting endocytosis project. Especially, I have to thank you for the freedom you gave me to venture into my own pet projects; and equally for your advice always to come back to the core questions.

I want to thank Monika Bug for the many and many ideas she gave me while discussing the project. Also I want to thank the other members of the endocytosis subgroup, Maja Vuk and Danilo Ritz, who set the basis for my research and introduced me to many experimental methods.

A special thank you and all the love goes out to the whole Meyer group. You made and continue to make this an exciting and fun lab; especially the ones who took it upon them to organize all the events that made me go outside.

I would like to thank all the members of the ZMB in Essen that provided input and technical assistance as well as company and coffee breaks.

I am especially grateful to my parents and sisters who supported me and my endeavors in every possible way. And finally, I would like to thank Anne Gregor for her love, laughter and untiring patience with me talking about stuff.

# Curriculum vitae

The curriculum vitae is omitted from the online version of this thesis for protection of data privacy.

## Publications

Kirchner, P., Bug, M., and Meyer, H. (2013). Ubiquitination of the N-terminal region of caveolin-1 regulates endosomal sorting by the VCP/p97 AAA-ATPase. J Biol Chem *288*, 7363-7372.

Ritz, D., Vuk, M., Kirchner, P., Bug, M., Schutz, S., Hayer, A., Bremer, S., Lusk, C., Baloh, R.H., Lee, H.*, et al.* (2011). Endolysosomal sorting of ubiquitylated caveolin-1 is regulated by VCP and UBXD1 and impaired by VCP disease mutations. Nat Cell Biol *13*, 1116-1123.

Essen 05.02.2014

## Affidavits/Erklärungen

**Erklärung:**

Hiermit erkläre ich, gem. § 6 Abs. (2) f) der Promotionsordnung der Fakultäten für Biologie, Chemie und Mathematik zur Erlangung der Dr. rer. nat., dass ich das Arbeitgebiet, dem das Thema „ **The role of ubiquitination and the p97-UBXD1 complex in regulating endosomal trafficking of caveolin-1** “ zuzuordnen ist, in Forschung und Lehre vertrete und den Antrag von **Philipp Kirchner** befürworte und die Betreuung auch im Falle eines Weggangs, wenn nicht wichtige Gründe dem entgegenstehen, weiterführen werde.

Essen, den _____ _____

Unterschrift eines Mitglieds der Universität Duisburg-Essen

**Erklärung:**

Hiermit erkläre ich, gem. § 7 Abs. (2) c) + e) der Promotionsordnung Fakultäten für Biologie, Chemie und Mathematik zur Erlangung des Dr. rer. nat., dass ich die vorliegende Dissertation selbständig verfasst und mich keiner anderen als der angegebenen Hilfsmittel bedient habe.

Essen, den _____ _____

Unterschrift des/r Doktoranden/in

**Erklärung:**

Hiermit erkläre ich, gem. § 7 Abs. (2) d) + f) der Promotionsordnung der Fakultäten für Biologie, Chemie und Mathematik zur Erlangung des Dr. rer. nat., dass ich keine anderen Promotionen bzw. Promotionsversuche in der Vergangenheit durchgeführt habe und dass diese Arbeit von keiner anderen Fakultät/Fachbereich abgelehnt worden ist.

Essen, den _____ _____

Unterschrift des Doktoranden